Isothermal Phase Transformations Below the Martensite Start Temperature in a Low-Carbon Steel

Navarro Lopez, Alfonso

DOI
10.4233/uuid:c51a53df-60cd-41ca-9418-364df17eba56

Publication date
2020

Document Version
Final published version

Citation (APA)
Navarro Lopez, A. (2020). *Isothermal Phase Transformations Below the Martensite Start Temperature in a Low-Carbon Steel*. [Dissertation (TU Delft), Delft University of Technology].
https://doi.org/10.4233/uuid:c51a53df-60cd-41ca-9418-364df17eba56

Important note
To cite this publication, please use the final published version (if applicable).
Please check the document version above.

Isothermal Phase Transformations Below the Martensite Start Temperature in a Low-Carbon Steel

Alfonso NAVARRO LÓPEZ

Isothermal Phase Transformations Below the Martensite Start Temperature in a Low-Carbon Steel

Dissertation

for the purpose of obtaining the degree of doctor
at Delft University of Technology
by the authority of the Rector Magnificus Prof. Dr. Ir. T.H.J.J. van der Hagen,
chair of the Board for Doctorates,
to be defended publicly on
Tuesday 23 June 2020 at 12.30 hours

by

Alfonso NAVARRO LÓPEZ

Ingeniero Industrial, Universidad Carlos III de Madrid, Spain
born in Albacete, Spain

This dissertation has been approved by the promoters.

Composition of the doctoral committee:

Rector Magnificus,	chairperson
Prof. dr. M.J. Santofimia,	Delft University of Technology, promoter
Prof. dr. ir. J. Sietsma,	Delft University of Technology, promoter
Dr. J. Hidalgo,	Delft University of Technology, copromoter

Independent members:

Dr. C. Garcia Mateo	CENIM (CSIC), Spain
Dr. S.M.C. van Bohemen	TATA Steel Europe, The Netherlands
Prof. Dr.-Ing. W. Bleck	RWTH Aachen University, Germany
Prof. dr. ir. J.M.C. Mol	Delft University of Technology

Reserve member:

Prof. dr. ir. Z. Li	Delft University of Technology

The research described in this dissertation was carried out in the Department of Materials Science and Engineering at Delft University of Technology, The Netherlands.

This research was carried out with the financial support of the Netherlands Organization for Scientific Research (NWO) and the Dutch Foundation for Applied Sciences (STW) through the VIDI-Grant 12376.

Printed by: ProefschriftMaken ‖ www.proefschriftmaken.nl
Cover by: arch. J.J. Horcajo-Gaspar

ISBN 978-94-6384-144-3
An electronic version of this dissertation is available at TUDelft repository.

Contents

Contents

Summary

Advanced High Strength Steels (AHSS) have been used extensively for the last three decades in the automotive industry as they exhibit an enhanced combination of strength and ductility which has successfully allowed the weight reduction of structural components. This breakthrough has been highly beneficial for the environment, as lighter vehicles have reduced the CO_2 emissions during use. In the last decade, the development of AHSS has been focused on the design of complex microstructures containing high strength phases, such as bainite and martensite, as well as a softer phase providing ductility and strain hardening, such as austenite. However, the thermomechanical processing of these multiphase steels requires long, complex, and energy-intensive thermal treatments with a high environmental footprint. New alternative processing routes are being developed for producing these multiphase steels sustainably, without compromise on strength and ductility, thus achieving reduced CO_2 emissions throughout the lifecycle of steel. In this framework, a new thermal treatment consisting of a rapid cooling below the martensite start temperature (M_s) followed by an isothermal treatment at the same quenching temperature is proposed as a promising environmentally sustainable alternative for the production of such multiphase steels. This Ph.D. thesis investigates, from a scientific point of view, the phase transformations and the interactions between the phases formed during the above-described novel isothermal treatment below M_s in a low-carbon high-silicon steel. The thermal treatment is applied in different combinations of quenching temperature and isothermal holding time in order to stimulate the formation of diverse phase fraction mixtures. The research also elucidates the effects of the formation of each of the phases on the microstructure-property relationships of these multiphase steels.

The main reason of considering the proposed thermal treatment as a promising processing route relies on the formation of prior athermal martensite (PAM) before the subsequent isothermal holdings below M_s. It has been reported that the presence of martensite accelerates the kinetics of the subsequent isothermal decomposition of austenite. A quantitative kinetic analysis of this isothermal transformation demonstrates that the formation of a small fraction of PAM causes a strong accelerating effect on the subsequent transformation kinetics due to the creation of a high number of nucleation sites in the form of martensite-austenite interfaces. This acceleration results to be, at least, two orders of magnitude higher at the start of the isothermal transformation below M_s compared to that obtained in an isothermal transformation occurring above M_s, where there is no formation of PAM. Regarding the nature of the product phase isothermally formed from the decomposition of austenite during the isothermal holding below M_s, different studies have identified it as bainite, isothermal martensite, or a neither purely

bainitic nor purely martensitic product phase. Based on a detailed microstructural characterization by Scanning Electron Microscopy (SEM) and Electron Back Scatter Diffraction (EBSD) of the product phases formed from the decomposition of austenite in holdings above and below M_s, bainitic ferrite is proven to be the isothermal product phase formed in isothermal treatments below M_s. This product phase mainly appears in the form of thin acicular units and/or irregularly shaped laths. On the other hand, PAM is typically found in the form of laths with a sharp tip at one of the edges and/or laths presenting wavy boundaries with ledge-like protrusions and containing carbides.

Once all product phases formed during the distinct stages of the proposed thermal treatment have been characterized in-depth individually, the research focuses on analysing the effects of a free surface on the microstructural evolution during isothermal holdings below M_s. Free surface effects are found to be responsible of a higher M_s temperature at the surface than within the bulk of steel specimens due to the easier accommodation of martensitic transformation strains at the surface. This may lead to a microstructural evolution at the surface which differs from that occurring in the bulk during the application of isothermal treatments below M_s. In-situ observations of the surface by Laser Confocal Microscopy (LCM) are complemented with EBSD measurements and verified by a thermodynamic model. These experiments demonstrate that a higher M_s temperature at the surface is a consequence of the minimized volume strain energy needed to accommodate the strains derived from martensite formation during rapid cooling below M_s. On the other hand, differences in the M_s temperature imply the formation of different multiphase microstructures at the surface compared to those formed in the bulk. These microstructural differences, also studied in terms of grain size and variant selection, can be decisive in the final mechanical performance of these multiphase steels, especially under the action of phenomena affecting the surface area.

Another interesting aspect to address of these newly designed multiphase microstructures is the carbon enrichment of the remaining austenite from the phases already formed, such as martensite and bainite, during the application of isothermal treatments below M_s. This process is generally studied by tracking the evolution of the austenite lattice parameter by means of conventional characterization techniques. However, since the austenite lattice parameter can be also affected below M_s by compressive strains introduced by martensite formation, the evaluation of carbon redistribution should be performed by advanced high-resolution characterization techniques. In-situ high energy X-ray diffraction (HE-XRD) measurements are carried out for a quantitative analysis of carbon partitioning from existing phases into the remaining austenite during an isothermal treatment below M_s. It turns out that the formation of a certain fraction of PAM (higher than 0.2) induces compressive strains in the untransformed austenite

which depend linearly on the increase in martensite fraction. Moreover, the kinetics of the relative carbon enrichment in austenite is proven to be slower than that of the isothermal bainite reaction. This difference is attributed to the slower kinetics of carbon redistribution within the untransformed austenite grains, which depends, at each temperature, on the combined effect of carbon diffusivity and the residual austenite fraction.

Having analysed the physical phenomena derived from the formation of distinct product phases, the research is focused next on the strengthening mechanisms acting in the newly designed multiphase microstructures below M_s and on their microstructure-property relationships. Uniaxial tensile tests are carried out to obtain the overall mechanical response of all multiphase microstructures. A thorough investigation is performed to determine the individual contribution of each product phase on the overall mechanical response of the microstructures formed by one-hour isothermal treatments below M_s, compared to those formed above M_s. The mechanical behaviour analysis shows that the initial formation of PAM and its tempering during the subsequent isothermal holding below M_s trigger several strengthening mechanisms, related to grain-boundary, solid-solution, and precipitation, which favour an increase of the yield stress of multiphase microstructures obtained below M_s. The presence of PAM, tempered to some extent, slightly reduces the strain hardening capacity of these microstructures, compared to those obtained above M_s where no initial formation of martensite occurs, because tempered PAM counteracts the contribution of the mechanical transformation of the retained austenite. In the present study, the mechanical stability of retained austenite is shown to be similar in all multiphase microstructures obtained from isothermal holdings either above or below M_s, where about 2/3 of the total fraction of retained austenite is mechanically transformed during the application of stress.

Finally, the effect of holding time on the microstructure-property relationship of microstructures isothermally formed below M_s is discussed. Variations in holding time lead to different degrees of tempering of the PAM which, in turn, results in a different mechanical response of this product phase within the multiphase microstructure. Results show that the tempering degree of PAM with holding time has a primary effect on the overall mechanical response of microstructures formed below M_s. For short holding times (several minutes), PAM yields similar to as-quenched martensite while, for longer holding times (up to one hour), its yielding behaviour becomes comparable to the one exhibited by typical tempered martensite. In addition, the bainitic character of the isothermal product phase formed below M_s is confirmed by the analysis of extended Kocks-Mecking curves, which shows that bainitic ferrite yields at a lower stress than as-quenched martensite and tempered martensite. Furthermore, a final comparative study of microstructure-property relations shows that small variations of temperature and

holding time in the application of isothermal treatments below M_s enable us to obtain bainitic-martensitic microstructures with mechanical properties comparable to those of conventional bainitic steels obtained above M_s. In turn, the reduction of processing times in treatments below M_s, as a consequence of the accelerating effect of PAM on the subsequent bainite reaction, entails a remarkable technological advantage for the manufacturing of more sustainable AHSS with a lower energy consumption and a reduced environmental footprint. This Ph.D. thesis provides fundamental understanding of the microstructural development and the interactions between phases occurring during isothermal treatments below M_s as well as of the mechanical performance of the created multiphase microstructures. This scientific knowledge can thus be valuable information for steelmakers willing to uptake the findings for investigating these newly designed AHSS at industrial scale and producing them commercially.

Samenvatting

Geavanceerde staalsoorten met hoge sterkte (AHSS) worden de laatste drie decennia veel gebruikt in de auto-industrie, aangezien ze een aantrekkelijke combinatie van sterkte en ductiliteit bezitten. Dit heeft tot een succesvolle gewichtsvermindering van structurele componenten geleid. Deze doorbraak was gunstig voor het milieu, aangezien lichtere voertuigen minder CO_2 uitstoten. In de afgelopen tien jaar was de ontwikkeling van AHSS gericht op het creëren van complexe microstructuren die fasen met een hoge sterkte bevatten, zoals bainiet en martensiet, evenals een zachtere fase die zorgt voor taaiheid en rekverharding, zoals austeniet. De thermomechanische verwerking van deze meerfasige staalsoorten vereist echter lange, gecompliceerde en energie-intensieve thermische behandelingen, die een groot ecologisch nadeel teweegbrengen. Er wordt daarom naar nieuwe alternatieve verwerkingsroutes gezocht om meerfasige staalsoorten duurzaam te produceren, zonder concessies te doen aan sterkte en ductiliteit, waardoor de CO_2-uitstoot gedurende de gehele levenscyclus vermindert. In dit kader wordt als veelbelovend duurzaam ecologisch alternatief een nieuwe thermische behandeling voorgesteld, bestaande uit een snelle afkoeling onder de martensiet start-temperatuur (M_s) gevolgd door isothermische ontlaten bij dezelfde afschrik temperatuur. In dit proefschrift worden, voor een koolstofarm staal met een hoog siliciumgehalte, vanuit wetenschappelijk oogpunt, de fasetransformaties en de onderlinge interacties tussen de verschillende fasen gevormd tijdens de nieuwe isotherme behandeling onder M_s beschreven. De thermische omvorming werd uitgevoerd in diverse combinaties van afschriktemperatuur en isothermische verblijftijd om de vorming van diverse fase-fractie mengsels te initiëren. In het proefschrift worden ook de effecten besproken van elk van de gevormde fasen op de relatie tussen microstructuur en eigenschappen van de nieuwe meerfasige staalsoorten.

De belangrijkste reden om de voorgestelde thermische behandeling als een veelbelovende verwerkingsroute te beschouwen, berust op de vorming van athermisch martensiet (PAM) nog voordat de isotherme omzetting onder M_s plaatsvindt. Het is bekend, dat de aanwezigheid van martensiet de kinetiek van de isotherme omzetting van austeniet versnelt. Een kwantitatieve analyse van de isotherme transformatie toont aan, dat de vorming van reeds een kleine fractie PAM de transformatiekinetiek sterk versneld, als gevolg van de creatie van een groot aantal kiemen in de vorm van martensiet-austeniet grensvlakken. Deze versnelling ligt minstens twee ordes van grootte hoger aan het begin van de isotherme transformatie onder M_s, vergeleken met die verkregen bij een isotherme transformatie boven M_s, waarbij geen PAM wordt gevormd. Wat betreft de aard van de fase die isotherm ontstaat door de afbraak van austeniet tijdens een isothermische

behandeling onder M_s, hebben verschillende studies deze geïdentificeerd als bainiet, isotherm martensiet, of een isotherm product dat noch puur bainitisch, noch puur martensitisch is. Op basis van een gedetailleerde microstructurele karakterisering met scanning elektronenmicroscopie (SEM) en Elektron Back Scatter Diffractie (EBSD) van de fasen die ontstaan door de ontbinding van austeniet boven en onder M_s, is bewezen dat bainitisch ferriet de fase is, die isothermisch wordt gevormd onder M_s. Deze fase komt voornamelijk voor in de vorm van dunne naaldvormige eenheden en/of onregelmatig gevormde latstructuren. Aan de andere kant neemt PAM meestal de vorm aan van latstructuren met een scherpe punt aan één van de randen en/of latstructuren die golvende grenzen vertonen met richelachtige uitsteeksels en carbiden.

Zodra alle fasen die tijdens de verschillende stadia in de voorgestelde thermische behandeling worden gevormd, diepgaand waren gekarakteriseerd, richtte het onderzoek zich op het analyseren van de effecten van vrije oppervlakken op de microstructurele evolutie tijdens isothermische omvorming onder M_s. Vrije oppervlakte-effecten blijken verantwoordelijk voor een hogere M_s-temperatuur aan het oppervlak vergeleken met die in het interne van de staalmonsters, vanwege de gemakkelijkere accommodatie van martensitische transformatie-vervormingen aan het oppervlak. Dit kan tot een andere microstructurele evolutie aan het oppervlak leiden dan in de massa, tijdens de isotherme behandelingen onder M_s. In-situ observatie van het oppervlak met Laser Confocal Microscopy (LCM) wordt aangevuld met EBSD-metingen en geverifieerd met behulp van een thermodynamisch model. De experimenten tonen aan, dat een hogere M_s-temperatuur aan het oppervlak het gevolg is van de geminimaliseerde vervormingsenergie die nodig is om de deformaties op te vangen, die ontstaan door martensiet-vorming tijdens snelle afkoeling onder M_s. Anderzijds, impliceren verschillen in de M_s temperatuur de vorming van verschillende meerfasige microstructuren aan het oppervlak in vergelijking met die in de bulk. Deze microstructurele verschillen, onderzocht in termen van korrelgrootte en variatieselectie, kunnen doorslaggevend zijn voor de uiteindelijke mechanische prestaties van de meerfasige staalsoorten, vooral onder invloed van fenomenen die de oppervlakte beïnvloeden.

Een ander interessant aspect van de nieuw ontworpen meerfasige microstructuren is het proces van koolstofverrijking van het resterende austeniet uit de reeds gevormde fasen, zoals martensiet en bainiet, door isotherme behandelingen onder M_s. Dit proces wordt over het algemeen bestudeerd door de evolutie van de austeniet-roosterconstante te volgen met conventionele karakteriseringstechnieken. Echter, aangezien de austeniet-roosterconstante onder M_s, ook kan worden beïnvloed door de samenpersing ten gevolge van de martensiet-vorming, moet de evaluatie van de koolstofherverdeling worden uitgevoerd met geavanceerde karakteriseringstechnieken met hoge resolutie. In-situ hoogenergetische röntgendiffractie (HE-XRD) metingen werden uitgevoerd voor

een kwantitatieve analyse van koolstofverdeling van de bestaande fasen in het resterende austeniet tijdens een isothermische behandeling onder M_s. Er kon worden aangetoond, dat de vorming van een bepaalde fractie van PAM (hoger dan 0,2) compressiestammen introduceert in het niet-getransformeerde austeniet, die lineair toenemen met de martensiet-fractie. Bovendien kon worden bewezen dat de kinetiek van de relatieve koolstofverrijking in austeniet langzamer is, dan die van de isotherme bainiet-reactie. Het verschil in de kinetiek wordt toegeschreven aan de tragere kinetiek van de koolstofherverdeling binnen de niet-getransformeerde austeniet-korrels, die afhangt van het gecombineerde effect van koolstof-diffusiviteit en de resterende austeniet-fractie.

Na de fysische verschijnselen te hebben geanalyseerd, die voortvloeien uit de vorming van verschillende fasen, werd het onderzoek gericht op de versterkingsmechanismen die actief zijn in de nieuw ontwikkelde meerfasige microstructuren onder M_s en op hun microstructuur-eigenschap relaties. Er werden uniaxiale trek-testen uitgevoerd om de totale mechanische respons van alle meerfasige microstructuren te bepalen. Er werd een grondig onderzoek uitgevoerd om eerst de individuele bijdrage van elke fase tot de algehele mechanische respons te bepalen van de microstructuren gevormd tijdens één-uur durende isothermische behandelingen onder M_s, en die vervolgens te vergelijken met die gevormd boven M_s. Uit de mechanische analyse blijkt, dat de initiële vorming van PAM en het temperen ervan tijdens de isothermische opslag onder M_s verschillende versterkingsmechanismen activeren, gerelateerd aan korrelgrens, vaste oplossing en precipitatie. Deze mechanismen verhogen de vloeispanning van meerfasige microstructuren verkregen onder M_s. De aanwezigheid van PAM, getemperd tot op een zeker niveau, vermindert de rekverhardingscapaciteit van deze microstructuren enigszins, in vergelijking met die verkregen boven M_s, waar geen initiële vorming van martensiet optreedt. Gehard PAM gaat de mechanische transformatie van het resterende austeniet immers tegen. In de huidige studie wordt aangetoond, dat de mechanische stabiliteit van resterend austeniet vergelijkbaar is met die van alle meerfasige microstructuren verkregen uit isotherme behandelingen boven of onder M_s, waarbij ongeveer 2/3 van de totale fractie achterblijvend austeniet mechanisch wordt getransformeerd tijdens de toepassing van spanning.

Ten slotte wordt het effect besproken van de verblijftijd op de microstructuur-eigenschap relatie van microstructuren isothermisch gevormd onder M_s. Variaties in de duur leiden tot verschillende gradaties van het temperen van PAM. Dit resulteert in een andere mechanische respons van deze fase binnen de meerfasige microstructuur. De resultaten tonen aan dat de mate van tempering van PAM een primair effect heeft op de totale mechanische respons van microstructuren gevormd onder M_s. Voor korte looptijden (enkele minuten) zwicht PAM zoals afgeschrikt martensiet, terwijl voor langere tijden (tot een uur), het zwichtgedrag vergelijkbaar wordt met dat van gehard martensiet. Het

bainitische karakter van de isothermisch, onder M_s, gevormde fase wordt bevestigd, door de analyse van de Kocks-Mecking-curven. Dit laat zien dat bainitisch ferriet bij een lagere spanning zwicht dan afgeschrikt en gehard martensiet. Bovendien liet een vergelijkende studie van microstructuur-eigenschap relaties zien, dat kleine variaties in temperatuur en looptijd bij isotherme behandelingen onder M_s het mogelijk maken bainitisch-martensitische microstructuren te verkrijgen met soortgelijke mechanische eigenschappen als die van conventionele bainitische staalsoorten verkregen boven M_s. De verkorting van de verwerkingstijden bij de omvorming onder M_s als gevolg van het versnellende effect van de PAM op de bainiet-reactie brengt een opmerkelijk technologisch voordeel met zich mee voor de duurzame productie van AHSS met lager energieverbruik en minder ecologische invloed. In dit proefschrift werden de microstructurele ontwikkeling en interactie tussen fasen die optreden tijdens isotherme behandelingen onder M_s en de mechanische prestaties van de verkregen meerfasige microstructuren behandeld. Dit werk kan waardevolle informatie opleveren voor staalproducenten die bereid zijn de bevindingen over te nemen voor onderzoek van deze nieuwe soort AHSS op industriële schaal en voor het commercieel produceren ervan.

Resumen

Los aceros avanzados de alta resistencia (AHSS) se han utilizado ampliamente en la industria automotriz durante las últimas tres décadas ya que estos aceros exhiben una buena combinación de resistencia y ductilidad que ha permitido, con éxito, la reducción de peso de los componentes estructurales. Este significativo avance ha sido altamente beneficioso para el medio ambiente, ya que los vehículos más ligeros han reducido sus emisiones de CO_2 durante el uso. En la última década, el desarrollo de AHSS se ha centrado en el diseño de microestructuras complejas formadas por fases con una alta resistencia, como la bainita y la martensita, así como una fase más blanda que proporciona ductilidad y endurecimiento por deformación, como es la austenita. Sin embargo, el procesado termo-mecánico de estos aceros multifase requiere de tratamientos térmicos largos, complejos, y energéticamente intensivos con un gran impacto medioambiental. Para conseguir una producción más sostenible de estos aceros, se están desarrollando nuevas rutas de procesado alternativas sin comprometer la resistencia y ductilidad de los mismos, logrando así una reducción de las emisiones de CO_2 durante todo el ciclo de vida del acero. En este marco, se propone para la producción de dichos aceros multifase un tratamiento térmico alternativo y sostenible medioambientalmente consistente en un enfriamiento rápido por debajo de la temperatura de inicio de la martensita (M_s) seguido de un tratamiento isotérmico a la misma temperatura de enfriamiento. En esta tesis doctoral se investiga, desde un punto de vista científico, las transformaciones de fase y las interacciones entre las fases formadas durante el novedoso tratamiento isotérmico por debajo de la M_s descrito anteriormente en un acero con bajo contenido en carbono y alto contenido en silicio. El tratamiento isotérmico se aplica a diferentes temperaturas y tiempos para lograr la formación de diversas combinaciones de fracciones de fase. La investigación también se centra en dilucidar los efectos de la formación de cada una de las fases en la relación microestructura-propiedad de estos aceros multifase.

El principal motivo para considerar el tratamiento térmico propuesto como una ruta de procesado alternativa de estos aceros radica en la formación de martensita atérmica (PAM) antes del tratamiento isotérmico por debajo de la M_s. Es sabido que la presencia de martensita acelera la cinética de la transformación isotérmica de la austenita. A partir de un análisis cuantitativo de la cinética de dicha transformación se demuestra que la formación de una pequeña fracción de PAM causa un fuerte efecto acelerante en la cinética de la transformación posterior debido a la creación de un gran número de sitios de nucleación en las intercaras martensita-austenita. Esta aceleración resulta ser, al menos, dos órdenes de magnitud mayor al comienzo de la transformación isotérmica por debajo de la M_s en comparación con la aceleración obtenida en una transformación

isotérmica que tiene lugar por encima de la M_s, donde no hay formación de PAM. Con respecto a la naturaleza de la fase formada a partir de la transformación isotérmica de la austenita por debajo de la M_s, diferentes estudios científicos la han identificado como bainita, martensita isotérmica, o una fase que no llega a ser puramente bainítica ni puramente martensítica. Gracias a una detallada caracterización microestructural mediante microscopía electrónica de barrido (SEM) y difracción de electrones por retrodispersión (EBSD) de las fases formadas a partir de la transformación isotérmica de la austenita por encima y por debajo de la M_s, se ha demostrado que es la bainita la fase formada isotérmicamente por debajo de dicha temperatura. Esta fase aparece principalmente en forma de unidades aciculares delgadas y/o lajas con forma irregular. Por otra parte, la PAM se presenta en forma de lajas con uno de sus bordes acabado en punta y/o lajas que presentan ondulaciones en su intercara(s) con protuberancias en forma de salientes y carburos.

Una vez caracterizadas en detalle cada una de las fases formadas durante las distintas etapas del tratamiento térmico propuesto, la investigación se centra en analizar los efectos de una superficie libre en la evolución microestructural que tiene lugar durante los tratamientos isotérmicos por debajo de la M_s. Los efectos de superficie libre son responsables de que la temperatura M_s sea más alta en la superficie que en el interior de las muestras de acero debido a que las deformaciones introducidas por la transformación martensítica se acomodan más fácilmente en la superficie. Esto puede dar lugar a una evolución microestructural totalmente distinta en la superficie y en el interior de dichas muestras durante la aplicación de tratamientos isotérmicos por debajo de la M_s. El estudio de esta evolución microestructural en superficie se realiza mediante observaciones in situ por microscopía confocal láser (LCM), que se complementan con medidas EBSD y, a su vez, se verifican con ayuda de un modelo termodinámico. Estos experimentos demuestran que la temperatura M_s es más alta en la superficie debido a que sólo es necesaria una mínima energía de deformación volumétrica para acomodar las deformaciones derivadas de la formación de martensita durante el enfriamiento rápido por debajo de la M_s. Por otra parte, estas diferencias en la temperatura M_s conllevan la formación de diferentes microestructuras multifase en la superficie con respecto al interior de la muestras de acero. Estas diferencias microestructurales, también estudiadas en términos de tamaño de grano y selección de variantes cristalográficas, pueden resultar decisivas en el comportamiento mecánico de estos aceros multifase, especialmente en aquellos bajo la acción de fenómenos que afectan al área superficial.

Otro aspecto interesante a estudiar en estas microestructuras multifase de nuevo diseño es el enriquecimiento de carbono de la austenita a partir de las fases ya formadas, como la martensita y la bainita, durante la aplicación de los tratamientos isotérmicos por debajo de la M_s. Este proceso generalmente se estudia analizando la evolución del parámetro de red

de la austenita mediante técnicas de caracterización convencionales. Sin embargo, dado que el parámetro de red de la austenita también puede verse afectado en los tratamientos isotérmicos por debajo de la M_s por las deformaciones de compresión inducidas por la transformación martensítica, la evaluación de la redistribución de carbono en la austenita debe realizarse mediante técnicas de caracterización de alta resolución. En este caso, medidas in-situ de difracción de rayos X de alta energía (HE-XRD) se llevan a cabo para obtener resultados cuantitativos con respecto a la partición de carbono entre la austenita y las fases existentes durante un tratamiento isotérmico por debajo de la M_s. Los resultados muestran que la formación de una cierta fracción de PAM (superior a 0.2) induce esfuerzos de compresión en la austenita no transformada que dependen linealmente del aumento de la fracción de martensita. Además, se ha demostrado que la cinética del enriquecimiento relativo de carbono de la austenita es más lenta que la de la reacción isotérmica de bainita. Esta diferencia se atribuye a una cinética más lenta de la redistribución del carbono dentro de los granos de austenita no transformados, que depende, en cada temperatura, del efecto combinado de la difusividad del carbono y de la fracción de austenita retenida.

Tras analizar los fenómenos físicos derivados de la formación de distintas fases, la investigación se centra a continuación en los mecanismos de endurecimiento que actúan en las microestructuras multifase obtenidas por debajo de la M_s y en sus relaciones de microestructura-propiedad. Para ello, se realizan ensayos de tracción uniaxial con el objetivo de obtener la respuesta mecánica de todas las microestructuras multifase. A partir de estos ensayos, se determina la contribución individual de cada fase a la respuesta mecánica de las microestructuras formadas mediante tratamientos isotérmicos de una hora de duración por debajo de la M_s y en comparación con las formadas por encima de la M_s. El análisis de dicho comportamiento mecánico muestra que la formación inicial de PAM y su posterior revenido durante el tratamiento isotérmico por debajo de la M_s desencadenan una serie de mecanismos de endurecimiento, relacionados con los límites de grano, los elementos en solución sólida y la precipitación de carburos, que favorecen un aumento del límite elástico de las microestructuras multifase obtenidas por debajo de la M_s. La presencia de PAM, revenida en cierto grado, reduce ligeramente la capacidad de endurecimiento por deformación de estas microestructuras en comparación con las obtenidas por encima de la M_s, donde no existe formación inicial de martensita, ya que la PAM revenida contrarresta la contribución de la transformación mecánica de la austenita retenida. En el presente estudio, se muestra que la estabilidad mecánica de la austenita retenida es similar en todas las microestructuras multifase obtenidas isotérmicamente, ya sea por encima o por debajo de la M_s, donde aproximadamente 2/3 de la fracción total de austenita retenida se transforma mecánicamente durante la aplicación de esfuerzos.

Finalmente, se discute el efecto del tiempo de tratamiento isotérmico en la relación microestructura-propiedad de las microestructuras formadas isotérmicamente por debajo de la M_s. Las variaciones en el tiempo de tratamiento isotérmico conducen a distintos grados de revenido de la PAM que, a su vez, dan como resultado una respuesta mecánica diferente de esta fase dentro de la microestructura. Los resultados muestran que el grado de revenido de la PAM según el tiempo de tratamiento tiene un efecto primario en la respuesta mecánica de las microestructuras formadas isotérmicamente por debajo de la M_s. Para tiempos de tratamiento cortos (varios minutos), el comportamiento mecánico de la PAM es similar al de la martensita obtenida tras un temple mientras que, para tiempos de tratamiento más largos (de hasta una hora), su comportamiento mecánico se vuelve comparable al exhibido por la típica martensita revenida. Además, el análisis de las curvas Kocks-Mecking confirma el carácter bainítico de la fase formada isotérmicamente por debajo de la M_s, mostrando que la bainita comienza a deformarse plásticamente a esfuerzos menores que la martensita al temple y la martensita revenida. Por último, un estudio comparativo de las relaciones entre microestructura y propiedades muestra que pequeñas variaciones en la temperatura y tiempo de tratamiento isotérmico por debajo de la M_s nos permiten obtener microestructuras bainítico-martensíticas con propiedades mecánicas comparables a las de los aceros bainíticos convencionales. A su vez, la reducción del tiempo de procesado en tratamientos por debajo de la M_s, como consecuencia del efecto acelerante de la PAM sobre la posterior reacción bainítica, conlleva una notable ventaja tecnológica para la fabricación de AHSS de forma más sostenible con un menor consumo de energía y una huella ambiental reducida. Este tesis doctoral proporciona una comprensión fundamental del desarrollo microestructural y de las interacciones entre las fases que se forman durante los tratamientos isotérmicos por debajo de la M_s, así como del comportamiento mecánico de las microestructuras multifase creadas. El conocimiento científico desarrollado puede resultar, por tanto, de información valiosa para los fabricantes de acero que estén dispuestos a usar los hallazgos presentados en esta tesis doctoral para la investigación de estos AHSS de nuevo diseño a escala industrial y producirlos comercialmente.

CHAPTER 1

Introduction

1.1. Introduction

Following the mythological description of the Ages of Man described by Hesiod, one of the first philosophers of Ancient Greece, origin of the current western societies, we could firmly affirm that, after the Iron Age, we are now immersed in the 'Age of Steel'. This material has been used for hundreds of years for all types of civilizations. However, it was not until the end of the 19th century and the beginning of the 20th century when the myth became a reality. The first scientific studies allowed to understand the phase transformations occurring in the internal structure of steel. Since then, and especially during the second half of the 20th century, a greater development of scientific knowledge about steel allowed extending the use of this material to all types of applications in different sectors due to its wide range of properties.

The development of the welfare state in our modern societies also brought the need of manufacturing new steels grades with increasingly better performance. However, in the last decades, small improvements in the performance of steels have resulted into a significant rise of their production costs. This is mainly due to 1) the use of higher additions of expensive and/or scarce alloying elements, such as titanium, nickel, niobium, or vanadium, and 2) the application of processing routes of long duration or with several heating-cooling cycles. Both alternatives imply a greater consumption of resources leading to an increase in greenhouse gas emissions. One of the examples that perfectly shows this evolution is the development over time of advanced high strength steels (AHSS), which can be classified into three types of categories or generations [1-4].

At the beginning of the 90s, the first generation of AHSS, primarily based on a ferrite matrix, began to be developed with the objective of increasing the strength of the conventional high strength steels. In the early 2000s, steelmakers managed to increase the formability of the existing AHSS through several methods to stabilize the austenite, developing the second generation of AHSS. The austenite stabilization was achieved by high additions of alloying elements such as nickel and/or manganese and through the refinement of the austenite grain size [2]. However, both implemented solutions resulted into higher production costs. From 2010, the third generation of AHSS results to be a good alternative to enhance significantly the combination of strength-ductility of the first generation AHSS at lower costs than the second one. This third generation of AHSS is based on complex multiphase microstructures formed by high strength phases, such as bainite and martensite, and a phase which provides ductility and strain hardening, such as austenite [1,5]. These multiphase-based AHSS exhibit an outstanding combination of strength and ductility, appropriate for a wide variety of applications.

Within the third generation of AHSS, the steels commonly-known as TRIP-aided bainitic (TRIP-B) steels and quenching and partitioning (Q&P) steels, alloyed with a

high silicon content, are two of the most used steels for the manufacturing of components for the automotive industry [1,3,5]. The use of both steels in these components permits the overall light-weighting of vehicles, which leads to savings in energy consumption and the reduction of emitted greenhouse gas emissions. The paradox is that to achieve these structural improvements and environmental benefits, it is necessary to apply long and complex thermal treatments which entail the increase of energy consumption and CO_2-emission during the manufacturing of these steels. Minimizing the overall carbon footprint thus requires looking for new alternative processing routes to obtain similar multiphase microstructures without loss of the strength-ductility performance.

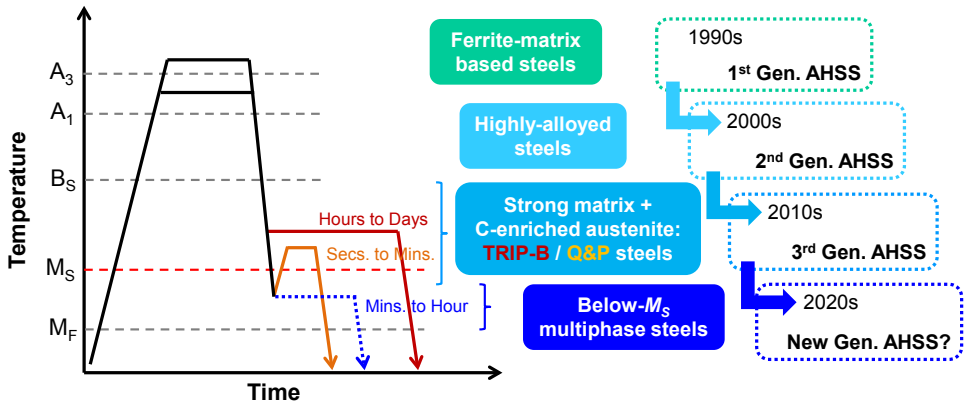

Figure 1.1. Schematic overview of the time evolution of advanced high strength steels (AHSS).

To overcome this trade-off, it results essential to understand the microstructural development during the thermal treatments applied for manufacturing TRIP-B and Q&P steels. On the one hand, TRIP-B steels are based on the slow formation of bainite at isothermal holdings between the bainite-start (B_s) and the martensite-start (M_s) temperatures (see Figure 1.1). During the isothermal holding, austenite is stabilized by the increasing carbon concentration due to the diffusion of carbon from bainite to austenite. On the other hand, Q&P microstructures are obtained through a complex thermal treatment in which the formation of martensite during an interrupted cooling below the M_s temperature is followed by a reheating and an isothermal holding at temperatures higher than M_s (around 400°C) (see Figure 1.1). As occurred in TRIP-B steels, austenite is stabilized during the isothermal holding due to its carbon enrichment but, in this case, carbon diffuses from martensite to austenite. In both steels, the presence of a high silicon content leads to the retardation, or even prevention, of carbide formation in the multiphase microstructure.

The interplay between the distinct phases during the microstructure formation is thus of great importance to obtain the desired multiphase microstructures leading to the excellent

final performance of these AHSS. But, how to develop such multiphase steels through more environmentally sustainable processing route? The answer lies in the formation of athermal martensite prior to an isothermal holding below the M_s temperature. The proposed thermal treatment simply consists of an interrupted cooling below M_s to form a certain fraction of martensite followed by an isothermal holding at the same quenching temperature to rapidly form an isothermal product phase (see Figure 1.1). After a certain holding time, martensite may probably form in a final cooling to room temperature at which a small fraction of austenite is retained.

The formation of prior athermal martensite provides an acceleration of the kinetics of the subsequent isothermal transformation [6-10]. However, there is a gap of scientific knowledge regarding the origin of such accelerating effect as well as the nature of the isothermal product phase formed. Investigations show discrepancies about the bainitic or martensitic character of this product phase and its growth mechanism [11-13,14-17]. In addition, the effects derived from the formation of prior athermal martensite on the overall mechanical behaviour of these multiphase microstructures are still questioned since diverging results arise with respect to their mechanical performance [10,18-20]. Apart from the fact that the formation of prior athermal martensite can trigger several strengthening mechanisms such as the refinement of the microstructure, variations in the tempering degree of this product phase with holding time can also affect the overall mechanical behaviour [21,22]. All phenomena derived from the formation and tempering of prior athermal martensite can in turn influence the carbon redistribution between phases, affecting the mechanical stability of the retained austenite.

As a first approach, the proposed thermal treatment has potential to be a more sustainable processing route for the development of third generation AHSS due to the acceleration of the isothermal phase transformations occurring below the M_s temperature. Understanding the microstructural development and the interactions between phases during the proposed thermal treatment represent a scientific challenge to face in order to provide fundamental knowledge regarding all involved phenomena. This scientific knowledge will give valuable information to steelmakers about the convenience of future industrial development and commercialization of these newly-designed AHSS.

1.2. Research Objective

The main objective of this Ph.D. thesis is to scientifically understand the decomposition reaction of austenite in the presence of prior athermal martensite and the interaction between the phases formed in isothermal holdings below the martensite-start (M_s) temperature in a low-carbon high-silicon steel. This Ph.D. thesis also focuses on understanding the effects of the formation and tempering of prior athermal martensite on the evolution of the microstructure-properties relationship of the multiphase

microstructures formed after the application of distinct isothermal times during holdings below M_s.

Microstructures are investigated by an in-depth micro-scale characterization by means of ex-situ and in-situ advanced characterization techniques, such as dilatometry, electron back scatter diffraction, laser confocal microscopy, and high energy X-ray diffraction, to determine the nature and morphology of all formed phases. Kinetics and thermodynamic analysis are also carried out to elucidate the effect of the formation of prior athermal martensite on the nucleation and growth of the phase isothermally formed below M_s. The microstructure-properties relationship of multiphase microstructures obtained below M_s is analysed through tensile tests to qualitatively and quantitatively determine the effect of prior athermal martensite and its tempering degree on the mechanical response of these microstructures.

1.3. Thesis Outline

This Ph.D. thesis contains an introductory chapter, six main chapters, and a final chapter of general conclusions and recommendations for future work. Chapters 2 and 3 present a basic study of transformation kinetics and multiphase microstructures formed in isothermal treatments above and below M_s. Chapters 4 and 5 are focused on a deeper analysis of these microstructures and the phenomena derived from the formation of the distinct micro-constituents. Finally, Chapters 6 and 7 present a detailed study on the strengthening mechanisms acting in the newly-designed multiphase microstructures and on their microstructure-properties relationships.

Chapter 2 examines the accelerating effect of the prior formation of martensite on the subsequent isothermal transformation occurring in isothermal holdings below the M_s temperature. Kinetics of the isothermal reaction are analysed, qualitatively, by dilatometry measurements and, quantitatively, by a kinetic model for isothermal transformations. The comparison of resulting kinetics results with those obtained by the application of isothermal holding above the M_s temperature provides insight into the possible microstructural mechanism responsible of the accelerated isothermal transformation.

Chapter 3 presents an in-depth microstructural characterization of the phases formed from the isothermal decomposition of austenite in holdings above and below the M_s temperature. The morphological characterization is carried out by the combination of images obtained by Scanning Electron Microscopy and Electron Back Scatter Diffraction. The combination of both techniques allows the identification of the bainitic or martensitic nature of the phase isothermally formed below M_s. Resulting features are also discussed based on previous investigations.

Chapter 4 investigates the effects of a free surface on the evolution of phase formation during isothermal holdings below the M_s temperature. These effects are determined qualitatively and quantitatively through in-situ observations of the surface by means of Laser Confocal Microscopy in combination with the use of a thermodynamic model. The microstructural characterization is complemented with Electron Back Scatter Diffraction measurements. Differences in the microstructural evolution during isothermal holding above and below M_s at a free surface and within the bulk are discussed in terms of the M_s temperature, nature of phases formed, grain size, and variant selection.

Chapter 5 explores the isothermal kinetics of carbon enrichment of austenite during holding below the M_s temperature. In-situ observations by X-ray diffraction using high-energy radiation are performed during the application of the newly-designed processing route in a unique attempt to quantitatively determine changes of carbon concentration in austenite. The kinetic evolution of these changes are directly compared with the kinetics of the isothermal bainite reaction as well as with the changes of carbon concentration in austenite obtained in conventional processing routes above M_s. The direct quantitative analysis of carbon enrichment suggests the diffusionless character of the bainite growth below M_s.

Chapter 6 focuses on determining the individual contribution of each phase on the overall mechanical response of the multiphase microstructures formed through isothermal holdings below the M_s temperature, compared to those formed above M_s. Uniaxial tensile tests are performed to obtain the overall mechanical behaviour of multiphase microstructures. This behaviour is discussed in terms of grain-boundary, solid-solution, and precipitation strengthening mechanisms derived from the formation of martensite and bainite. The capacity of strain hardening is also analysed based on the stability of the austenite due to carbon enrichment.

Chapter 7 explores and compares the evolution of the microstructure-properties relationship with the increasing holding time at temperatures above and below M_s. The comparative analysis is qualitatively performed by the use of extended Kocks-Mecking curves. This new approach confirms the nature of the phase that is isothermally formed in holdings below M_s and highlights the relevance of the tempering of the martensite on the mechanical performance of the multiphase microstructures. The resulting properties from this analysis are globally benchmarked within the commonly-known diagram of steel properties for AHSS.

Chapter 8 summarizes the general outcomes obtained from this research work. The importance of the fundamental understanding of phase transformations and interaction between phases in these advanced multiphase steels is highlighted as the main factor to

successfully achieve an efficient production of final steel components with the desired characteristics. Future recommendations are suggested for the extension of the present research work.

References

[1] D.K. Matlock, J.G. Speer. Third generation of AHSS: microstructure design concepts. Proceed. Inter. Conf. on Microstructure and Texture in Steels, 2008, pp. 185-205.

[2] M.Y. Demeri. Advanced high-strength steels – Science, technology, and applications. Chapter 3: Advanced high-strength steels. ASM Inter., 2013, pp. 59-70.

[3] C. Garcia-Mateo, F.G. Caballero. Comprehensive Materials Processing. Chapter: Advanced high strength bainitic steels. Elsevier Ltd., First Edition, 2014, vol. 1, pp. 165-166.

[4] T. Nanda, V. Singh, V. Singh, A. Chakraborty, S. Sharma. Third generation of advanced high-strength steels: Processing routes and properties. Mat.: Design & Appl., 2016, pp. 1-30.

[5] D.K. Matlock, J.G. Speer. Processing opportunities for new advanced high-strength sheet steels. Mater. Manuf. Process., 2010, vol. 25, pp. 7-13.

[6] R.T. Howard, M. Cohen. Austenite transformation above and within the martensite range. Trans. AIME, 1948, vol. 176, pp. 384-397.

[7] C.E. Ericsson, M.S. Bhat, E.R. Parker, V.F. Zackay. Isothermal studies of bainitic and martensitic transformations in some low alloy steels. Metall. Trans. A, 1976, vol. 7, pp. 1800-1803.

[8] H. Kawata, K. Hayashi, N. Sugiura, N. Yoshinaga, M. Takahashi. Effect of martensite in initial structure on bainite transformation. Mater. Sci. Forum, 2010, vols. 638-642, pp. 3307-3312.

[9] M.J. Santofimia, S.M.C. van Bohemen, D.N. Hanlon, L. Zhao, J. Sietsma. Perspectives in high-strength steels: Interactions between non-equilibrium phases. Inter. Symp. on AHSS, 2013, AIST, pp. 331-339.

[10] L. Zhao, L. Qian, J. Meng, Q. Zhou, F. Zhang. Below-M_s austempering to obtain refined bainitic structure and enhanced mechanical properties in low-C high-Si/Al steels. Scr. Mater., 2016, vol. 112, pp. 96-100.

[11] S.M.C. van Bohemen, M.J. Santofimia, J. Sietsma. Experimental evidence for bainite formation below M_s in Fe-0.66C. Scr. Mater., 2008, vol. 58, pp. 488–491.

[12] D. Kim, S.J. Lee, B.C. De Cooman. Microstructure of low carbon steel isothermally transformed in the M_s to M_f temperature range. Metall. Mater. Trans. A, 2012, vol. 43, pp. 4967–4983.

[13] M.C. Somani, D.A. Porter, L.P. Karjalainen, R.D.K. Misra. On various aspects of decomposition of austenite in a high-Si steel during Q & P. Metall. Mater. Trans. A, 2014, vol. 45, pp. 1247–1257.

[14] A. Borgenstam, M. Hillert, J. Ågren. Metallographic evidence of carbon diffusion in the growth of bainite. Acta Mater., 2009, vol. 57, pp. 3242-3252.

[15] M. Hillert, A. Borgenstam, J. Ågren. Do bainitic and Widmanstätten ferrite grow with different mechanisms? Scripta Mater., 2010, vol. 62, pp. 75-77.

[16] H.K.D.H. Bhadeshia. The nature, mechanism and properties of strong bainite. Proceedings 1st Int. Symp. on Steel Science, Iron Steel Inst. Japan, 2007, pp. 1-10.

[17] F.G. Caballero, M.K. Miller, C. Garcia-Mateo, J. Cornide. New experimental evidence of the diffusionless transformation nature of bainite. Journal Alloys & Comp., 2013, vol. 577S, pp. 626-630.

[18] J.C. Hell, M. Dehmas, S. Allain, J.M. Prado, A. Hazotte, J.P. Chateau. Microstructure-properties in carbide-free bainitic steels. ISIJ Int., 2011, vol. 51, pp. 1724-1732.

[19] J. Feng, T. Frankenbach, M. Wettlaufer. Strengthening 42CrMo4 steel by isothermal transformation below martensite start temperature. Mater. Sci. Eng. A, 2017, vol. 683, pp. 110-115.

[20] J. Tian, G. Xu, M. Zhou, H. Hu. Refined bainite microstructure and mechanical properties of a high-strength low-carbon bainitic steel treated by austempering below and above M_s. Steel Res. Int., 2018, pp. 1-10.

[21] S. Yan, X. Liu, W.J. Liu, T. Liang, B. Zhang, L. Liu, Y. Zhao. Comparative study on microstructure and mechanical properties of a C-Mn-Si steel treated by quenching and partitioning (Q&P) processes after a full and intercritical austenitization. Mater. Sci. Eng. A, 2017, vol. 684, pp. 261-269.

[22] A. Zinsaz-Borujerdi, A. Zarei-Hanzaki, H.R. Abedi, M. Karam-Abian, H. Ding, D. Han, N. Kheradmand. Room temperature mechanical properties and microstructure of a low alloyed TRIP-assisted steel subjected to one-step and two-step quenching and partitioning process. Mater. Sci. Eng. A, 2018, vol. 725, pp. 341-349.

2

CHAPTER 2

Effect of Prior Athermal Martensite on the Isothermal Transformation Kinetics Below M_s

**This chapter corresponds to the article "Effect of prior athermal martensite on the isothermal transformation kinetics below M_s in a low-C high-Si steel" by A. Navarro-López, J. Sietsma, and M.J. Santofimia, Metall. Mater. Trans A (2016), vol. 47A, 1028-1039.*

Abstract

Thermomechanical processing of Advanced Multiphase High Strength Steels often includes isothermal treatments around the martensite start temperature (M_s). It has been reported that the presence of martensite formed prior to these isothermal treatments accelerates the kinetics of the subsequent transformation. This kinetic effect is commonly attributed to the creation of potential nucleation sites at martensite-austenite interfaces. The aim of this study is to determine qualitatively and quantitatively the effect of a small volume fraction of martensite on the nucleation kinetics of the subsequent transformation. For this purpose, dilatometry experiments were performed at different temperatures above and below the M_s temperature for athermal martensite in a low-carbon high-silicon steel. Microstructural analysis led to the identification of the isothermal decomposition product formed above and below M_s as bainitic ferrite. The analysis of the transformation processes demonstrated that the initial stage of formation of bainitic ferrite at heat treatments below M_s is at least two orders of magnitude faster than above M_s due to the presence of martensite.

2.1. Introduction

The industrial sector is continuously looking for new steels for a range of applications. Those efforts have led to the development of a new generation of Advanced Multiphase High Strength Steels with very good combination of properties: high tensile strength and good ductility. Thermomechanical processing of these advanced multiphase steels often includes isothermal treatments around the martensite start temperature (M_s). When isothermal treatments are applied below the M_s temperature, a predetermined fraction of athermal martensite is present prior to the application of the isothermal treatment. This prior athermal martensite has an accelerating effect on the overall isothermal transformation close to the M_s temperature, which is generally known as the "swing-back" phenomenon [1-4].

But, how can athermal martensite contribute to this acceleration? It is well known that martensite preferentially nucleates at prior-austenite grain boundaries, i.e., at austenite-austenite (γ-γ) interfaces [5]. In an isothermal treatment after quenching, the athermal martensite formation is stopped before the completion of the transformation and thus martensite-austenite (α'-γ) interfaces are present in the material, which can act as potential nucleation sites [6]. Kawata et al. [5] reported that a further acceleration of the isothermal transformation above M_s is achieved by increasing the volume fraction of prior athermal martensite and, as a consequence, the density of α'-γ interfaces. However, the mechanisms of this acceleration are not well understood and the effect of these α'-γ boundaries on later transformation kinetics remains unclear.

Microstructures obtained in isothermal treatments around the M_s temperature depend on the chemical composition and the temperature of the isothermal holding. Above M_s, in hypoeutectoid steels, researchers agree about the nature of the isothermal product obtained from the decomposition of austenite. Microstructures are generally formed by a bainitic ferrite matrix with or without carbides, depending on the alloying elements and the isothermal holding time, and retained austenite, in the form of thin films or martensite-austenite (MA) islands [7-13]. The isothermally obtained phase product is generally called bainite. While the bainitic ferrite is free of carbides in upper bainite, lower bainitic ferrite can contain a fine dispersion of plate-like carbides, depending on the silicon content [14].

However, below M_s, there is discussion about which phase product is obtained from the isothermal decomposition of austenite. Different observations have shown that isothermal products formed below the M_s temperature can be purely bainitic, purely martensitic or a product nor purely martensitic nor bainitic, as is explained below:

1. Kim et al. [13,15,16] state that the nature of the isothermal product obtained in 0.2C-1.5Mn-1.5Si (wt.%) alloys, after applying isothermal treatments below M_s, is neither purely martensitic nor purely bainitic. The units of this characteristic product are, for instance, much wider than the laths in athermal martensite, and the boundaries are wavy and contain ledges. However, the presence of multivariant carbides in the isothermal product below M_s implies that it has clear similarities with athermal martensite.

2. Van Bohemen et al. [10] report that bainite can form below the martensite start temperature in a steel with 0.66 wt. % C. The microstructure obtained below the M_s temperature in a medium carbon alloy is formed by sheaves of lower bainite in a martensitic matrix and some blocks of tempered martensite exhibiting a typical multivariant carbide precipitation. This microstructure has been compared with one that was isothermally formed above the M_s temperature. A very similar bainitic microstructure is obtained in the form of long, thin sheaves containing carbides. Therefore, Van Bohemen et al. consider that the transformation product observed below M_s in their experiments is best described as bainite. Kinetics analysis supports this observation.

3. Kolmskog et al. [17] report that although it is possible that bainitic ferrite can form below the martensite start temperature, this bainitic ferrite grows slowly, similar to Widmanstätten ferrite growth above the M_s temperature. This explanation is linked to the controversy surrounding the bainite growth mechanisms. Two schools of thought differ about the mechanism of bainite formation. One argues that bainitic ferrite grows without diffusion of carbon by a displacive mechanism like martensitic growth; the transformation kinetics is thus determined by the nucleation process. The other school argues that bainitic ferrite grows by a diffusion-controlled mechanism; the transformation kinetics is thus governed by diffusion processes.

4. Oka and Okamoto [3] report the formation of isothermal martensite in treatments above and below the M_s temperature in hypereutectoid steels. Isothermal martensite was observed in the form of thin plates and/or leaf-like units. The formation of isothermal martensite has mainly been studied in high-nickel alloys and high-carbon steels [18-20], but it has not been reported in hypoeutectoid steels.

As shown, there are several unresolved issues with respect the effect of prior athermal martensite on the subsequent isothermal transformations below M_s. Although this martensite introduces new potential nucleation sites in the form of martensite-austenite interfaces, their quantitative contribution to the subsequent transformation kinetics still remains unclear. In addition, the mechanisms involved in the accelerating effect of

the prior athermal martensite in the later formation of an isothermal product are not fully clarified. Also, there is still controversy about the nature of the isothermal product obtained in isothermal treatments below the M_s temperature.

The goal of this study is to qualitatively and quantitatively determine the contribution of a certain volume fraction of martensite to the subsequent transformation kinetics. This will provide insight into the microstructural mechanism that causes the acceleration of the transformation. Additionally, a microstructural study is performed in order to identify the transformation product formed during isothermal heat treatments above and below M_s. For this purpose, dilatometry experiments are performed at different temperatures above and below M_s in a low-carbon high-silicon steel.

2.2. Experimental Procedure

The steel investigated was a hot rolled steel of composition 0.2C-3.51Mn-1.52Si-0.25Mo-0.04Al (wt. %). Manganese enhances the austenite stability and thus retards the formation of ferrite, pearlite and bainite, which results in a shift of the TTT- and CCT-curves of these phases to longer times. The combination of low-carbon and high-silicon contents minimizes and delays the carbide precipitation during the isothermal holding. The as-received material was hot rolled into a 4 mm-thick steel slab. Dilatometry specimens were taken from hot rolled slabs, parallel to the rolling direction. These were cylindrical of dimensions 10 mm in length and 3.5 mm in diameter. All specimens were heat-treated using a Bähr 805A dilatometer. The specimens were placed between two quartz rods, heated by an induction coil, and cooled using nitrogen gas. A thermocouple was spot-welded in the middle of the specimens to measure and control the temperature.

Two sets of heat treatments were applied:

(i) A direct-quench treatment was used to determine the experimental M_s temperature and the volume fraction of martensite as a function of temperature. The treatment consisted of heating to a fully austenitizing temperature (900°C) at a rate of 2°C/s, austenitization at 900°C for 240 s, and cooling until room temperature at a cooling rate of 20°C/s. From this treatment, the experimental M_s was determined as $M_{s\,(1\%)}$ = 320°C ± 5°C, at which temperature the volume fraction of martensite formed is 0.01.

(ii) Isothermal treatments were performed at different temperatures above and below M_s to evaluate the effect of the previously formed athermal martensite on the subsequent isothermal transformation kinetics. The heat treatments consisted of heating at 2°C/s to a fully austenitization at 900°C for 240 s, followed by a rapid cooling at 20°C/s until the isothermal temperature, ranging from 370°C to 270°C as

shown in Figure 2.1, where the specimens were held for 3600 s. The heat treatments ended with a final cooling to room temperature at a rate of 20°C/s.

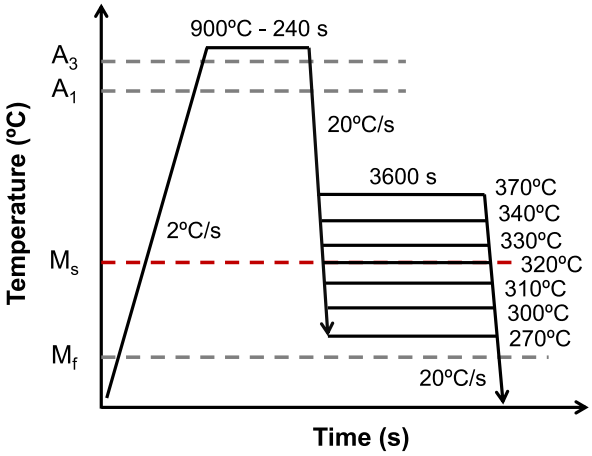

Figure 2.1. Schematic representation of heat treatments applied to the selected steel.

The heat-treated specimens were metallographically prepared by grinding and polishing. 2% Nital etching was applied to the specimens to observe the phases formed by Light Optical Microscopy (LOM). Specimens were also analysed with a JEOL JSM-6500F Scanning Electron Microscope (SEM) using a 15 kV electron beam and the Secondary Electron Imaging (SEI) detection mode. X-ray diffraction (XRD) experiments were performed on all specimens to determine the volume fraction of retained austenite (RA) at room temperature. These experiments were carried out in a Bruker D8-Advance diffractometer equipped with a Bruker Vantec Position Sensitive Detector. CoKα radiation was used in the 2θ scan from 40° to 130° with a step size of 0.035°. The fractions of austenite and ferrite were calculated by the integrated area method using the (111), (200), (220), and (311) austenite peaks, and the (110), (200), (211), and (220) ferrite peaks [21].

2.3. Results and Discussion

2.3.1. Martensite Fraction and M_s temperature

Having information on the evolution of the martensite volume fraction and the M_s temperature is crucial to determine the effect of prior athermal martensite on the subsequent formation of the isothermal product phase. Figure 2.2.a shows the change in length as a function of temperature during cooling obtained from the quench treatment. The martensite volume fractions formed during cooling to different temperatures below M_s were calculated applying the lever rule. The contraction occurring during cooling

from austenitization to the M_s temperature follows a straight line, which indicates that ferrite, pearlite, and bainite are not forming before the martensitic transformation. The dilatation below the M_s temperature is characteristic for fcc-bcc transformation indicating the formation of athermal martensite. The experimental M_s temperature for the alloy studied was determined at 320°C ± 5°C, at which the volume fraction of martensite formed was 0.01.

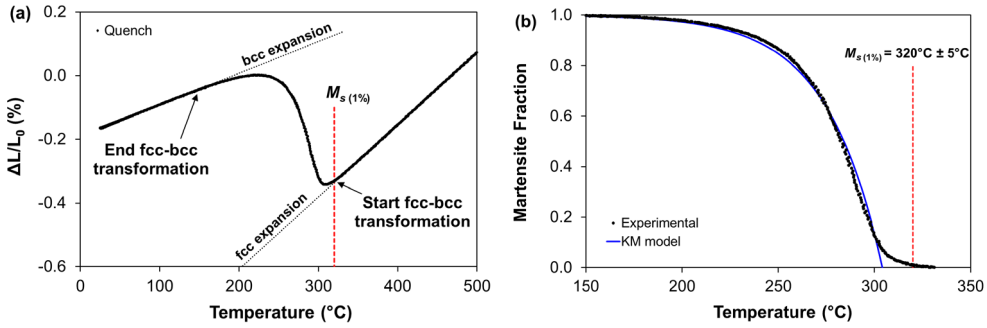

Figure 2.2. (a) Change in length versus temperature during cooling at 20°C/s. (b) Experimental volume fraction of martensite calculated applying the lever rule and fitting of this volume fraction by the Koistinen and Marburger model.

Figure 2.2.b shows the evolution of the experimental volume fraction of martensite obtained after applying the lever rule to the curve of Figure 2.2.a. A comparison with the theoretical fitting of the Koistinen and Marburger model (KM) is also displayed. The KM model quantitatively describes the progress of the austenite-to-martensite transformation as [22]:

$$f^{\alpha'} = 1 - \exp\left[-\alpha_m \cdot \left(T_{KM} - T_q\right)\right] \tag{2.1}$$

where $f^{\alpha'}$ is the volume fraction of martensite formed at a temperature T_q below the M_s temperature, T_{KM} is the theoretical martensite start temperature, which is typically somewhat lower than the experimentally determined M_s, and α_m is the rate parameter [23]. T_{KM} and α_m are taken as fitting parameters. In this case, the values of T_{KM} and α_m obtained from the fit are 304°C and 0.035°C^{-1}, respectively. This model was not finally considered for determining the M_s temperature as it does not provide accurate values at the very beginning of the martensite transformation (see Figure 2.2.b) [23].

2.3.2. Microstructures

Figure 2.3 shows the microstructures of the specimens after isothermal treatments for 3600 s at 370°C, 330°C, and 320°C (above and just at M_s) and at 310°C, 300°C, and 270°C (below M_s).

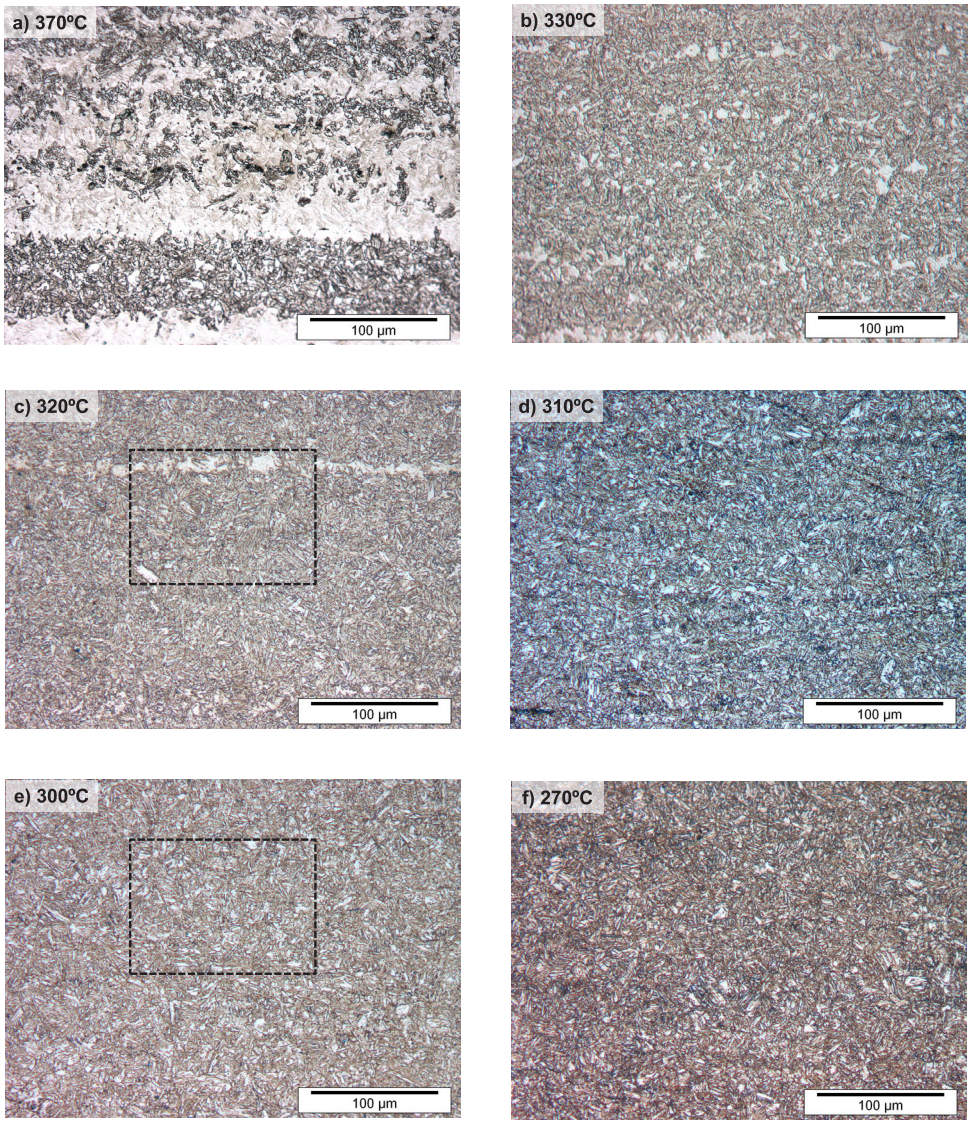

Figure 2.3. Microstructures after isothermal treatments for one hour at temperatures above M_s, a) 370°C and b) 330°C, just at M_s, c) 320°C, and below M_s, d) 310°C, e) 300°C, and f) 270°C. The dashed rectangles are enlarged in Figures 2.4.a and 2.4.b, respectively.

A structure formed by alternating bands of bainitic ferrite and martensite can be clearly observed in microstructures obtained at 370, 330, and 320°C (above or just at M_s). Microstructural banding is a very common characteristic in hot-rolled low-carbon high-alloyed steels. This phenomenon occurs due to the segregation of substitutional alloying elements during dendritic solidification. After processes such as hot rolling, areas with different segregation levels will align in the form of bands following the rolling direction. In this case, the high manganese content and its heterogeneous distribution explain the microstructures obtained. Manganese is a γ-stabilizer and decreases the A_3 and M_s temperatures. The M_s temperature is locally affected by banding, so it will be lower in Mn-rich areas than in Mn-poor ones. This implies that athermal martensite will firstly form in Mn-poor areas. Therefore, since the M_s temperature is defined as $M_{s(1\%)}$, this means that a 0.01 volume fraction of athermal martensite has already formed and, due to banding, the formation of that martensite has probably taken place at Mn-poor areas.

Due to the Mn γ-behaviour, austenite is thus more stable in Mn-rich areas, and bainitic ferrite will first grow in the areas where the Mn content is lower. After the isothermal treatment, some of the remaining untransformed austenite will transform into fresh martensite in the final cooling to room temperature. Although microstructural bands are not visible below M_s (310, 300, and 270°C), Mn segregation is also present in these specimens.

Figure 2.3 shows that as the isothermal temperature decreases, from 370°C to 270°C, the microstructures appear more homogeneous and microstructural bands are thinner, whereas they cannot be distinguished below M_s. A possible explanation of this is related with the undercooling at the transformation temperatures with respect to the A_3 temperature. When the undercooling is higher (lower transformation temperature), the driving force for the transformation is also higher, and the difference in terms of this driving force between Mn-rich and Mn-poor areas is not so pronounced as at high temperature. Thus, the effect of the inhomogeneous distribution of Mn on the microstructure development is smaller.

In isothermal treatments above and just at M_s, bainitic ferrite (BF) appears in the form of sheaves of acicular units of ferrite and can be distinguished from the fresh martensite (FM) formed in the final cooling, as shown in Figure 2.4.a. Fresh martensite is observed in the form of irregular areas within the banded structure. However, below M_s, it is rather difficult to differentiate between tempered martensite, bainitic ferrite, and fresh martensite (see Figure 2.4.b). Tempered martensite in the microstructures refers to prior athermal martensite formed during cooling which tempers to some extent during the isothermal holding. Acicular units of bainitic ferrite are not clearly identified and can be confused with laths of tempered martensite. Retained austenite can also be present

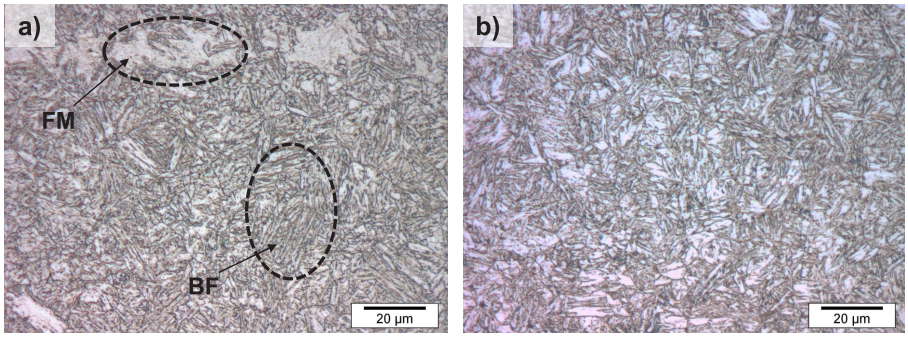

Figure 2.4. Enlarged images of the area surrounded by dashed squares in Figures 2.3.c and 2.3.e, corresponding to microstructures obtained in specimens isothermally treated for 3600 s: a) just at M_s at 320°C, and b) below M_s at 300°C. Bainitic ferrite is indicated by BF, and fresh martensite by FM.

in these microstructures in the form of interlath films between bainitic ferrite units, and/or as coarser particles. Retained austenite films as well as carbides cannot be clearly distinguished by optical microscopy due to its nanometric size.

To clarify the nature of the isothermal product obtained in treatments around M_s, three specimens treated at 340°C (above M_s), at 320°C (just at M_s) and at 300°C (below M_s) were analysed by Scanning Electron Microscopy (SEM). Figure 2.5 shows that, at 340°C, the microstructure is a mixture of bainitic ferrite, retained austenite and MA islands. Bainitic ferrite mainly appears in the form of acicular units with interlath retained austenite. MA islands with irregular shape can also be distinguished. Carbides are not identified in this microstructure.

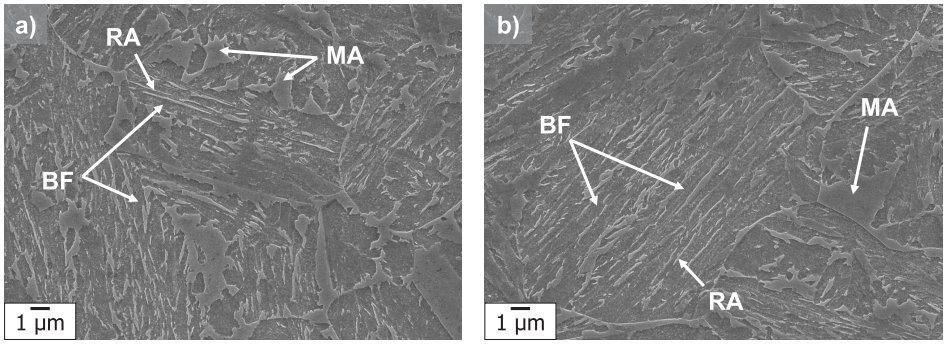

Figure 2.5. Microstructures obtained in a specimen isothermally treated above M_s at 340°C for 3600 s. Bainitic ferrite is indicated by BF, martensite-austenite islands by MA, and retained austenite by RA.

At 320°C, acicular units of bainitic ferrite with interlath retained austenite appear in the microstructure, as shown in Figure 2.6.a. Irregular-shaped MA islands can also be distinguished in both Figures. These microstructures are similar to those obtained at temperatures above M_s. In Figure 2.6.b, a lath-shaped phase product with carbides within the lath can be observed. This product could be identified as either lower bainite or tempered martensite, so it is labelled as LB/TM in the micrographs. In this case, carbides are aligned in the same direction within the lath, which is argued to be characteristic of lower bainite microstructures. However, at this temperature, a very small fraction of prior athermal martensite might have formed during cooling from austenitization. If this were so, this martensite would temper during the isothermal holding and could be confused with bainitic ferrite.

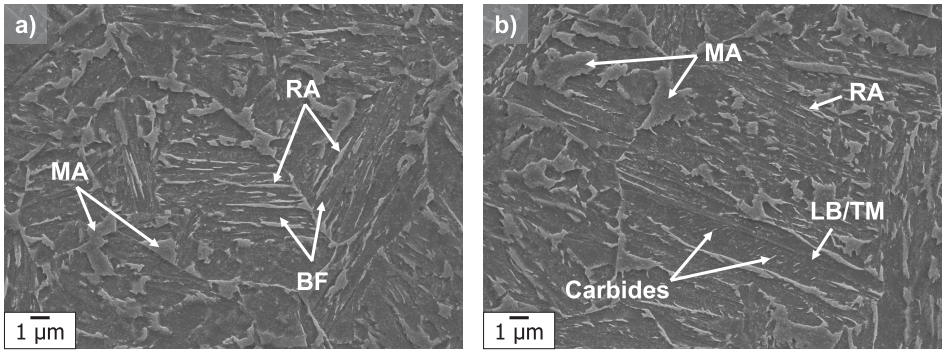

Figure 2.6. Different microstructures obtained in a specimen isothermally treated at 320°C for 3600 s. Bainitic ferrite is indicated by BF, martensite-austenite islands by MA, retained austenite by RA, and lower bainite or tempered martensite by LB/TM.

Figures 2.7.a and 2.7.b show that, at 300°C, acicular units appear in similar structures as the bainitic ones identified in Figures 2.5 and 2.6. This indicates the formation of bainitic ferrite in isothermal treatments below M_s with similar morphological characteristics to that formed in treatments above and just at M_s. LB/TM can also be distinguished in Figure 2.7.c. This product contains carbides aligned in the same direction within the lath, similar to the product observed at 320°C. On the other hand, at 300°C, a 0.16 volume fraction of athermal martensite has previously been formed during cooling from austenitization. This martensite is tempered during the isothermal holding. Tempered martensite (TM) can be clearly observed in Figure 2.7.d in the form of lath units with multivariant carbides within them. Below M_s, Figures 2.7.a and 2.7.c show other different structures, in the shape of blocks, with almost no carbides inside. These structures might be formed by different subunits of a phase product or be a unique coarse one.

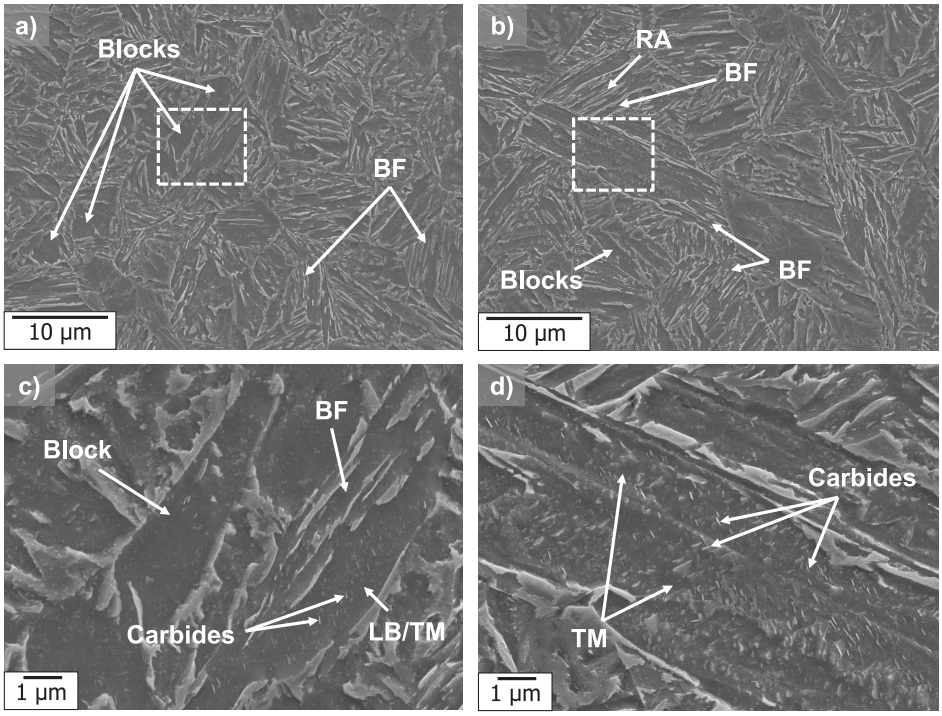

Figure 2.7. a), b) Microstructures obtained in a specimen isothermally treated at 300°C for 3600 s. c), d) Enlarged images of the area surrounded by a dashed square in a) and c), respectively. Bainitic ferrite is indicated by BF, retained austenite by RA, lower bainite or tempered martensite by LB/TM, and tempered martensite by TM.

2.3.3. Isothermal Transformation Kinetics

Figures 2.8.a and 2.8.b show the change in length of the specimens as a function of temperature during cooling for the specimens isothermally treated: a) at 370, 340, 330 (above M_s), and 320°C (just at M_s), and b) at 310, 300, and 270°C (below M_s). Above M_s, there is a linear contraction during cooling until the isothermal temperature is reached. An increase of the thermal length takes place during the isothermal holding, as shown in Figure 2.8.a. This indicates the formation of the isothermal product previously identified as bainitic ferrite.

However, below M_s, a deviation occurs from the linear contraction during cooling before the isothermal temperature is reached (see Figure 2.8.b). This means that a fraction of prior athermal martensite has formed. In these cases, once the isothermal temperature is reached, the prior athermal martensite stops forming, and an increase of the change in length takes place due to the formation of the isothermal product. All experimental curves exhibit a non-linear change in length during quenching after the isothermal holding. This indicates that the isothermal transformation is an incomplete reaction

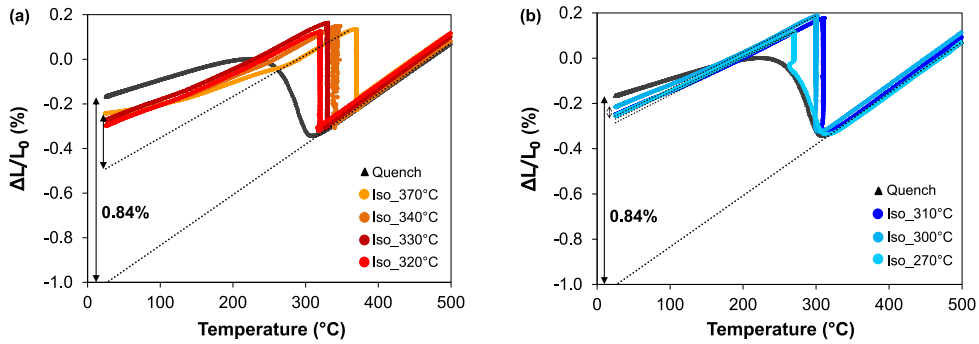

Figure 2.8. Change in length as a function of temperature for isothermal treatments above and just at M_s (a) at 370, 340, 330, and 320°C, and below M_s (b) at 310, 300, and 270°C.

and the remaining austenite partially transforms into fresh martensite during cooling to room temperature, as can be observed in Figures 2.5, 2.6, and 2.7.

In order to quantify the fresh martensite fractions [24,25], the net dilatations at room temperature (25°C) of all isothermal treatments are compared with the maximum net dilatation with respect to the austenitic phase obtained at the same temperature in the direct-quench treatment, which is 0.84% (see Figure 2.8). Net dilatations (indicated by double-ended arrows) are obtained calculating the difference of change in length between the experimental curves and the dashed lines. These dashed lines indicate the linear length change in case of absence of the martensitic transformation during cooling. XRD results show that the volume fraction of retained austenite in the directly quenched specimen is approximately 0.01, so the formation of 0.99 martensite leads

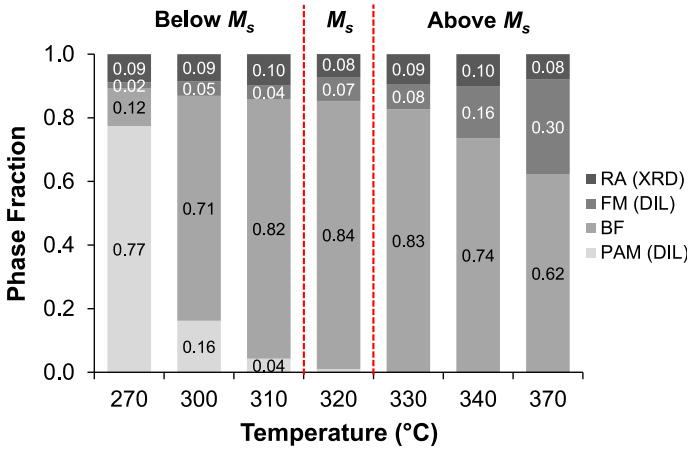

Figure 2.9. Phase fractions obtained after the application of selected heat treatments including isothermal treatments at temperatures above, just, and below M_s. Prior athermal martensite is indicated by PAM, Bainitic ferrite by BF, fresh martensite by FM, and retained austenite by RA.

to a net dilatation of 0.84%. The fractions of fresh martensite and retained austenite determined for all specimens are given in Figure 2.9. Bainitic ferrite volume fractions are calculated balancing the fractions of prior athermal martensite, retained austenite, and fresh martensite formed in the final cooling to room temperature.

Before analysing the experimental kinetic curves of the isothermal formation of bainitic ferrite, a "zero" (start) time and change in length must be established. First, a cubic spline interpolation is applied to the length data measured by dilatometry in order to obtain a value for a fixed incremental time interval. After that, the resulting data is smoothed by moving average to decrease the scatter. Finally, above M_s, the start of the isothermal transformation is considered at the minimum change in length. Below M_s, the start of the isothermal transformation corresponds to the point of minimum temperature reached during cooling when athermal martensite stops forming.

Figure 2.10 shows the bainite fraction obtained during the isothermal treatments at each temperature by means of dilatometry. The transformation kinetics above M_s increases as the temperature decreases and approaches M_s (320 ± 5°C). Above and just at M_s (Figure 2.10.a), bainitic transformation kinetics follows an S-shape curve which is shifted to shorter times as the temperature of the treatment decreases. The maximum fraction of bainitic ferrite increases with the decrease of the holding temperature. Below M_s (Figure 2.10.b), the shape of the curves changes and the isothermal transformation instantaneously reaches the maximum transformation rate. The highest bainitic ferrite fractions are reached in a range of ±20°C around M_s. The temperature dependence of the maximum fractions of bainitic ferrite can be observed in Figure 2.9.

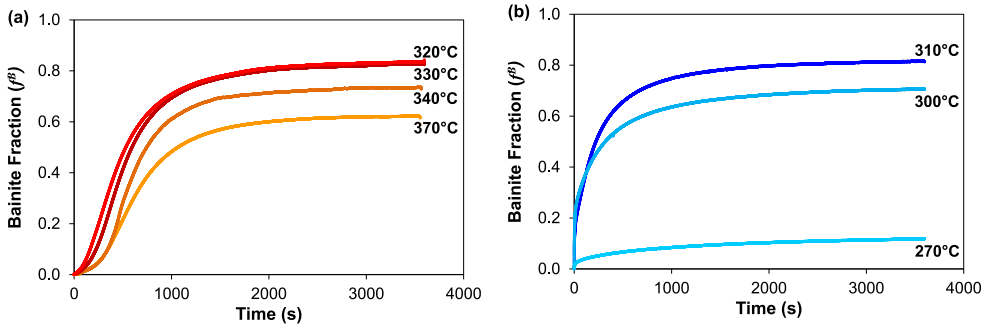

Figure 2.10. Volume fractions of bainitic ferrite as a function of isothermal holding time at different temperatures above and just at M_s (a) and below M_s (b).

The change in the kinetics of the bainitic ferrite formation above and below M_s is highlighted in Figure 2.11. This figure shows the bainitic ferrite formation as a function of time during two isothermal holdings at 330°C and 310°C, above and below M_s,

respectively. In these treatments, the fraction of bainitic ferrite formed is very similar, around 0.82 (see Figure 2.9). However, the shape of the curves is different, changing from an "S" curve at 330°C without any athermal martensite formation, to an initially rapidly ascending curve at 310°C, when there is a small fraction of prior athermal martensite formed (approximately 0.04). This confirms that at an early stage, the transformation at 310°C (below M_s) is much faster than that at 330°C (above M_s) and that the presence of martensite strongly accelerates the subsequent isothermal transformation kinetics.

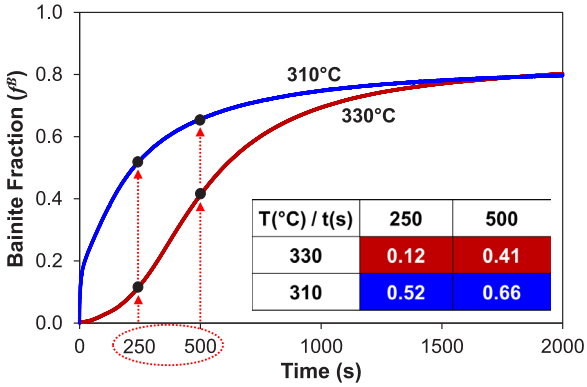

Figure 2.11. Evolution of bainite fraction as a function of time at 330°C and 310°C, above and below M_s, respectively.

The effect of prior athermal martensite on the bainitic ferrite formation is studied in terms of nucleation rate and density of potential nucleation sites, assuming that the bainitic ferrite growth mechanism is governed by nucleation without diffusion of carbon. The variation of bainitic ferrite fraction (f^B) with time (t) can be described by [6]:

$$\frac{\mathrm{d}f^B}{\mathrm{d}t} = \frac{\mathrm{d}N}{\mathrm{d}t} \cdot V_u \tag{2.2}$$

where $\mathrm{d}N/\mathrm{d}t$ is the nucleation rate per unit of volume and V_u is the average volume of a bainitic subunit. This volume is sometimes assumed constant with temperature in the literature, with dimensions of 0.2 x 10 x 10 μm^3 [26], but investigations have shown that the average volume of a bainitic subunit actually depends on different factors, such as temperature, austenite strength and driving force, as described by Singh and Bhadeshia [27]. Parker [28] empirically modelled the bainitic subunit thickness as a temperature-dependent parameter, based on previous experimental work of Chang and Bhadeshia [29] on silicon-rich steels with carbon contents between 0.095 and 0.5 wt. %, isothermally treated between 250 and 500°C. The thickness of bainitic subunits, z', was then modelled as:

$$z' = z_0 \cdot \frac{(T - 528\,\mathrm{K})}{150\,\mathrm{K}} \tag{2.3}$$

where T is the isothermal holding temperature in Kelvin and z_0 is a reference thickness. Assuming that bainitic ferrite has a plate shape and all the plate dimensions vary with temperature as described in Equation (2.3), the volume of bainitic subunits can be described as [26]:

$$V_u = V_0 \cdot \left(\frac{T - 528\,\mathrm{K}}{150\,\mathrm{K}} \right)^3 \tag{2.4}$$

where V_0 is the previously mentioned volume of 0.2 x 10 x 10 μm^3. In this study, the nucleation rate ($\mathrm{d}N/\mathrm{d}t$) is calculated from Equation (2.2) for all isothermal treatments using the experimental data for $\mathrm{d}f^{\beta}/\mathrm{d}t$ and considering that the volume of the bainitic subunits changes with the applied temperature as described in Equation (2.4). This latter equation can be used for the steel studied and the isothermal treatments performed since the composition is within the above-mentioned ranges and temperatures are higher than 255°C.

The evolution of the nucleation rate in different treatments above and below M_s, obtained from the fraction curves of Figure 2.10 and Equations (2.2) and (2.4), can be observed in Figure 2.12. In treatments above and just at M_s, for instance at 330 and 320°C (Figure 2.12.a), the nucleation rate increases rapidly until reaching a maximum at bainitic ferrite fractions between 0.2 and 0.3. This maximum coincides with the inflection point of the experimental S-shaped kinetic curve of the bainitic ferrite formation (see Figure 2.11). Then, the decrease of nucleation rate is gradual until the formation of the maximum bainitic ferrite fraction is completed. In treatments below M_s, at 310 and 300°C (Figure 2.12.b), the maximum nucleation rate is obtained at the very beginning of the transformation and it is 2 to 3 orders of magnitude higher than that of treatments above M_s. The nucleation rate decreases rapidly until reaching similar values to those obtained in treatments above M_s.

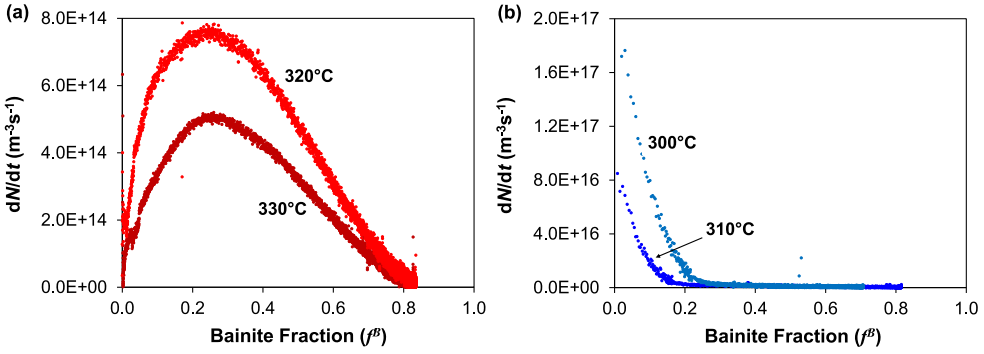

Figure 2.12. Evolution of nucleation rates during different isothermal holdings at temperatures (a) above M_s and (b) below M_s assuming a temperature-dependent volume of the bainitic subunits.

Figure 2.12.a also shows that the nucleation rate increases as the isothermal temperature decreases. This fact is in good agreement with the shift of bainite fraction curves to shorter times as shown in Figure 2.10.a. The lower the isothermal temperature, the higher the undercooling, so the driving force for nucleation will be higher, increasing the transformation kinetics. Consequently, a faster transformation implies a smaller size of the bainitic subunits, which is in accordance with Equation (2.4) used for the nucleation rate calculations. If this reflection is applied to the isothermal treatments below M_s, in conjunction with the increase of the density of potential nucleation sites introduced by the prior athermal martensite, the nucleation rate in those treatments will be much faster, as observed in Figure 2.12.b. The higher density of nucleation sites facilitates a faster isothermal bainite kinetics, even when the formed units are smaller.

Table 2.I shows the theoretical values of the volume of the bainitic subunits (V_u) as well as the experimental values of nucleation rate $(\mathrm{d}N/\mathrm{d}t)_{0.5}$, calculated by Equation (2.2), at 0.5 seconds after the start of the isothermal transformation for all heat treatments. The elapsed time selected has been 0.5 seconds in order to only study the effect of prior martensite on the nucleation rate, minimizing the autocatalytic nucleation effects. Autocatalytic nucleation is related to the induced formation of new nuclei due to the stresses and strains introduced after the formation of a phase product, in this case, prior athermal martensite.

Table 2.I. Calculated and experimental values of different parameters obtained for the isothermal treatments performed at temperatures above, just, and below M_s. V_u (volume of bainitic subunits), f^{PAM} (fraction of prior athermal martensite), t_i (elapsed time since the start of the isothermal transformation), $(\mathrm{d}N/\mathrm{d}t)_{0.5}$ (nucleation rate at t_i = 0.5 s), n_{sites} (number of nuclei forming per second and austenite grain at t_i), and f^{β} (experimental volume fraction of bainitic ferrite formed after t_i).

Temperature (°C)	V_u (m^3)	f^{PAM}	t_i (s)	$(\mathrm{d}N/\mathrm{d}t)_{0.5}$ ($m^{-3}s^{-1}$)	n_{sites} (s^{-1})	f^{β}
370	9.0×10^{-18}	0	0.5	1.9×10^{12}	1.0×10^{-3}	8.8×10^{-6}
340	3.7×10^{-18}	0	0.5	3.2×10^{12}	1.7×10^{-3}	5.9×10^{-6}
330	2.5×10^{-18}	0	0.5	2.5×10^{14}	1.3×10^{-1}	1.1×10^{-3}
320	1.6×10^{-18}	0	0.5	1.3×10^{14}	6.7×10^{-2}	1.3×10^{-4}
310	9.9×10^{-19}	0.04	0.5	6.2×10^{16}	32	3.6×10^{-2}
300	5.5×10^{-19}	0.16	0.5	1.4×10^{17}	74	4.6×10^{-2}
270	2.1×10^{-20}	0.77	0.5	4.9×10^{17}	255	6.8×10^{-3}

A logarithmic representation of the initial nucleation rates $(\mathrm{d}N/\mathrm{d}t)_{0.5}$ for all isothermal transformations is shown in Figure 2.13. The M_s temperature represents an inflection point in the initial nucleation rate since it changes sharply from temperatures above M_s to those just below M_s. The nucleation rates below M_s are on the order of 10^{16} $m^{-3}s^{-1}$ or higher. Above M_s, the nucleation rates are on the order of 10^{14} $m^{-3}s^{-1}$ or less. Therefore,

small fractions of athermal martensite prior to isothermal treatments below M_s increase the nucleation rate by at least two orders of magnitude at the start of the subsequent isothermal transformations, compared to those above M_s where prior martensite does not form. This confirms the differences described in the evolution of the bainitic ferrite formation and the nucleation rates above and below M_s, as shown in Figures 2.11 and 2.12, respectively.

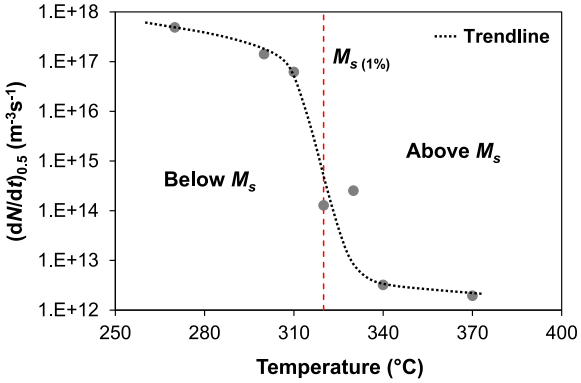

Figure 2.13. The initial nucleation rate as a function of the isothermal temperature at 0.5 seconds after the start of the isothermal transformations above, just, and below M_s.

As the prior athermal martensite volume fraction increases, the nucleation rate of bainitic ferrite at α'-γ interfaces at the start of the transformation also increases. This means that the volume fraction of bainitic ferrite formed after 0.5 s will be higher due to a faster transformation kinetics. However, to understand why the transformation kinetics increases, it is necessary to determine the relationship between the volume fraction of prior athermal martensite, the interfaces involved in the transformation, and the bainitic ferrite fraction formed. To tackle this problem, a new variable has been defined, which is called as n_{sites}. This variable represents the number of nucleation events per second and prior austenite grain. Experimental values of n_{sites} at t_i = 0.5 s since the start of the isothermal transformations are listed in Table 2.I. These values have been calculated by multiplying the nucleation rate (dN/dt) by the average volume of an austenite grain (V^{γ}_{grain}), as expressed by:

$$n_{sites}\left(t_i\right) = \left(\frac{\mathrm{d}N}{\mathrm{d}t}\right)_{t_i} \cdot V^{\gamma}_{grain} \tag{2.5}$$

The austenite grain diameter has been determined by SEM, obtaining an average value of 10 μm. Above M_s, γ-γ interfaces are the only potential nucleation sites at the start of the isothermal transformations. Below M_s, γ-γ interfaces and also α'-γ interfaces will provide potential nucleation sites for the bainitic ferrite formation. Assuming that there is no contribution of nucleation sites from bainite-austenite (α^b-γ) interfaces at the very

beginning of isothermal transformations, the difference in the values of n_{sites} between treatments above and below M_s can be attributed to α'-γ interfaces, due to the presence of prior athermal martensite, and to a temperature difference itself, from which the driving force will increase as temperature decreases. If comparing treatments above M_s with those below M_s, differences in n_{sites} are more than two orders of magnitude higher than those obtained comparing treatments only above or only below M_s. Although the temperature difference will contribute to the transformation kinetics, the increase of the density of nucleation sites has a stronger contribution to the nucleation rate at the beginning of the isothermal transformation below M_s.

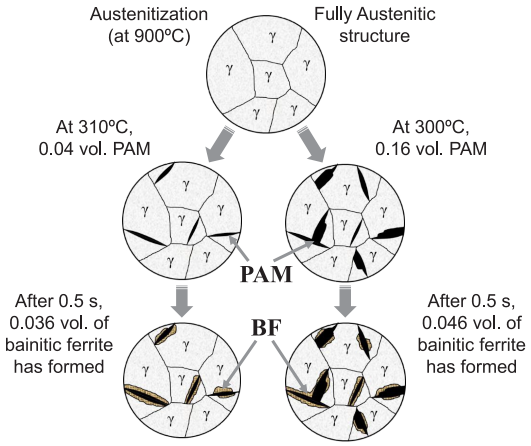

Figure 2.14. Schematic evolution of the initial microstructure at the very beginning of the isothermal holding at temperatures 310°C and 300°C, both below M_s.

Table 2.I shows that, in treatments below M_s, n_{sites} does not increase proportionally to the martensite volume fraction. To clarify the relationship between martensite fraction and nucleation behaviour, a diagram of the evolution of the initial microstructure from the austenitization until 0.5 s after the start of the isothermal transformation at 310°C and 300°C is shown in Figure 2.14. The values presented are extracted from Table 2.I. At 900°C, the microstructure is fully austenitic. In the subsequent cooling until temperatures below M_s, 310 and 300°C, small fractions of athermal martensite form depending on the quenching temperature. After 0.5 s, a small fraction of bainitic ferrite has formed, and that fraction is different depending on the prior athermal martensite fraction.

As observed in Table 2.I, the increase of the volume fraction of bainitic ferrite formed after 0.5 s at lower temperatures is not proportional to the volume of prior athermal martensite previously formed. The reason is that the subunits of bainitic ferrite nucleate at α'-γ interfaces, so the nucleation process will depend on the interfacial area, rather than

on the volume fraction of athermal martensite. Hence, the arrangement of martensite units within the austenite grain should be considered. Martensite generally forms in clusters or blocks, and not in the form of individual units homogeneously distributed in the material (see Figures 2.7.b and 2.7.d). For this reason, n_{sites} does not increase in the same proportion as the volume fraction of prior athermal martensite. Nevertheless, experimental results (Table 2.I) suggest a relationship between n_{sites} and $(f^{PAM})^{2/3}$ at the very beginning of the isothermal transformations below M_s. This indicates that the α'-γ interfacial area plays a dominant role in the transformation kinetics in treatments below M_s. Further investigations are required for a better understanding of the mentioned relationship.

The acceleration effect of prior athermal martensite on the bainitic ferrite formation could lead to significant advantages in steel technology. Bainitic steels could be created through much faster processing routes; these steels can be manufactured with the same fractions of bainitic ferrite by heat treatments below M_s in less time than above M_s. The good combination of mechanical properties would be very similar to bainitic steels obtained above M_s; small fractions of prior athermal martensite can provoke a strong accelerating effect on the subsequent transformation, and prior martensite would be tempered without adding brittleness.

2.4. Conclusions

The effect of prior athermal martensite and its contribution to the subsequent transformation kinetics was qualitatively and quantitatively determined in isothermal treatments below M_s in a low-C high-Si steel. The main conclusions obtained are the following:

1. Bainitic ferrite was identified as the isothermal product formed in treatments below M_s, where prior athermal martensite had already formed. This bainitic ferrite appears in the form of acicular units with interlath retained austenite, similar morphological characteristics to that obtained in treatments above and just at M_s.

2. A phase product with morphological similarities to lower bainite and/or tempered martensite was identified in treatments below and just at M_s. This product appears in the form of laths containing carbides aligned in the same direction.

3. Prior athermal martensite has a strong accelerating effect on the subsequent isothermal transformation kinetics due to the creation of a high number of nucleation sites in the form of martensite-austenite (α'-γ) interfaces.

4. Small fractions of prior athermal martensite cause an acceleration by at least two orders of magnitude of the nucleation rate at the start of the subsequent isothermal transformations below M_s, compared to those above M_s where prior martensite does not form.

5. There appears to be a relationship between the initial nucleation rate at each temperature and the martensite-austenite interfacial area, confirming the important role of martensite-austenite interfaces on the subsequent isothermal transformation kinetics.

References

[1] R.T. Howard, M. Cohen. Austenite transformation above and within the martensite range. Trans. AIME, 1948, vol. 176, pp. 384-397.

[2] S.V. Radcliffe, E.C. Rollason. J. Iron Steel Inst., 1959, vol. 191, pp 56-65.

[3] M. Oka, H. Okamoto. Swing back in kinetics near M_s in hypereutectoid steels. Metall. Trans. A, 1988, vol. 19A, pp. 447-452.

[4] D.H. Kim, J.G. Speer, H.S. Kim, B.C. De Cooman. Observation of an isothermal transformation during quenching and partitioning processing. Metall. Mater. Trans. A, 2009, vol. 40, pp. 2048-2060.

[5] H. Kawata, K. Hayashi, N. Sugiura, N. Yoshinaga, M. Takahashi. Effect of martensite in initial structure on bainite transformation. Mater. Sci. Forum, 2010, vols. 638-642, pp. 3307-3312.

[6] M.J. Santofimia, S.M.C. van Bohemen, D.N. Hanlon, L. Zhao, J. Sietsma. Perspectives in high-strength steels: Interactions between non-equilibrium phases. Inter. Symp. on AHSS, 2013, AIST, pp. 331-339.

[7] K. Sugimoto, T. Ilda, J. Sakaguchi, T. Kashima. Retained austenite characteristics and tensile properties in a TRIP type bainitic sheet steel. ISIJ Inter., 2000, vol. 40, pp. 902-908.

[8] K. Sugimoto, M. Murata, S.M. Song. Formability of Al-Nb bearing ultra-high strength TRIP-aided sheet steels with bainitic ferrite and/or martensite matrix. ISIJ Inter., 2010, vol. 50, pp. 162-168.

[9] Y. Jiang, R. Zhou, R. Zhou, D. Lu, Z. Li. Microstructures and properties of a bainite and martensite dual-phase cast steel fabricated by combination of alloying and controlled cooling heat treatment. Trans. Tech. Publications, 2005, Mater. Sci. Forum, vol. 475-479, pp. 93-96.

[10] S.M.C. van Bohemen, M.J. Santofimia, J. Sietsma. Experimental evidence for bainite formation below M_s in Fe-0.66C. Scripta Mater., 2008, vol. 58, pp. 488-491.

[11] J.C. Hell, M. Dehmas, S. Allain, J.M. Prado, A. Hazotte, J.P. Chateau. Microstructure-properties relationships in carbide-free bainitic steels. ISIJ Inter., 2011, vol. 51, pp. 1724-1732.

[12] I.A. Yakubtsov, G.R. Purdy. Analyses of transformation kinetics of carbide-free bainite above and below the athermal martensite start temperature. Metall. Mater. Trans. A, 2012, vol. 43A, pp. 437-446.

[13] D. Kim, J.G. Speer, B.C. De Cooman. The isothermal transformation of low-alloy low-carbon CMnSi steels below M_s. Trans. Tech. Publications, 2010, Mater. Sci. Forum, vol. 654-656, pp. 98-101.

[14] M. Takahashi, H.K.D.H. Bhadeshia. Model for transition from upper to lower bainite. Mater. Sci. Technol., 1990, vol. 6, pp. 592-603.

[15] D. Kim, J.G. Speer, B.C. De Cooman. Isothermal transformation of a CMnSi steel below the M_s temperature. Metall. Mater. Trans. A, 2011, vol. 42A, pp. 1575-1585.

[16] D. Kim, S.J. Lee, B.C. De Cooman. Microstructure of low carbon steel isothermally transformed in the M_s to M_f temperature range. Metall. Mater. Trans. A, 2012, vol. 43A, pp. 4967-4983.

[17] P. Kolmskog, A. Borgenstam, M. Hillert, P. Hedstrom, S.S. Babu, H. Terasaki, Y.I. Komizo. Direct observation that bainite can grow below M_s. Metall. Mater. Trans. A, 2012, vol. 43A, pp. 4984-4988.

[18] S.R. Pati, M. Cohen. Nucleation of the isothermal martensitic transformation. Acta Metall., 1969, vol. 17, pp. 189-199.

[19] A. Borgenstam, M. Hillert, J. Ågren. Critical temperature for growth of martensite. Acta Metall. Mater., 1995, vol. 43, pp. 945-954.

[20] A. Borgenstam, M. Hillert, Activation energy for isothermal martensite in ferrous alloys. Acta Mater., 1997, vol. 45, pp. 651-662.

[21] C.F. Jatczak, J.A. Larson, S.W. Shin. Retained austenite and its measurements by X-ray diffraction. Soc. Autom. Eng. Special Publication 453, 1980.

[22] D.P. Koistinen, R.E. Marburger. A general equation prescribing the extend of the austenite-martensite transformation in pure iron-carbon alloys and plain carbon steels. Acta Metall., 1959, vol. 7, pp. 59-60.

[23] S.M.C. van Bohemen, J. Sietsma. Effect of composition on kinetics of athermal martensite formation in plain carbon steels. Mater. Sci. Technol., 2009, vol. 25, pp. 1009-1012.

[24] S.M.C. van Bohemen, D.N. Hanlon. A physically based approach to model the incomplete bainitic transformation in high-Si steels. Int. J. Mat. Res., 2012, 103-8, pp. 987-991.

[25] S.M.C. van Bohemen. Austenite in multiphase structures quantified by analysis of thermal expansion. Scripta Mater., 2014, vol. 75, pp. 22-25.

[26] H. Matsuda, H.K.D.H. Bhadeshia. Kinetics of the bainite transformation. Proc. R. Soc. Lond. A, 2004, 460, pp. 1707-1722.

[27] S.B. Singh, H.K.D.H. Bhadeshia. Estimation of bainite plate-thickness in low-alloy steels. Mater. Sci. Eng. A, 1998, 245, pp. 72-79.

[28] S.V. Parker. Modelling of phase transformations in hot-rolled steels. PhD Thesis, 1997, University of Cambridge, UK.

[29] L.C. Chang and H.K.D.H. Bhadeshia. Austenite films in bainitic microstructures. Mater. Sci. Technol., 1995, vol. 11, pp. 874-881.

3

CHAPTER 3

Characterization of Bainitic/Martensitic Structures formed in Isothermal Treatments Below M_s

**This chapter corresponds to the article "Characterization of bainitic/martensitic structures formed in isothermal treatments below the M_s temperature" by A. Navarro-López, J. Hidalgo, J. Sietsma, and M.J. Santofimia, Mater. Charact. (2017), vol. 128, 248-256.*

Abstract

Previous investigations have shown that bainitic ferrite can form from austenite in isothermal treatments below M_s, where its formation kinetics is accelerated by the presence of the athermal martensite. That athermal martensite is tempered during the isothermal treatment, and fresh martensite may form during the final cooling to room temperature. The distinction between product phases present after the application of this type of heat treatments is difficult due to morphological similarities between these transformation products. The aim of this study is to characterize the structural and morphological features of the product phases obtained in isothermal treatments below the M_s temperature in a low-carbon high-silicon steel. Multiphase microstructures, having controlled fractions of product phases, were developed by applying isothermal treatments above and below M_s, and were further studied by electron back scatter diffraction (EBSD) and scanning electron microscopy (SEM). The bainitic or martensitic nature of these product phases is discussed based on this characterization. Results showed that bainitic ferrite appears in the form of acicular units and irregularly shaped laths. Tempered martensite appears as laths with a sharp tip and as relatively large elongated laths with wavy boundaries containing protrusions.

3.1. Introduction

Based on the microstructural characterization presented in the previous chapter, the bainitic or martensitic nature of the distinct microstructural features formed in isothermal treatments below the martensite start temperature (M_s) results challenging to determine by usual microscopy techniques. This difficulty comes from the formation of bcc-phases such as tempered martensite and bainitic ferrite with morphological similarities. The use of advanced microscopy techniques for a detailed comparison of microstructural features observed in multiphase microstructures obtained from isothermal treatments above and below M_s is thus needed to elucidate the nature of those bcc-phases. Researchers agree that, in hypoeutectoid steels, the multiphase microstructure obtained from isothermal treatments above M_s is mainly formed by bainitic structures with retained austenite in the form of thin films and/or martensite-austenite (MA) islands [1-7]. Bainite is thus the isothermal product phase obtained from the decomposition of austenite. Carbides can also be present in bainite, depending on the composition of the steel and the isothermal holding temperature and time.

On the other hand, cooling from austenitization to a temperature below M_s leads to the formation of a certain volume fraction of prior athermal martensite. This martensite has a strong accelerating effect on the subsequent transformation kinetics, mainly due to a higher density of potential nucleation sites [8-11]. Although bainite has been reported in hypoeutectoid steels as an isothermal decomposition product from austenite in isothermal treatments below M_s [4,10-14], there is experimental evidence showing the formation of other types of product phases in similar heat treatments. For example, several authors observed an isothermal product characterized by wide laths with characteristic wavy boundaries with ledges [16,17]. Kim et al. [7,15,16] stated that this isothermal product is neither purely martensitic nor purely bainitic, since it shows similarities with both types of product phases. Somani et al. [17] identified this product as isothermal martensite since it presents clear similarities to athermal martensite. According to the literature, isothermal martensite has mainly been reported in high-carbon steels and high-nickel alloys [18-20], but not in hypoeutectoid steels. Independently of the growth mechanism of these product phases, the dilemma is which microstructural features observed in isothermal treatments below M_s correspond to each phase formed in those treatments, such as bainitic ferrite, tempered martensite or fresh martensite.

The goals of this study are: to characterize the microstructural features obtained in isothermal treatments performed at temperatures above and below M_s; relate those features to the product phases formed at each isothermal temperature; and determine, based on that characterization, the martensitic or bainitic nature of those product phases. For this purpose, isothermal heat treatments were applied at different temperatures above and below M_s based on the microstructural analysis of Chapter 2. Various

microstructures formed by combinations of different volume fractions of bainitic ferrite, tempered martensite, and fresh martensite were created. Volume fractions of those product phases were extracted from the dilatometry results presented in Chapter 2. The identification of phases by dilatometry in combination with the characterization of microstructures formed at different temperatures by electron backscatter diffraction (EBSD) and scanning electron microscopy (SEM) provided a straight and systematic way of phase analysis.

3.2. Experimental Procedure

The experimental procedure regarding the application of heat treatments in steel specimens is the same as that described in Chapter 2. The chemical composition of the investigated steel is 0.2C-3.51Mn-1.52Si-0.25Mo-0.04Al (wt. pct). Cylindrical dilatometry specimens were extracted from a 4 mm-thick hot rolled slab, parallel to the rolling direction, with dimensions of 10 mm in length and 3.5 mm in diameter. Heat treatments were carried out in a Bähr 805A dilatometer. Specimens were placed between two quartz rods, heated by an induction coil, and cooled using nitrogen gas. A thermocouple was spot-welded in the middle of the specimens to control the temperature.

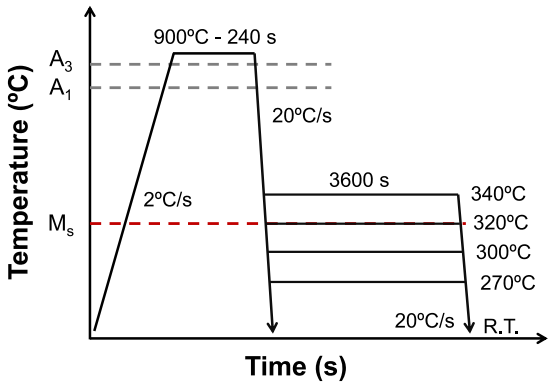

Figure 3.1. Schematic representation of the heat treatments applied by dilatometry to the selected steel.

Different heat treatments were applied above and below the M_s temperature, after a full austenitization at 900°C for 240 seconds. The applied heat treatments are described as follows (Figure 3.1):

(i) A direct-quench treatment was performed to determine the experimental M_s temperature and the kinetics of the martensite formation. The analysis of the dilatometric curve, presented elsewhere [11], determined an experimental $M_{s\ (1\%)}$ = 320°C ± 5°C, at which temperature the volume fraction of martensite formed is 0.01.

(ii) An isothermal treatment above the M_s temperature was carried out at 340°C to obtain a microstructure formed by a mixture of bainite, retained austenite and fresh martensite.

(iii) Three isothermal treatments between M_s and room temperature (RT) were performed at 320°C, 300°C and 270°C to obtain a multiphase microstructure formed by martensite obtained during cooling from austenitization to the isothermal temperature, bainitic ferrite, retained austenite, and fresh martensite obtained in the final cooling to room temperature.

The volume fractions of retained austenite at room temperature were determined by X-ray diffraction (XRD) experiments using a Bruker D8-Advance diffractometer equipped with a Bruker Vantec Position Sensitive Detector. CoKα radiation was used in the 2θ scan from 40° to 130° with a step size of 0.035°. The fractions of austenite and ferrite were calculated by the integrated area method using the (111), (200), (220), and (311) austenite peaks, and the (110), (200), (211), and (220) ferrite peaks [21]. The heat-treated specimens were metallographically prepared by grinding and polishing. 2% Nital etching was applied to the specimens to reveal the microstructure. A pre-analysis of microstructures by Light Optical Microscopy (LOM) and Scanning Electron Microscopy (SEM) was presented in Chapter 2.

Electron Back Scatter Diffraction (EBSD) in combination with SEM was used to perform a detailed characterization of the transformation products obtained in the heat treatments previously described. In order to analyse the same area by EBSD and SEM, various micro-indentations (HV1) were made in the specimens to select representative areas. As a final preparation step, the specimens were mechanically polished with a colloidal silica solution in order to exhaustively clean the specimens and remove surface deformation. Areas selected in the specimens were first analysed by EBSD.

The EBSD patterns were acquired on a FEI Quanta 450 scanning electron microscope equipped with a Field Emission Gun (FEG-SEM) by means of the OIM Data Collection software. The analysis was performed under the following conditions: acceleration voltage of 20 kV, spot size 5, working distance of 16 mm, tilt angle of 70°, and step size of 50 nm in a hexagonal scan grid. The orientation data were post-processed with TSL OIM® Analyses 6.0 software. First, a grain confidence index (CI) standarization was applied to the raw data, selecting a tolerance angle of 5° and a minimum grain size of 6 pixels, and considering that grains are formed by multiple pixel rows. The second step of the post-processing procedure included neighbour-orientation correlation with a tolerance angle of 5° and a minimum confidence index of 0.1. Finally, a down-filtering

criterion of confidence index higher than 0.1 was applied to reduce the number of pixels poorly indexed, i.e., not attributed to either fcc or bcc phases.

After a comprehensive EBSD analysis, specimens were carefully polished with a colloidal silica solution for 5 to 10 minutes in order to remove the carbon deposition layer of the specimen surface. Afterwards, 2% Nital etching was applied to the specimens to reveal the different phases formed during the heat treatments. The EBSD-analysed areas were then studied with a JEOL JSM-6500F Scanning Electron Microscope (SEM) using a 15 kV electron beam and the Secondary Electron Imaging (SEI) detection mode.

3.3. Results and Discussion

3.3.1. Volume Fraction of Phases

Dilatometry results analysed in Chapter 2 showed no evidence of the formation of ferrite, pearlite, or bainite during the initial cooling to the isothermal temperatures above and below M_s. Only when the temperature decreased below the M_s temperature, a dilatation was observed due to the formation of a certain fraction of athermal martensite prior to the isothermal holding. Dilatometric curves showed a significant dilatation during the isothermal holding, which implies the formation of an isothermal product phase identified as bainitic ferrite (see Chapter 2). There was also a small deviation from linearity of the dilatometric curves during the final cooling to room temperature, showing the formation of fresh martensite during that cooling. The determination of the volume fractions of product phases obtained in the applied heat treatments is explained in detailed in Chapter 2 and shown in Table 3.I.

Table 3.I. Phase fractions obtained after the application of the selected heat treatments. f^{PAM}, f^{BF}, f^{FM}, and f^{RA} are the experimental fractions of prior athermal martensite, bainitic ferrite, fresh martensite, and retained austenite, respectively, extracted from Chapter 2.

Temperature (°C)	f^{PAM}	f^{BF}	f^{FM}	f^{RA}
340	—	0.74	0.16	0.10
320	< 0.02	0.84	0.07	0.08
300	0.16	0.71	0.05	0.09
270	0.77	0.12	0.02	0.09

3.3.2. Microstructural Features

Microstructures were characterized by a combined analysis of SEM and EBSD images in order to find patterns regarding the structure and morphology of the different product phases. Distinct microstructural features with specific characteristics were observed and described in detail below. The descriptions will allow a better characterization

and understanding of the nature of the product phases obtained in each isothermal treatment. A schematic representation of these features is shown in Figure 3.2. Examples of these microstructural features will be shown in further sections.

- ***Thin features (S_T)***

This microstructural feature, defined as *'S_{Thin}'* (S_T), appears in the form of a thin unit with acicular shape. S_T units are aligned parallel with each other and appear as low-relief microstructures after etching. Their aspect ratio (*a/c*), where *'a'* and *'c'* are the length and width, respectively, can vary in a wide range between 5 and 15. The width of S_T units is generally less than 1 μm, and the length varies from 3.5 μm to 15 μm. Most of them have a mean length between 5 and 8 μm and a mean width between 0.6 and 0.8 μm. Carbides are not observed within this type of microstructural feature.

- ***Irregular features (S_I)***

This second microstructural feature has an irregular lath-shaped morphology without carbides and is defined as *'$S_{Irregular}$'* (S_I). These lath-shaped features also appear as low-relief microstructures after etching. The length of the S_I features varies between 4 and 7 μm and the width between 1 and 3 μm, so S_I features are wider than S_T, with a lower aspect ratio.

- ***Thick features (S_{TK})***

The third type of microstructural feature appears in the form of laths with a sharp tip at one of its edges. These lath-shaped features are defined as *'S_{Thick}'* (S_{TK}). They are aligned parallel and appear as low-relief microstructures after etching. Carbides are generally visible within these features. The aspect ratio of S_{TK} varies in the range of 2.5 to 6. These lath-shaped structures have a mean length and width of 5 μm and 1.1 μm, respectively. S_{TK} features seem to grow from the prior austenite grain boundaries, and are surrounded by S_T units.

- ***Elongated features (S_E)***

This fourth microstructural feature presents a big elongated, lath-shaped morphology, so it is defined as *'$S_{Elongated}$'* (S_E). This type of lath-shaped features are aligned parallel to adjacent constituent units and appear as low-relief microstructures. Their size is larger than that of the previous microstructural features described. S_E features have a mean length and width of 12 μm and 2 μm, respectively. In general, S_E features are longer and wider than S_T. There is an abundant presence of carbides within most of S_E features.

The most relevant characteristic of S_E is the presence of wavy boundaries. These wavy boundaries were first reported by Kim et al. [16], who concluded that the nature of these isothermal products formed below M_s was neither purely martensitic nor purely

bainitic. More recently, Somani et al. [17] identified an isothermal product in the form of laths with wavy boundaries, formed during isothermal treatments below M_s. Ledge-like protrusions are also observed in these laths. Somani et al. identified this product phase as isothermal martensite.

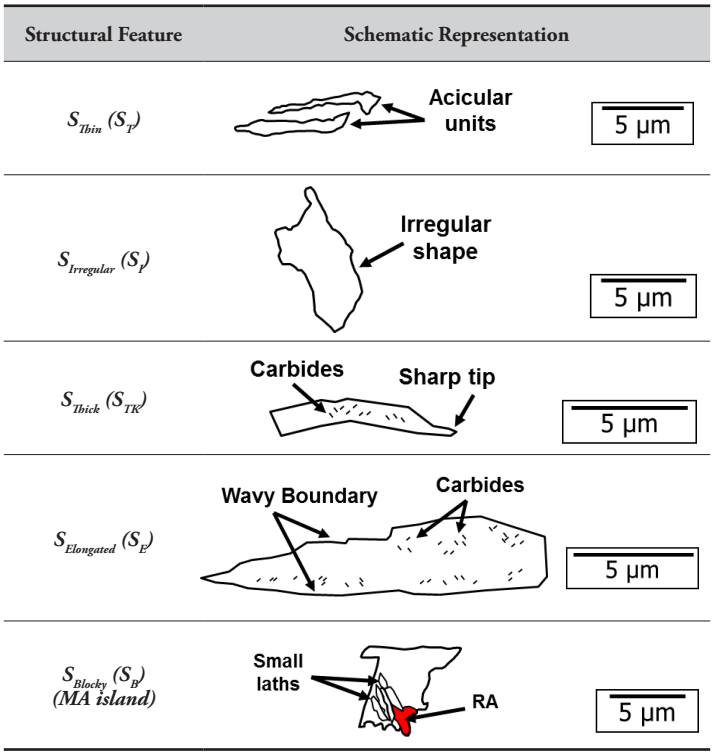

Figure 3.2. Schematic representations of the different features described, directly derived from actual micrographs.

➢ ***Blocky features (S_B) (also known as MA islands)***

This microstructural feature is characterized by a blocky structure which combines small parallel aligned laths within the structure with irregular blocks at its boundaries. This feature, defined as 'S_{Blocky}' (S_B), is generally known as martensite-austenite island (MA), which is formed from partly untransformed austenite in the final cooling to room temperature. SEM shows the MA island as a non-etched structure with a smooth surface. However, EBSD analysis displays that the MA island is formed by an internal structure of very small martensite laths surrounded by small blocks of retained austenite (RA) at the boundaries. These small laths appear aligned parallel within the island. The length of the laths is less than 2 μm.

3.3.3. Microstructures obtained from Heat Treatments

➢ ***At 340°C (above M_s)***

According to dilatometry results, bainitic ferrite and fresh martensite coexist in this microstructure in volume fractions of 0.74 and 0.16, respectively (see Table 3.I), completed by 0.10 of retained austenite. In this case, there is no formation of athermal martensite prior to the isothermal treatment. The microstructure is thus a mixture of bainitic ferrite, retained austenite and MA islands. Figure 3.3 shows the SEM micrograph, the Image Quality (IQ) map, and the Phase Distribution (PD) map of the same area of the specimen. The combined analysis of images allows to distinguish two different sub-areas: Region A, in which different features of fresh martensite appear in combination with small bainitic ones, and Region B, in which bainitic ferrite is the dominant product phase. Bainitic ferrite mainly appears as S_T features with retained austenite (RA) between them. These bainitic areas are generally better indexed in EBSD than the martensitic ones, so they appear as bright areas in the IQ map due to a higher

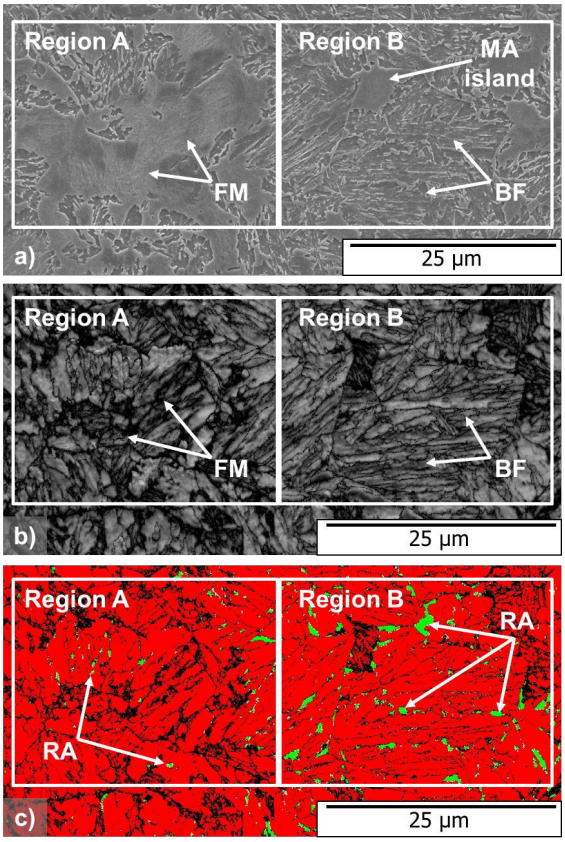

Figure 3.3. a) SEM micrograph, b) Image Quality (IQ) map, and c) Phase Distribution (PD) map of a determined area of the specimen isothermally treated at 340°C (above M_s).

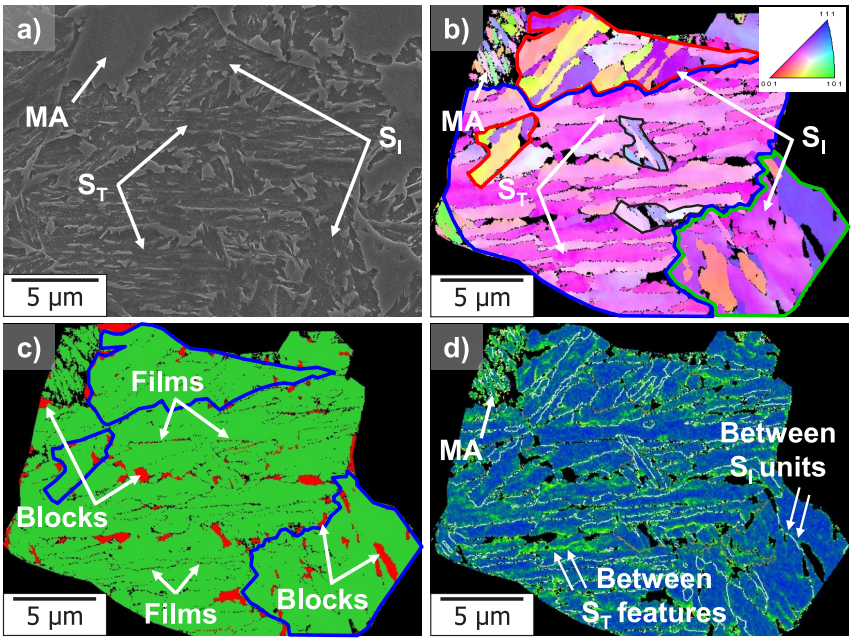

Figure 3.4. a) SEM micrograph, b) IPF map, c) PD map, and d) KAM map of a selected prior austenite grain of the specimen isothermally treated at 340°C. Regions are marked on the IPF map by different colours.

confidence index (see Figure 3.3.b). Conversely, fresh martensite areas have a poorer indexing than the bainitic ones due to internal strains and dislocations. This means that the confidence index will be lower in those areas, and darker regions will appear in the IQ map, as shown in Figure 3.3.b.

The distribution and morphology of the retained austenite is also an important factor to distinguish between different product phases. Figure 3.3.c shows the Phase Distribution (PD) map of the above-mentioned specimen. As observed, retained austenite (in green) mainly appears within the bainitic ferrite areas (Region B) in the form of small blocks or thin films between bainitic ferrite units. This means that, after the incomplete isothermal transformation (approx. 0.74 of bainitic ferrite), the remaining austenite in the bainitic areas is more stable than in the areas that become martensitic due to a higher carbon enrichment during the isothermal holding. In the final cooling, while the remaining austenite in bainitic areas will be retained, most of the remaining austenite present in martensitic areas will transform into fresh martensite due to its lower stability. This explains the lower fraction of retained austenite obtained in martensitic areas.

For a detailed description of the different product phases, a prior austenite grain was selected and analysed by a combined study of SEM and three different EBSD maps,

as shown in Figure 3.4. Inverse Pole Figures (IPF) and Kernel Average Misorientation (KAM) maps were used to determine the morphology (size and shape) of the different product phases and the distribution of local grain misorientations, respectively. KAM maps were calculated by considering the 1st neighbours as the nearest neighbour points of the kernel in order to include information about the surroundings of the measured point.

The selected grain is mainly formed by four regions with different orientation relationships (ORs) (see Figure 3.4.b). Analysing the central region of the austenite grain (marked by a blue contour), a typical bainitic structure can be distinguished, which is mainly formed by S_T features. Retained austenite appears in the form of very thin films between the units (see Figure 3.4.c). Elongated blocky structures of retained austenite are also distinguished close to region boundaries and at the boundaries of the MA island, as shown in Figure 3.4.c.

S_I features can be observed in the microstructure (see Figures 3.4.a and 3.4.b). Although the morphology of these laths is not acicular, their nature may be bainitic. The reason for this proposition is that there is no dilatometric evidence of the formation of prior athermal martensite, so bainitic ferrite cannot be confused with tempered martensitic structures in this microstructure. Figure 3.4 also shows a martensite-austenite (MA) island in which its internal structure of small martensite laths can be observed (Figure 3.4.b). The KAM map (Figure 3.4.d) shows that these martensitic structures present higher concentrations of local misorientation than the bainitic ones, so the internal structure is more distorted. The KAM map also shows that higher local misorientations are concentrated at the boundaries between S_T features, and/or between S_I units, as shown in Figure 3.4.d (white arrows).

- ***At 320°C (at M_s)***

This isothermal temperature corresponds to the experimental M_s temperature when the volume fraction of martensite formed is approximately 0.01. This prior athermal martensite formed during cooling from austenitization to the isothermal temperature will be tempered during the isothermal holding, so its appearance will be different from that of the fresh martensite obtained in the final cooling. A complex multiphase microstructure is thus obtained at this temperature (see Table 3.I), where bainitic ferrite represents more than 80% of the volume fraction.

S_T features containing films of retained austenite appear in the microstructure, as shown in Figures 3.5.a and 3.5.b. According to the previous characterization done above M_s, these features correspond to bainitic ferrite structures. MA islands can also be distinguished in the microstructure (see Figure 3.5.a). S_{TK} features are also present at this temperature

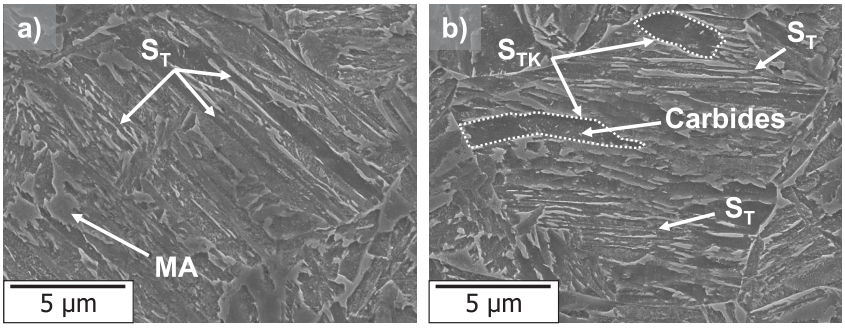

Figure 3.5. SEM micrographs of two distinct areas of the specimen isothermally treated at 320°C (at M_s), showing the presence of S_{Ithin} and S_{Ithick} features in a selected prior austenite grain.

with their characteristic sharp tip at one of the edges. These lath-shaped structures are different from the ones identified at 340°C, above M_s. Figure 3.6.a shows an S_E feature, i.e., a large elongated lath containing carbides. This S_E feature presents wavy boundaries, which can be observed in Figures 3.6.b (marked with white arrows) and 3.6.c (marked with blue dashed line). In addition to this specific characteristic, ledge-like protrusions can be observed in one of the boundaries of this S_E feature (see Figures 3.6.b and 3.6.c). Since these two types of features are not present in microstructures above M_s, they should correspond to martensitic structures, which are tempered during the isothermal holding of the heat treatment.

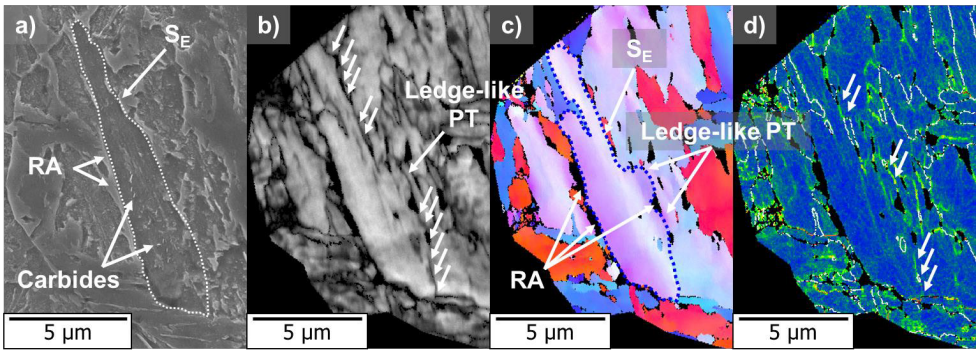

Figure 3.6. a) SEM micrograph, b) IQ map, c) IPF map, and d) KAM map of a region within a prior austenite grain of the specimen isothermally treated at 320°C.

Retained austenite is present in this microstructure in two different morphologies. Within S_T features, retained austenite generally appears as thin films. In S_E features, however, retained austenite appears in the form of elongated blocks along boundaries and/or as irregular blocks between ledge-like protrusions, as shown in Figure 3.6.c. The KAM map shows high local misorientations at the boundaries of the S_E feature, as shown

in Figure 3.6.d (white arrows). Lower local misorientations are also observed within the S_E feature, which can correspond to low-angle boundaries of its internal structure.

➢ ***At 300°C (below M_s)***

At this temperature, a volume fraction of approximately 0.16 of prior athermal martensite is formed during the cooling below M_s until reaching the isothermal temperature. This prior athermal martensite will be tempered during the isothermal holding. The microstructure is thus a mixture of bainitic ferrite, prior athermal martensite, and MA islands (see Table 3.I). S_T features, identified as bainitic ferrite in previously described microstructures, are shown in Figure 3.7. This indicates the formation of bainitic ferrite in isothermal treatments below M_s with similar morphological characteristics as the bainite formed in treatments above and at the M_s temperature.

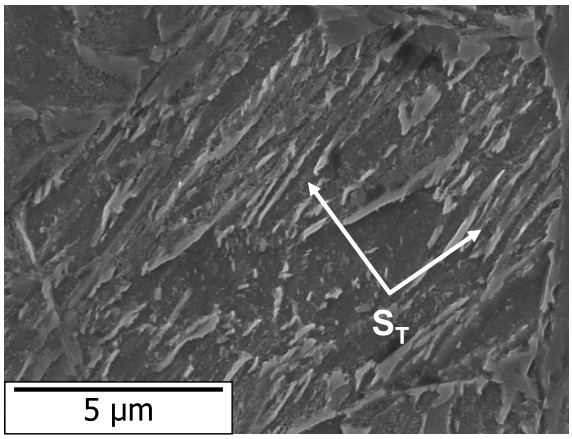

Figure 3.7. Presence of S_{Thin} microstructural features in the specimen isothermally treated at 300°C (below M_s).

Other types of product phases can be distinguished in this microstructure. Figure 3.8 shows the SEM micrograph, Inverse Pole Figure (IPF), Phase Distribution (PD), and Kernel Average Misorientation (KAM) maps of a specific prior austenite grain of the specimen treated at 300°C. An S_E feature with wavy boundaries can be observed at the top part of the grain (marked with a dashed blue line). This specific feature has also been observed in microstructures formed during isothermal treatments at 320°C (at M_s). As pointed out in the microstructural description of that heat treatment, S_E features should be characterized as martensite since this type of feature does not appear in treatments above M_s and its presence in the microstructures becomes more pronounced when the volume fraction of prior athermal martensite increases. Carbides are visible within these S_E features, and there seem to be multi-directional carbides. Bainitic structures are also characterized at this temperature in the form of S_T and S_I features (see Figure 3.8.a and 3.8.b).

Figure 3.8.a also shows an interesting feature in the surroundings of S_E. This feature corresponds to very small acicular units (S_T features), identified as bainitic ferrite, just next to the wavy boundary of the lath. These S_T features are indicated by a dashed white or red oval in the SEM figure and EBSD maps. As observed in Figure 3.8.a, the S_T features seem to grow from the S_E and appear aligned at both sides of the lath-shaped S_E. However, in the EBSD maps (Figures 3.8.b, 3.8.c, and 3.8.d), there is no clear indication of the existence of these features, apart from a small concentration of high local misorientations (see Figure 3.8.d). According to the analysis, bainitic ferrite (S_T) may be growing from the prior athermal martensite (S_E), maintaining a similar crystallographic orientation relationship. This fact could contribute to the formation of the ledge-like protrusions which can give rise to a wavy appearance of the boundaries of the lath-shaped S_E features.

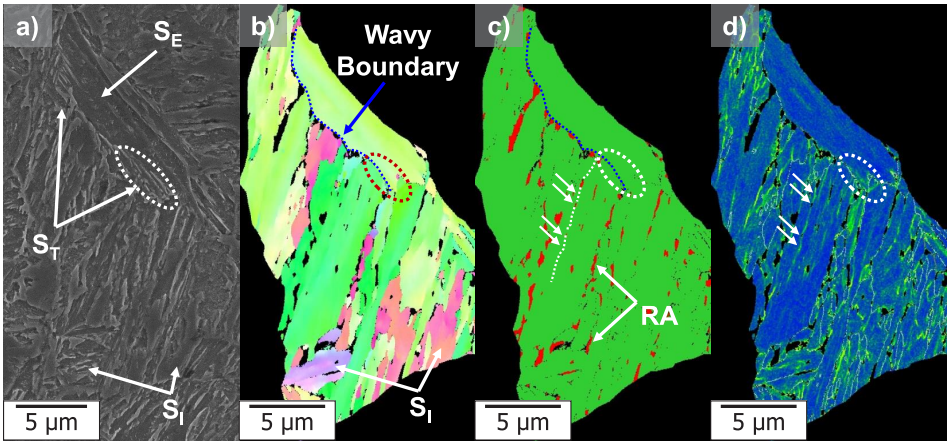

Figure 3.8. a) SEM micrograph, b) IPF map, c) PD map, and d) KAM map of a selected prior austenite grain of the specimen isothermally treated at 300°C.

Retained austenite mainly appears in the form of small elongated blocks, as shown in Figure 3.8.c. These blocks could form a continuous film at the boundaries between microstructural constituents, as marked by the dashed white line in Figure 3.8.c. A high density of low-angle boundaries with misorientations lower than 5-7° can be observed in Figure 3.8.d (marked with white arrows). These boundaries separate the different sub-units present within the same microstructural constituent. The described boundaries coincide with the discontinuous "films" of retained austenite.

➢ ***At 270°C (below M_s)***

At 270°C, 50°C below the experimental M_s temperature, almost 80% of the microstructure is formed by prior athermal martensite, which is tempered, with only 12% of bainitic ferrite formed during the isothermal holding (see Table 3.I) and 9%

of retained austenite. The microstructure is mainly formed by lath-shaped structures of different sizes and shapes, containing carbides inside (see Figure 3.9.a). In this case, no bainitic structures similar to the ones described to be formed above M_s are observed. Although the studied steel has a 1.5 wt. percent silicon, carbide precipitation is not completely supressed.

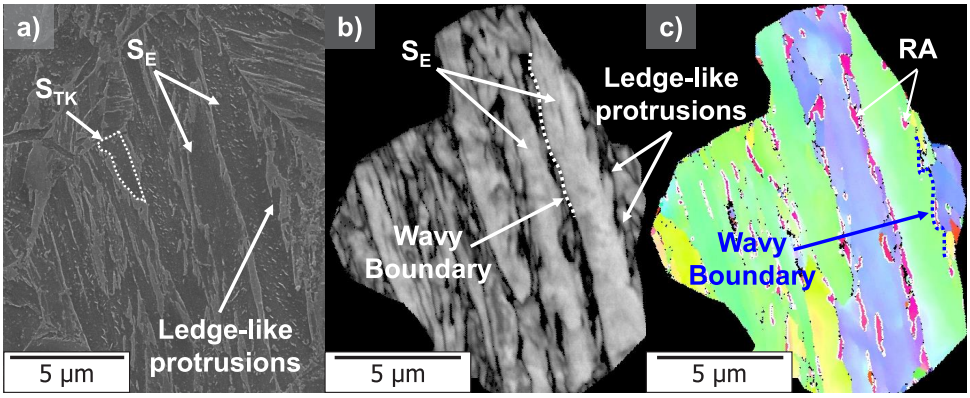

Figure 3.9. a) SEM micrograph, b) IQ map, and c) IPF map of a selected prior austenite grain of the specimen isothermally treated at 270°C. This specimen contains a volume fraction of prior athermal martensite of approximately 80%. This martensite is tempered during the isothermal holding.

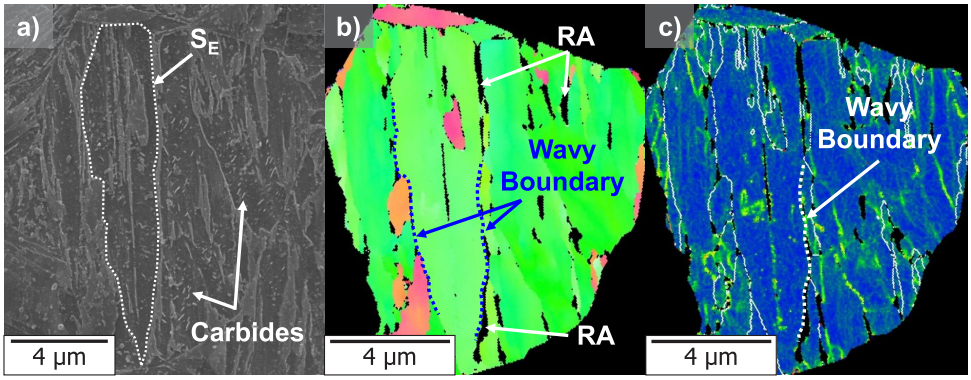

Figure 3.10. a) SEM micrograph, b) IPF map, and c) KAM map of a selected prior austenite grain of the specimen isothermally treated at 270°C.

Figure 3.9.a shows two types of microstructural features: S_{TK} and S_E. Wavy boundaries with ledge-like protrusions, a specific microstructural characteristic of S_E, can be observed in Figures 3.9.b and 3.9.c. Retained austenite is also present in this microstructure in the form of elongated blocks between S_E features (see Figure 3.9.c). Figure 3.10 shows another example of S_E features, which are characteristic for this microstructure. The S_E feature, indicated by a dashed white contour in Figure 3.10.a, is extended along the

grain from one boundary to the opposite one. This specific lath-shaped structure is characterized by wavy boundaries at its both sides, marked with dashed blue lines in Figure 3.10.b. The KAM map shows high local misorientations at the wavy boundaries of the S_E feature (see Figure 3.10.c).

According to volume fractions obtained and previous microstructural analysis at higher temperatures, both features S_{TK} and S_E are definitively characterized as prior athermal martensite, tempered during the isothermal holding. As described in the microstructural characterization at 300°C, the existence of ledge-like protrusions may produce the characteristic wavy boundaries observed in S_E. Although there are carbides along the entire S_E feature, these protrusions do not present any carbides inside, as shown in Figure 3.9.a. Based on the EBSD maps (Figures 3.9.b and 3.9.c), the protrusions exhibit a similar orientation as the rest of the S_E feature. As is pointed out for the microstructure formed at 300°C, these protrusions can correspond to bainitic ferrite structures growing from the prior athermal martensite.

3.3.4. Nature of Product Phases

Table 3.II shows a summary of the main characteristics of the five microstructural features observed in the analysis of the four isothermal treatments performed at 340°C (above M_s), and 320°C (at M_s), 300°C, and 270°C (below M_s), as well as at which temperature that specific feature was observed. The possible nature of the each microstructural feature is also specified.

Considering the thermal cycle followed in these heat treatments, the bainitic structures, S_T and S_I, were only formed during the isothermal holdings of one hour performed at temperatures of 300°C and higher. However, the martensitic structures, S_{TK} and S_E, were previously formed during the cooling from austenitization to the selected isothermal temperature. MA islands were finally formed in the cooling to room temperature from the remaining austenite, which was not fully transformed during the isothermal holding.

As shown in Table 3.II, S_T and S_I are considered bainitic structures since they are the main features observed in the isothermal treatment performed above M_s, where there is no formation of athermal martensite prior to the isothermal holding. Both types of features are also observed in isothermal treatments below M_s. Besides, S_{TK} and S_E are considered martensitic structures. The reason for this conclusion is the majority presence of these two microstructural features after applying the isothermal treatment at 270°C (below M_s), where almost 80% of the volume corresponds to the prior athermal martensite formed during cooling until reaching the isothermal temperature. Furthermore, as the isothermal temperature below M_s is increased and approaches M_s, the presence of these microstructural features in the microstructures is reduced. Martensite-austenite islands,

formed in the final cooling to room temperature, are present in the microstructures of all heat treatments.

The martensitic nature of S_E is partially in agreement with previous investigations done by Kim et al. [16] and Somani et al. [17]. Both authors characterized an isothermal product with wavy boundaries and ledge-like protrusions in isothermal treatments performed below M_s in low-carbon steels with similar compositions as the one investigated in the present work. In both studies, the authors conclude that the nature of these laths with wavy boundaries is not purely bainitic since they have a stronger similarity with athermal martensite. However, there are some descriptive details which differ between each characterization. These characterization details are presented as follows:

1. Kim et al. [16] compare by TEM observations the product phases obtained in an isothermal treatment above M_s, below M_s (with 10% of prior athermal martensite), and in a direct quench. The authors suggest that the presence of wavy boundaries containing ledges in the mentioned laths formed below M_s is the result of the thickening of those laths during the isothermal transformation. Additionally, multi-variant carbides were also distinguished within those isothermal laths and the athermal martensite, but not in lower bainite. Kim et al. thus state that although there was a stronger similarity with athermal martensite than with lower bainite, the nature of those isothermal laths is neither purely martensitic nor purely bainitic.

2. Somani et al. [17] also compared by TEM observations the nature of the different products phases obtained during two-step quenching and partitioning (Q&P) treatments. Such isothermal laths with wavy boundaries and ledge-like protrusions were also characterized. In this case, these laths are considered the result of the isothermal growth, through the migration of ledges, during the partitioning step of the prior athermal martensite laths already formed. These laths were thus identified as martensite.

Although both identifications are feasible, the thermal conditions of the heat treatments analysed in each investigation are different between them and with respect to the present work. In the investigation of Kim et al., there is no microstructural characterization of existing tempered martensite formed in the treatment below M_s (with 10% volume fraction), so those S_E features could also be considered as tempered martensite. In the investigation of Somani et al., the nature of S_E is certainly considered martensitic.

However, there is another possible explanation which has not been considered yet. The formation of bainitic ferrite below M_s could be the reason of the appearance of ledge-like protrusions in the S_E features, which lead to the formation of wavy boundaries. Several

Table 3.II. Summary of the microstructural features observed in isothermal treatments at 340, 320, 300, and 270°C. The nature and characteristics of each feature are also detailed.

Structural Feature	Characteristics	340°C	320°C	300°C	270°C	Phase Nature
S_{Thin} (S_T)	- Above and below M_s. - Thin units with acicular shape. - Parallel aligned. - Length: 5-8 um. - No carbides distinguished.	✓	✓	✓	?	***Bainitic***
$S_{Irregular}$ (S_I)	- Above and below M_s. - Laths with irregular shape. - Wider than S_T. - No carbides distinguished.	✓	✓	✓	---	***Bainitic***
S_{Thick} (S_{TK})	- Below M_s. - Laths with sharp tip at an edge. - Surrounded by S_T. - Contain carbides.	---	✓	✓	✓	***Martensitic***
$S_{Elongated}$ (S_E)	- Below M_s. - Longer and wider than S_T. - Wavy boundaries. - Contain carbides.	---	✓	✓	✓	***Martensitic***
S_{Blocky} (S_B) ***(MA island)***	- Smooth surface (not etched). - Internal structure. - Very small laths. - Surrounded by RA blocks.	✓	✓	✓	✓	***Martensite / Austenite***

studies have shown that the formation of athermal martensite prior to isothermal treatments leads to the creation of new potential nucleation sites in the form of martensite-austenite interfaces [8-11]. At the same time, as the isothermal temperature decreases and approaches M_s, there is a reduction in the size of the bainitic units due to an increase of the transformation kinetics. The lower the temperature, the higher the undercooling and driving force for nucleation. So, very small units of bainitic ferrite may grow from the initial martensitic laths (S_E features) in the form of ledge-like protrusions at the very beginning of the isothermal treatments below M_s.

This fact can be observed in the microstructure obtained after the isothermal treatment at 300°C (below M_s), shown in Figure 3.8.a. In that figure, small units of a few micrometres length (less than 5 μm) appear just next to the wavy boundary of an S_E feature. The morphology (shape and size) of these units strongly differs from the one of the S_E, so they can be considered as different product phases. Their orientation may be the same (or similar) to that of the main S_E feature (see Figure 3.8.b). Only a small concentration of local deformation around the area where those small units appear (see Figure 3.8.d) indicates their possible existence. Although these observations can suggest the different nature of these ledge-like protrusions in treatments below M_s, further investigations are needed for a detailed characterization of these protrusions and a better understanding of the interactions between prior athermal martensite and the subsequently formed bainitic ferrite.

3.4. Conclusions

The nature of the different microstructural features obtained in isothermal treatments below M_s is determined as bainitic or martensitic by comparing experimental volume fractions of the product phases, which were extracted from previous dilatometry and XRD analysis, with the morphology (size and shape) of the specific features characterized at each isothermal temperature by SEM and EBSD analysis. The main conclusions obtained from this methodology are the following:

1. Bainitic ferrite appears in the form of thin acicular units and/or irregularly shaped laths in isothermal treatments performed above and below the M_s temperature. Acicular units are aligned parallel to each other. They have a mean length between 5 and 8 μm and a mean width between 0.6 and 0.8 μm. Irregular laths are wider than acicular units. Carbides are not observed within any of these features.

2. Martensite appears as lath-shaped structures in isothermal treatments performed below the M_s temperature. Two different martensitic structures are characterized in the form of laths with a characteristic sharp tip at one of the edges and/or laths presenting wavy boundaries with ledge-like protrusions. The latter martensitic structures are longer and wider than acicular units of bainitic ferrite, with a mean length and width of 12 μm and 2 μm, respectively. Both types of lath-shaped structures contain carbides within them. Based on the characterization methodology described above, these microstructures correspond well to tempered martensite.

3. Martensite-austenite islands are characterized in all isothermal treatments performed above and below M_s. These islands present an internal structure formed by very small martensite laths (smaller than 2 μm) parallel aligned, surrounded by retained austenite blocks.

4. The appearance of some protrusions in martensitic structures can be related to the formation of bainitic ferrite in isothermal treatments below M_s, which might lead to the formation of wavy boundaries in such martensitic laths.

References

[1] K. Sugimoto, T. Ilda, J. Sakaguchi, T. Kashima. Retained austenite characteristics and tensile properties in a TRIP type bainitic sheet steel. ISIJ Int., 2000, vol. 40, pp. 902-908.

[2] K. Sugimoto, M. Murata, S.M. Song. Formability of Al-Nb bearing ultra-high strength TRIP-aided sheet steels with bainitic ferrite and/or martensite matrix. ISIJ Int., 2010, vol. 50, pp. 162-168.

[3] Y. Jiang, R. Zhou, R. Zhou, D. Lu, Z. Li. Microstructures and properties of a bainite and martensite dual-phase cast steel fabricated by combination of alloying and controlled cooling heat treatment. Trans. Tech. Publications, 2005, Mater. Sci. Forum, vol. 475-479, pp. 93-96.

[4] S.M.C. van Bohemen, M.J. Santofimia, J. Sietsma. Experimental evidence for bainite formation below M_s in Fe-0.66C. Scripta Mater., 2008, vol. 58, pp. 488-491.

[5] J.C. Hell, M. Dehmas, S. Allain, J.M. Prado, A. Hazotte, J.P. Chateau. Microstructure-properties relationships in carbide-free bainitic steels. ISIJ Int., 2011, vol. 51, pp. 1724-1732.

[6] I.A. Yakubtsov, G.R. Purdy. Analyses of transformation kinetics of carbide-free bainite above and below the athermal martensite start temperature. Metall. Mater. Trans. A. 2012, vol. 43A, pp. 437-446.

[7] D. Kim, J.G. Speer, B.C. De Cooman. The isothermal transformation of low-alloy low-carbon CMnSi steels below M_s. Trans. Tech. Publications, 2010, Mater. Sci. Forum, vol. 654-656, pp. 98-101.

[8] H. Kawata, K. Hayashi, N. Sugiura, N. Yoshinaga, M. Takahashi. Effect of martensite in initial structure on bainite transformation. Mater. Sci. Forum, 2010, vols. 638-642, pp. 3307-3312.

[9] M.J. Santofimia, S.M.C. van Bohemen, D.N. Hanlon, L. Zhao, J. Sietsma. Perspectives in high-strength steels: Interactions between non-equilibrium phases. Inter. Symp. on AHSS, 2013, AIST, pp. 331-339.

[10] L. Zhao, L. Qian, J. Meng, Q. Zhou, F. Zhang. Below-M_s austempering to obtain refined bainitic structure and enhanced mechanical properties in low-C high-Si/Al steels. Scripta Mater., 2016, vol. 112, pp. 96-100.

[11] A. Navarro-López, J. Sietsma, M.J. Santofimia. Effect of prior athermal martensite on the isothermal transformation kinetics below M_s in a low-C high-Si steel. Metall. Mater. Trans. A, 2016, vol. 47A, pp. 1028-1039.

[12] P. Kolmskog, A. Borgenstam, M. Hillert, P. Hedstrom, S.S. Babu, H. Terasaki, Y.I. Komizo. Direct observation that bainite can grow below M_s. Metall. Mater. Trans. A, 2012, vol. 43A, pp. 4984-4988.

[13] E.P. Da Silva, D. De Knijf, W. Xu, C. Föjer, Y. Houbaert, J. Sietsma, R. Petrov. Isothermal transformations in advanced high strength steels below martensite start temperature. Mater. Sci. Technol., 2015, vol. 31, pp. 808-816.

[14] S. Samanta, P. Biswas, S. Giri, S.B. Singh, S. Kundu. Formation of bainite below the M_s temperature: kinetics and crystallography. Acta Mater., 2016, vol. 105, pp. 390-403.

[15] D. Kim, J.G. Speer, B.C. De Cooman. Isothermal transformation of a CMnSi steel below the M_s temperature. Metall. Mater. Trans. A, 2011, vol. 42A, pp. 1575-1585.

[16] D. Kim, S.J. Lee, B.C. De Cooman. Microstructure of low carbon steel isothermally transformed in the M_s to M_f temperature range. Metall. Mater. Trans. A, 2012, vol. 43A, pp. 4967-4983.

[17] M.C. Somani, D.A. Porter, L.P. Karjalainen, R.D.K. Misra. On various aspects of decomposition of austenite in a high-Si steel during Q&P. Metall. Mater. Trans. A, 2014, vol. 45A, pp. 1247-1257.

[18] S.R. Pati, M. Cohen. Nucleation of the isothermal martensitic transformation. Acta Metall., 1969, vol. 17, pp. 189-199.

[19] A. Borgenstam, M. Hillert, J. Ågren. Critical temperature for growth of martensite. Acta Metall. Mater., 1995, vol. 43, pp. 945-954.

[20] A. Borgenstam, M. Hillert. Activation energy for isothermal martensite in ferrous alloys. Acta Mater., 1997, vol. 45, pp. 651-662.

[21] C.F. Jatczak, J.A. Larson, S.W. Shin. Retained austenite and its measurements by X-ray diffraction. Society of Automotive Engineers, Special Publication 453, 1980.

CHAPTER 4

Effect of a Free Surface on Low Temperature Phase Transformations by In-situ Laser Confocal Microscopy

**This chapter corresponds to the article "Free surface effects on low temperature phase transformations in a multiphase steel by laser confocal microscopy" by A. Navarro-López, J. Hidalgo, G. Miyamoto, T. Furuhara, J. Sietsma, and M.J. Santofimia, to be submitted for publication.*

Abstract

The development of fundamental knowledge in advanced high strength steels has enabled the increasingly lightweigthing of automotive steel structural components by reducing their thickness. The use of thin steel sheets for such applications diminishes the surface-to-volume ratio of steel components, leading to a significantly importance of the free surface effects in the development of multiphase microstructures. For example, there is experimental evidence confirming the onset of the martensitic transformation at higher temperatures at the steel surface compared to the bulk. Free surface effects can thus lead to microstructural differences along the thickness of steel sheets, causing local gradients of mechanical properties due to the formation of distinct multiphase mixture at surface and bulk. The objective of this study is to determine the free surface effects on the phase transformations involved during isothermal treatments at low temperatures in a low-carbon high-silicon steel. With that aim, experimental surface observations by in-situ laser confocal microscopy are combined with theoretical thermodynamic models. It is demonstrated that the higher M_s temperature at a free surface compared to the bulk is consequence of the minimized volume strain energy needed to accommodate the strains induced by martensite formation. Furthermore, differences between the micro-constituents formed at the surface and within the bulk of steel specimens are identified and characterized in terms of their bainitic or martensitic nature, grain size, and growth direction by electron back scatter diffraction and dilatometry measurements. Finally, the crystallographic analysis show a preferential variant selection in both surface and bulk grains, though a larger deviation of the crystallographic pattern of surface grains is observed with respect to the theoretical K-S orientation relationship.

4.1. Introduction

The manufacture of increasingly lightweight steel structural components has led to the progressive use of thin sheets of advanced high strength steels (AHSS) for such applications. The use of thin steel sheets implies, in turn, the precise control of the temperature and time during the application of thermal treatments to obtain the desired microstructure homogenously along the sheet thickness. The temperature-time control results decisive on the microstructural development of multiphase steels, especially for those obtained through the application of isothermal holdings above and below the martensite-start (M_s) temperature. Small variations in temperature and time can lead to significant differences in the final multiphase microstructure, as demonstrated in Chapters 2 and 3.

The main microstructural difference between multiphase steels obtained by isothermal treatments above and below M_s lies on the formation of a certain fraction of prior athermal martensite (PAM) before the isothermal bainite transformation. The accelerated formation of bainitic ferrite below M_s stems from the introduction of additional sites for bainite nucleation resulting from PAM formation [1-5]. The final multiphase microstructure of these steels, which also includes fresh martensite and retained austenite, will depend on the applied holding time. Furthermore, the reduced surface-to-volume ratio of the steel sheets can create a microstructural gradient along the sheet thickness in these multiphase steels as a consequence of a different microstructural development at the free surface with respect to the bulk. The formation of this microstructural gradient can be decisive in the final performance of these steels, especially under the action of fatigue, impact, or corrosion, which severely affect the surface area.

Several investigations reported that the M_s temperature is higher at the surface than within the bulk of steel specimens [6-9]. This is generally attributed to the easier accommodation of martensitic transformation strains at the surfaces due to a lower associated strain energy. In addition to this effect, the coalescence of several bainite or martensite laths into coarser grains was also observed to occur at free surfaces in high strength steels [6,10-14]. This increase of grain size due to coalescence is considered to be detrimental for toughness [11]. Apart from these studies, there is scarce literature about the effects of a free surface on the microstructure development of advanced high strength steels. On the other hand, free surface effects are generally studied by means of in-situ observations using laser confocal microscopy (LCM), which is a powerful tool for the in-situ study of phase transformations in steel. This technique has been extensively used for the analysis of the transformation kinetics, morphological growth, and crystallography of bainite in high strength steels [12,14-22].

The main goal of this research work is to determine the effect of a free surface on the microstructural evolution of a low-C high-Si steel during isothermal treatments performed at low temperatures. For this purpose, surface observations by in-situ laser confocal microscopy experiments are carried out in combination with theoretical calculations using thermodynamic models for heterogeneous martensite nucleation. Direct observations are also combined with electron back scatter diffraction (EBSD) measurements to characterize qualitatively the morphological differences and the internal structure of the final micro-constituents formed at the surface and within the bulk. Differences in the microstructure evolution between surface and bulk are further investigated by dilatometry measurements.

4.2. Experimental Procedure

This research work was carried out at the Institute for Materials Research, placed at Tohoku University in Sendai, Japan. Disc-shaped specimens of 3.5 mm diameter and 1.0 mm thickness, machined from a hot-rolled slab of a low-carbon high-silicon steel with 0.2C–3.51Mn–1.52Si–0.25Mo–0.04Al (wt.%), were used for in-situ experiments performed by laser confocal microscopy (LCM). Before performing experiments, the surface of the disc-shaped specimens was first grinded and polished until mirror finish. Subsequently, a surface area of 400 x 400 μm^2 was marked in the centre of the specimens by several micro-indentations (HV1) to facilitate the later performance of electron back scattering diffraction (EBSD) measurements over the same surface area studied in LCM experiments. As a final preparation step, specimens were mechanically polished with a colloidal silica solution in order to exhaustively clean the specimen surface and remove any superficial deformation. On the other hand, cylindrical specimens of 3.5 mm diameter and 10 mm length, extracted from the same hot rolled steel slab as the LCM specimens, were used in dilatometry measurements to characterize the phase transformations occurring during the thermal treatments applied in LCM experiments.

The in-situ experimental set-up consisted of a laser confocal microscope VL200 LaserTec in combination with a Yonekura heating stage controlled by a high temperature observation system (HiTOS). Figure 4.1.a shows a detailed scheme of the complete experimental set-up. Specimens were placed within an alumina cylindrical crucible covered by an alumina cap with a central hole to allow the laser beam illuminating the marked central surface of the specimens. The crucible was in turn held by a platinum plate inside the chamber of the heating stage. A thermocouple was attached to the platinum plate to control and monitor the temperature during the heat treatments. The interior volume of this chamber was formed by two ellipsoids, where the crucible with the specimen was placed at the centre of their union. Two lamps were located at both extremes of the chamber to heat the specimen homogenously. A real image of the described configuration is shown in Figure 4.1.b. Since the specimen was heated by

infrared, the interior surface of the chamber was covered by a thin layer of gold, this element being a good infrared reflective and unreactive to oxidation.

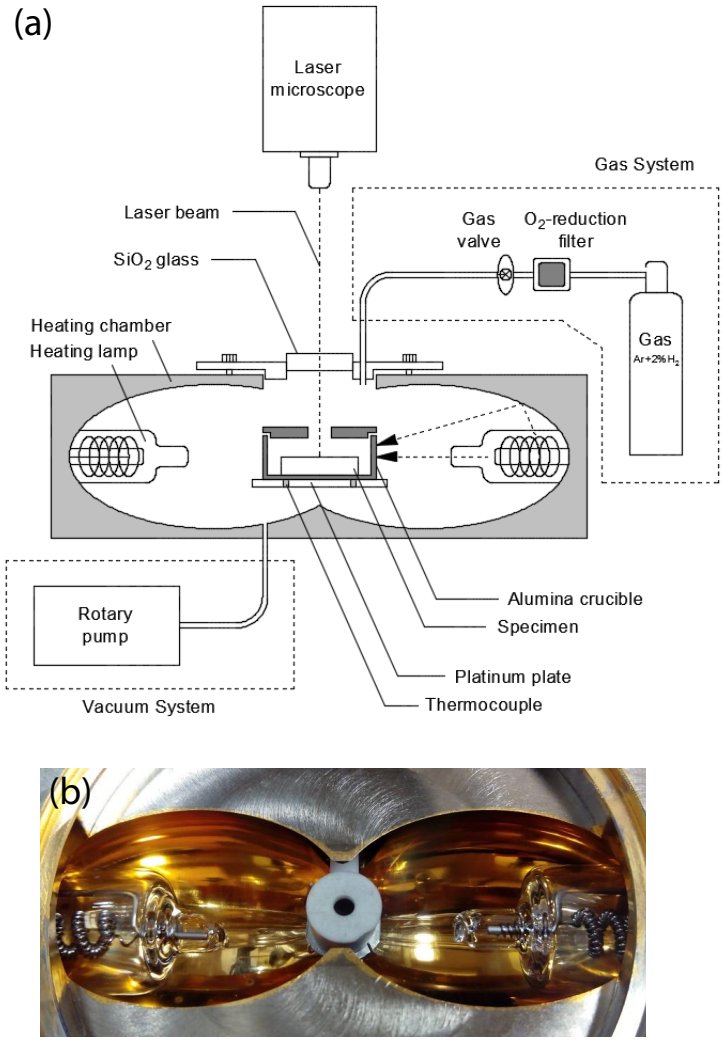

Figure 4.1. a) Schematic of the transversal cross-section of the heating stage and the complete experimental set-up, including temperature, vacuum, and gas control systems; b) Real image of the interior of the heating chamber where the steel specimen was placed within an alumina crucible in the centre of the union of the two ellipsoids.

The experimental set-up contains two complementary parts (see Figure 4.1.a): 1) a rotary pump used to evacuate the air and make vacuum within the heating chamber before starting the experiments and 2) the gas system throughout which argon gas with 2 pct. hydrogen (Ar-2%H_2) was continuously flushed into the heating chamber to create a protective atmosphere during the heat treatments avoiding the surface oxidation

of the specimens. The protective gas was conducted through an oxygen reduction filter before being flushed into the chamber to eliminate residuary oxygen contained in the gas system.

The disc-shaped specimen was introduced into the alumina crucible within the heating chamber together with two thin foils of a high-Mn (12 wt.%) and a high-C (1.8 wt.%) steels, respectively. These foils were placed within the crucible and surrounding the disc-shaped specimen in all experiments to provide an extra cathodic protection and induce a source of manganese in order to avoid its evaporation at high temperatures from the surface of the studied specimen. Before the start of LCM experiments, low pressure was achieved within the heating chamber until reaching a minimum initial value of 0.02 mbar. During the experiments, the vacuum valve was completely closed and a gas flow of 80-90 ml/min of Ar-2%H_2 was continuously flushed into the heating chamber.

In laser confocal microscopy experiments, there exists a temperature gradient between the controlling temperature measured by the thermocouple attached to the platinum plate and the temperature reached at the specimen surface. This temperature gradient is a consequence of the heat transfer through the alumina crucible placed onto the platinum plate and the specimen itself. Calibration measurements were thus necessary to determine at any time the temperature at the specimen surface during the heat treatments. The calibration was carried out by spot-welding a thermocouple to the top surface of the specimen, repeating the heat treatments in the experimental conditions previously described, and comparing the temperatures measured at the specimen surface and at the platinum plate. All temperatures recorded in laser confocal microscopy experiments and presented in this work were corrected in accordance to this calibration.

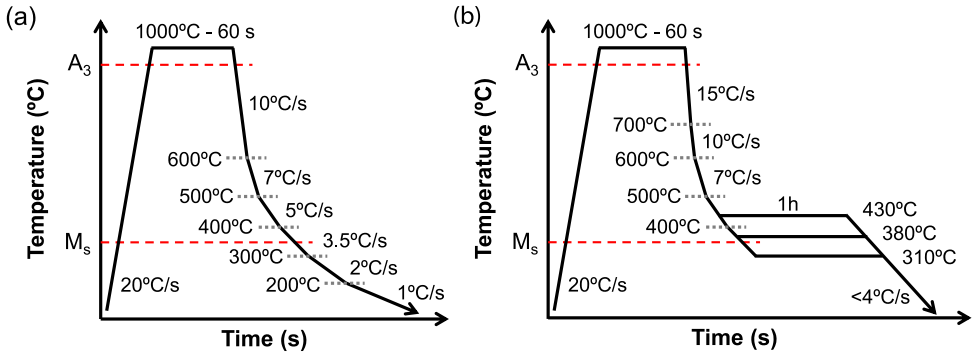

Figure 4.2. (a) Continuous cooling and (b) one-hour isothermal treatments at 430°C, 380°C, and 310°C applied in laser confocal microscopy experiments. These temperature profiles were recorded at the specimen surface during these in-situ experiments. The same temperature profiles were also applied in dilatometry experiments.

Figure 4.2 shows the temperature profiles applied in each of the heat treatments. All heat treatments consisted of a full austenitization at 1000°C for 60 seconds followed by a continuous cooling to room temperature (Figure 4.2.a) or an isothermal annealing for one hour before cooling to room temperature (Figure 4.2.b). The direct-cooling treatment was performed to determine the experimental M_s temperature at the surface of the specimens, referred as $M_{s\text{-}surf}$. The isothermal treatments were performed at the three selected temperatures to study phase transformations occurring at the specimen surface above and below $M_{s\text{-}surf}$. Due to technical limitations of the experimental set-up to accomplish high cooling rates, the cooling stage in all heat treatments was performed in several continuous steps in which the cooling rates used were the maximum allowed by the experimental set-up.

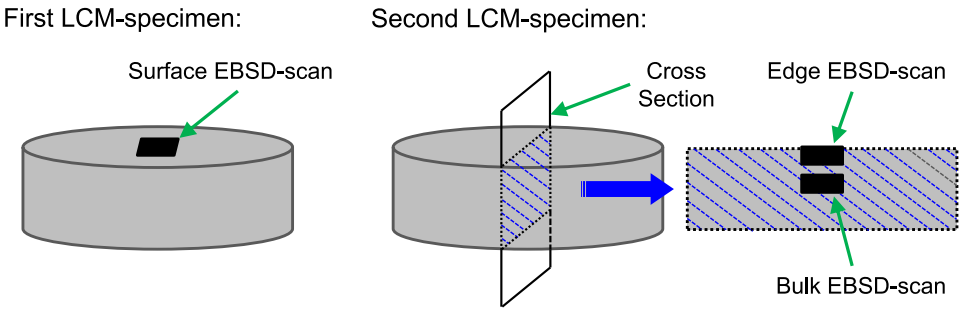

Figure 4.3. Scheme of the locations of EBSD measurements performed at the surface and cross-section of the two disc-shaped specimens previously heat treated during LCM in-situ experiments.

Two disc-shaped specimens were thermally treated for each of the heat treatments described in Figure 4.2. Figure 4.3 shows a schematic illustration of how both specimens were microstructurally analysed. The first of the two specimens was used for the microstructural characterization of the surface, which was performed by EBSD measurements carried out within the marked superficial centre area where previously the LCM observations were performed. The second specimen was used for the microstructural characterization of the specimen bulk. In this case, a cross-section slice with respect to the surface was cut from the specimen by electric discharge machining (EDM). The cross-section surface was microstructurally characterized by EBSD measurements (bulk and edge scans) after metallography preparation by grinding and polishing with colloidal silica.

The EBSD patterns were acquired on a FEI Quanta 450 scanning electron microscope equipped with a Field Emission Gun (FEG-SEM) by means of the OIM Data Collection software. The analysis was performed under the following conditions: acceleration voltage of 20 kV, working distance of 15 mm, tilt angle of 70°, and step size of 50 nm

in a hexagonal scan grid. The orientation data were post-processed with TSL OIM® Analyses 7.0 software. First, a grain confidence index (CI) standardization was applied to the raw data, selecting a tolerance angle of 5°, a minimum grain size of 6 pixels, and considering that grains are formed by multiple pixel rows. The second step of the post-processing procedure included neighbour-orientation correlation with a tolerance angle of 5° and a minimum confidence index of 0.1. Finally, a down-filtering criterion of confidence index higher than 0.1 was applied to reduce the number of pixels poorly indexed, i.e., not attributed to either fcc or bcc phases.

Dilatometry measurements were performed to determine the M_s temperature and the microstructural constituents formed within the bulk of the specimens while applying the same heat treatments as those applied in laser confocal microscopy experiments (see Figure 4.2). Cylindrical specimens were thermally treated with a Bähr 805A/D dilatometer, in which heating was performed by an induction coil under a vacuum of the order of 10^{-4} mbar, and cooling by a continuous flow of helium gas. An S-type thermocouple was spot-welded to the surface of each cylindrical specimen at the middle of the length to monitor and control the temperature. Specimens were placed between two quartz rods to measure changes in the length of specimens occurring during the application of thermal treatments.

4.3. Results

4.3.1. Microstructural Evolution

❖ ***In the Bulk***

Phase transformations occurring in the bulk of steel specimens during the described heat treatments were investigated by dilatometry. Figure 4.4.a shows the experimentally-obtained relative change in length as a function of temperature during continuous cooling to room temperature according to the thermal profile presented in Figure 4.2.a. The dilatometric curve shows a linear thermal contraction during cooling until reaching the martensite-start temperature, indicating the absence of any phase transformation (ferrite, pearlite, or bainite) before martensite starts to form. The M_s temperature was determined to be 333°C ± 5°C, according to the procedure described in Chapter 2, and is defined as *'*$M_{s\text{-}bulk\ (1\%)}$*'* since it corresponds to the temperature at which 1% of athermal martensite is formed within the bulk of the specimen. An additional direct-cooling treatment at a rate of 20°C/s was performed by dilatometry to verify these observations. As shown in Figure 4.4.a, both dilatometry curves superimpose during cooling until the beginning of the martensitic transformation, verifying the presented descriptions.

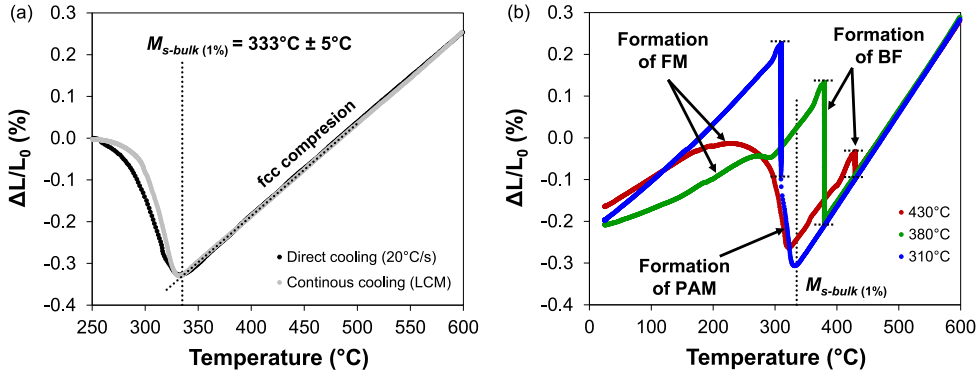

Figure 4.4. Relative change in length as function of temperature from dilatometry following the same thermal profiles performed in LCM experiments: (a) continuous cooling treatment presented in Figure 4.2.a and direct-cooling at 20°C/s, and (b) cooling followed by distinct isothermal treatments as presented in Figure 4.2.b. The following terms refer to 'BF: bainitic ferrite', 'PAM: prior athermal martensite', and 'FM: fresh martensite'.

Figure 4.4.b shows the relative change in length as a function of temperature following the thermal profiles presented in Figure 4.2.b, which were also applied in LCM experiments. Dilatometry curves of specimens cooled to temperatures above $M_{s\text{-}bulk}$, 430°C and 380°C, exhibit a linear contraction until reaching the isothermal temperature, which indicates the absence of formation of any bcc-phase during cooling. This thermal contraction deviates from its linearity when the specimen is cooled to a temperature below $M_{s\text{-}bulk}$, 310°C, due to the formation of a certain fraction of prior athermal martensite (PAM) before the isothermal holding. A dilatation takes place during the one hour isothermal holding in all heat treated specimens as consequence of the formation of bainitic ferrite (BF). A larger isothermal dilatation indicates a larger volume fraction of bainitic ferrite formed. The bainite reaction is incomplete after one hour of isothermal holding at the three selected temperatures, as evident from the non-linear relative change in length during the final cooling to room temperature, showing the formation of fresh martensite (FM) from the untransformed remaining austenite.

❖ *At the Surface*

The in-situ evolution of the microstructure at the surface of LCM specimens was studied through the analysis of the video frames obtained by laser confocal microscopy. In this case, observations reveal that the initiation of the martensitic transformation at the specimen surface takes place at a temperature of 388°C ± 8°C, which is defined as *'$M_{s\text{-}surf.}$'* in the present work. The formation of martensite was directly observed by LCM as the sudden fast growth of acicular units. The microstructural evolution at the surface of specimens isothermally treated at 430°C, 380°C, and 310°C is shown in Figure 4.5.

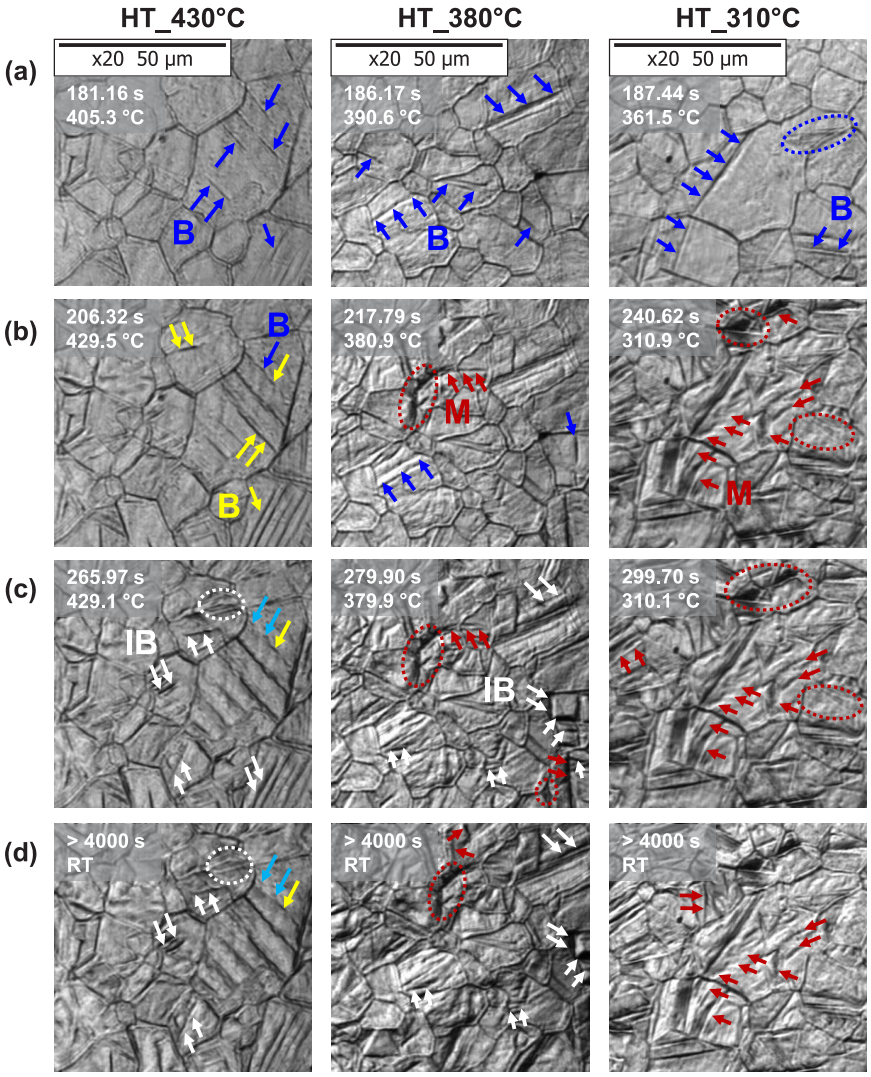

Figure 4.5. Video frames illustrating the microstructural evolution at the surface of LCM specimens isothermally treated at 430°C, 380°C, and 310°C through four time instants corresponding to a) the formation of bainitic ferrite (B) during cooling from austenitization, b) the formation of bainitic (B) and martensitic structures (M) until the stabilization of the applied isothermal temperature, c) the isothermal formation of bainitic ferrite (IB) after applying the first 60 seconds of holding time, d) the final microstructure after one hour of isothermal holding and final cooling to room temperature.

Micro-constituents are indicated in the video frames by coloured arrows. Every column of video frames corresponds to the microstructural evolution during a different heat treatment (HT), while every row shows the formation of a specific micro-constituent. For a better understanding of the analysis, the microstructural evolution is described as follows:

a) Figures 4.5.a shows the formation of bainitic ferrite (blue arrows) in the surface of the specimens during cooling from austenitization before reaching the corresponding isothermal temperature. Bainitic ferrite is observed to grow in the form of acicular units from prior austenite grain boundaries and/or from unobservable defects within the parent austenite grains.

b) In the specimen isothermally treated at 430°C, bainitic ferrite is observed to continuously grow during an existing undercooling of approximately 30°C until the isothermal temperature is stabilized. These bainitic structures are indicated by yellow arrows in Figure 4.5.b. On the other hand, a certain fraction of prior athermal martensite (PAM) is observed to form at the surface of specimens isothermally treated at 380°C and 310°C before reaching the corresponding isothermal temperature, which in both cases is below the $M_{s\text{-}surf.}$ temperature. These martensitic structures are indicated by red arrows.

c) Once the isothermal temperature is stable, bainitic ferrite continues forming isothermally at the specimen surface during the following 60 seconds of holding at 430°C (above $M_{s\text{-}surf.}$ and $M_{s\text{-}bulk}$) and at 380°C (below $M_{s\text{-}surf.}$), as indicated by white arrows in Figure 4.5.c. Figure 4.6 shows, in more detail, the superficial growth of bainitic ferrite at 380°C by several video frames during the first 30 seconds of the isothermal holding, confirming bainite formation below M_s. However, the isothermal formation of bainitic ferrite is not observed in the specimen treated at 310°C due to the larger martensite formation occurred during cooling.

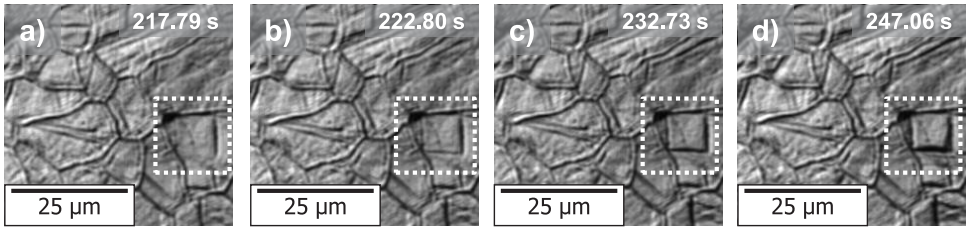

Figure 4.6. Isothermal growth of bainitic ferrite at specimen surface during the first 30 s of holding at the stable temperature of 380°C, in this case, below the $M_{s\text{-}surf.}$ temperature. The video frames obtained by LCM measurements correspond to the time instants of a) 0 s, b) 5 s, c) 15 s, and d) 30 s.

d) Figures 4.5.d show the microstructures defined after the application of one hour holding and the subsequent cooling to room temperature. Fresh martensite is observed to form during cooling from the isothermal temperatures of 430°C and 380°C, but not from 310°C. In this final cooling, the formation of martensite can only be detected by LCM observations as the appearance of a small and localized bump of the specimen surface.

4.4. Discussion

4.4.1. The M_s temperature

It is evident from surface observations and dilatometry measurements that the onset of the austenite-to-martensite transformation at the surface occurs at higher temperatures than within the bulk. This fact was already reported in several studies on plain-carbon steels [6], Fe-Ni alloys [7,8], and stainless steels [9]. Reported differences in temperature between the formation of surface and bulk martensite can vary from 5°C to more than 100°C. In this work, the average difference in the M_s temperature between surface and bulk is 55°C ± 9°C. This difference is likely related to a lower driving force required for the martensitic transformation to occur at the surface as consequence of the lower resistance exerted by the austenite for the transformation [23]. Compared to the bulk, the free surface provides fewer constraints for the accommodation of strains derived from the formation of athermal martensite.

The initiation of the martensitic transformation requires a certain degree of undercooling below T_0, the temperature at which the Gibbs free energy of the austenite and the martensite phases is the same for a given chemical composition. The degree of undercooling needed to drive the austenite-to-martensite transformation depends on the energy balance between the chemical free energy change ($\Delta G_{chem}^{\gamma\text{-}\alpha}$) associated to both phases and the non-chemical free energy opposing the formation of martensite [24,25]. At the martensite start temperature, this energy balance results to be 'zero', and the minimum chemical free energy change associated to the onset of the martensitic transformation is known as critical driving force ($\Delta G_c^{\gamma\text{-}\alpha}$). Figure 4.7 shows the chemical free energy change for the austenite-to-martensite transformation ($\Delta G_{chem}^{\gamma\text{-}\alpha}$) as a function of temperature for the steel composition studied in this work calculated with

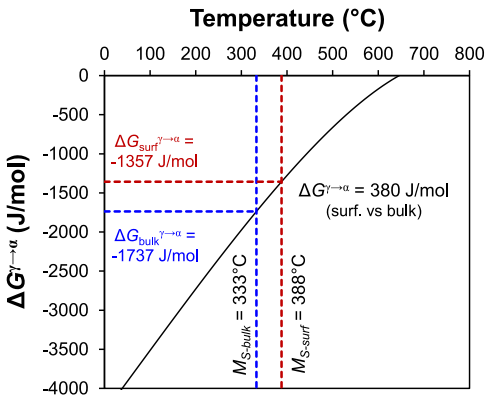

Figure 4.7. Chemical Gibbs free energy change for austenite-to-martensite transformation as a function of temperature, calculated by Thermo-Calc software using the TCFE9 database. The critical driving force for martensite nucleation at surface and bulk are indicated.

Thermo-Calc software (TCFe9 database). The critical driving forces for martensite nucleation at the surface ($\Delta G_{surf.}^{\gamma-\alpha}$ = 1357 J/mol) and bulk ($\Delta G_{bulk}^{\gamma-\alpha}$ = 1737 J/mol) were extracted from this thermodynamic data, considering the experimental $M_{s\text{-}surf.}$ and $M_{s\text{-}bulk}$ temperatures. In this case, there is a difference of 380 J/mol in the critical driving force required for martensitic transformation at the surface compared to the bulk.

The need of a lower critical driving force at the surface to initiate the martensitic transformation can be thermodynamically proven by means of the extended model developed by Van Bohemen and Morsdorf [26], which is based on the mechanism for heterogeneous martensite nucleation proposed by Olson and Cohen [27]. Van Bohemen and Morsdorf modify the thermodynamic model of Ghosh and Olson [24,25], which describes the resistance of austenite to the martensite-austenite interface motion during martensite formation, to account also for the effect of the austenite grain size. The critical driving force for heterogeneous martensite nucleation is given by the energy balance [24,26]:

$$-\Delta G_c^{\gamma-\alpha} = K_1 + W_\mu + W_{th} + W_{HP} + W_C \tag{4.1}$$

where K_1 accounts for the strain energy, the interfacial energy, and the critical defect size. W_μ and W_{th} represent the athermal and thermal components of the interfacial frictional work, respectively, due to interface mobility. The athermal component is only composition dependent while the thermal one is both composition and temperature dependent. Generally, the thermal component of the frictional work (W_{th}) is considered to be negligible at temperatures higher than 300 K (room temperature). W_{HP} accounts for the Hall-Petch effect due to the inversely proportional relationship between the austenite grain size and the austenite strengthening, which, in turn, directly affects the M_s temperature and the martensite transformation [28,29]. W_C accounts for the change in the aspect ratio of the martensite laths below a critical austenite grain size, which influences the stored energy in the surroundings of the untransformed austenite.

The first non-chemical free energy term of Equation (4.1) can be expressed as

$$K_1 = E^{str} + \frac{2 \cdot \sigma}{n^* \cdot \rho_A} \tag{4.2}$$

where E^{str} is the volume strain energy, σ is the semi-coherent interfacial energy per unit area (0.15 J/m^2 [27]), ρ_A refers to the atomic density per unit area in a close-packed plane of the parent austenite (its value is of approximately $2.99 \cdot 10^{-5}$ mol/m^2 in the (111) austenite plane), and n^* is the critical defect size, which represents the number of planes in the thickness of the fault from where martensite nucleates. A value of 20 is considered as the critical defect size, based on the work of Celada-Casero et al. [23] on the effect of

austenite grain size in the martensitic transformation using a similar composition as the one used in the present work. The semi-coherent interfacial energy (σ) and the critical defect size (n^*) are assumed to be independent of whether the martensitic transformation occurs at the surface or within the bulk, but not the volume strain energy (E^{str}) which, in this case, remains as an unknown parameter.

The athermal component of the frictional work (W_μ) can be expressed as

$$W_\mu = K_\mu^C \cdot x_C^{0.5} + \sqrt{\sum_i \left(K_\mu^i \cdot x_i^{0.5} \right)^2} \tag{4.3}$$

where K_μ are the coefficients of the interfacial frictional work for the martensite-austenite semi-coherent interface (which can be found in ref. [26]), and x_i represents the concentration of the alloying element i in wt. %. Considering that there are no compositional changes between surface and bulk in all specimens during the application of heat treatments, W_μ is equal for surface and bulk martensitic transformation with a value of 716 J/mol.

The non-chemical free energy terms related to the Hall-Petch strengthening (W_{HP}) and the aspect ratio of martensite laths (W_C) can be expressed as

$$W_{HP} = \frac{K_{HP}}{\sqrt{d^\gamma}} \tag{4.4}$$

and

$$W_C = K_C \cdot \exp\left(\frac{-6 \cdot d^\gamma}{d_C^\gamma} \right) \tag{4.5}$$

where K_{HP} and K_C are proportionality constants with a value of approximately $350 \cdot 10^{-3}$ $Jm^{1/2}$/mol and 370 J/mol, respectively, derived and experimentally validated by Van Bohemen and Morsdorf [26], d_γ is the average austenite grain size, corresponding to 25 μm in the present work, and d_C^γ is the critical austenite grain size below which there is a pronounced decrease in the M_s temperature due to variations in the *c/a* ratio of martensite laths. This latter parameter is considered to be 14 μm based on the experimental observations of several authors [23,30] in low-carbon steels with similar composition to the steel studied in the present work. In this case, W_{HP} and W_C are also considered to be the same for surface and bulk since there are no differences in the austenite grain size (due to the use of the same austenitization conditions), so the calculated values are W_{HP} = 70 J/mol and W_C = 0.01 J/mol.

Substituting all calculated values in Equation (4.1), the K_1 parameter and, consequently, the volume strain energy (E^{str}) for surface and bulk martensitic transformation in the

heat-treated specimens can be obtained. The resulting values of both terms are indicated in Table 4.I. The value of E^{str} = 449 J/mol in bulk martensitic transformation is similar to the typical values of strain energy (450-500 J/mol) reported in literature [23,24,27]. For the same transformation conditions, the value of K_1 = 951 J/mol lies in a range defined between 900 J/mol and 1010 J/mol, minimum and maximum values reported by Celada-Casero [23], Ghosh and Olson [24], and Van Bohemen and Morsdorf [26].

Table 4.I. Experimental values of the M_s temperature and calculated values of the critical driving force ($\Delta G_c^{\gamma-\alpha}$), the K_1 parameter, and the volume strain energy (E^{str}) for the austenite-to-martensite transformation at the surface and within the bulk of heat-treated specimens.

Parameter/Term	At Surface	In Bulk	Determined from
M_s (°C)	388	333	Measurements
$\Delta G_c^{\gamma-\alpha}$ (J/mol)	-1357	-1737	Thermo-Calc (Fig. 4.7)
E^{str} (J/mol)	**69**	**449**	Eq. (4.1)
K_1 (J/mol)	571	951	Eq. (4.2)

On the contrary, the values of E^{str} and, consequently, the K_1 parameter are drastically reduced in surface martensitic transformation, indicating a significantly smaller resistance to the volume change accompanying the transformation at the surface compared to bulk. This is due to the existence of a free surface where constraints to the expansion or contraction of the lattice are not imposed in the normal direction to the surface. Therefore, it is demonstrated that differences in the M_s temperature between surface and bulk are mainly related to differences in the volume strain energy, i.e., in the resistance exerted by the free surface or the bulk for the accommodation of strains due to the volume change that accompanies the martensitic transformation.

4.4.2 Product Phases

The higher-temperature onset of the martensitic transformation at surface in comparison to the bulk strongly affects the microstructural evolution between surface and bulk during the application of heat treatments. Extrapolating this free-surface effect to the onset of the bainitic transformation, the formation of bainitic ferrite should be more energetically favourable at the surface than within the bulk. Experimental observations made by LCM and dilatometry agree with this assessment: LCM experiments showed the formation of bainitic ferrite at the surface of all specimens during cooling from austenitization to the isothermal temperature (see Figure 4.5), while this bainite formation was not detected by dilatometry.

Dilatometry measurements detect volume changes in the longitudinal direction of the cylindrical specimens. Considering that surface effects affect a depth equal to an average austenite grain size (d^{γ}), in this case, the first 25 μm from the surface towards the centre of the specimens, the total 'surface' volume in which bainite can form represent

approximately 2% of the total volume of the cylindrical specimen. In principle, the formation of a 0.02 volume fraction of bainitic ferrite should lead to a detectable length change by the dilatometer. However, since volume changes inherent to bainitic ferrite formation in the majority 'surface' volume mostly occur in the transversal direction of the cylindrical specimen, the possibility that these changes are detected by the dilatometer is drastically reduced.

Taking into consideration LCM observations and dilatometry measurements, the main microstructural differences at the surface compared to the bulk of the isothermally-treated specimens are the following:

i) *Specimen isothermally treated at 430°C.* There is a higher degree of formation of bainitic ferrite at the cost of fresh martensite at the surface compared to the bulk, where fresh martensite is the majority phase within the phase mixture.

ii) *Specimen isothermally treated at 380°C.* At the surface, a certain fraction of prior athermal martensite (PAM) forms, followed by bainitic ferrite formation. In the bulk, there is no formation of PAM and the phase mixture is mainly formed by bainitic ferrite and fresh martensite. This microstructural difference is consequence of the applied isothermal temperature being lower than the M_s temperature at the surface, but higher than the M_s temperature in the bulk.

iii) *Specimen isothermally treated at 310°C.* The formation of PAM is observed to occur in almost the entire surface area, where there is an undercooling of more than 80°C

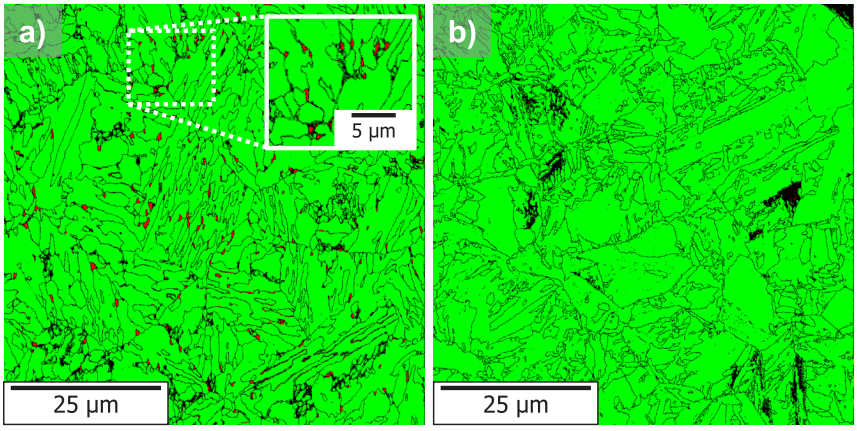

Figure 4.8. Phase Distribution (PD) maps from the a) surface and b) bulk of a determined area of the LCM specimen isothermally treated at 380°C for one hour. Retained austenite is identified in red colour, while black contours represent high-angle boundaries with misorientations of 15°-65°.

below the $M_{s\text{-}surf}$, resulting difficult to observe the formation of bainitic ferrite and/or fresh martensite. In the bulk, the microstructure is mainly formed by a significant fraction of PAM and bainitic ferrite.

The last effect of the free surface on phase transformations to account for is related to the stability of the retained austenite within the phase mixture. Figure 4.8 shows the phase distribution maps of bcc- and fcc- phases (from EBSD measurements) at the surface and in the bulk (cross-section) of the LCM specimen isothermally treated at 380°C. Both at the surface and within the bulk there is a well-balanced mixture of martensitic-bainitic structures, whereas retained austenite is observed to appear only within the bulk in the form of blocky shaped grains between the laths (Figure 4.8.a) and not at the surface of the heat-treated specimen (Figure 4.8.b). This difference can be also attributed to the lower volume strain energy associated to the free surface since the constraints resulting from the presence of micro-constituents such as martensite and/or bainitic ferrite opposing the transformation of the austenite are significantly diminished.

4.4.3. Grain Size

The grain size of the micro-constituents is also affected by the presence of a free surface. Figure 4.9 shows the evolution of the average grain size of the micro-constituents formed during the thermal cycles at the three selected isothermal temperatures, independently of the bainitic or martensitic nature of these micro-constituents. In this work, the average grain size is determined from the average diameter obtained from the image analysis of Unique Grain Colour (UGC) maps (EBSD measurements) in which an average number of 600-750 grains were analysed. A grain was defined by a tolerance angle of 2.5° and a minimum grain size of 10 pixels. Figure 4.9 shows that, at the surface and within the bulk, the grain size decreases when the temperature decreases below the corresponding M_s temperatures.

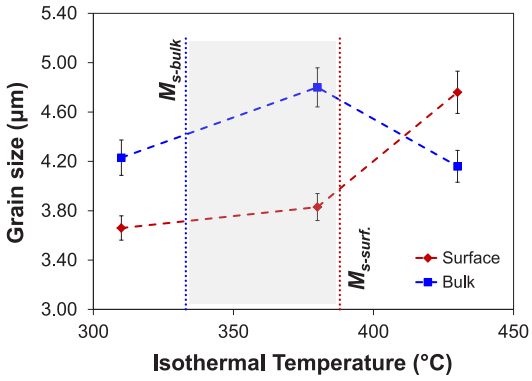

Figure 4.9. Average grain size of bainitic/martensitic micro-constituents formed at the surface and within the bulk of LCM specimens isothermally treated for one hour at 430°C, 380°C, and 310°C.

The decrease of the average grain size is mainly attributed to the refinement of micro-constituents, such as bainitic ferrite, as consequence of the presence of a certain fraction of athermal martensite prior to the bainite reaction [31]. The formation of athermal martensite leads to the fragmentation of the prior austenite grains into smaller ones [32] and to the acceleration of the bainitic ferrite formation due to the introduction of potential nucleation sites at martensite-austenite interfaces [1-5]. Both mechanisms induce the refinement of microstructures isothermally obtained below M_s compared to those ones obtained above M_s.

The largest differences in grain size between the micro-constituents formed at the surface and within the bulk of the heat-treated specimens are observed within the temperature range defined by both experimental M_s temperatures (see Figure 4.9). This temperature range can be considered as critical since the formation of PAM and the consequent drastic reduction of the grain size of micro-constituents at the surface in comparison to the bulk can cause large differences in the relative mechanical responses at both locations. This effect can thus be critical during the manufacturing of these advanced multiphase steels for industrial applications in which the thickness is a key factor for the final mechanical performance.

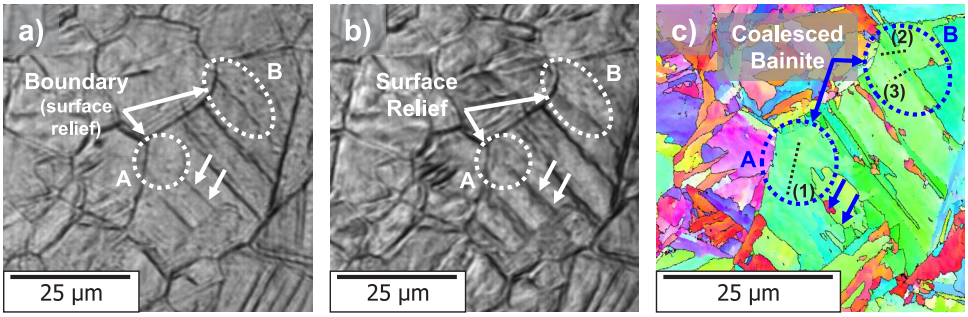

Figure 4.10. Coalescence of bainitic ferrite units at the surface of the specimen isothermally treated at 430°C. The video frames (from LCM) represented in a) and b) are the surface images corresponding to the microstructure at the beginning of the isothermal holding and at the end of the final cooling to room temperature, respectively. The orientation map presented in c) corresponds to the Inverse Pole Figure (IPF) of the same surface area observed in a) and b).

It can be also observed in Figure 4.9 that the average grain size in the specimen isothermally treated at 430°C is higher at the surface than within the bulk. In this case, higher grain sizes at the surface of this specimen can be attributed to the coalescence of bainitic ferrite units. The phenomenon of coalescence of bainite units or martensite laths has been extensively studied in high strength steels [6,10-14]. In the case of bainitic ferrite, it consists of the merging of several units to form a single larger plate in which the thin austenite films initially present between the bainitic ferrite units decompose

as the coarser bainitic structure is formed [10]. There are, in principle, two conditions necessary for the coalescence to occur: 1) the chemical driving force should be sufficient to sustain the increase in strain energy associated with the process [10], and 2) the units of bainitic ferrite to coalesce must have the same crystallographic orientation [12].

These conditions can be fulfilled in the presence of a free surface due to 1) the reduced strain energy associated to the transformation and 2) the preferential growth direction of the micro-constituents that can lead to a strong variant selection. Figure 4.10 shows an example of possibly coalesced bainitic ferrite at the surface of the specimen isothermally treated at 430°C. At the beginning of the isothermal holding, bainitic ferrite forms at the prior austenite grain boundaries creating austenite-bainite interfaces with an observable surface relief, as indicated in the video frame of Figure 4.10.a. The bainitic reaction continues during the isothermal holding, so new units of bainitic ferrite with their corresponding boundaries are formed adjacent to the initially-formed ones. However, at the end of the heat treatment, although surface reliefs created by the formation of bainitic ferrite are visible (see video frame of Figure 4.10.b), the orientation map

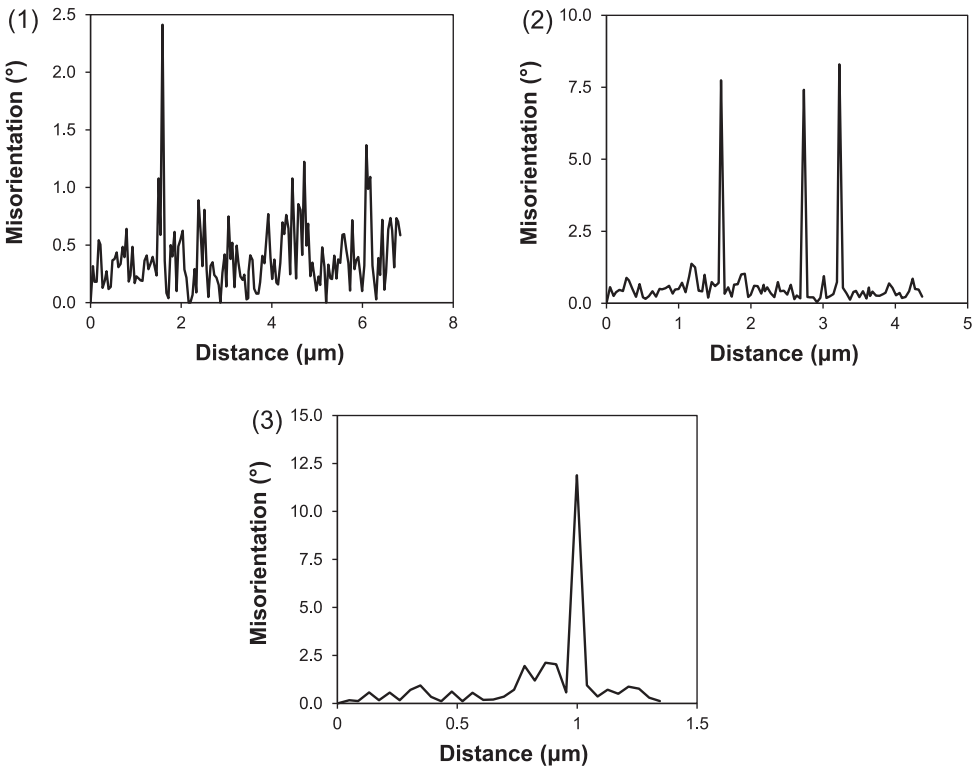

Figure 4.11. Point-to-point misorientation profiles between the coalesced bainitic ferrite units formed within the marked areas A and B along the dashed lines (1), (2), and (3) indicated in Figure 4.10.

(obtained from EBSD measurement) shows the disappearance of the initial boundaries in the areas A and B, respectively (see Figure 4.10.c).

Figure 4.11 shows the misorientation profiles, marked by dashed lines (1), (2), and (3) in Figure 4.10.c. The misorientation profile (1) shows a misorientation lower than 3° within the bainitic structure, which indicates the coalescence of several units of bainitic ferrite into a coarser grain with crystallographic homogeneity. On the other hand, the misorientation profiles (2) and (3) show a larger misorientation, in the range of 7.5°-12.5°, between adjacent units of bainitic ferrite. This misorientation is lower than 15°, the minimum limit of misorientation between two units/laths to be considered as two different grains. However, the coalescence of bainite units in area B may be considered partial since these units can exhibit different crystallographic orientations despite the existence of low-angle boundaries between them.

Another interesting observation is the different growing direction of the bainitic and martensitic structures originated close to the free surface. Figure 4.12 shows the growth of these structures along the cross-section of the upper surface of the isothermally treated specimens. As observed, most of the structures originated close to the free surface, independently of their bainitic or martensitic nature, prefer to grow nearly parallel to this surface, which in turn favours the coalescence of bainitic units and/or martensitic

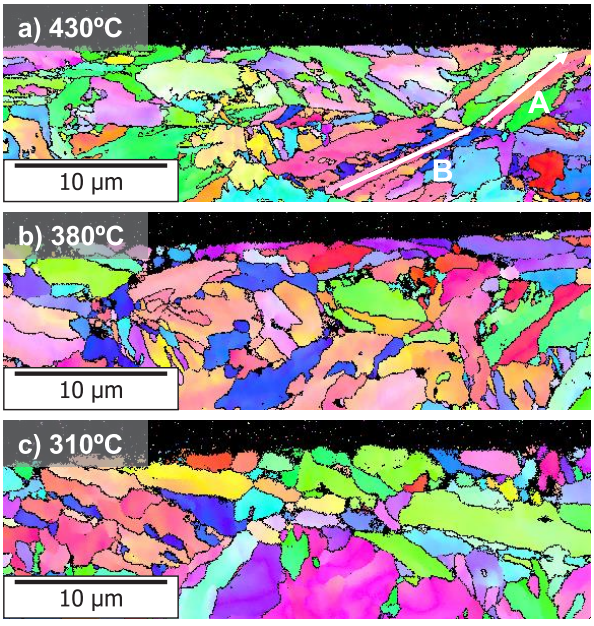

Figure 4.12. Growth of bainitic and martensitic structures along the cross-section of the upper surface of the specimens isothermally treated at a) 430°C, b) 380°C, and c) 310°C. IPF maps from EBSD measurements are used to distinguish individual grains of such structures.

laths. This preferential growth may be due to the maximum reduction of strain energy that a unit or lath can experience by growing in such direction [33].

However, a different growth direction of some structures can be also observed in Figure 4.12.a (indicated by white arrows), where the growth direction of units/laths (A) close to the free surface tends to be more vertical than that of the units/laths (B) at further depth. This preferential growth was also observed in a similar research study performed by Pak et al. [6]. The more vertical growth direction of units/laths (A) (compared to (B) ones) indicates that these units/laths probably start to grow from below the free surface due to a higher reduction of the associated strain energy.

4.4.4. Variant Selection

The reduction at the free surface of the strain energy associated to the formation of bainitic and martensitic structures also affects the diversity of orientation relationships (variant selection) in which bainitic ferrite and martensite grow within an austenite grain. It is well known that bainite and martensite mainly grow with an orientation relationship with respect to the parent austenite close to the one described by the Kurdjumov-Sachs (K-S) [34] orientation model. From this general orientation relationship, 24 equivalent crystallographic variants can be formed from a single austenite grain [35]. Figure 4.13 shows the {001} pole figure of the theoretical K-S orientation relationship. In principle, all variants are expected to be found in a single transformed austenite grain. However, the existence of a free surface can lead to preferential formation of crystallographic variants. This fact is confirmed by the {001} pole figures of individual prior austenite grains obtained from the surface of specimens isothermally treated at 430°C and 310°C,

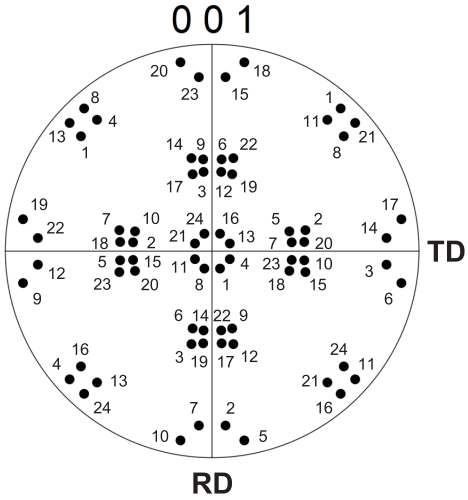

Figure 4.13. {001} pole figure of the theoretical K-S orientation relationship, showing the 24 crystallographic variants that can be formed from an austenite grain.

presented in Figures 4.14.a,c, respectively. In both specimens, the crystallographic patterns of surface grains are incomplete compared to the theoretical pole figure of the K-S orientation relationship [35].

The incompleteness of the crystallographic patterns of surface austenite grains cannot uniquely be attributed to the presence of a free surface since, in the present work, bulk austenite grains also present certain variant selection due to their incomplete crystallographic patterns (see Figures 4.14.b,d). Crystallographic differences may be related to a distinct number of crystallographic variants present in surface grains in comparison to the bulk ones [36]. Results reported by Nambu et al. [36] on a crystallographic analysis of the martensitic transformation in a low-C low-alloyed steel

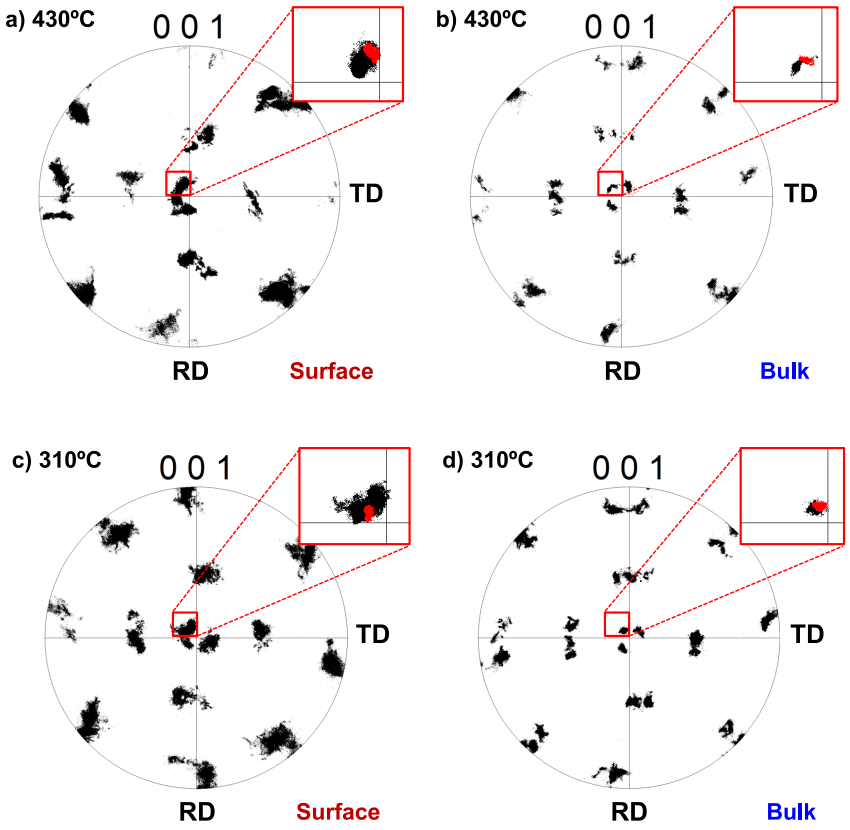

Figure 4.14. {001} pole figures obtained from a single prior austenite grain at the surface and within the bulk of specimens isothermally treated at a-b) 430°C and c-d) 310°C. Note that the EBSD measurements performed in the cross-section of specimens (i.e., in the bulk) were rotated 90° over the TD axis in order to have the same coordination system as that of the surface measurements. Enlarged images of part of the {001} pole figures show the selection (in red colour) of one crystallographic variant for the determination of the dispersion between all data points.

showed the appearance of an increasing number of martensite variants with increasing distance from the free surface until an analysed depth of approximately 30 μm. This was attributed to the presence of a free surface. The reduced strains that need to be accommodated at a free surface and the coalescence of bainite units and/or martensite laths may result in the likely formation of fewer crystallographic variants in surface grains than in the bulk ones. In the present work, however, the distortion of the crystallographic pattern of surface grains in comparison with the theoretical K-S pattern makes it challenging to accurately determine the number of crystallographic variants in surface grains for later comparison.

Table 4.II. Average dispersion between all data points belonging to the crystallographic variant indicated by red colour in {001} pole figures of surface and bulk grains of specimens isothermally treated at 430°C and 310°C, above and below both M_s temperatures, respectively (see Figure 4.14).

Specimen	Grain Location	Dispersion (°)
430°C	Bulk	1.6 ± 0.3
	Surface	1.8 ± 0.3
310°C	Bulk	1.5 ± 0.3
	Surface	1.9 ± 0.3

The more distorted crystallographic patterns obtained from the surface grains in comparison with those obtained from the bulk are clearly observed in pole figures of Figure 4.14. The observed variants in bulk grains are found to be better defined, showing a crystallographic pattern close to the theoretical K-S one. On the contrary, surface grains show more dispersed variants in the crystallographic pattern, showing a certain degree of distortion with respect to the theoretical K-S one. To determine a possible difference in the dispersion of variants in surface and bulk grains, one crystallographic variant was selected from the {001} pole figure of each grain shown in Figure 4.14, where the selected variant is highlighted in red in an enlarged partial image of the crystallographic pattern. Table 4.II shows the average dispersion between all points corresponding to the selected crystallographic variant of the surface and bulk grains of specimens isothermally treated at 430°C and 310°C. The dispersion was determined by considering the crystallographic orientation of a random point of each variant as reference for calculating the alignment of the rest of the points of the variant. This process was performed five times per selected variant to obtain the average dispersion. Results show that differences regarding the dispersion of the crystallographic variants between surface and bulk grains are not significant, although variants formed in surface grains seem to have a higher dispersion. This tendency may be an indication of a larger deviation of the crystallographic pattern of bainitic ferrite and/or martensite formed in surface grains with respect to the theoretical K-S orientation relationship. A further crystallography analysis will be needed in order to determine the deviation from the theoretical K-S orientation model.

4.5. Conclusions

The effects derived from the existence of a free surface on phase transformations involved during isothermal treatments at low temperatures in a low-carbon high-silicon steel were investigated through the combination of in-situ observations by laser confocal microscopy (LCM) and microstructural analysis by electron back scatter diffraction (EBSD) and dilatometry. The conclusions obtained are the following:

1. The final bainitic-martensitic microstructure obtained after the application of heat treatments strongly differs from surface to bulk due to differences on the onset of the martensitic transformation. A higher M_s temperature at a free surface is consequence of the minimized volume strain energy needed for strain accommodation during martensite formation, which implies a lower resistance at the free surface for the transformation to occur. This lower resistance is attributed to the reduction of compression constraints surrounding the surface austenite grains due to the presence of a free surface. Differences on the M_s temperature lead to the formation of distinct volume fractions of micro-constituents, such as bainitic ferrite and martensite, at the free surface compared to the bulk.

2. The temperature range defined by the M_s temperatures corresponding to the free surface and bulk can be considered a critical temperature range for manufacturing these bainitic-martensitic steels due to the observation of larger microstructural differences during isothermal treatments at that temperature range in terms of the type of micro-constituents formed and of their grain size. Such differences are mainly caused by the additional refinement of the micro-constituents originated by the formation of prior athermal martensite at the surface with respect to the bulk. However, this refinement effect can be reduced by the occurrence of grain coalescence, more energetically favourable at a free surface and potentially enhanced by the nearly parallel preferential growing direction of micro-constituents originated close to the surface.

3. There is preferential selection of crystallographic variants in surface grains, independently of the bainitic or martensitic nature of the micro-constituents formed. This may be attributed to the reduced constraints imposed by the free surface and the coalescence of bainitic and martensitic micro-constituents. On the other hand, a higher dispersion of the crystallographic variants formed in surface grains may indicate a larger deviation of the crystallographic pattern of bainitic ferrite and/or martensite from the theoretical K-S orientation relationship. Further investigations are needed to determine this possible deviation.

References

[1] C.E. Ericsson, M.S. Bhat, E.R. Parker, V.F. Zackay. Isothermal studies of bainitic and martensitic transformations in some low alloy steels. Metall. Trans. A, 1976, vol. 7, pp. 1800-1803.

[2] D.H. Kim, J.G. Speer, H.S. Kim, B.C. De Cooman. Observation of an isothermal transformation during quenching and partitioning processing. Metall. Mater. Trans. A, 2009, 40, pp. 2048-2060.

[3] H. Kawata, K. Hayashi, N. Sugiura, N. Yoshinaga, M. Takahashi. Effect of martensite in initial structure on bainite transformation. Mater. Sci. Forum, 2010, vols. 638-642, pp. 3307-3312.

[4] A. Navarro-López, J. Sietsma, M.J. Santofimia. Effect of prior athermal martensite on the isothermal transformation kinetics below M_s in a Low-C High-Si Steel. Metall. Mater. Trans. A, 2016, vol. 47, pp. 1028-1039.

[5] L. Zhao, L. Qian, J. Meng, Q. Zhou, F. Zhang. Below-M_s austempering to obtain refined bainitic structure and enhanced mechanical properties in low-C high-Si/Al steels. Scripta Mater., 2016, vol. 112, pp. 96-100.

[6] J. Pak, D.W. Suh, H.K.D.H. Bhadeshia. Displacive phase transformation and surface effects associated with confocal laser scanning microscopy. Metall. Mater. Trans. A, 2012, vol. 43, pp. 4520-4524.

[7] J.A. Klostermann, W.G. Burgers. Surface martensite in iron-nickel. Acta Metall., 1964, vol. 12, pp. 355-360.

[8] A.P. Baur, C. Cayron, R.E. Logé. Variant selection in surface martensite. J. Appl. Cryst., 2017, vol. 50, pp. 1646-1652.

[9] J.D. Escobar, G.A. Faria, L. Wu, J.P. Oliveira, P.R. Mei, A.J. Ramirez. Austenite reversion kinetics and stability during tempering of a Ti-stabilized supermartensitic stainless steel: Correlative in situ synchrotron x-ray diffraction and dilatometry. Acta Mater., 2017, vol. 138, pp. 92-99.

[10] L.C. Chang, H.K.D.H. Bhadeshia. Microstructure of lower bainite formed at large undercoolings below bainite start temperature. Mater. Sci. Technol., 1996, vol. 12, pp. 233-236.

[11] F.G. Caballero, J. Chao, J. Cornide, C. Garcia-Mateo, M.J. Santofimia, C. Capdevila. Toughness deterioration in advanced high strength bainitic steels. Mater. Sci. Eng. A, 2009, vol. 525, pp. 87-95.

[12] J.H. Pak, D.W. Suh, H.K.D.H. Bhadeshia. Promoting the coalescence of bainite platelets. Scripta Mater., 2012, vol. 66, pp. 951-953.

[13] J.H. Pak, H.K.D.H. Bhadeshia, L. Karlsson. Mechanism of misorientation development within coalesced martensite. Mater. Sci. Tech., 2012, vol. 28, pp. 918-923.

[14] H.F. Lan, L.X. Du, Q. Li, C.L. Qiu, J.P. Li, R.D.K. Misra. Improvement of strength-toughness combination in austempered low carbon bainitic steel: The key role of refining prior austenite grain size. Journal Alloys Compounds, 2017, vol. 710, pp. 702-710.

[15] M. Kang, M.X. Zhang, M. Zhu. In situ observation of bainite growth during isothermal holding. Acta Mater., 2006, vol. 54, pp. 2121-2129.

[16] P. Kolmskog, A. Borgenstam, M. Hillert, P. Hedstrom, S.S. Babu, H. Terasaki, Y. Komizo. Direct observation that bainite can grow below M_s. Metall. Mater. Trans. A, 2012, vol. 43, pp. 4984-4988.

[17] G. Xu, F. Liu, L. Wang, H. Hu. A new approach to quantitative analysis of bainitic transformation in a superbainitic steel. Scripta Mater., 2013, vol. 68, pp. 833-836.

[18] Z. Hu, G. Xu, H. Hu, L. Wang, Z. Xue. In situ measured growth rates of bainite plates in an Fe-C-Mn-Si superbainitic steel. Int. J. Miner. Metall. Mater., 2014, vol. 21, pp. 371-378.

[19] G. Mao, R. Cao, X. Guo, Y. Jiang, J. Chen. In situ observation of kinetic processes of lath bainite nucleation and growth by laser scanning confocal microscope in reheated weld metals. Metall. Mater. Trans. A, 2017, vol. 48, pp. 5783-5798.

[20] S. Sainis, H. Farahani, E. Gamsjäger, S. van der Zwaag. An in-situ LSCM study on bainite formation in a Fe-0.2C-1.5Mn-2.0Cr alloy. Metals, 2018, vol. 8, 498, pp. 1-22.

[21] X. Long, F. Zhang, Z. Yang, M. Zhang. Study on bainitic transformation by dilatometer and in situ LSCM. Metals, 2019, vol. 12, 1534, pp. 1-9.

[22] B. An, C. Zhang, G. Gao, X. Gui, Z. Tan, R.D.K. Misra, Z. Yang. Experimental and theoretical analysis of multiphase microstructure in a newly designed MnSiCrC quenched and partitioned steel to promote bainitic transformation: The significant impact on mechanical properties. Mater. Sci. Eng. A, 2019, vol. 757, pp. 117-123.

[23] C. Celada-Casero, J. Sietsma, M.J. Santofimia. The role of the austenite grain size in the martensitic transformation in low carbon steels. Mater. Design, 2019, vol. 167, 107625.

[24] G. Ghosh, G.B. Olson. Kinetics of fcc → bcc heterogeneous martensitic nucleation I. The critical driving force for athermal nucleation. Acta Metall. Mater., 1994, vol. 42, pp. 3361-3370.

[25] G. Ghosh, G.B. Olson. Kinetics of fcc → bcc heterogeneous martensitic nucleation II. Thermal activation. Acta Metall. Mater., 1994, vol. 42, pp. 3371-3379.

[26] S.M.C. van Bohemen, L. Morsdorf. Predicting the M_s temperature of steels with a thermodynamic based model including the effect of the prior austenite grain size. Acta Mater., 2017, vol. 125, pp. 401-415.

[27] G.B. Olson, M. Cohen. A general mechanism of martensitic nucleation: Part II. Fcc → bcc and other martensitic transformations. Metall. Trans. A, 1976, vol. 7, pp. 1905-1914.

[28] T.J. Nichol, G. Judd, G.S. Ansell. The relationship between austenite strength and the transformation to martensite in Fe-10 pct Ni-0.6 pct C alloys. Metall. Trans. A, 1977, vol. 8, pp. 1877-1883.

[29] P.J. Brofman, G.S. Ansell. On the effect of fine grain size on the M_s temperature in Fe-27Ni-0.025C alloys. Metall. Trans. A, 1983, vol. 14, pp. 1929-1931.

[30] J. Hidalgo, M.J. Santofimia. Effect of prior austenite grain size refinement by thermal cycling on the microstructural features of as-quenched lath martensite. Metall. Mater. Trans. A, 2016, vol. 47, pp. 5288-5301.

[31] A. Navarro-López, J. Hidalgo, J. Sietsma, M.J. Santofimia. Influence of the prior athermal martensite on the mechanical response of advanced bainitic steel. Mater. Sci. Eng. A, 2018, vol. 735, pp. 343-353.

[32] J. Feng, T. Frankenbach, M. Wettlaufer. Strengthening 42CrMo4 steel by isothermal transformation below martensite start temperature. Mater. Sci. Eng. A, 2017, vol. 683, pp. 110-115.

[33] F.R.N. Nabarro. Dislocations in solids: dislocations in crystals. North Holland, The Netherlands, 1979.

[34] G. Kurdjumov, G. Sachs. Über den Mechanismus der Stahlhärtung. Z. Phys., 1930, vol. 64, pp.325-343.

[35] S. Morito, H. Tanaka, R. Konishi, T. Furuhara, T. Maki. The morphology and crystallography of lath martensite in Fe-C alloys. Acta Mater., 2003, vol. 51, pp. 1789-1799.

[36] S. Nambu, N. Shibuta, M. Ojima, J. Inoue, T. Koseki, H.K.D.H. Bhadeshia. In situ observations and crystallographic analysis of martensitic transformation in steel. Acta Mater., 2013, vol. 61, pp. 4831-4839.

5

CHAPTER 5

In-situ Investigation of Carbon Enrichment in Austenite during Isothermal Holdings around the M_s Temperature by High Energy X-Ray Diffraction

**This chapter is based on the article "In-situ investigation of carbon enrichment in austenite during isothermal holdings around the M_s temperature by high energy X-ray diffraction" by A. Navarro-López, J. Hidalgo, C.A. Fitriani, R.M. Huizenga, B. Kim, J. Sietsma, and M.J. Santofimia, to be submitted for publication.*

Abstract

The isothermal growth of bainitic ferrite in low-carbon steels generally implies the diffusion of carbon to the surrounding untransformed austenite, increasing its thermal and mechanical stability. During isothermal holdings above the martensite start (M_s) temperature, the carbon enrichment of austenite can be directly evaluated from the evolution of the austenite lattice parameter since only bainite and austenite coexist in the microstructure. However, during isothermal holdings below M_s, the austenite lattice parameter is affected by the compressive strains associated to martensite formation and by the carbon diffusion from bcc-phases martensite and bainite. This makes the evaluation of the process of carbon redistribution below M_s very challenging by means of conventional characterization techniques. For this reason, in-situ high energy X-ray diffraction measurements are carried out to quantitatively determine the kinetics of carbon partitioning from bcc-phases into austenite during an isothermal treatment below M_s in a low-carbon high-silicon steel. Results show that the formation of a certain fraction of martensite (> 0.2) induces compressive strains in the untransformed austenite, showing a linear dependence with the increasing martensite fraction. Furthermore, the kinetics of the relative carbon enrichment of austenite during isothermal holdings above and below M_s is observed to be slower than the kinetics of bainite formation. This is attributed to a slower carbon redistribution kinetics throughout the austenite grains, which depends on the combined effect of carbon diffusivity and the remaining austenite fraction at each temperature.

5.1. Introduction

The isothermal formation of bainite above the martensite start (M_s) temperature has been widely studied in different steel compositions for years. It is well-accepted that carbon will diffuse into the untransformed austenite during the formation of bainitic ferrite. However, there exists an extensive debate about the bainite growth mechanism. The main point of discrepancy between the two theories proposed for bainite growth is whether it is controlled by carbon diffusion (diffusional theory) [1-6] or, on the contrary, carbon diffuses into the untransformed austenite once bainite growth has finished (diffusionless theory) [7-11]. Independent of the growth mechanism, there is carbon enrichment of the untransformed austenite as a consequence of the bainite reaction, increasing the austenite stability against the thermal and mechanical martensite formation.

Carbon enrichment of austenite is also expected to occur in isothermal holdings below M_s due to carbon redistribution coming from bainite formation, but also from the carbon-supersaturated prior athermal martensite (PAM) formed in the interrupted cooling below M_s. The carbon trapped within the carbon-supersaturated martensite can be partially segregated to defects, partially released into the surrounding austenite, and partially precipitated in the form of carbides within the martensite. These processes can occur simultaneously during the isothermal holding below M_s, overlapping with the formation of bainitic ferrite. Carbon enrichment of austenite thus depends on the effectiveness of each one of the described competing phenomena. Changes in the austenite chemical composition are reflected, to some extent, in its lattice parameter, from which values of carbon concentration can be determined. An increase of the carbon concentration in the austenite diffusing from martensite and/or bainitic ferrite during isothermal holdings below M_s implies an increase in the austenite lattice parameter. However, compressive strains induced in the untransformed austenite due to martensitic transformation, as reported in [12-15], can lead to an underestimation of the austenite carbon concentration.

The complexity of the simultaneous phenomena occurring in isothermal holdings below M_s makes it challenging to elucidate the effectiveness of carbon enrichment in the untransformed austenite by conventional characterization techniques. In addition, there is limited scientific knowledge regarding the evolution of austenite carbon enrichment during holdings below M_s. Recent research on quenching and partitioning low-carbon steels by high-energy X-ray diffraction has demonstrated that this high-resolution technique is a reliable method to in-situ characterize the transformation of austenite into martensite (and bainitic ferrite) as well as the austenite carbon enrichment [16,17]. In the present work, the kinetics of the austenite carbon enrichment during phase transformations occurring in isothermal holdings below M_s is quantitatively determined by in-situ high energy X-ray diffraction measurements in a low-carbon high-silicon

steel. For comparison, similar measurements are performed during additional thermal treatments, such as a direct quench and an isothermal holding above M_s, to support the interpretation of the phenomena.

5.2. Experimental Procedure

The steel investigated in this study has a chemical composition of 0.2C-3.51Mn-1.52Si-0.25Mo-0.04Al (wt. pct). The material was produced by casting followed by a hot rolling process of several steps to obtain a final 4 mm-thick steel slab. Small blocks of 50 x 10 x 4 mm^3 were machined from the hot-rolled slab, parallel to the rolling direction (RD), for later homogenization to reduce the inhomogeneous distribution of substitutional alloying elements, such as manganese (Mn) and silicon (Si), along the slab thickness, as reported in Chapter 2. These blocks were first sealed within quartz tubes, as shown in Figure 5.1.a, and then introduced into a furnace chamber to apply a homogenization treatment at 1250°C for 48 hours. All quartz tubes contained an inert atmosphere of argon (Ar) gas at a pressure of 200 mbar to avoid oxidation or decarburization.

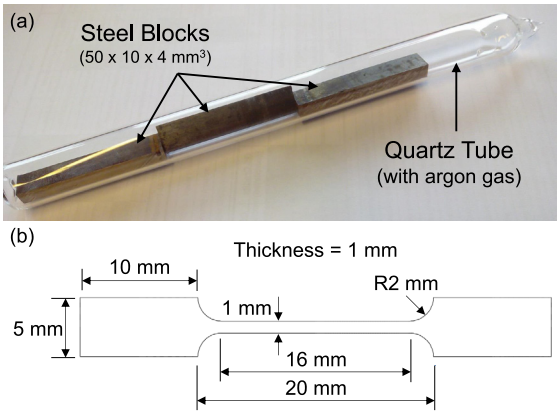

Figure 5.1. (a) Quartz tube containing several steel blocks before applying the homogenization treatment. (b) Scheme of the flat double T-shaped specimen used for in-situ SXRD measurements.

After homogenization, the steel blocks were extracted from the quartz tubes and fully austenitized twice in a salt bath at 900°C for 4 minutes followed by water quenching in order to refine the prior austenite grain size. Grain refinement was performed to obtain an austenite grain size similar to that of specimens of the same steel composition studied in Chapters 2 and 3 and, in turn, to avoid spotty X-rays diffraction patterns during in-situ high energy X-ray diffraction (HE-XRD) measurements. Flat double T-shaped specimens were finally electro-discharge machined from the homogenized and grain-refined blocks. Two specimens were extracted from the bulk of each steel block, discarding the material close to its surfaces. The dimensions of these specimens are depicted in Figure 5.1.b. The specimen gauge had a length of 16 mm with a cross-

section of 1.0 x 1.0 mm^2. Specimen surfaces were metallographically prepared for in-situ measurements by grinding until a 2000 grit silicon carbide sandpaper to remove the oxide superficial layer originated after machining.

In-situ X-ray diffraction measurements using high-energy radiation were carried out at the ID11 beamline of the European Synchrotron Radiation Facility (ESRF) in Grenoble, France. A mono-chromatic X-ray beam of about 80 keV (measured wavelength of λ = 0.15582 Å) with a beam size of 200 x 200 µm^2 was used in transmission measurements through the gauge geometry of the specimen, as shown in Figure 5.2.a. Diffraction patterns were recorded by a two dimensional CCD FReLoN (charge coupled device – fast readout, low noise [18]) detection camera system of 2048 x 2048 pixel^2 with a dimension of 50 x 50 µm^2/pixel, placed at a distance from the specimen of approximately 300 mm. A cerium dioxide (CeO_2) standard calibrant (NIST SRM 674b) was placed on the top surface of each specimen to determine relevant instrumental parameters, such as the position of the beam centre, the tilt angle of the detector with respect to the direct beam, and the specimen-to-detector distance, for a correct post-processing of the diffraction data. From this experimental set-up, the diffraction rings of the first four {hkl} planes of fcc and bcc phases were able to be captured during in-situ time-resolved measurements, as indicated in Figure 5.2.b. The 2D diffraction patterns were acquired at an exposure time of 0.1 s and continuously recorded during the application of the heat treatments with an effective measurement interval of 0.7 s.

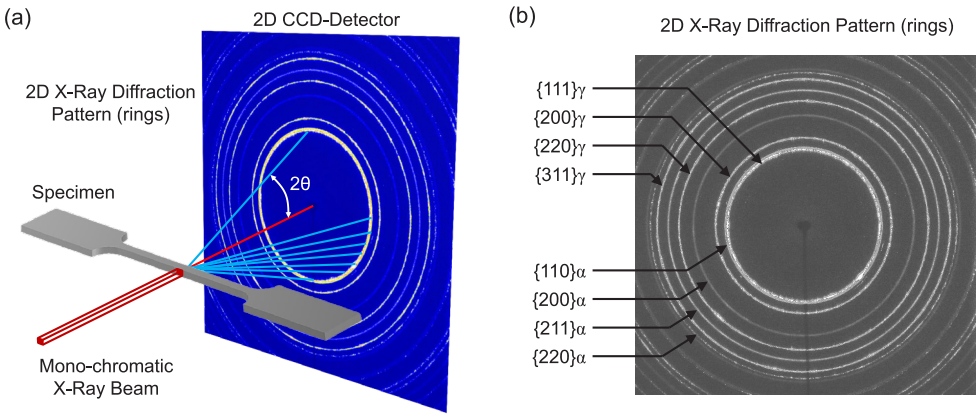

Figure 5.2. (a) Schematic representation of the transmission measurements by in-situ SXRD. (b) Characteristic 2D diffraction pattern obtained by the CCD detection camera system, where the diffraction rings of the main {hkl} planes of fcc and bcc phases are captured (indicated by arrows).

An Instron/NPL electro-thermal mechanical testing (ETMT) machine was used to apply the heat treatments. This machine works similarly as the commonly known Gleeble. In this case, the 'load control' mode was selected to perform the heat treatments without

the application of any load, obtaining as output parameter the displacement (change in length) of the specimen as a function of temperature. Specimens were gently placed between the clamps of the device and thermally treated by ohmic heating, which consists of the passage of electric current through the specimen to heat it. The temperature during the heat treatments was controlled by an R-type thermocouple spot-welded on the bottom surface at the centre of the gauge of the specimens. A continuous flow of argon (Ar) gas was flushed into the ETMT heating chamber during the application of heat treatments providing an inert atmosphere to avoid oxidation and decarburization. Figure 5.3 shows the heat treatments applied after a full austenitization at 900°C for 240 s, consisting of (i) a rapid cooling at 40°C/s to determine the experimental M_s temperature as well as the strains introduced due to the formation of athermal martensite, and (ii) isothermal treatment at 350°C and 305°C for one hour to determine the kinetic evolution of the bainite reaction and the carbon enrichment of the untransformed austenite during holding at temperatures above and below M_s, respectively. The isothermal treatments ended with a final cooling to room temperature at a rate of 20°C/s.

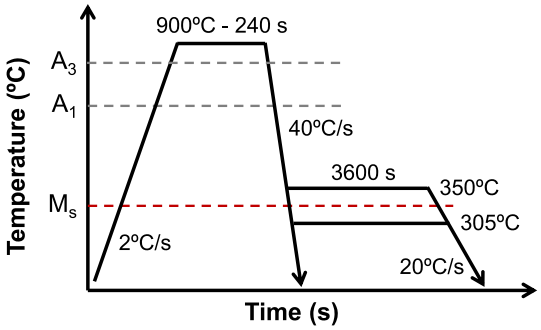

Figure 5.3. Heat treatments applied during in-situ HE-XRD measurements.

Once the experimental measurements were performed, the acquired 2D diffraction patterns were post-processed using the Fit2D data analysis software [19,20]. Three corrections were first applied to the raw diffraction patterns to minimize possible distortion introduced by the 2D detector system during the acquisition of diffraction data [21]. These corrections consisted of: 1) subtraction of the dark current signal (background), 2) correction for the detector flat field (related to the sensitivity of each detector pixel), and 3) correction for the detector spatial distortion. The corrected diffraction patterns were then refined by fine-tuning the beam centre, the tilt angle of the detector with respect to the direct beam, and the specimen-to-detector distance using the values obtained from the calibration measurement. The 2D diffraction patterns (rings) were finally integrated along the scattering angle (2θ) over the total range of 360° azimuthal angle to obtain a 1D diffraction pattern in which the diffraction intensity is represented as a function of 2θ angle.

The {200}γ and {220}γ reflections from fcc phase (austenite) and the {200}α and {211}α reflections from bcc phases (martensite and bainitic ferrite) were individually fitted to a pseudo-Voigt function. The position, intensity, and width of these {hkl} reflections were determined. Diffraction peaks of bcc phases martensite and bainitic ferrite cannot be distinguished since both phases exhibit the same crystal structure and, as consequence, there is an almost total overlapping of their respective {hkl} reflections. The volume fractions of fcc and bcc phases were calculated from the integrated intensity of the {hkl} reflections selected for the analysis. The volume fraction of austenite (f_γ) was obtained from the ratio of the measured integrated intensities of fcc ($I_{\gamma,i}$) and bcc ($I_{\alpha,i}$) diffraction peaks with respect to the R-values by [22]:

$$f_\gamma = \frac{\frac{1}{N}\sum_{i=1}^{N}\left(\frac{I_{\gamma,i}}{R_{\gamma,i}}\right)}{\frac{1}{N}\sum_{i=1}^{N}\left(\frac{I_{\gamma,i}}{R_{\gamma,i}}\right)+\frac{1}{M}\sum_{i=1}^{M}\left(\frac{I_{\alpha,i}}{R_{\alpha,i}}\right)} \tag{5.1}$$

where the subscript i refers to the Miller indexes {hkl} of the analysed reflection, N and M are the total number of {hkl} reflections of the fcc and bcc phases considered in the calculation, respectively, $R_{\gamma,i}$ and $R_{\alpha,i}$ are the normalization factors for the corresponding reflections of fcc and bcc phases, respectively. These latter factors depend on the interplanar spacing (d_{hkl}), the Bragg's angle (θ), the crystal structure (fcc or bcc), and the composition of the phase, and were calculated as described in [12]. In the present work, the possible effect of texture on the relative intensity of the {hkl} reflections is considered to be negligible since the integrated intensity of all reflections was obtained from the integration of the diffraction ring over the total range of 360° azimuthal angle. The volume fraction of bcc phase (f_α) was then calculated from the balance $f_\alpha = 1\text{-}f_\gamma$.

Changes in lattice parameter of the fcc and bcc phases are related to variations in the diffraction angle (2θ) at which the {hkl} reflections are found in the diffraction pattern. The lattice parameter of both phases (a_γ and a_α) was determined as the average value of those obtained from the individual {hkl} reflections considered for the analysis using

$$a_{\gamma/\alpha} = \frac{1}{N}\cdot\sum_{1}^{N}\left(\frac{\lambda}{2\cdot\sin(\theta_{hkl})}\cdot\sqrt{h^2+k^2+l^2}\right) \tag{5.2}$$

where the well-known Bragg's Law, which relates the diffraction angle with the wavelength (λ) of the mono-chromatic incident X-ray beam and the interplanar spacing (d_{hkl}) between {hkl} planes, was combined with the formula for cubic crystals that relates the interplanar spacing with the lattice parameter. The average carbon concentration

in the fcc-austenite phase was determined from its average lattice parameter at a given temperature (T) following the expression:

$$a_\gamma(T) = \left(a_{\gamma 0} + k_C \chi_C + \sum\left(k_i \chi_i\right)\right) \cdot \left(1 + \beta_\gamma \left(T - 300\text{K}\right)\right) \quad (5.3)$$

where $a_{\gamma 0}$ is the austenite lattice parameter in pure iron at room temperature (300 K), k_C and k_i are the proportionality factors for carbon and the alloying element i (where i = Mn, Si, Mo, Al), respectively, χ_C and χ_i are the concentration (wt.%) of carbon and the alloying element i within austenite, respectively, the parameter β_γ is the coefficient of thermal expansion of austenite, and T is the applied temperature expressed in Kelvin. In the present work, the concentration of alloying elements (Mn, Si, Mo, Al) in austenite is assumed to be constant during the heat treatments.

5.3. Results & Discussion

5.3.1. The M_s temperature

The evolution of the volume fraction and lattice parameter of the bcc-phase determined from HE-XRD measurements during rapid cooling from austenitization to room temperature is shown in Figures 5.4.a and 5.4.b. These results originate from different heat-treated specimens, namely (I) and (II), respectively, which were cooled under the same conditions. Particularly, the M_s temperature results difficult to be determined from these HE-XRD measurements. As observed, bcc-phase starts to form at temperatures higher than 400°C. However, there is no significant deviation from linearity in the evolution of its lattice parameter until reaching temperatures in a range between 315°C and 335°C. Within this temperature range, a rather abrupt change in the lattice parameter of the bcc-phase occurs (see Figures 5.4.a and 5.4.b). From this inflection point, there is an initial increase of the lattice parameter until a certain fraction of bcc-phase is formed, from where the lattice parameter starts to decrease with decreasing temperature.

To determine a more accurate value of the M_s temperature, a similar heat treatment (austenitization at 900°C for 240 s followed by rapid cooling at 20°C/s) as that performed in HE-XRD experiments was applied by dilatometry to a cylindrical specimen of 10 mm length and 3.5 mm diameter of the same steel composition. Previously, this specimen was sealed in a quartz tube and homogenized in the same conditions as those applied to HE-XRD specimens (see 'Experimental Procedure'). Subsequently, two grain-refinement treatments were performed by dilatometry to the homogenized cylindrical specimen. Figure 5.4.c shows the evolution of martensite fraction during cooling from austenitization to room temperature as well as the change in length of the cylindrical specimen due to the austenite-to-martensite transformation.

The experimental M_s temperature is determined as $M_{s\,(1\%)}$ = 327°C ± 5°C, following the procedure described in Chapter 2. This value corresponds well with the start temperature of bulk martensitic transformation. The continuous linear contraction during cooling until the M_s temperature indicates the absence of any decomposition of austenite into ferrite, pearlite, or bainite within the bulk of the specimen.

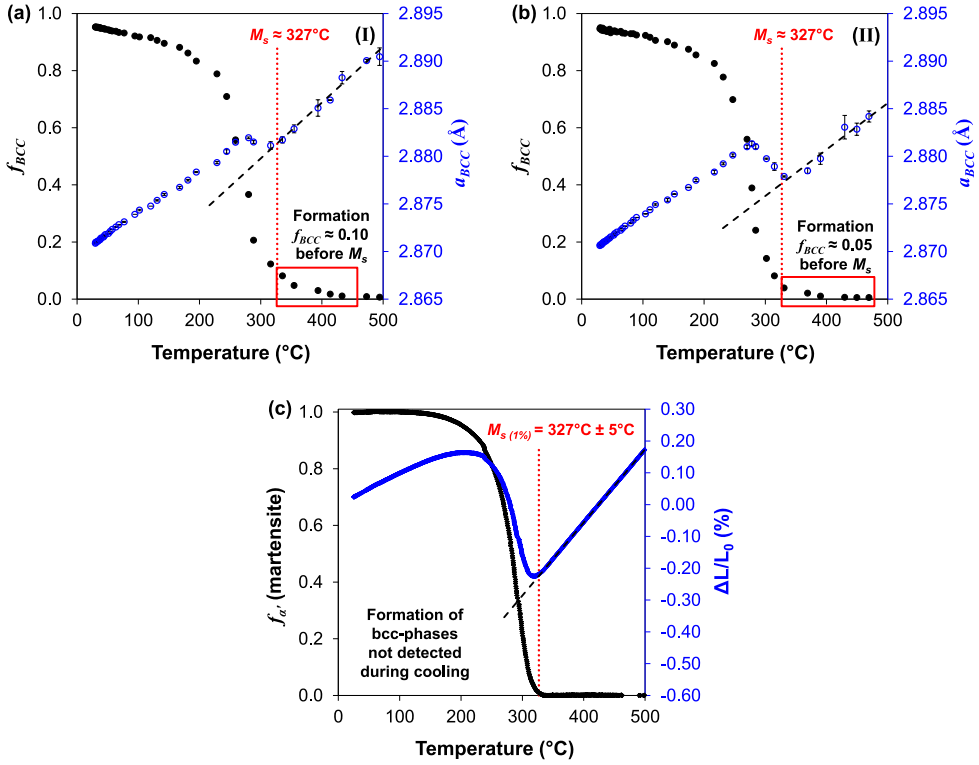

Figure 5.4. Evolution of the volume fraction and lattice parameter of bcc-phase during rapid cooling from austenitization in steel specimens (a) (I) and (b) (II). (c) Evolution of the volume fraction of athermal martensite and the change in length (expansion) originated by the martensitic transformation during a rapid cooling at 20°C/s applied by dilatometry.

Implementing the experimental M_s temperature obtained by dilatometry in the evolution of the bcc-phase lattice parameter, as depicted in Figures 5.4.a and 5.4.b, this temperature fits perfectly well within the previously defined temperature range (315-335°C) at which a significant change in the lattice parameter occurs. The M_s temperature is thus considered to be 327°C for further analysis of HE-XRD results. However, if this is so, a certain fraction of bcc phase is formed before reaching the M_s temperature, as observed in Figures 5.4.a and 5.4.b. In this case, the formed volume fraction varies between 0.05 and 0.10. The fact that dilatometry does not detect such a significant bcc phase fraction during cooling till M_s suggests that phase transformations detected in

HE-XRD measurements in that particular temperature range are primarily taking place at the free surface of heat-treated specimens.

Investigations performed in Chapter 4 on austenite-to-martensite transformations by in-situ laser confocal microscopy (LCM) in the same steel showed the formation of athermal martensite (and even bainitic ferrite) at the free surface of specimens at a temperature approximately 60°C higher than the temperature for martensite formation within the specimens' bulk. This fact has been repeatedly reported for different types of steels, with differences between surface and bulk M_s temperatures ranging from 5°C to more than 150°C [13,23-26]. In the present work, the results obtained from HE-XRD measurements are consistent with these observations. The formation of a certain fraction of bcc phase before reaching M_s is considered to take place mainly at the free surface of specimens as a consequence of the higher temperature at which the martensitic transformation starts to occur at the surface compared to bulk.

On the other hand, the initial increase of the lattice parameter of bcc-phase (in this case, athermal martensite) can be attributed to the rapid martensite formation taking place within the bulk of specimens. The reasons of such abrupt increase can derive from two different phenomena. Assuming that athermal martensite inherits the carbon concentration of the parent austenite during its transformation, a carbon concentration gradient in the parent austenite can partially cause the increase of the martensite lattice parameter. The bulk martensitic transformation would start on austenite regions that are poorer in carbon to continue in the ones richer in carbon. However, the homogenization pre-treatment performed to all specimens makes this phenomenon less likely.

The abrupt changes of the lattice parameter of bcc-phase could be also caused by the evolution of the state of stress of the untransformed austenite as the martensite formation progresses. This state of stress balances with the thermal compression of both phases derived from decreasing temperature. However, there is still debate within the scientific community about the type of micro-stresses (compressive or tensile) developed in both phases during the austenite-to-martensite transformation. A further analysis of the state of strains in austenite due to martensite formation is presented in the following section.

5.3.2. Strains Imposed by Martensite Formation

Figures 5.5.a and 5.5.c show the austenite lattice parameter during cooling from austenitization until room temperature of the specimens (I) and (II), respectively. In both coolings, the austenite lattice parameter linearly decreases with temperature until reaching M_s. When bulk martensite starts to form, the austenite lattice parameter contracts with respect to the linear fit of the measured thermal contraction (represented by a dashed blue line). This deviation is consequence of martensite formation, which is

known to induce compressive strain in the untransformed austenite [12-15,17]. Figures 5.5.b and 5.5.d show the estimated transformation strain, $\varepsilon_{transf.}$, induced in the austenite as a function of the volume fraction of martensite formed during cooling from the M_s temperature. The transformation strain was calculated by

$$\varepsilon_{transf.} = \frac{a_{\gamma,\exp} - a_{\gamma,TC}}{a_{\gamma,TC}} \tag{5.4}$$

where $a_{\gamma,exp}$ is the experimentally measured lattice parameter of untransformed austenite and $a_{\gamma,TC}$ is the lattice parameter of austenite extrapolated from the linear fit of its thermal contraction.

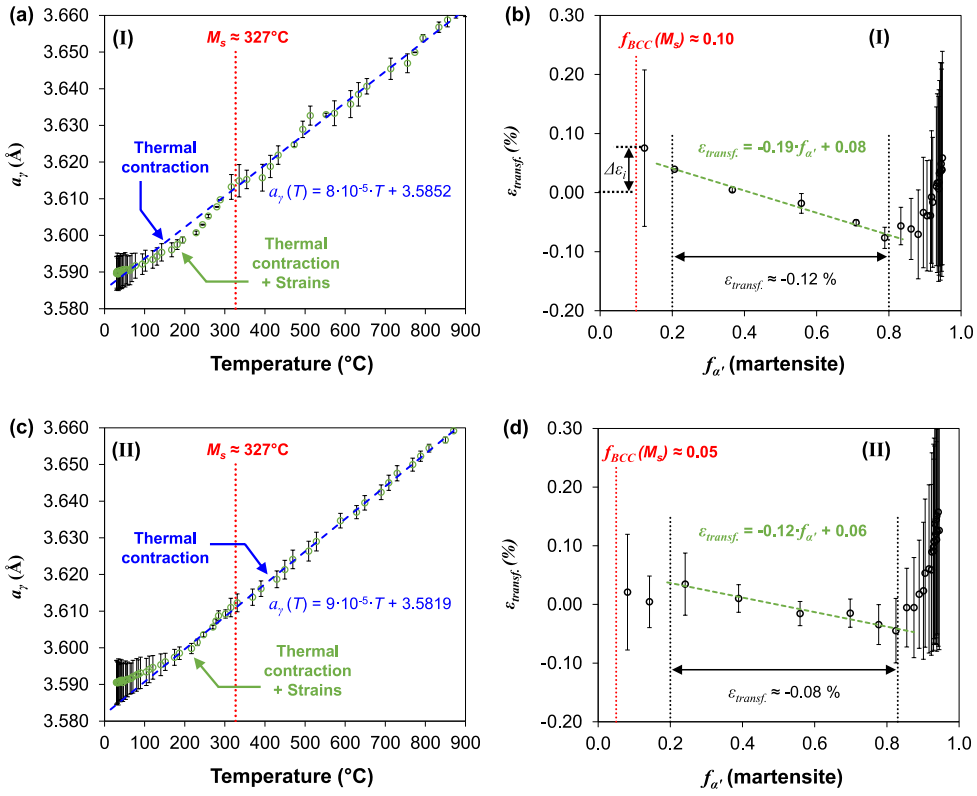

Figure 5.5. (a)-(c) Evolution of the average lattice parameter of austenite during cooling from austenitization until room temperature. The dashed blue line represents the linear fit of the thermal contraction of austenite until reaching the M_s temperature. (b)-(d) Estimated transformation strain built up in the untransformed austenite as function of the martensite fraction.

As observed in Figures 5.5.b and 5.5.d, the austenite experiences a small tensile strain when the volume fraction of martensite formed is still lower than 0.2. As the formation of martensite progresses, the state of strain in the untransformed austenite reverses. Thus,

when the formation of martensite varies from 0.2 to 0.8 volume fraction, significant compressive strains are experienced by the remaining untransformed austenite. There seems to be a linear relationship between the compressive strains built up in the untransformed austenite and the volume fraction of martensite formed. Similar observations have been recently reported by Villa et al. [13]. The reversion of the state of strain of the untransformed austenite with the progress of the martensitic transformation is related to the type of micro-stresses (compression or tension) acting in both phases. These micro-stresses are generally compressive in the minority phase and tensile in the majority phase as the austenite-to-martensite transformation progresses [13].

In the present work, the calculated strain introduced by martensite volume fractions lower than 0.2 is uncertain due mainly to a significant scatter in these measurements (see Figures 5.5). Due to these uncertainties, for volume fractions of martensite lower than 0.20 formed prior the isothermal bainite reaction, the effect of strains associated to the martensitic transformation on the austenite lattice parameter will not be considered in further analysis of carbon enrichment.

5.3.3. Coefficient of Thermal Expansion of Austenite

The coefficient of thermal expansion (CTE) of austenite is determined based on the evolution of the austenite lattice parameter during the cooling stage of all heat treatments considering the temperature range between 500°C and 900°C. In this range, austenite is the only phase present in the microstructure. Table 5.I displays the average CTE of austenite obtained from each heat treatment as well as the average CTE of austenite of the steel composition. The CTE of austenite is calculated from the evolution of the average austenite lattice parameter obtained from the individual {200}γ and {220}γ reflections of the austenite phase. In the present work, the average CTE of austenite results to be $(2.42 \pm 0.04)\cdot10^{-5}$ K^{-1}. This value is in good agreement with those reported in similar in-situ investigations of quenching and partitioning treatments of low-carbon steels [16,17]. It is also noted that the calculated average CTE of austenite corresponds well with the thermal expansion coefficients evaluated for a wide range of carbon concentrations in steel by Onink et al. [27] and Van Bohemen [28].

Table 5.I. Coefficient of thermal expansion (CTE) of austenite calculated from the evolution of the austenite lattice parameter during rapid cooling between 900°C and 500°C for all heat treatments.

Heat Treatment	CTEγ (10^{-5} K^{-1})
Direct cooling (I)	2.28 ± 0.06
Direct cooling (II)	2.46 ± 0.12
Holding at 350°C	2.62 ± 0.08
Holding at 305°C	2.43 ± 0.03
AVERAGE	**2.42 ± 0.04**

5.3.4. Kinetics of Bainite Reaction

The decomposition of austenite into bcc-phases during the application of the isothermal treatments is shown in Figure 5.6.a. Above M_s, the formation of approximately 0.05 volume fraction of bcc-phase(s) is observed before the isothermal holding. As indicated in previous sections, these bcc-phases can correspond to bainitic ferrite and martensite formed at the free surface of the heat-treated specimen. During the isothermal holding at 350°C, there is formation of a maximum fraction of bainitic ferrite of 0.55. Once the isothermal holding is finished, part of the remaining austenite is decomposed into fresh martensite (approximately 0.29 volume fraction) during the final cooling from the isothermal temperature. The rest of the untransformed austenite (0.11 volume fraction) is retained at room temperature.

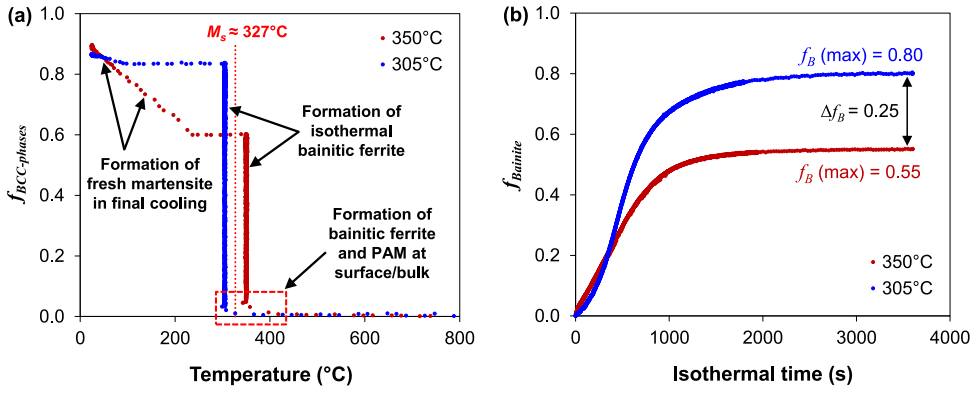

Figure 5.6. (a) Evolution of the bcc-phase(s) volume fraction during the isothermal treatments performed at 350°C and 305°C, including both coolings, from austenitization to the isothermal temperature and the final cooling to room temperature. (b) Kinetics curves of the bainite reaction obtained from the one hour isothermal holding performed at 350°C and 305°C.

The sequence of phase transformations during the isothermal treatment at 305°C, below M_s, is similar to the one previously described, as observed in Figure 5.6.a. During the rapid cooling from the austenitization, only 0.01 volume fraction of bcc-phase(s) is formed at the free surface of the heat-treated specimen before reaching the M_s temperature. The continued cooling until the isothermal temperature leads to the formation of approximately 0.02 volume fraction of athermal martensite. During the isothermal holding at 305°C, a maximum volume fraction of 0.80 bainitic ferrite is formed after one-hour holding time. During the final cooling from the isothermal temperature, less than 0.04 volume fraction of the remaining untransformed austenite decomposes into fresh martensite, while 0.13 volume fraction is retained at room temperature.

Based on experiments (I) and (II) (Figure 5.5), the martensite fraction formed just before reaching 305°C (below M_s) should have been higher than 0.02. In addition,

previous dilatometry measurements using the same steel composition also show the formation of martensite fractions ranging from 0.1 to 0.2 before applying isothermal holdings at similar temperatures (see Chapter 2). The discrepancy between the measured and the expected fraction can be due to differences in chemical composition and/or deviations in the temperature measurement. Electron probe micro-analysis (EPMA) measurements performed after heat treatments show that all specimens present similar concentrations of alloying elements. Therefore, the most probable source of discrepancy may be an instrumental error introduced in the temperature measurement due to the use of distinct thermocouples for each thermal treatment.

On the other hand, Figure 5.6.b shows that, at 350°C, the transformation kinetics is faster at the beginning of the bainite reaction and becomes slower as it progresses. However, at 305°C, the bainite reaction kinetics is slower at the beginning of the transformation and becomes faster, up to a certain point, with holding time. As opposed to the kinetic results shown in Chapter 2, the expected acceleration on bainite kinetics below M_s as consequence of the formation of prior athermal martensite is not observed in bainite reaction kinetics at 305°C. The non observation of this accelerating effect can be ascribed to the progressive formation of bcc-phases during cooling, starting at the specimen's surface and continuing towards the centre of the bulk, and to the formation of a non-significant enough martensite fraction within the specimen's bulk. Further investigations are needed to elucidate the origin of the observed kinetic discrepancy.

Comparing both isothermal holdings, the volume fraction of bainitic ferrite formed below M_s is 0.25 higher than that formed above M_s. At both temperatures, the bainite reaction is incomplete after the isothermal holding since part of the austenite still remains untransformed. Furthermore, as observed in Figure 5.6.a, the experimental M_s temperature during the final cooling, at which fresh martensite starts to form, is found to be at 240°C and 98°C after the application of the isothermal holding at 350°C and 305°C, respectively. This difference is an indication of the higher stability of the remaining austenite after the bainite reaction at 305°C. This higher stability may be primarily due to a higher carbon enrichment of austenite during the isothermal holding below M_s.

5.3.5. Carbon-enrichment in Austenite

Figure 5.7 shows the evolution of the average lattice parameter of the austenite during the isothermal holding at 350°C and 305°C. As observed, there is an increase in the austenite lattice parameter at both temperatures, although this increase is much higher after the one-hour holding at 305°C, coinciding with the formation of a higher volume fraction of bainite (Figure 5.6.b). Changes in the austenite lattice parameter can be directly affected by 1) strains introduced by the formation of prior athermal martensite,

2) relaxation of these transformation strains, 3) carbon enrichment from bcc-phases, and 4) strains derived from bainite formation. Results described in Section 5.3.2 show that martensite formation introduces compressive strains in the untransformed austenite when the martensite fraction formed is higher than 0.2. In the present work, despite uncertainty in the type of strains introduced for martensite fractions lower than 0.2, these transformation strains are unlikely to significantly affect the average lattice parameter of austenite since the fraction of martensite formed before both isothermal holdings is small (< 0.05). Consequently, there should not be a detectable effect of the phenomenon of strain relaxation in the austenite lattice parameter.

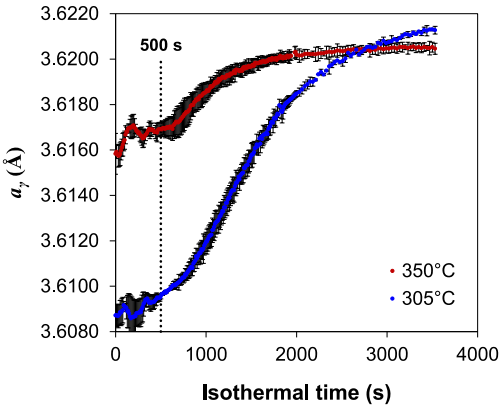

Figure 5.7. Evolution of the average lattice parameter of austenite during isothermal holdings at 350°C and 305°C.

The evolution of the austenite lattice parameter during the isothermal holding at both temperatures is thus considered to be mainly affected by the increase of its carbon concentration and the possible introduction of strains by bainite formation. Several empirical formulae correlating the austenite lattice parameter with its chemical composition can be used to estimate the evolution of carbon enrichment of the untransformed austenite [12,27,29-32]. Considering the generic expression of Equation (5.3), all empirical formulae differ quantitatively in the main terms such as the austenite lattice parameter in pure iron ($a_{\gamma 0}$) at room temperature and/or the proportionality factors for carbon and alloying elements (k_C and k_i, respectively). Distinct levels of uncertainty for the carbon enrichment in austenite can thus result due to differences in these terms as well as in the CTE of austenite used to consider the effect of temperature on the austenite lattice parameter.

For a better interpretation of the phenomenon of carbon enrichment, three formulae are used in the present work to determine the carbon concentration within austenite during the isothermal holding. These formulae are described as:

$$a_\gamma = 3.556 + 0.0453\chi_C + 0.00095\chi_{Mn} + 0.0056\chi_{Al} \quad [12] \quad (5.5)$$

$$a_\gamma = 3.578 + 0.033\chi_C + 0.00095\chi_{Mn} + 0.0056\chi_{Al} + 0.0031\chi_{Mo} \quad [30] \quad (5.6)$$

$$a_\gamma = 3.572 + 0.033\chi_C + 0.0012\chi_{Mn} + 0.0056\chi_{Al} - 0.00157\chi_{Si} \quad [32] \quad (5.7)$$

where the austenite lattice parameter is expressed in Ångstrom (Å) and χ_i corresponds to the weight percent of the element i in the austenite (i = C, Mn, Al, Si, Mo). The effect of the temperature on the lattice parameter is corrected by applying the CTE of austenite calculated for each specific isothermal treatment (see Table 5.I) through the second factor of Equation (5.3). It is noted that Equation (5.5) [12] significantly differs from Equation (5.6) [30] and Equation (5.7) [32] with respect to the values used for the austenite lattice parameter in pure iron and the proportionality factor of carbon. On the other hand, Equation (5.6) presents a distinct proportionality factor for manganese and considers the effect of silicon to be negligible, compared to Equation (5.7) which takes into consideration this element but neglects molybdenum.

Table 5.II. Estimation of carbon concentration in austenite by Equations (5.5)-(5.7) at the initial (C_i) and at the end (C_f) of the isothermal bainite reaction at 350°C and 305°C. Differences between the estimated initial carbon concentration and the nominal one as well as the absolute carbon enrichment in austenite after the isothermal holding are calculated.

T (°C)	Eq. [ref.]	C_i in γ (wt.%)	$(C_i - C_{nom.})$ (wt.%)	C_f in γ (wt.%)	$(C_f - C_i)$ (wt.%)
350	(5.5) [12]	0.57 ± 0.02	+0.37	0.67 ± 0.01	+0.10
	(5.6) [30]	0.09 ± 0.03	-0.11	0.23 ± 0.01	+0.14
	(5.7) [32]	0.34 ± 0.03	+0.14	0.48 ± 0.01	+0.14
305	(5.5) [12]	0.55 ± 0.01	+0.35	0.82 ± 0.01	+0.27
	(5.6) [30]	0.06 ± 0.01	-0.14	0.43 ± 0.01	+0.37
	(5.7) [32]	0.31 ± 0.01	+0.11	0.68 ± 0.01	+0.37

Table 5.II shows the estimated average carbon concentration (in weight percent) in the untransformed austenite at the start (C_i) and at the end (C_f) of the isothermal holding at both temperatures, as well as the absolute increase in carbon concentration calculated by means of Equations (5.5)-(5.7). Assuming that austenite contains the nominal carbon concentration ($C_{nom.}$ = 0.20 wt.%) at the start of the isothermal holding, Equations (5.6) and (5.7) give a closer estimation of the initial carbon concentration in austenite with approximately ±0.10 wt.% difference with respect to the nominal one. Both equations give the same estimation of the absolute carbon enrichment of austenite at the end of the holding time. On the other hand, Equation (5.5) gives a far too high estimation of the initial carbon concentration in austenite and a lower estimation of the absolute carbon enrichment of austenite compared to that obtained by the other two equations.

Based on these results, Equations (5.6) and (5.7) provide the 'best' estimations and can be considered as a lower and upper limit, respectively, for the carbon concentration in austenite.

Deviations in the estimation of the initial carbon concentration in austenite at the beginning of both isothermal holdings also result from uncertainty of the austenite lattice parameter derived from the fitting process of the {hkl} reflections of austenite. Fluctuations are observed in the first 500 s of the bainite reaction at both isothermal temperatures (see Figure 5.7). In the present work, the use of a symmetrical pseudo-Voigt function to fit all austenite diffraction peaks leads to the over- or underestimation of the 2θ position of the asymmetrical peaks of some of the austenite {hkl} reflections. Figure 5.8 shows two fitting examples of the asymmetrical peak shape of the {220} γ reflection. The asymmetry of certain austenite diffraction peaks at the early stage of the isothermal bainite formation has also been observed in in-situ studies of the bainite transformation in medium-carbon steels [33,34]. This phenomenon, also referred to as peak splitting, is mainly attributed to an inhomogeneous carbon distribution within the untransformed austenite. Consequently, the formation of carbon-poor and carbon-rich austenite regions may affect the interpretation of results concerning the evolution of carbon enrichment in austenite during bainite formation.

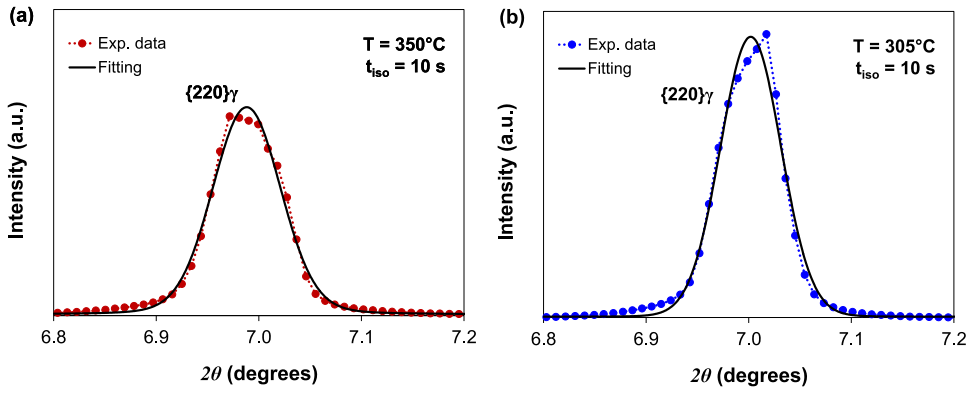

Figure 5.8. Example of the {220}γ reflection from untransformed austenite at t_{iso} = 10 s from the onset of the isothermal bainite reaction at (a) 350°C and (b) 305°C.

Figure 5.9.a shows the comparison between the kinetics of the relative carbon enrichment in austenite and the bainite formation during the isothermal holdings at 350°C and 305°C. The relative carbon enrichment was estimated based on Equation (5.6) (lower limit). At both temperatures, the kinetics of carbon enrichment in the remaining untransformed austenite is observed to be slower than the kinetics of the bainite reaction. For example, the increase of carbon concentration in austenite is

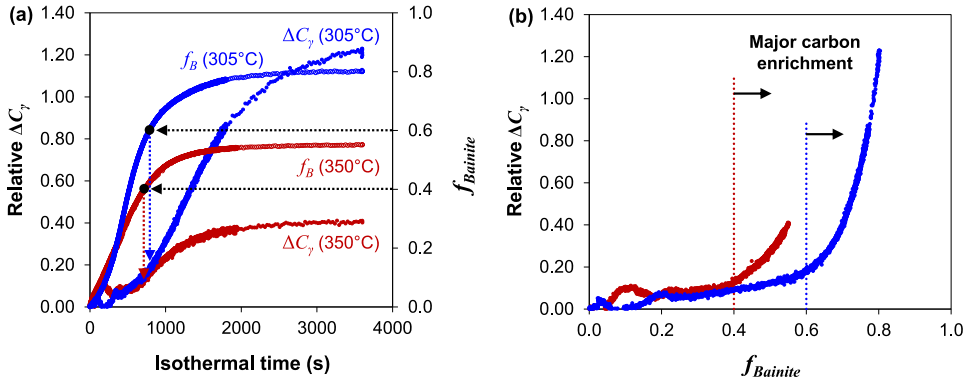

Figure 5.9. (a) Comparison between the kinetics of relative carbon enrichment in the untransformed austenite and the bainite reaction and (b) evolution of carbon enrichment in the untransformed austenite as a function of bainite fraction formed during the isothermal holdings at 350°C and 305°C.

unexpectedly low after the formation of 0.4 and 0.6 volume fraction of bainite at 350°C and 305°C, respectively, which corresponds to approximately 75% of the progress of the transformation at both isothermal temperatures. The evolution of carbon enrichment of austenite as a function of the bainite fraction formed during both isothermal holdings is depicted in Figure 5.9.b. As observed, a significant increase of carbon concentration in austenite occurs approximately after 0.4 and 0.6 bainite fraction is already formed at 350°C and 305°C, respectively. This indicates that there is a phenomenological mismatch between bainite formation and carbon enrichment of austenite.

The observed delay between carbon enrichment of austenite and bainite formation can be mainly attributed to the process of carbon redistribution within the untransformed austenite grains. The carbon redistribution in austenite is conditioned by the diffusivity of carbon and the remaining austenite fraction at each temperature. The combined effect of both factors determines the kinetics of carbon enrichment of austenite during the bainite reaction. Carbon diffusivity is higher at 350°C than at 305°C, but the distances within austenite grains to reach an homogeneous carbon profile are also bigger at 350°C due to the higher austenite fraction remaining untransformed. A further detailed analysis is thus needed to determine the individual effect of both factors on the carbon enrichment kinetics. As a first approach, the carbon concentration profile within austenite grains is expected to be heterogeneous at the beginning of the bainite reaction, when there is still a high untransformed austenite fraction. The centre of the austenite grains will contain the nominal carbon concentration (carbon-poor areas) while the surroundings at the newly-formed austenite-bainite interfaces will exhibit higher carbon concentrations (carbon-rich areas). This interpretation is consistent with the asymmetry observed in certain austenite diffraction peaks at the beginning of the bainite reaction at both isothermal temperatures (see Figure 5.8).

Nishikawa et al. [35] recently demonstrated through simulations that, at the early stage of the bainite reaction, the carbon profile in the untransformed austenite grains is heterogeneous with carbon-rich areas close to the bainite-austenite interfaces and carbon-poor areas in the centre of the austenite grains. The total redistribution of carbon along the austenite grains is shown to be reached after a certain time. Assuming the same behaviour in the steel of the present work, the homogenization of carbon within the untransformed austenite grains takes place from the beginning of the bainite reaction. However, a significant increase of carbon enrichment in the untransformed austenite is not detected until the carbon concentration within austenite grains reaches a certain degree of homogeneity. This inflexion point coincides, at both temperatures, with a certain percentage of progression of the bainite reaction, as observed in Figure 5.9. After 2000 s from the onset of the isothermal holding, the carbon redistribution within untransformed austenite grains seems to continue since carbon concentration in austenite continues increasing even though the bainite formation has reached a plateau, considering the isothermal reaction finished.

5.4. Conclusions

An in-situ microstructural characterization of the phase transformations occurring during isothermal treatments above and below M_s was performed by means of in-situ high-energy X-ray diffraction measurements on a low-carbon high-silicon steel. Microstructural changes throughout heat treatments were characterized by the analysis of the diffraction peaks and lattice parameters of fcc- and bcc-phases, from which the kinetics of the isothermal bainite reaction and carbon enrichment of fcc-phase were quantitatively determined. The conclusions obtained from this work are the following:

1. The formation of 0.2 to 0.8 volume fractions of athermal martensite induces compressive strains in the untransformed austenite. These strains show a linear dependence on the martensite fraction. When the fraction of martensite is lower than 0.2, the compressive or tensile character of the transformation strains induced in the untransformed austenite remains uncertain.

2. The isothermal evolution of the relative increase of carbon concentration in untransformed austenite indicates a higher carbon enrichment at the end of the bainite reaction below M_s, mainly due to the formation of a higher fraction of bainitic ferrite than above M_s. A higher carbon concentration implies a higher chemical stability of the austenite. As a consequence, the remaining austenite after the holding below M_s partially decomposes into fresh martensite during final cooling at a lower secondary M_s temperature, compared to the lower carbon-enriched austenite that remains after the holding above M_s.

3. Asymmetry in the diffraction peak of the {220} reflection from austenite is observed at the early stage of the isothermal transformation above and below M_s. The asymmetric peak shape is related to the development of austenite regions with different carbon concentrations due to the slower kinetics of carbon redistribution along the untransformed austenite grains compared to the bainite reaction kinetics.

4. Kinetics of the relative austenite carbon enrichment during isothermal holdings above and below M_s is observed to be slower than the kinetics of the isothermal bainite formation. Differences in kinetics between both processes are attributed to slower kinetics of carbon redistribution throughout the untransformed austenite grains. The rate of carbon redistribution mainly depends on the combined effect of carbon diffusivity and the remaining austenite fraction at each temperature, though further analysis is needed to determine the individual effect of each factor.

References

[1] A. Hultgren. Trans. ASM, 1947, vol. 39, pp. 915-89.

[2] T. Ko, S.A. Cottrell. J. Iron Steel Inst., 1952, vol. 172, pp. 307-13.

[3] M. Hillert. Diffusion in growth of bainite. Metall. Mat. Trans. A, 1994, vol. 25, pp. 1957-1966.

[4] A. Borgenstam, M. Hillert, J. Ågren. Metallographic evidence of carbon diffusion in the growth of bainite. Acta Mater., 2009, vol. 57, pp. 3242-3252.

[5] M. Hillert, A. Borgenstam, J. Ågren. Do bainitic and Widmanstätten ferrite grow with different mechanisms? Scripta Mater., 2010, vol. 62, pp. 75-77.

[6] M. Hillert, A. Borgenstam. Centennial of the diffusionless paradigm of bainite. Metall. Mat. Trans. A, 2012, vol. 43, pp. 4487-4495.

[7] C. Zener. Trans. AIME, 1946, vol. 167, pp. 550-83.

[8] H.K.D.H. Bhadeshia. Bainite in Steels: Transformations, Microstructure and Properties. Second Edition, 2001.

[9] F.G. Caballero, M.K. Miller, S.S. Babu, C. Garcia-Mateo. Atomic scale observations of bainite transformation in a high carbon high silicon steel. Acta Mater., 2007, vol. 55, pp. 381-90.

[10] H.K.D.H. Bhadeshia. The nature, mechanism and properties of strong bainite. Proceedings 1st Int. Symp. on Steel Science, Iron Steel Inst. Japan, 2007, pp. 1-10.

[11] F.G. Caballero, M.K. Miller, C. Garcia-Mateo, J. Cornide. New experimental evidence of the diffusionless transformation nature of bainite. Journal Alloys & Comp., 2013, vol. 577S, pp. 626-630.

[12] N.H. van Dijk, A.M. Butt, L. Zhao, J. Sietsma, S.E. Offerman, J.P. Wright, S. van der Zwaag. Thermal stability of retained austenite in TRIP steels studied by synchrotron X-ray diffraction during cooling. Acta Mater., 2005, vol. 53, pp. 5439-5447.

[13] M. Villa, F. Niessen, M.A.J. Somers. In situ investigation of the evolution of lattice strain and stresses in austenite and martensite during quenching and tempering of steel. Metall. Mater. Trans. A, 2018, vol. 49, pp. 28-40.

[14] N. Nakada, Y. Ishibashi, T. Tsuchiyama, S. Takaki. Self-stabilization of untransformed austenite by hydrostatic pressure via martensitic transformation. Acta Mater, 2016, vol. 110, pp. 95-102.

[15] S.Y.P. Allain, S. Gaudez, G. Geandier, J.C. Hell, M. Gouné, F. Danoix, M. Soler, S. Aoued, A. Poulon-Quintin. Internal stresses and carbon enrichment in austenite of quenching and partitioning steels from high energy X-ray diffraction experiments. Mater. Sci. Eng. A, 2018, vol. 710, pp. 245-250.

[16] S.Y.P. Allain, G. Geandier, J.C. Hell, M. Soler, F. Danoix, M. Gouné. In-situ investigation of quenching and partitioning by high energy X-ray diffraction experiments. Scripta Mater., 2017, vol. 131, pp. 15-18.

[17] P. Huyghe, M. Caruso, J.L. Collet, S. Depinoy, S. Godet. Into the quenching and partitioning of a 0.2C steel: An in-situ synchrotron study. Mater. Sci. Eng. A, 2019, vol. 743, pp. 175-184.

[18] J.C. Labiche, O. Mathon, S. Pascarelli, M.A. Newton, G.G. Ferre, C. Curfs, G. Vaughan, A. Homs, D.F. Carreiras. Rev. Sci. Instrum., 2007, vol. 78, p. 091301.

[19] A.P. Hammersley. ESRF Internal Report, ESRF98HA01T, FIT2D V9.129 Reference Manual V3.1, 1998.

[20] A.P. Hammersley. FIT2D: a multi-purpose data reduction, analysis, and visualization program. J. Appl. Crystallogr., 2016, vol. 49, pp. 646-652.

[21] A.P. Hammersley, S.O. Svensson, M. Hanfland, A.N. Fitch, D. Hausermann. Two-dimensional detector software: From real detector to idealised image or two-theta scan. High Press. Res., 1996, vol. 14, pp. 235-248.

[22] ASTM International. Standard practice for X-ray determination of retained austenite in steel with near random crystallographic orientation. West Conshohocken, PA, 2013.

[23] J. Pak, D.W. Suh, H.K.D.H. Bhadeshia. Displacive phase transformation and surface effects associated with confocal laser scanning microscopy. Metall. Mater. Trans. A, 2012, vol. 43, pp. 4520-4524.

[24] J.A. Klostermann, W.G. Burgers. Surface martensite in iron-nickel. Acta Metall., 1964, vol. 12, pp. 355-360.

[25] A.P. Baur, C. Cayron, R.E. Logé. Variant selection in surface martensite. J. Appl. Cryst., 2017, vol. 50, pp. 1646-1652.

[26] J.D. Escobar, G.A. Faria, L. Wu, J.P. Oliveira, P.R. Mei, A.J. Ramirez. Austenite reversion kinetics and stability during tempering of a Ti-stabilized supermartensitic stainless steel: Correlative in situ synchrotron x-ray diffraction and dilatometry. Acta Mater., 2017, vol. 138, pp. 92-99.

[27] M. Onink, C.M. Brakman, F.D. Tichelaar, E.J. Mittemeijer, S. van der Zwaag. The lattice parameters of austenite and ferrite in Fe-C alloys as functions of carbon concentration and temperature. Scripta Metall. Mater., 1993, vol. 29, pp. 1011-1016.

[28] S.M.C. van Bohemen. The non-linear lattice expansion of iron alloys in the range 100-1600 K. Scripta Mater., 2013, vol. 69, pp. 315-318.

[29] N. Ridley, H. Stuart, L. Zwell. Lattice parameters of Fe-C austenites at room temperature. Trans. AIME, 1969, vol. 245, pp. 1834-1840.

[30] D.J. Dyson, B. Holmes. Effect of alloying additions on the lattice parameter. J. Iron Steel Res. Inst., 1970, vol. 208, pp. 469-474.

[31] L. Cheng, A. Böttger, T.H. de Keijser, E.J. Mittemeijer. Lattice parameters of iron-carbon and iron-nitrogen martensites and austenites. Scripta Metall. Mater., 1990, vol. 24, pp. 509-514.

[32] J.B. Seol, D. Raabe, P.P. Choi, Y.R. Im, C.G. Park. Atomic scale effects of alloying, partitioning, solute drag and austempering on the mechanical properties of high-carbon bainitic-austenitic TRIP steels. Acta Mater., 2012, vol. 60, pp. 6183-6199.

[33] S.S. Babu, E.D. Specht, S.A. David, E. Karapetrova, P. Zschack, M. Peet, H.K.D.H. Bhadeshia. In-situ observations of lattice parameter fluctuations in austenite and transformation to bainite. Metall. Mater. Trans. A, 2005, vol. 36, pp. 3281-3289.

[34] I.B. Timokhina, K.D. Liss, D. Raabe, K. Rakha, H. Beladi, X.Y. Xiong, P.D. Hodgson. Growth of bainitic ferrite and carbon partitioning during the early stages of bainite transformation in a 2 mass % silicon steel studied by in situ neutron diffraction, TEM, and APT. J. Appl. Cryst., 2016, vol. 49, pp. 1-16.

[35] A.S. Nishikawa, G. Miyamoto, T. Furuhara, A.P. Tschiptschin, H. Goldenstein. Phase transformation mechanisms during quenching and partitioning of a ductile cast iron. Acta Mater., 2019, vol. 179, pp. 1-16.

CHAPTER 6

Influence of the Prior Athermal Martensite on the Overall Mechanical Response

**This chapter corresponds to the article "Influence of the prior athermal martensite on the mechanical response of advanced bainitic steels" by A. Navarro-López, J. Hidalgo, J. Sietsma, and M.J. Santofimia, Mater. Sci. Eng. A (2018), vol. 735, 343-353.*

Abstract

The accelerated formation of bainite in presence of martensite is opening a new processing window for the steel industry. However, for a feasible industrial implementation, it is necessary to determine the mechanical behaviour of the steels developed under such conditions. This study focuses on analysing the effects of the formation of athermal martensite, followed by the formation of bainitic ferrite, on the mechanical response of a low-C high-Si steel. For this purpose, microhardness measurements and tensile tests have been performed on specimens that were thermally treated either above or below the martensite-start temperature (M_s). Specimens isothermally treated below M_s exhibit a good combination of mechanical properties, comparable with that of the specimens heat treated by conventional treatments above M_s, where there was no prior formation of martensite. Investigations show an increase of the yield stress and a decrease of the ultimate tensile strength as the isothermal holding temperature is decreased below M_s. The formation of prior athermal martensite and its tempering during the isothermal holding leads to the strengthening of the specimens isothermally heat treated below M_s at the expense of slightly decreasing their strain hardening capacity.

6.1. Introduction

Steel industry aims to develop steels with a better balance of mechanical properties through more efficient, cost-effective, and sustainable manufacturing processes. Particularly, obtaining bainitic microstructures by the application of isothermal treatments below the martensite-start temperature (M_s) is now one of the most promising processing routes within the steel sector. This is due to the accelerating effect of the partial formation of martensite on the subsequent bainitic reaction [1-7]. These thermal treatments involve an isothermal holding below M_s after an interrupted cooling. Adequate cooling rates and alloy compositions are used to avoid the formation of ferrite, pearlite or bainite during cooling from austenitization. Bainitic ferrite forms from the untransformed austenite during the subsequent isothermal holding below M_s [6-10]. Finally, the remaining austenite will either be retained or transform into fresh martensite during the final cooling to room temperature. A multiphase microstructure is thus formed in which specific fractions of martensite and bainite coexist with carbon-enriched retained austenite.

These multiphase microstructures are comparable to the ones present in carbide-free bainitic (CFB) steels and quenching and partitioning (Q&P) steels. These steels are also developed through thermal cycles in which an isothermal holding around the M_s temperature is performed [11-15]. In CFB steels, the phase mixture is generally formed by a bainitic matrix with certain fractions of retained austenite and fresh martensite. In Q&P steels, the primary matrix is martensitic and it is tempered to some extent during the partitioning step. The final microstructure also contains certain fractions of retained austenite and fresh martensite. Regarding their mechanical behaviour, CFB and Q&P steels exhibit a composite mechanical response to the application of stress [13-15]. The relationship between their complex microstructure and their mechanical performance has been extensively studied in the last decade [11-12,14-19]. Both types of steels exhibit a good combination of strength and ductility as well as a considerable strain hardening due to the presence of high fractions of chemically stabilized retained austenite which can mechanically transform into martensite during deformation.

In multiphase steels developed through isothermal holding below M_s, the presence of prior athermal martensite leads to a different phase mixture compared to typical CFB and Q&P microstructures, which consequently affects the mechanical response of these steels. Recent studies on steels that were isothermally-treated below M_s have focused on studying the relationship between their phase mixture and their mechanical response [7,11,20-24]. Most of the reported results show an increase of the yield strength in specimens isothermally treated below M_s compared to the ones heat treated by conventional holding above M_s [7,11,22]. However, according to the results reported by [23], the application of isothermal holding below M_s leads to a general deterioration of

the mechanical properties of the heat treated specimens. Despite the effects derived from the distinct chemical compositions of the analysed steels and the fractions of product phases formed during the isothermal holding below M_s, these diverging results can also result from the applied holding time and, consequently, from the tempering of the prior athermal martensite. In that sense, there is not a clear insight into the effects introduced by the prior athermal martensite and their significance for the mechanical response of these bainitic steels. A common observation is the refinement of the subsequently-formed bainitic ferrite [7,11,22,23]. This fact is directly related to the formation of prior athermal martensite and has been considered one of the main factors responsible for the improvement of the mechanical properties of specimens heat treated below M_s [7,22]. However, the influence of other effects resulting from the introduction of prior athermal martensite into the phase mixture, such as the precipitation of carbides due to tempering and the mechanical transformation of the unstable retained austenite, can also result decisive in the overall mechanical response of the below-M_s microstructures [20,23].

Another factor that might explain discordant results in the literature is the mechanical stability of retained austenite. The stability of austenite is affected by its composition (mainly carbon concentration), morphology, and grain size [25-27], and is generally related to the strain hardening capacity of the steel under the application of stress. The strain hardening capacity has been studied in specimens isothermally treated above and below M_s, resulting in a lower strain hardening capacity being exhibited by specimens heat treated below M_s compared to the ones treated above M_s [7,11,22,23]. This lower capacity is attributed to a lower volume fraction of blocky-shaped retained austenite (in the form of martensite-austenite (MA) islands) which potentially can transform into martensite [11,23]. Moreover, a lower strain hardening capacity is also attributed to the chemical stability of the retained austenite due to carbon enrichment. Film-shaped retained austenite is more difficult to mechanically transform into martensite than the blocky-shaped type since it can enrich from carbon more easily due to its high area to volume ratio [24]. However, this carbon enrichment of the austenite in multiphase steels isothermally treated below M_s may be also affected by the possible formation of iron carbides as a consequence of tempering of the prior athermal martensite. This phenomenon reduces the carbon concentration available to diffuse from the prior athermal martensite into the surrounding austenite, possibly leading to a less carbon enrichment of the untransformed austenite in steels isothermally treated below M_s in comparison with those treated above M_s. This latter fact has not been taken into consideration in previous research studies, so the effect of the retained austenite in the overall strain hardening capacity of multiphase steels isothermally treated below M_s remains unclear.

In this context, there is a need of performing a deeper analysis of the individual contribution of the different phases forming the multiphase matrix of these steels to their overall mechanical response. This research work mainly focuses on the effect of prior athermal martensite and its tempering during the isothermal holding on the mechanical response of multiphase steels obtained through isothermal treatments below M_s in a low-C high-Si steel, confronting with observations through conventional treatments without prior formation of martensite. Individual contributions of the different phases to the overall mechanical response are analysed in terms of grain-boundary, solid-solution, and precipitation strengthening mechanisms.

6.2. Experimental Procedure

The chemical composition of the investigated steel is 0.2C-3.51Mn-1.52Si-0.25Mo-0.04Al (wt. pct). The as-received material was hot rolled into a 4 mm-thick steel slab. Tensile specimens were machined from the hot rolled slabs, parallel to the rolling direction. These specimens were extracted from a different area of the same hot rolled slab than that studied in Chapters 2 and 3. Small local variations in the chemical composition of the extracted specimens were observed with respect the specimens analysed in previous chapters, which gave rise to variations in the critical temperatures of the steel with respect to the values presented in Chapters 2 and 3.

The dimensions of the tensile specimens are shown in Figure 6.1. These specimens were thermally treated with a Bähr 805A/D dilatometer, in which heating was performed by an induction coil under a vacuum of the order of 10^{-4} mbar, and cooling by a continuous flow of helium gas. Three tensile specimens per condition were heat treated by dilatometry. Two S-type thermocouples were spot-welded to the surface of each tensile specimen: one in the middle of the reduced area (T_1) to monitor and control the temperature, and the second one in the border of the reduced area (T_2) to check the temperature gradient. The mean temperature difference measured in all specimens during austenitization and isothermal holdings was $\Delta T = T_1 - T_2 \approx 15$°C.

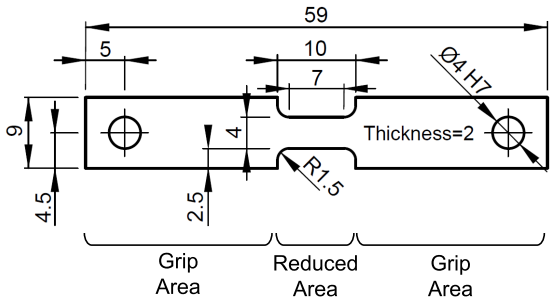

Figure 6.1. Scheme of the tensile specimens (dimensions in mm).

Cylindrical dilatometry specimens were extracted from the same zone of the hot rolled slab as the tensile specimens. The dimensions of the cylinders were 10 mm in length and 3.5 mm in diameter. These specimens were heat treated with the Bähr 805A/D dilatometer in the same conditions previously described for the tensile specimens. The heat treatments applied to tensile and cylindrical specimens are presented in Figure 6.2. Dilatometry data obtained from the heat treatments performed to cylindrical specimens were used to determine the phase fractions involved in each treatment.

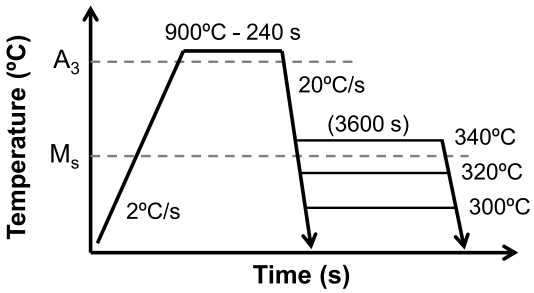

Figure 6.2. Heat treatments performed by dilatometry to tensile and cylindrical specimens.

Vickers HV1 (1 kgf) micro-indentations were done with a DuraScan 70 (Struers) microhardness tester machine to check the homogeneity of the resulting microstructures obtained in the heat-treated tensile specimens. Average values of microhardness were obtained from three rows of equidistant indentations performed along the 7 mm gauge length of the tensile specimens. These indentations rows were separated by 1 mm, covering the total width of the gauge area.

Tensile tests were performed with an Instron 5500R electromechanical tester machine, equipped with a maximum load cell of 100 kN, at room temperature and in extension control. The elongation during the tensile tests was recorded by a clip-on extensometer with knife edges, which was attached to the tensile specimen by elastic bands. The extensometer had a gauge length of 7.8 mm with a maximum extension of ±2.5 mm. Stress-strain curves of all specimens were obtained from the tensile tests. The yield stress (YS) was determined by the 0.2% offset method, so the yield-stress value obtained should be considered as the 0.2% proof.

Heat-treated cylindrical specimens were metallographically prepared by grinding and polishing, and etched with 2% Nital. Microstructures were analyzed with a JEOL JSM-6500F Scanning Electron Microscope (SEM) using a 15 kV electron beam and the Secondary Electron Imaging (SEI) detection mode. X-ray diffraction (XRD) measurements were performed to determine the volume fraction of retained austenite (RA) and its lattice parameter at room temperature as well as the volume

fraction of untransformed retained austenite after the application of uniaxial stress. The measurements were carried out using a Bruker D8-Advance diffractometer equipped with a Bruker Vantec Position Sensitive Detector. Co-Kα radiation was used in the 2θ scan from 40° to 130° with a step size of 0.035°. The fractions of austenite were calculated by the integrated area method using the (111), (200), (220), and (311) austenite peaks, and the (110), (200), (211), and (220) ferrite peaks [28]. The austenite lattice parameter was calculated by the application of the Nelson-Riley method [29] to the peak positions of the four austenite reflections.

6.3. Results

6.3.1. Phase Fractions

Figure 6.3.a shows the change in length as a function of temperature of the specimen directly quenched to room temperature from the austenitization conditions. The derivative of the change in length is also represented to accurately determine the M_s temperature of the studied alloy. The experimental M_s temperature at 0.01 volume fraction of athermal martensite was determined to be 335°C ± 5°C. The linear contraction during cooling from austenitization to the M_s temperature indicates the absence of formation of ferrite, pearlite, or bainite before the martensitic transformation. The dilatation occurring below the M_s temperature indicates the formation of athermal martensite. The total net dilatation caused by the athermal martensitic transformation with respect to the austenitic phase was approximately 0.88% at room temperature (indicated by a double-ended arrow in Figure 6.3.a).

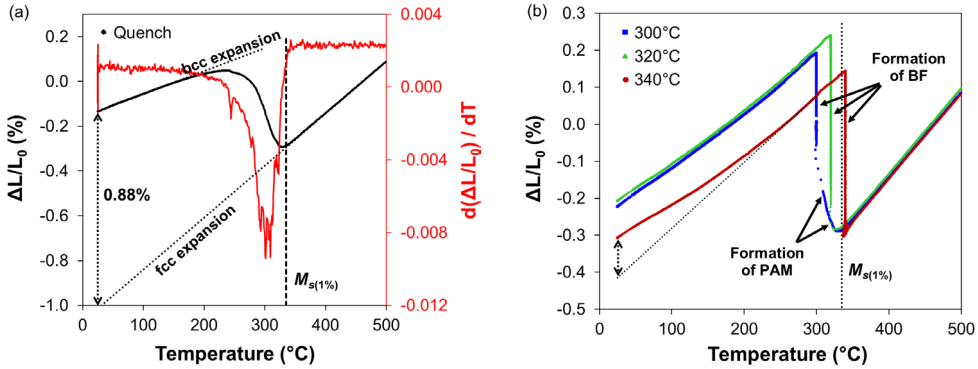

Figure 6.3. Change in length as a function of temperature obtained from dilatometry measurements performed to cylindrical specimens heat treated by (a) direct quench, and (b) isothermal holding at 340°C (above M_s), 320°C (below M_s), and 300°C (below M_s) for one hour.

Figure 6.3.b shows the dilatometric curves of specimens isothermally treated for one hour at 340°C (above M_s), 320°C, and 300°C (below M_s). During cooling from austenitization until the isothermal holding temperature, a deviation from linearity is only observed in

the dilatometry curves of specimens cooled down below M_s. This deviation indicates the formation of prior athermal martensite (PAM). The distinct martensite volume fractions formed at the two selected temperatures below M_s were calculated by applying the lever rule to the dilatometric curve of the quenched specimen. Once the isothermal temperature is reached, a dilatation takes place in all specimens during the one-hour isothermal holding applied above or below M_s, which is related to the formation of bainitic ferrite, as reported in Chapters 2 and 3.

A non-linear change in length occurs during cooling from the isothermal temperatures to room temperature as a consequence of the formation of athermal martensite, called fresh martensite (FM) in this work, from the untransformed remaining austenite. Such martensitic transformation causes a relative net dilatation with respect to the microstructure obtained at the end of the isothermal holding, as shown by the double-ended arrow in Figure 6.3.b, which allows the quantification of the fresh martensite fraction following the procedure described in Chapter 2. The formation of athermal martensite during the final cooling indicates the incompleteness of the isothermal bainitic transformation after one hour of holding time. A certain fraction of remaining austenite is also retained at room temperature. Volume fractions of bainitic ferrite were calculated by balancing the fractions of prior athermal martensite, fresh martensite, and retained austenite (the latter is obtained from XRD). Figure 6.4 shows the volume fractions of the different phases obtained in each isothermal treatment.

6.3.2. Mechanical Properties

The mean 0.2% offset yield stress (YS) and ultimate tensile strength (UTS) (with their standard deviations) of the tensile specimens isothermally treated at temperatures above and below M_s are presented in Figure 6.4. These values were obtained from the corresponding engineering stress-strain curves (see Figure 6.5). There is an opposite tendency of the YS and the UTS with the isothermal holding temperature. The specimens isothermally treated for one hour at a temperature above M_s (340°C) exhibit lower YS and higher UTS than the ones treated at temperatures below M_s (320°C and 300°C), as shown in Figure 6.4.

Figure 6.5.a shows the engineering stress-strain curves obtained from the performed uniaxial tensile tests. Mean values of uniform elongation with their corresponding standard deviations are also shown. The directly quenched specimens exhibit the highest yield stress and ultimate tensile strength and the lowest uniform elongation and fracture strain. On the other hand, similar stress-strain engineering curves are obtained for specimens isothermally treated at temperatures above and below M_s. However, differences in yield strength can be observed in an amplified view of these engineering curves, as shown in Figure 6.5.b. Moreover, for lower holding temperatures, a lower

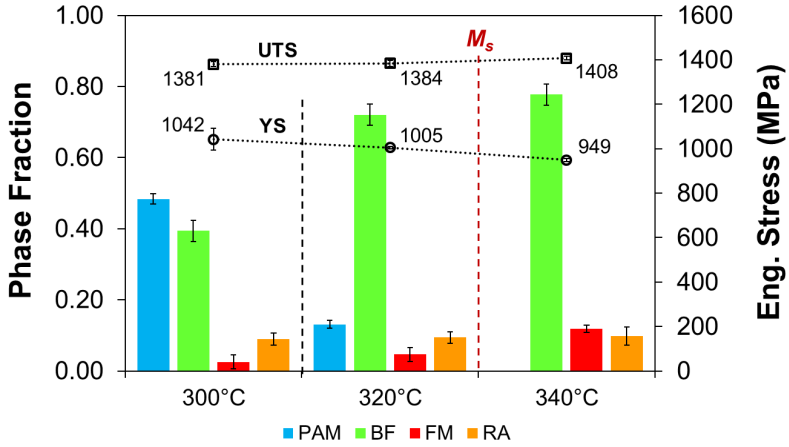

Figure 6.4. Volume fractions of prior athermal martensite (PAM), bainitic ferrite (BF), fresh martensite (FM), and retained austenite (RA) obtained after the application of one-hour isothermal holdings at 340°C (above M_s), 320°C (below M_s), and 300°C (below M_s). Mean values of 0.2% offset yield stress (YS) and ultimate tensile strength (UTS) exhibited by the heat-treated tensile specimens are also presented. The M_s temperature (335°C) of the studied alloy is indicated by a dashed line.

uniform elongation is exhibited (see the table included in Figure 6.5.a). Fracture strains are in the range of 18-23%. Note that elongation values are affected by the sub-size dimensions of the tensile specimens since a reduced gauge length leads to a significant contribution to the overall elongation from the necked region [30]. In the present work, all tensile tests were performed in sub-size specimens with exactly the same dimensions, and results were only used for the relative comparison of their mechanical response.

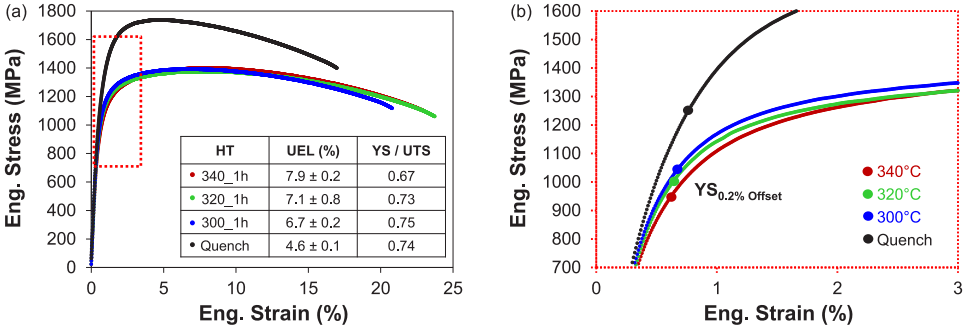

Figure 6.5. (a) Engineering stress-strain curves and average values of uniform elongation (UEL) and *'YS/UTS'* ratio of the tensile specimens heat-treated by a direct-quench and one-hour isothermal holdings at temperatures of 340°C (above M_s), 320°C, and 300°C (below M_s); (b) Amplified view of the engineering curves (marked by a red dashed-line rectangle in (a)).

Figure 6.5 also shows the ratio of the yield stress to the tensile strength *'YS/UTS'* for all heat-treated specimens. The *'YS/UTS'* ratio represents the capacity of a material to

harden by plastic deformation and it is a widely-used parameter to determine the strain hardening potential of alloys. A lower *'YS/UTS'* ratio means that higher strain hardening will take place in the material. In this study, all heat-treated specimens exhibit *'YS/UTS'* ratios in a range of 0.67-0.75, which are typical values of strain hardening of multiphase steels [16,21]. The degree of strain hardening is lower in specimens isothermally treated below M_s.

Microhardness values Vickers HV1 of the heat-treated tensile specimens are presented in Figure 6.6. In this case, microhardness values can vary from a minimum of 400 HV1 (dark green) to a maximum of 525 HV1 (dark red). Each group of measurements is represented by a hardness matrix, where each individual hardness value is assigned a specific colour within a colour scale. The hardness matrices show a uniform hardness within the gauge area for each heat-treated specimen (see Figure 6.6), which is reflected in the small standard deviations obtained. These results indicate a uniform microstructure throughout the gauge of the heat-treated tensile specimens.

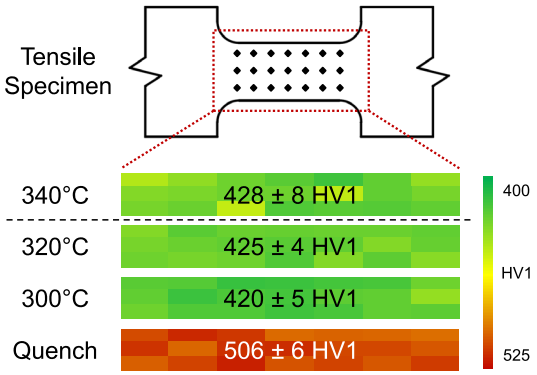

Figure 6.6. Mean values of microhardness Vickers HV1 obtained from measurements performed along the gauge length of the heat-treated tensile specimens. Each group of microhardness measurements is represented by a hardness matrix, following the colours code indicated.

Quenched specimens are the hardest of the analysed heat-treated specimens. This fact is consistent with the highest UTS obtained from the engineering stress-strain curve. The microhardness of the isothermally treated specimens slightly decreases from temperatures above M_s to temperatures below M_s. This decreasing variation of the microhardness is also in agreement with the decrease of the UTS as the isothermal temperature is decreased.

6.3.3. Microstructures

The microstructural analysis of this work is based on the microstructural description of features presented in Chapter 3, which facilitate the characterization and comparison of multiphase microstructures obtained after the application of isothermal holdings above and below the M_s temperature. Figures 6.7.a-d show the microstructures obtained from the quenched specimen and the one-hour isothermally treated specimens. The quenched specimen has a fully martensitic matrix which corresponds well with 0.97 fresh martensite fraction (calculated from XRD). Fresh martensite appears in the form of laths, with different shapes and sizes, containing carbides that grow along specific habit planes within the block-shaped substructures. The presence of carbides indicates the auto-tempering of the martensite during the fast cooling. These carbides are marked by white arrows within the magnified view of the dashed-rectangular area indicated in Figure 6.7.a.

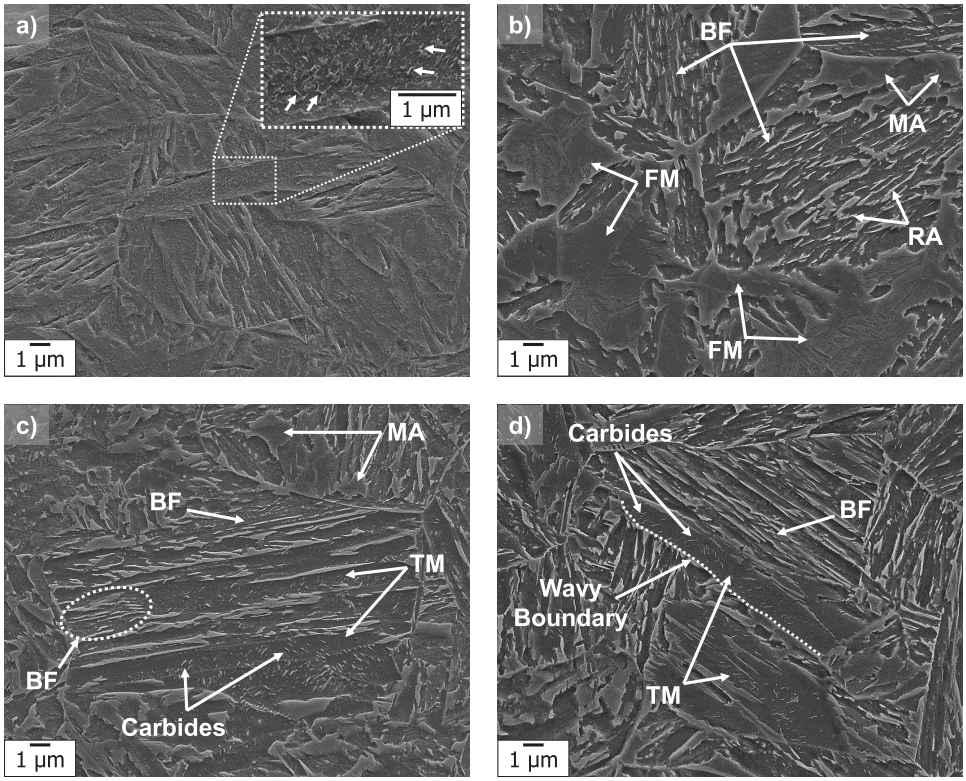

Figure 6.7. Microstructures obtained after applying a) a direct-quench treatment, and isothermal treatments for one hour at the selected temperatures of b) 340°C (above M_s), c) 320°C (below M_s), and d) 300°C (below M_s). BF (Bainitic Ferrite), FM (Fresh Martensite), RA (Retained Austenite), MA (Martensite-Austenite islands), and TM (Tempered Martensite, also referred as PAM).

Concerning specimens isothermally treated for one hour above M_s, at 340°C, the microstructure is mainly formed by a bainitic matrix with fresh martensite areas (FM) and isolated martensite-austenite islands (MA) at the prior austenite grain boundaries (see Figure 6.7.b). Bainitic ferrite (BF) appears in the form of acicular units with retained austenite films (RA) between them. Below M_s, at 320°C, a small fraction (less than 0.15) of athermal martensite was formed prior to the one-hour isothermal holding. As shown in Figure 6.7.c, tempered martensite (TM) appears in the form of elongated laths with carbides within them. As occurred above M_s, acicular units of bainitic ferrite with film-like retained austenite have formed in the microstructure. Some of these acicular units appear next to the lath boundaries of tempered martensite. Fresh martensite only appears in the form of isolated martensite-austenite islands.

Finally, when the isothermal temperature is decreased to 300°C (below M_s), a considerable volume fraction of tempered martensite (approximately 0.50) is present after one hour of isothermal holding. This tempered martensite can be distinguished from bainitic ferrite, as shown in Figure 6.7.d. The microstructure is then formed by a matrix of acicular units of bainitic ferrite and elongated laths of tempered martensite with wavy boundaries and carbides within them.

6.4. Discussion

6.4.1. Influence of Phase Mixture on Strength

Specimens isothermally treated for one hour above and below M_s present similar engineering tensile curves (see Figure 6.5), with maximum differences of less than 95 MPa and 30 MPa for YS and UTS, respectively. However, careful observation reveals an increase of the YS as well as a decrease of the UTS as the isothermal temperature is decreased below M_s (see Figure 6.4). Since the fraction of bainitic ferrite formed at 340°C (above M_s) and 320°C (below M_s) is in the range of 0.72-0.78, this evolution of the YS and UTS should be related to the formation of PAM in treatments below M_s. A qualitative analysis of the effects derived from the formation of this product phase on the overall mechanical response is presented in the following sub-sections.

Strengthening via refinement of structures

One of the strengthening effects is the refinement of the bainitic structures formed during isothermal holding below M_s. The formation of PAM implies three mechanisms leading to a refinement of such structures:

1) The fragmentation of the prior austenite grains formed during austenitization into smaller parts [22]. As shown in the scheme of Figure 6.8, the initial austenite grain

size is reduced as the volume fraction of PAM is increased, inducing the formation of finer bainitic structures.

2) The increase of the density of potential nucleation sites for bainitic ferrite introduced in the form of martensite-austenite interfaces due to the formation of PAM, which leads to an accelerating effect on its transformation kinetics, as reported in Chapter 2. The new martensite-austenite interfaces are represented as a light blue shading in Figure 6.8. This refinement effect can be enhanced by the decrease of the applied isothermal temperature, which leads to a higher driving force for bainite formation [31,32].

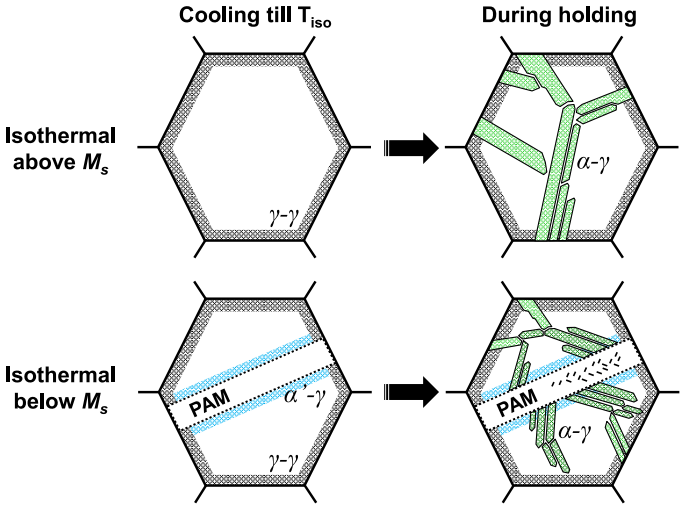

Figure 6.8. Schematic representation of the refining effects caused by the formation of a certain fraction of PAM on the bainitic structures subsequently formed in isothermal holdings below M_s, in comparison with those structures formed by conventional treatments above M_s.

3) The introduction of plastic strain through the formation of PAM into the surrounding untransformed austenite. This fact leads to the strengthening of the untransformed austenite, constraining the free movement of bainite-austenite interfaces and impeding their growth [22,23].

These refinement mechanisms contribute to the grain boundary strengthening of the specimens isothermally treated for one hour below M_s. To determine the individual contribution of prior martensite laths and bainitic ferrite structures to the grain boundary strengthening of the heat treated specimens, the mean width of both types of microstructural features is estimated. The mean width of the martensitic laths (PAM), $w_{\alpha'}$, is considered as a temperature-independent value of 2.0 ± 0.6 μm (Figure 6.9.a), which is extracted from the microstructural analysis of Chapter 3. This value was

determined from width measurements of the same type (morphology) of martensitic laths as those described in the present work, which were characterized in specimens isothermally treated for one hour at several temperatures below M_s (270°C, 300°C, and 320°C). The mean width of bainitic ferrite structures (BF), w_b, is assumed to be temperature-dependent as follows [33]:

$$w_b = w_0 \cdot \left(\frac{T - 528\,\mathrm{K}}{150\,\mathrm{K}} \right) \tag{6.1}$$

where T is the isothermal holding temperature in Kelvin and w_0 is a reference width. In this case, a width of 1.6 μm is considered as the reference value, which is determined from the bainitic ferrite features measured in previous microstructural analysis (see Chapter 3). This equation can be used for this research since the steel composition and the applied isothermal temperatures are within its validity ranges [33].

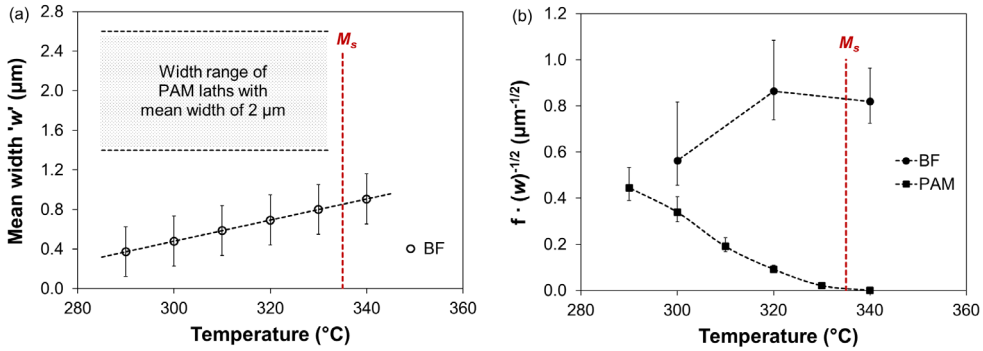

Figure 6.9. (a) Mean width of prior athermal martensite (PAM) laths and bainitic ferrite structures (BF), and (b) the contribution factor from PAM and BF to the grain boundary strengthening of isothermally treated specimens as a function of the applied holding temperature.

Figure 6.9.a shows the estimated mean width of the bainitic ferrite structures, w_b, as a function of the applied isothermal temperature as well as the estimated width range of the prior martensite laths. The width range of bainitic ferrite structures obtained from Equation (6.1) is in accordance with the width ranges of similar structures (between 0.1 and 0.8 μm) obtained through EBSD and TEM measurements by other researchers [7,11,22]. Using the values estimated by Equation (6.1), the contribution of each phase to the grain boundary strengthening (σ_{gb}) of the one-hour isothermally treated specimens is obtained as

$$\sigma_{gb}^{i} \propto f^{i} \cdot \left(w_i \right)^{-1/2} \tag{6.2}$$

where f is the volume fraction of each phase obtained at the corresponding temperature and w_i is the estimated mean width of the martensitic or bainitic ferrite structures.

According to general literature, a Hall-Petch type relationship as that described by Equation (6.2) is applicable in micro-structured steels with grain sizes higher than 20 nm [34,35]. Equation (6.2) can be thus used in the present work since the smallest size of the mean width of bainitic ferrite structures used to estimate the effect of grain refinement on the grain boundary strengthening is approximately 0.3 μm (300 nm).

Figure 6.9.b shows this contribution factor as a function of the applied temperature. The contribution of bainitic ferrite structures to the strengthening of the one-hour isothermally treated specimens is higher at 320°C than at 340°C due to a greater refinement of a similar fraction (0.72-0.78) of bainitic ferrite below M_s. When the isothermal temperature is decreased from 320°C to 300°C, the individual contribution of bainitic ferrite to the grain boundary strengthening is reduced due to the formation of a lower fraction of bainitic ferrite in comparison with that formed at 320°C. The contribution factor of bainitic ferrite then shows a maximum at 320°C. Figure 6.9.b also displays that the strengthening contribution of the PAM increases when the temperature of the isothermal holding decreases due to an increase of the volume fraction of this product phase.

Combining these observations, and assuming the same proportionality factor in Equation (6.2) for all phases, it can be concluded that, at 320°C, the strengthening contribution of bainitic ferrite by grain refinement is higher than that of the PAM due to a great difference between the volume fractions of both product phases and to the much smaller dimensions of bainitic ferrite structures in comparison with the prior martensite laths. When decreasing the isothermal temperature to 300°C, these differences are reduced due to the increase of the volume fraction of PAM at the expense of the bainitic ferrite volume fraction.

Strengthening by carbon in solid solution

The yield stress can be also modified via the strengthening effect of carbon atoms and substitutional elements in solid solution within the different phases. Substitutional elements (manganese, silicon, and molybdenum) are assumed not to partition during the tempering of PAM and the isothermal formation of bainitic ferrite in all heat treatments. Therefore, the contribution of substitutional atoms to any variation of the individual strengthening of a phase is considered negligible. On the contrary, carbon in solid solution does partition between the different phases. The contribution of interstitial carbon atoms to the solid solution strengthening depends on the carbon concentration (X_C) of each individual phase. For $X_C \leq 0.2$ wt.%, the contribution of the bainitic and martensitic phases can be expressed as [36]:

$$\sigma_{C-ss}^{i} = 1722.5 \text{ MPa}/\left(\text{wt\%}\right)^{1/2} \cdot \left(X_C^i\right)^{1/2} \tag{6.3}$$

while for X_C > 0.2 wt.%, it can be calculated as [37]

$$\sigma_{C-ss}^{i} = 1171.3 \text{ MPa}/\left(\text{wt\%}\right)^{1/3} \cdot \left(X_C^i\right)^{1/3} \tag{6.4}$$

where the strength is in MPa and the concentration of carbon in solid solution of phase *i* is in wt.%. Regarding the retained austenite, its strengthening contribution via carbon in solid solution can be determined from an empirical relation proposed by Young and Bhadeshia [38], which is expressed as [32]:

$$\sigma_{C-ss}^{RA} = 15.4 \text{ MPa}/\left(\text{wt\%}\right) \cdot \left(23 X_C^{RA}\right) \tag{6.5}$$

where the carbon concentration in solid solution (X^{RA}_C) within the retained austenite is in wt.%. To determine the contribution of each phase to the overall yield stress, the carbon concentration was first estimated as follows:

(i) Bainitic ferrite is assumed to have a carbon concentration of 0.03 wt.% [38] for all isothermal treatments.

(ii) Carbon concentrations of fresh martensite were calculated from the experimental secondary M_s temperature extracted from the dilatometric curves obtained during the final cooling to room temperature (Figure 6.3.b). This secondary M_s temperature depends on the carbon concentration of the remaining austenite that transforms. Carbon concentrations of secondary, fresh martensite were calculated by using the empirical equation proposed by Van Bohemen [39]

$$M_s = 565 - \left(31x_{Mn} + 13x_{Si} + 10x_{Cr} + 18x_{Ni} + 12x_{Mo}\right) - 600 \cdot \left[1 - \exp\left(-0.96x_C\right)\right] \tag{6.6}$$

where the secondary M_s temperature is in degrees Celsius and the concentrations of the different elements are expressed in wt.%. The size reduction of the remaining austenite grains is assumed to have a negligible influence on the decrease of the secondary M_s temperature in comparison to the effect of the carbon enrichment.

(iii) The carbon concentration in the retained austenite at room temperature was calculated from [40]

$$a^{\gamma} = 3.572 + 0.033x_C + 0.0012x_{Mn} - 0.00157x_{Si} + 0.0056x_{Al} \tag{6.7}$$

where the lattice parameter a^{γ} is in Ångström and the concentrations of the different elements, x_i, are in wt.%. The lattice parameters were determined by XRD.

(iv) The carbon concentration in solid solution within PAM was derived from additional quenching and tempering (Q&T) heat treatments. In multiphase steels, the fraction of carbon trapped in the interstitial sites of the martensite lattice can be drastically reduced during an isothermal holding. This reduction is due to the precipitation of a certain fraction of carbon atoms in the form of carbides and the diffusion of another fraction of carbon atoms from the PAM into the surrounding untransformed austenite. The aim of these additional Q&T treatments is to create a fully martensitic matrix tempered in similar temperature-time conditions as the PAM obtained in the isothermally treated specimens below M_s. Since no significant carbon partitioning to austenite takes place in the Q&T microstructure, the determination of the final carbon concentration in tempered martensite for each temperature-time condition will be considered as the maximum carbon concentration that PAM can contain in solid-solution after the one-hour isothermal treatments at the same temperatures.

Quenching and tempering (Q&T) treatments were carried out in the dilatometer by a direct quench from austenitization to room temperature, followed by a tempering stage of one hour at 320°C and/or 300°C. The microstructure obtained in both Q&T treatments was formed by a 0.97-0.98 volume fraction of tempered martensite and a 0.02-0.03 fraction of retained austenite. X-ray diffraction measurements were performed to determine the bcc-phase lattice parameter, which, in this case, corresponds to the lattice parameter of the one-hour tempered martensite since no other bcc-phases formed in Q&T treatments. The carbon concentration in tempered martensite was calculated using [41]

$$X_C^{TM} = 31\ \text{wt.\%} / \text{Å} \cdot \left(a^{TM} - a^{\alpha} \right) \tag{6.8}$$

where a^{TM} is the lattice parameter of the tempered martensite and a^{α} is the lattice parameter of a reference sample, containing no carbon in the bcc-phase, with a value of 2.866 Å [42].

Applying Equation (6.8), the carbon concentration in solid solution of the tempered martensite formed in Q&T treatments at temperatures of 320°C and 300°C (below M_s) was 0.08 and 0.09 wt.%, respectively. This loss of carbon in solid solution within the initial carbon-supersaturated martensite is mainly attributed to the formation of carbides during tempering. The volume fraction of retained austenite is so small that the fraction of carbon atoms diffusing from tempered martensite to retained austenite is considered negligible in Q&T treatments.

Table 6.I. Phase fractions (f) and carbon concentrations in wt.% (XC) of the prior athermal martensite (PAM), bainitic ferrite (BF), fresh martensite (FM), and retained austenite (RA) of specimens isothermally treated at 340°C (above M_s), 320°C (below M_s), and 300°C (below M_s). The sum of the products of the phase fractions (PAM, BF, FM, and RA) by their respective carbon concentration in solid solution is also shown for the three selected temperatures. The remaining carbon concentration is considered to be in the form of carbides.

HT	PAM		BF		FM		RA		$\Sigma(f^i \cdot X_{C\text{-}ss})$ (wt.%)	$X_{C\text{-}prec.}$ (wt.%)	X_{CT} (wt.%)
	f^{PAM}	$X_{C\text{-}ss}$	f^{BF}	$X_{C\text{-}ss}$	f^{FM}	$X_{C\text{-}ss}$	f^{RA}	$X_{C\text{-}ss}$			
340°C	0.00 ± 0.00	0.00	0.78 ± 0.03	0.03	0.12 ± 0.01	0.41	0.10 ± 0.03	0.91	**0.16**	**0.04**	**0.20**
320°C	0.13 ± 0.01	0.08	0.72 ± 0.03	0.03	0.05 ± 0.02	0.59	0.09 ± 0.02	0.91	**0.15**	**0.05**	**0.20**
300°C	0.48 ± 0.01	0.09	0.39 ± 0.03	0.03	0.03 ± 0.02	0.65	0.09 ± 0.02	0.85	**0.15**	**0.05**	**0.20**

Table 6.I shows the balance of phase fractions and their corresponding carbon concentrations ($X_{C\text{-}ss}$) of the specimens isothermally treated at temperatures above and below M_s. A certain concentration of carbon atoms ($X_{C\text{-}prec.}$) is considered to precipitate as carbides during the isothermal holding since micrographs of specimens isothermally treated below M_s (see Figures 6.7.c-d) show their presence within the tempered laths of PAM. Note that a certain fraction of carbides can also be present within phases such as bainitic ferrite and fresh martensite obtained in treatments above and below M_s. The final balance of carbon concentrations was obtained by applying the equation:

$$X_{CT} = 0.2 = \sum \left(f^i \cdot X^i_{C-ss} \right) + \left(X_{C-prec.} \right) \tag{6.9}$$

where f^i represents the volume fraction of the phase i (prior athermal martensite, bainitic ferrite, fresh martensite, or retained austenite), and the quantities X_{CT}, $X_{C\text{-}ss}$, and $X_{C\text{-}prec.}$ are the nominal carbon concentration of the steel (in this case, 0.2 wt.%), the carbon concentration in solid solution of the phase i, and the carbon concentration in the form of carbides, respectively.

The individual strengthening contributions by carbon atoms in solid solution (σ_{ss}) of the prior athermal martensite, bainitic ferrite, fresh martensite, and retained austenite were calculated by

$$\sigma^i_{ss} = f^i \cdot \sigma^i_{C-ss} \tag{6.10}$$

where f^i is the experimental volume fraction of each phase and $\sigma_{C\text{-}ss}$ is the contribution of the solute carbon atoms calculated from Equations (6.3), (6.4), or (6.5).

Figure 6.10.a shows the corresponding individual contributions of PAM, bainitic ferrite (BF), fresh martensite (FM), and retained austenite (RA) to the strengthening by solute carbon atoms in the isothermally treated specimens at temperatures above and below M_s. All heat treated specimens present a small and similar strengthening by carbon in solid solution derived from the presence of retained austenite. Despite retained austenite exhibiting the highest carbon concentration between all phases (see Table 6.I), its strengthening contribution by solute carbon atoms results to be not significant compared to the individual contributions of the other phases at the three selected temperatures. At 340°C (above M_s), the main strengthening contribution stems from the bainitic ferrite due to its high volume fraction. The second greatest contribution derives from the 0.12 volume fraction of fresh martensite and represents approximately 30% of the total strengthening contribution.

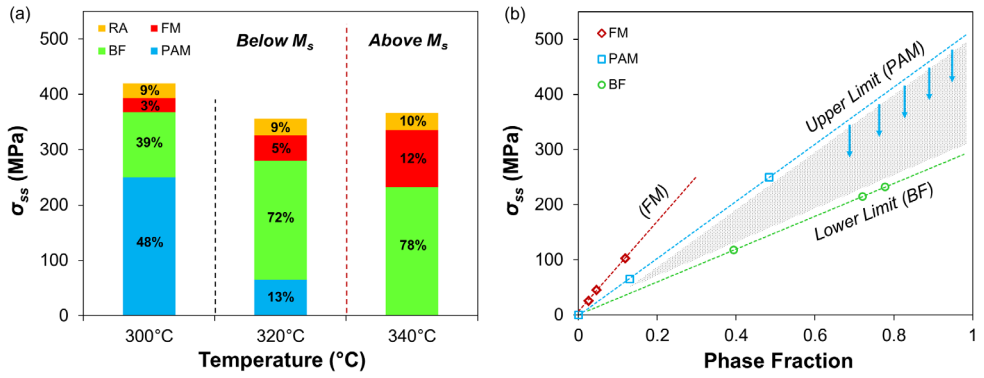

Figure 6.10. Comparison of the product of the volume fractions and the individual strengthening contributions by carbon in solid solution of the prior athermal martensite (PAM), bainitic ferrite (BF), and fresh martensite (FM) as a function of (a) the isothermal temperature and (b) the phase fraction. The numbers in percentage indicated in (a) correspond to the volume fractions of each phase.

At 320°C (below M_s), the main contribution to solid-solution strengthening also comes from the bainitic ferrite since it represents 0.72 of the total phase fraction. This contribution is similar to that of the bainitic ferrite at 340°C due to similar volume fractions (in the range of 0.72-0.78). At this lower temperature, the presence of a certain fraction of PAM also contributes to the overall solid-solution strengthening of the heat-treated specimens, compensating to some extent the lower contribution exhibited by 0.05 of fresh martensite. The sum of individual contributions of the different phases to the overall strengthening of the specimens isothermally treated at 320°C is not significantly different to that obtained at 340°C (see Figure 6.10.a).

At 300°C (below M_s), as a higher fraction of PAM is formed, the individual contribution by carbon in solid solution of this product phase becomes dominant within the

multiphase matrix. As observed in Figure 6.10.a, a similar strengthening contribution by carbon in solid solution is obtained with 0.48 volume fraction of PAM formed in specimens isothermally treated at 300°C than with 0.78 volume fraction of bainitic ferrite formed in those treated at 340°C. This means that formation of PAM has a greater effect than bainitic ferrite on the overall solid-solution strengthening of the isothermally treated specimens below M_s.

Figure 6.10.b shows a comparison of the individual strengthening contributions by carbon in solid-solution of the prior athermal martensite, bainitic ferrite, and fresh martensite as a function of their volume fraction. The solid-solution strengthening contribution of PAM to the overall yield stress per unit of fraction is 1.7 times higher than that of the bainitic ferrite. This relationship is directly dependent on the carbon concentrations attributed to PAM and bainitic ferrite. If the diffusion of carbon from the PAM to the remaining untransformed austenite is also considered to occur during the isothermal holding, the strengthening contribution of PAM will decrease as a consequence of the additional reduction of its carbon concentration in solid solution; this decrease is represented by blue arrows in Figure 6.10.b. Then, differences (shaded area) between the individual strengthening contributions via carbon in solid solution of PAM and bainitic ferrite will be smaller.

Maintaining a similar fraction of bainitic ferrite (0.72-0.78), there is a decrease of the UTS as the isothermal temperature is decreased from 340°C to 320°C (see Figure 6.4). This is mainly due to the reduction of the fresh martensite fraction formed (which is the hardest phase) as well as the formation of a certain fraction of PAM at 320°C (which is tempered). When the isothermal temperature is decreased from 320°C to 300°C, the UTS remains almost constant (see Figure 6.4) in spite of the variations of the fractions of PAM and bainitic ferrite. During the isothermal holding below M_s, the PAM reduces its carbon concentration by carbide precipitation and presumably also reduces its dislocation density, leading to a softening of this product phase. In both specimens, the sum of volume fractions of PAM and bainitic ferrite is approximately 0.85-0.87, confirming that tempered PAM may have a similar influence on the UTS as the isothermally formed bainitic ferrite.

The formation of carbides by the precipitation of part of the carbon contained within the PAM acts as a strengthening mechanism of the specimens heat treated below M_s, partly compensating the strengthening decrease by the loss of carbon in solid solution. This precipitation strengthening, together with the grain boundary strengthening, leads to an increase of the yield stress of these specimens with respect the ones heat treated above M_s. In turn, precipitation strengthening can imply the softening of the phase(s)

in which carbides are contained, explaining the decrease of the UTS of the specimens heat treated below M_s.

6.4.2. Influence of Phase Mixture on Strain Hardening

Figure 6.5 shows an increase of the *'YS/UTS'* ratio as the isothermal temperature is decreased from above M_s to below M_s, which implies a decrease of the strain hardening potential in specimens isothermally treated below M_s. This decreasing tendency is consistent with the observations of other researchers in similar studies [7,11,22,23]. In order to understand this tendency, two microstructural aspects are considered: (i) the presence of tempered PAM in these heat treated specimens and (ii) the possible differences in the mechanical stability of the retained austenite compared to the specimen heat treated above M_s. These aspects are discussed below:

(i) The presence of tempered PAM in the phase mixture of specimens heat treated below M_s gives rise to two opposing effects. On the one hand, PAM has a softer character than the fresh martensite obtained during the final cooling to room temperature due to the reduction of its carbon concentration in solid solution and a presumable reduction in dislocation density. Both phenomena are a direct consequence of the tempering process and lead to a decrease in UTS. On the other hand, the presence of higher fractions of tempered PAM with the decreasing annealing temperature lead to an increase of the yield stress due to a greater presence of carbides, compared to bainitic microstructures. These carbides can act as pinning points of the dislocations, impeding their movement. The combination of both effects narrows the difference between YS and UTS to the decreased capacity of plastic deformation of specimens isothermally treated below M_s.

(ii) The volume fractions of retained austenite (obtained by XRD) present in the isothermally treated specimens before and after performing the uniaxial tensile tests are shown in Figure 6.11. Results indicate that about 2/3 of the total volume fraction of retained austenite is mechanically transformed during the application of stress in all heat treated specimens. These observations suggest that the mechanical transformation of the retained austenite in multiphase microstructures is contributing in a similar way to the strain hardening of all heat treated specimens. However, slight differences in the mechanical stability of the retained austenite are due to variations in its composition, size, and morphology, but also to the strength of the surrounding phase [43-46].

High and similar carbon concentrations in the retained austenite are exhibited by all heat treated specimens (see Table 6.I) as a consequence of the carbon enrichment of the untransformed austenite during the isothermally bainite formation. These

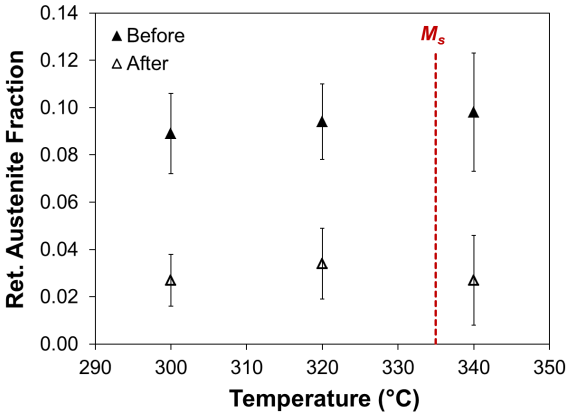

Figure 6.11. Volume fraction of retained austenite contained in specimens isothermally treated at the three selected temperatures above and below M_s before and after the application of tensile tests.

carbon concentrations should be sufficiently high to hinder the mechanical transformation of the retained austenite up to reaching the yield stress [47-50], so austenite transformation is assumed to effectively contribute to the strain hardening capacity. Small differences in the strain hardening contribution of the retained austenite between specimens heat treated at the three selected temperatures may be related to the mechanical stability of the distinct types of retained austenite present in these multiphase microstructures (see Figures 6.7.b-d). Thin films of retained austenite are mechanically more stable than coarser blocky grains of austenite in bainitic steels obtained through conventional treatments above M_s [51]; moreover, coarser grains are easier to mechanically transform than smaller ones. However, further investigations are needed to elucidate the individual contribution of the different types of retained austenite to the strain hardening of the heat treated specimens.

The analysis of the mechanical stability of retained austenite within these multiphase microstructures shows that the individual contribution of the mechanically-induced transformation of the retained austenite to the strain hardening capacity is similar in specimens heat treated above and below M_s due to the formation of similar fractions of retained austenite with similar levels of carbon enrichment and the transformation of similar fractions of retained austenite into martensite under the application of stress. At the same time, the formation and tempering of PAM gives rise to a lower strain hardening capacity of specimens annealed at temperatures below M_s. Combining both observations, it is concluded that the presence of tempered PAM within the multiphase microstructure slightly reduces the strain hardening capacity of specimens heat treated below M_s compared to those treated above M_s since tempered PAM counteracts the contribution of the mechanical transformation of the retained austenite.

6.5. Conclusions

The effects derived from the formation and tempering of prior athermal martensite on the overall mechanical response of a low-C high-Si steel were studied in terms of grain-boundary, solid-solution, and precipitation strengthening mechanisms in specimens isothermally treated for one hour at temperatures below M_s and confronted, in similar terms, with observations extracted from conventional treatments performed above M_s, where athermal martensite is not formed prior to the isothermal holding. The main conclusions obtained are the following:

1. Specimens isothermally treated for one hour below M_s exhibit higher yield stress and lower ultimate tensile strength than those treated by conventional heat treatments above M_s. Since the gap between yield stress and ultimate tensile strength is narrowed with the decreasing annealing temperature, specimens that were isothermally treated below M_s exhibit a smaller capacity of strain hardening during deformation than the ones treated above M_s.

2. The formation of small fractions of prior athermal martensite leads to an increase of the yield stress of the specimens treated below M_s with similar volume fractions of bainitic ferrite as those treated above M_s. This increasing tendency continues with the decreasing annealing temperature due to the formation of higher fractions of prior athermal martensite at the cost of bainitic ferrite and fresh martensite.

3. The formation of prior athermal martensite and its tempering during the one-hour isothermal holdings below M_s triggers several strengthening mechanisms, favouring the increase of the yield stress of these multiphase specimens. These phenomena are: the introduction of martensite-austenite interfaces, the presence of a higher carbon concentration in solid solution in prior athermal martensite (compared to bainitic ferrite), and the formation of carbides within laths of prior athermal martensite during the isothermal holding.

4. There is a similar contribution of the mechanical transformation of the retained austenite, upon the application of uniaxial stress, to the strain hardening of multiphase microstructures obtained by one-hour isothermal holdings above and below M_s. However, the presence and tempering of prior athermal martensite counteract this contribution in specimens heat treated below M_s and, consequently, slightly reduce their strain hardening capacity. This mainly occurs due to the softening of the tempered PAM as consequence of losing carbon in solid-solution (decreasing ultimate tensile strength) and the higher presence of carbides as the volume fraction of PAM is increased within the phase mixture (increasing yield stress).

References

[1] R.T. Howard, M. Cohen. Austenite transformation above and within the martensite range. Trans. AIME, 1948, vol. 176, pp. 384-397.

[2] C.E. Ericsson, M.S. Bhat, E.R. Parker, V.F. Zackay. Isothermal studies of bainitic and martensitic transformations in some low alloy steels. Metall. Trans. A, 1976, vol. 7, pp. 1800-1803.

[3] D.H. Kim, J.G. Speer, H.S. Kim, B.C. De Cooman. Observation of an isothermal transformation during quenching and partitioning processing. Metall. Mater. Trans. A, 2009, 40, pp. 2048-2060.

[4] H. Kawata, K. Hayashi, N. Sugiura, N. Yoshinaga, M. Takahashi. Effect of martensite in initial structure on bainite transformation. Mater. Sci. Forum, 2010, vols. 638-642, pp. 3307-3312.

[5] M.J. Santofimia, S.M.C. van Bohemen, D.N. Hanlon, L. Zhao, J. Sietsma. Perspectives in high-strength steels: Interactions between non-equilibrium phases. Inter. Symp. on AHSS, 2013, AIST, pp. 331-339.

[6] A. Navarro-López, J. Sietsma, M.J. Santofimia. Effect of prior athermal martensite on the isothermal transformation kinetics below M_s in a Low-C High-Si Steel. Metall. Mater. Trans. A, 2016, vol. 47, pp. 1028-1039.

[7] L. Zhao, L. Qian, J. Meng, Q. Zhou, F. Zhang. Below-M_s austempering to obtain refined bainitic structure and enhanced mechanical properties in low-C high-Si/Al steels. Scripta Mater., 2016, vol. 112, pp. 96-100.

[8] P. Kolmskog, A. Borgenstam, M. Hillert, P. Hedstrom, S.S. Babu, H. Terasaki, Y.I. Komizo. Direct observation that bainite can grow below M_s. Metall. Mater. Trans. A, 2012, vol. 43A, pp. 4984-4988.

[9] E.P. Da Silva, D. De Knijf, W. Xu, C. Föjer, Y. Houbaert, J. Sietsma, R. Petrov. Isothermal transformations in advanced high strength steels below martensite start temperature. Mater. Sci. Technol., 2015, vol. 31, pp. 808-816.

[10] S. Samanta, P. Biswas, S. Giri, S.B. Singh, S. Kundu. Formation of bainite below the M_s temperature: kinetics and crystallography. Acta Mater., 2016, vol. 105, pp. 390-403.

[11] J.C. Hell, M. Dehmas, S. Allain, J.M. Prado, A. Hazotte, J.P. Chateau. Microstructure-properties in carbide-free bainitic steels. ISIJ Int., 2011, vol. 51, pp. 1724-1732.

[12] X.Y. Long, J. Kang, B. Lu, F.C. Zhang. Carbide-free bainite in medium carbon steel. Mat. and Design, 2014, vol. 64, pp. 237-245.

[13] J. Sun, H. Yu, S. Wang, Y. Fan. Study of microstructural evolution, microstructure-mechanical properties correlation and collaborative deformation-transformation behaviour of quenching and partitioning (Q&P) steel. Mater. Sci. Eng. A, 2014, vol. 596, pp. 89-97.

[14] I. de Diego-Calderón, D. De Knijf, M.A. Monclus, J.M. Molina-Aldareguia, I. Sabirov, C. Föjer, R.H. Petrov. Global and local deformation behaviour and mechanical properties of individual phases in a quenched and partitioned steel. Mater. Sci. Eng. A, 2015, vol. 630, pp. 27-35.

[15] F. HajyAkbary, J. Sietsma, G. Miyamoto, N. Kamikawa, R. Petrov, T. Furuhara, M.J. Santofimia. Analysis of the mechanical behaviour of a 0.3C-1.6Si-3.5Mn quenching and partitioning steel. Mater. Sci. Eng. A, 2016, 677, pp. 505-514.

[16] E.P. Bagliani, M.J. Santofimia, L. Zhao, J. Sietsma, E. Anelli. Microstructure, tensile and toughness properties after quenching and partitioning treatments of a medium-carbon steel. Mater. Sci. Eng. A, 2013, vol. 559, pp. 486-495.

[17] I. de Diego-Calderón, M.J. Santofimia, J.M. Molina-Aldareguia, M.A. Monclus I. Sabirov. Deformation behaviour of a high strength multiphase steel at macro- and micro- scales. Mater. Sci. Eng. A, 2014, vol. 611, pp. 201-211.

[18] D. De Knijf, R. Petrov, C. Föjer, L.A.I. Kestens. Effect of fresh martensite on the stability of retained austenite in quenching and partitioning steel. Mater. Sci. Eng. A, 2014, vol. 615, pp. 107-115.

[19] K.O. Findley, J. Hidalgo, R.M. Huizenga, M.J. Santofimia. Controlling the work hardening of martensite to increase the strength/ductility balance in Q&P steels. Mater. Design, 2017, vol. 117, pp. 248-256.

[20] X. Tan, Y. Xu, X. Yang, D. Wu. Microstructure-properties relationship in a one-step quenched and partitioned steel. Mater. Sci. Eng. A, 2014, vol. 589, pp. 101-111.

[21] G. Mandal, S.K. Ghosh, S. Bera, S. Mukherjee. Effect of partial and full austenitisation on microstructure and mechanical properties of quenching and partitioning steel. Mater. Sci. Eng. A, 2016, vol. 676, pp. 56-64.

[22] J. Feng, T. Frankenbach, M. Wettlaufer. Strengthening 42CrMo4 steel by isothermal transformation below martensite start temperature. Mater. Sci. Eng. A, 2017, vol. 683, pp. 110-115.

[23] J. Tian, G. Xu, M. Zhou, H. Hu. Refined bainite microstructure and mechanical properties of a high-strength low-carbon bainitic steel treated by austempering below and above M_s. Steel Research Inter. 2018, pp. 1-10.

[24] A. Zinsaz-Borujerdi, A. Zarei-Hanzaki, H.R. Abedi, M. Karam-Abian, H. Ding, D. Han, N. Kheradmand. Room temperature mechanical properties and microstructure of a low alloyed TRIP-assisted steel subjected to one-step and two-step quenching and partitioning process. Mater. Sci. Eng. A, 2018, vol. 725, pp. 341-349.

[25] Z.C. Li, H. Ding, R.D.K. Misra, Z.H. Cai. Microstructure-mechanical property relationship and austenite stability in medium-Mn TRIP steels: the effect of austenite-reverted transformation and quenching-tempering treatments. Mat. Sci. Eng. A, 2017, vol 682, pp. 211-219.

[26] D. De Knijf, C. Föjer, L.A.I. Kestens, R. Petrov. Factors influencing the austenite stability during tensile testing of quenching and partitioning steel determined via in-situ Electron Backscatter Diffraction. Mat. Sci. Eng. A, 2015, vol. 638, pp. 219-227.

[27] R.D.K. Misra, V.S.A. Challa, P.K.C. Venkatsurya, Y.F. Shen, M.C. Somani, L.P. Karjalainen. Interplay between grain structure, deformation mechanisms and austenite stability in phase-reversion-induced nanograined/ultrafine-grained austenitic ferrous alloy. Acta Mater., 2015, vol. 84, pp. 339-348.

[28] C.F. Jatczak, J.A. Larson, S.W. Shin. Retained austenite and its measurements by X-ray diffraction. Society of Automotive Engineers, 1980, 453, Special Publication.

[29] J.B. Nelson, D.P. Riley. An experimental investigation of extrapolation methods in the derivation of accurate unit-cell dimensions of crystals. Proc. Phys. Soc., 1945, vol. 56, pp. 160-176.

[30] G.E. Dieter. Mechanical Metallurgy, SI Metric Edition. McGraw-Hill, 1988.

[31] L.C. Chang, H.K.D.H. Bhadeshia. Austenite films in bainitic microstructures. Mater. Sci. Technol., 1995, vol. 11, pp. 874-81.

[32] S.B. Singh, H.K.D.H. Bhadeshia. Estimation of bainite plate-thickness in low-alloy steels. Mater. Sci. Eng. A, 1998, vol. 245, pp. 72-79.

[33] H. Matsuda, H.K.D.H. Bhadeshia. Kinetics of the bainite transformation. Proc. R. Soc. Lond. A, 2004, vol. 460, pp. 1707-1722.

[34] H.K.D.H. Bhadeshia, R.W.K. Honeycombe. Steels: microstructure and properties. 4th Ed., Elsevier Ltd., 2017, pp. 41-42.

[35] S.H. Whang. Nanostructured metals and alloys: processing, microstructure, mechanical properties and applications. 1st Ed., Woodhead Publishing Limited, 2011.

[36] G.R. Speich, H. Warlimont. Yield strength and transformation substructure of low-carbon martensite. J. Iron Steel Inst., 1968, vol. 206, pp. 385-392.

[37] P.G. Winchell, M. Cohen. The strength of martensite. Trans. ASM, 1962, vol. 55, pp. 347-361.

[38] C.H. Young, H.K.D.H. Bhadeshia. Strength of mixtures of bainite and martensite. Mater. Sci. Technol., 1994, vol. 10, pp. 209-214.

[39] S.M.C. van Bohemen. Bainite and martensite start temperature calculated with exponential carbon dependence. Mater. Sci. Technol., 2012, vol. 28, pp. 487-495.

[40] J.B. Seol, D. Raabe, P.P. Choi, Y.R Im, C.G. Park. Atomic scale effects of alloying, partitioning, solute drag and austempering on the mechanical properties of high-carbon bainitic-austenitic TRIP steels. Acta Mater., 2012, vol. 60, pp. 6183-6199.

[41] B. Hutchinson, J. Hagström, O. Karlsson, D. Lindell, M. Tornberg, F. Lindberg, M. Thuvander. Microstructures and hardness of as-quenched martensites (0.1-0.5%C). Acta Mater., 2011, vol. 59, pp. 5845-5858.

[42] N. Ridley, H. Stuart. Lattice parameter anomalies at the curie point of pure iron. J. Phys. D. Appl. Phys., 1968, vol. 1, pp. 1291-1295.

[43] X.C. Xiong, B. Chen, M.X. Huang, J.F. Wang, L. Wang. The effect of morphology on the stability of retained austenite in a quenched and partitioned steel. Scripta Mater., 2013, vol. 68, pp. 321-324.

[44] Z.P. Xiong, A.A. Saleh, R.K.W. Marceau, A.S. Taylor, N.E. Stanford, A.G. Kostryzhev, E.V. Pereloma. Site-specific atomic-scale characterization of retained austenite in a strip cast TRIP steel. Acta Mater., 2017, vol. 134, pp. 1-15.

[45] P.J. Jacques, J. Ladriere, F. Delannay. On the influence of interactions between phases on the mechanical stability of retained austenite in TRIP multiphase steels. Metall. Mater. Trans. A, 2001, vol. 32, pp. 2759-2768.

[46] J. Hidalgo, K.O. Findley, M.J. Santofimia. Thermal and mechanical stability of retained austenite surrounded by martensite with different degrees of tempering. Mater. Sci. Eng. A, 2017, vol. 690, pp. 337-347.

[47] J.G. Speer, E. De Moor, A.J. Clarke. Critical assessment 7: quenching and partitioning. Mater. Sci. Tech-Lond., 2015, vol. 31, pp. 3-9.

[48] A.J. Clarke, J.G. Speer, M.K. Miller, R.E. Hackenberg, D.V. Edmonds, D.K. Matlock, F.C. Rizzo, K.D. Clarke, E. De Moor. Carbon partitioning to austenite from martensite of bainite during the quench and partition (Q&P) process: a critical assessment. Acta Mater., 2008, vol. 56, pp. 16-22.

[49] M.J. Santofimia, L. Zhao, R. Petrov, C. Kwakernaak, W.G. Sloof, J. Sietsma. Microstructural development during the quenching and partitioning process in a newly designed low-carbon steel. Acta Mater., 2011, vol. 59, pp. 6059-6068.

[50] Y. Toji, G. Miyamoto, D. Raabe. Carbon partitioning during quenching and partitioning heat treatment accompanied by carbide precipitation. Acta Mater., 2015, vol. 86, pp. 137-147.

[51] H.K.D.H. Bhadeshia, D.V. Edmonds. Bainite in silicon steels: new composition-property approach – Part 1. Metal Science, 1983, vol. 17, pp. 411-419.

CHAPTER 7

Effect of Holding Time on Microstructure-Properties Relationship of Multiphase Microstructures Isothermally Obtained Below M_s

This chapter corresponds to the article "Unravelling the mechanical behaviour of advanced multiphase steels isothermally obtained below M_s" by A. Navarro-López, J. Hidalgo, J. Sietsma, and M.J. Santofimia, Mater. Design (2020) vol. 188, 108484.

Abstract

The initial formation of athermal martensite was proven to accelerate the subsequent bainite formation kinetics during isothermal holdings below the martensite-start temperature (M_s). In turn, the presence of prior athermal martensite (PAM) within the phase mixture modifies the overall mechanical response of these newly-designed multiphase steels. Differences stem not only from the balance of product phases, but also from the effect of tempering of the PAM with variations in the applied holding time. This work investigates the effect of tempering time on the mechanical behaviour of the PAM and, as consequence, on the overall mechanical response of these microstructures. Results show that, for short holding times (several minutes), PAM yields similar to as-quenched martensite while, for longer holding times, its yielding behaviour becomes comparable to the one exhibited by typical tempered martensite. Furthermore, the use of Kocks-Mecking curves for the analysis of the mechanical performance confirms the bainitic character of the product phase isothermally formed below M_s. Tailoring the bainitic-martensitic microstructure with variations of the holding time below M_s enables to obtain advanced multiphase steels with comparable mechanical properties to those exhibited by conventional bainitic steels, but in shorter processing times due to the acceleration of bainite formation.

7.1. Introduction

Recent investigations on low-carbon steels, alloyed with medium-manganese and/or high-silicon contents, heat treated through isothermal holdings below the martensite start (M_s) temperature show that a good combination of mechanical properties can be attained, similar, in many cases, to the ones exhibited by conventional bainitic steels [1-9]. The main difference between both types of multiphase steels lies in the presence of prior athermal martensite (PAM) in the microstructures obtained below M_s. In Chapter 2, the formation of a certain fraction of PAM was proven to accelerate significantly the kinetics of the subsequent bainite reaction at the onset of the transformation. In turn, PAM also affects the overall mechanical response of these multiphase steels, as was demonstrated in Chapter 6. Firstly, PAM can contribute, in principle, to the strengthening of the phase mixture since it is initially a carbon-supersaturated martensitic phase. Secondly, the fragmentation of the initial austenite grains due to the formation of PAM favours the increase of the yield stress through the reduction of the average bainite sheaf size [1,9]. Finally, the tempering of PAM with holding time leads to the softening of this micro-constituent due to the precipitation of carbon in solid solution in the form of carbides as well as dislocations recovery, affecting both phenomena the mechanical behaviour of the steel.

Variation of the holding time gives rise to different degrees of tempering of the PAM, resulting in different individual mechanical response of this product phase within the final phase mixture. The tempering process can be divided into several stages, arranged in order of increasing tempering temperature. At low temperatures, carbon atoms segregate at dislocations, phenomenon that can occur even during quenching. At intermediate temperatures, transitional carbides start to precipitate within the martensitic matrix. Finally, at highest temperatures of the tempering range, transitional carbides transform into cementite, which coarsens upon extended tempering times [10]. All these phenomena lead to the softening of the PAM due to changes in its matrix, which can be aggravated by the recovery of dislocations from intermediate holding temperatures (generally, higher than approximately 400°C). Previous investigations on this type of multiphase steels show that the presence of PAM leads to an increase of the yield stress together with a reduction of the tensile strength in specimens annealed below M_s in comparison to those isothermally treated above M_s [1,2,5,6,8,9]. Among these investigations, only a few research studies show the evolution of the mechanical properties of specimens isothermally treated below M_s at different holding times [5,8]. These studies report a rapid decrease of the yield stress at short holding times (only a few minutes) and, then, an increase of the yield stress with longer holding times. On the contrary, a decreasing evolution of the ultimate tensile strength is reported with respect to the increasing holding time.

A deeper analysis of the evolution of the mechanical properties is still needed by taking into consideration all product phases formed in these advanced multiphase steels. This will allow to understand the effect of holding time not only on the degree of tempering of PAM and its individual mechanical behaviour, but also on the microstructure-properties relationship derived from the multiphase mixture formed in which bainitic ferrite and/or retained austenite are also present. This research work investigates the mechanical behaviour of prior athermal martensite after the application of different holding times below M_s and, consequently, its effect on the formation of other phases and on the overall mechanical behaviour of these multiphase steels. The evolution of the microstructure and the resulting properties are studied by the application of different isothermal treatments above and below M_s in a low-carbon steel. The resulting properties are compared and benchmarked against the mechanical properties reported in other research studies as well as other conventional grades of advanced high strength steels.

7.2. Experimental Procedure

The chemical composition of the alloyed steel investigated in the present work is indicated in Table 7.I. Double T-shaped tensile specimens and cylindrical dilatometry specimens were machined parallel to the rolling direction of a hot rolled slab of 4 mm thickness. The dimensions of these specimens are indicated in Figure 7.1. The two types of specimens were extracted from a different area of the same hot rolled slab used to extract the specimens analysed in Chapters 2 and 3. Local compositional variations of the hot rolled slab led to slight differences in the critical temperatures of the steel, such as the M_s temperature. A Bähr 805A/D dilatometer was primarily used to thermally treat all specimens and, secondarily, to identify phase transformations occurring during the applied heat treatments. All specimens were inductively heated up under vacuum conditions of the order of 10^{-4} mbar and cooled down under a protective atmosphere of continuously-flushed helium gas. An S-type thermocouple was spot-welded on the surface of each specimen to control and monitor the temperature at any instant.

Figure 7.2 shows a schematic overview of the heat treatments applied to both types of specimens. Three tensile specimens were used per each thermal condition to obtain a statistical representativeness of their mechanical performance under tensile deformation. On the other hand, only one dilatometry specimen was used per thermal condition to identify the phase transformations occurring during each heat treatment. A direct-quench from full austenitization to room temperature was carried out to determine the mechanical response of a fully untempered martensitic microstructure. The experimental M_s temperature was determined at $M_{s\,(1\%)}$ = 335°C ± 5°C, as described in Chapter 6. Three isothermal treatments with different holding times ('t1', 't2', 't3', see Table 7.II) after full austenitization were performed at each of the three selected temperatures to obtain intermediate fractions of bainitic ferrite and determine the mechanical response

Table 7.I. Chemical composition (in wt. pct) of the alloyed steel with balanced iron (Fe).

C	Mn	Si	Mo	Al
0.20	3.51	1.52	0.25	0.04

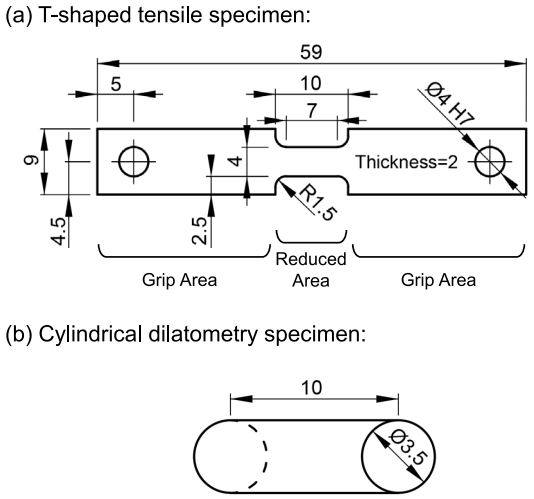

Figure 7.1. Schematic representation of tensile and cylindrical specimens with dimensions in mm.

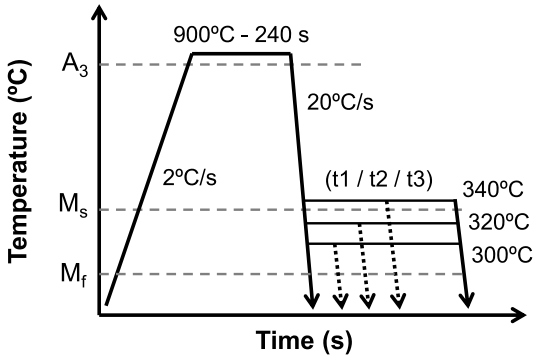

Figure 7.2. Direct-quench and isothermal treatments (t1 / t2 / t3) performed to both types of specimens.

of the resulting microstructures. The phase fractions formed after each heat treatment were determined from the dimensional changes detected by dilatometry of the heat-treated cylindrical specimens. Experimental results derived from isothermal treatments 't3' at the three selected temperatures were previously analysed in Chapter 6.

Table 7.II. Holding times ('t1', 't2', 't3') of the isothermal treatments performed at the selected temperatures above and below M_s.

HT	Isothermal holding time (s)		
	300°C	320°C	340°C
t1	7	253	441
t2	151	422	615
t3	3600	3600	3600

An Instron 5500R electromechanical tester machine was used to perform all tensile tests, which were carried out in extension control at room temperature. A clip-on extensometer with knife edges was used to measure the elongation of the specimen gauge during the tensile test. The attachment of the extensometer to the tensile specimen consisted of fixing firmly by elastic bands the knife edges of the extensometer in both extremes of the specimen gauge. The extensometer, with a separation between knife edges of 7.8 mm, completely covered the gauge length of the double T-shaped specimen. Once tensile tests were performed, mechanical properties such as yield stress, tensile strength, and uniform elongation were determined from the corresponding engineering stress-strain curves of all heat treated specimens. In this work, the 0.2% offset method was used for the determination of the yield stress (σ_y).

Cross sections of heat-treated cylindrical specimens were grinded and polished to 1 μm, and etched with 2% Nital to observe the microstructures obtained after heat treatments. A JEOL JSM-6500F Scanning Electron Microscope (SEM) was used for the microstructural characterization, using a 15 kV electron beam and the Secondary Electron Imaging (SEI) detection mode. A Bruker D8-Advance diffractometer was used to perform X-ray diffraction (XRD) measurements in order to determine the retained austenite fraction in the cylindrical specimens. These measurements were carried out by using Co-Kα radiation. A 2θ scan from 40° to 130° was performed in all specimens with a step size of 0.035°. The integrated area method was used to calculate the fractions of retained austenite by comparing the areas under the {200}, {220}, and {311} diffraction peaks of fcc-austenite with the areas under the {110}, {200}, {211}, and {220} diffraction peaks of the bcc- phase(s) [11].

7.3. Results

7.3.1. Formation of Product Phases

Dilatometry curves for cylindrical specimens isothermally treated at 340°C, 320°C, and 300°C for holding times 't1', 't2', and 't3' are shown in Figures 7.3.a-c. All specimens exhibit a linear behaviour during cooling from austenitization until reaching the M_s temperature. This is an indication of the non-decomposition of austenite into bcc-

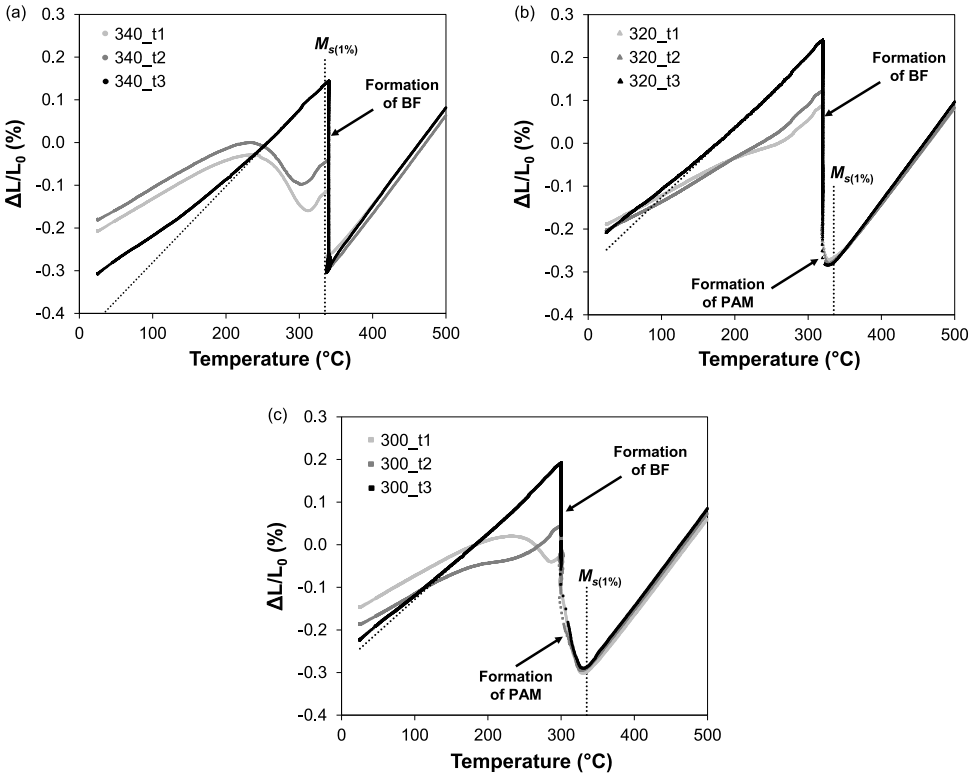

Figure 7.3. Change in length of cylindrical dilatometry specimens during cooling stages and isothermal holdings at (a) 340°C, (b) 320°C, and (c) 300°C for different holding times (t1, t2, and t3). The experimental M_s temperature is also shown.

phases, such as ferrite, pearlite, or bainite, before the onset of the austenite-to-martensite transformation. In treatments performed at 340°C (above M_s), there is a length increase (dilatation) in all specimens during the isothermal holding which is originated by the formation of bainitic ferrite (BF) (see Figure 7.3.a). In treatments performed at 320°C and 300°C (below M_s), a deviation from linearity occurs once the M_s temperature is overcome during cooling due to the formation of prior athermal martensite (PAM), as indicated in Figures 7.3.b-c. The austenite-to-martensite transformation stops when the cooling is interrupted at the corresponding isothermal temperature. Subsequently, dilatation takes place during all isothermal holdings as consequence of the formation of bainitic ferrite (see Figures 7.3.b-c).

Finally, there is a deviation from linearity of the change in length during the final cooling from the isothermal temperatures to room temperature in all experimental dilatometric curves, as shown in Figures 7.3.a-c. This deviation is an indicative of the decomposition of untransformed austenite into fresh martensite (FM). In all cases, the isothermal bainitic transformation is incomplete even after one hour of holding time

and the remaining untransformed austenite partially transforms into fresh martensite, while the rest is partially retained at room temperature.

The quantification of the phase fractions was first performed in the one-hour isothermal treatments ('t3'). In these heat treatments, the volume fractions of fresh martensite, originated from the untransformed austenite decomposition during the final cooling, were obtained from the dilatometry data by following the procedure described in Chapter 2. The bainitic ferrite fractions were balanced from volume fractions of the rest of product phases, i.e., from prior athermal martensite, fresh martensite (both obtained from dilatometry), and retained austenite (obtained from XRD). For the isothermal treatments 't1' and 't2', bainitic ferrite fractions were extracted from the dilatometry curves of the one-hour isothermal treatments ('t3') by considering the fraction formed at the selected holding times for each of the three temperatures (see Table 7.II). In these heat treatments, the fresh martensite fractions were balanced from the volume fractions of prior athermal martensite, bainitic ferrite (both obtained from dilatometry), and retained austenite (obtained from XRD).

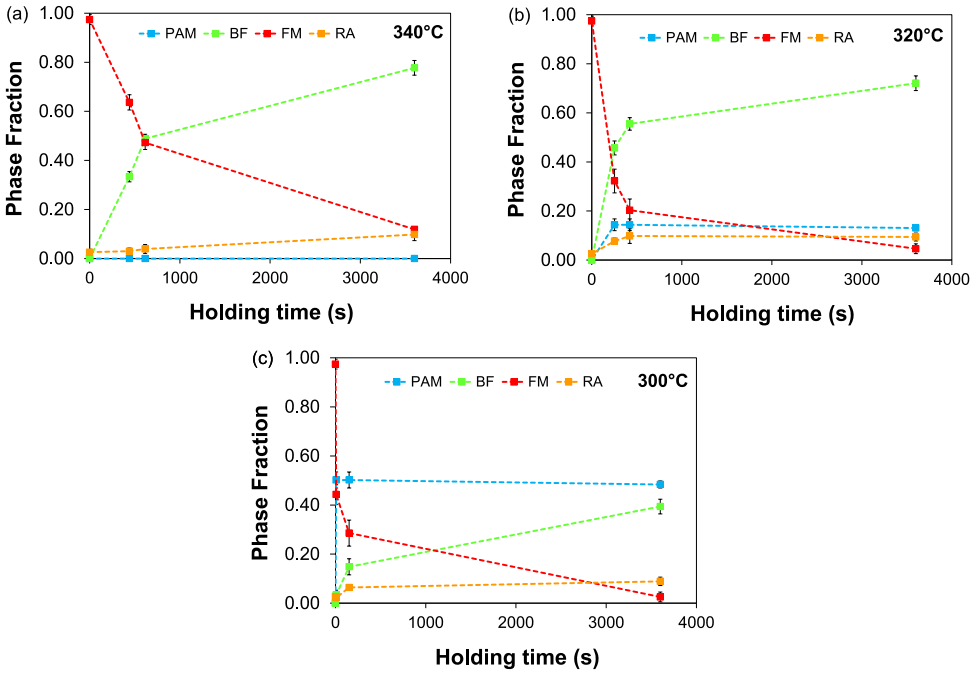

Figure 7.4. Evolution of the multiphase mixture after the application of isothermal treatments at (a) 340°C, (b) 320°C, and (c) 300°C for holding times 't1', 't2', and 't3'. The phase mixture of the direct quenched specimen is considered in all figures as the reference value at holding time '0 s'. The following terms refer to: 'PAM: prior athermal martensite', 'BF: bainitic ferrite', 'FM: fresh martensite', and 'RA: retained austenite'.

Figures 7.4.a-c show the evolution of the volume fractions of the distinct phases of the multiphase mixture formed after the application of the previously described isothermal treatments at 340°C, 320°C, and 300°C, respectively. Implicitly, the final balance of phase fractions for each thermal-temporal condition can be extracted from these figures. As is observed, the volume fraction of PAM is maintained constant with holding time at each temperature since it only depends on the undercooling below M_s. The volume fraction of bainitic ferrite increases with holding time at all temperatures and, as consequence, a lower volume fraction of fresh martensite is formed from the untransformed austenite during the final cooling to room temperature. The final fraction of retained austenite also increases with holding time at all temperatures, reaching maximum values of 0.10 in specimens heat treated for one hour of holding time.

7.3.2. Microstructural Evolution

The microstructural characterization of the direct-quenched specimen and specimens isothermally treated at the selected temperatures for the holding time 't3' is presented in Chapter 6. Figure 7.5 shows the microstructures obtained in specimens heat treated by isothermal holdings 't1' and 't2' at temperatures above and below M_s. At 340°C (above M_s), the microstructure evolves from a martensitic matrix, formed by large fresh martensite (FM) areas surrounded by small acicular units of bainitic ferrite (BF) after a holding time of 441 s ('t1') (see Figure 7.5.a), to a bainitic-martensitic matrix of similar phase fractions, where bainitic ferrite and fresh martensite appear in the form of acicular units and laths, respectively, after a holding time of 615 s ('t2') (see Figure 7.5.b). Retained austenite is present in the form of thin films between the units of bainitic ferrite, as observed in the dashed-rectangular magnified area of Figures 7.5.a-b.

At 320°C (below M_s), tempered martensite (TM) is present in the microstructure since a 0.14 volume fraction of prior athermal martensite is formed before applying the isothermal holdings. After the holding time of 253 s ('t1') (Figure 7.5.c), there is a bainitic-martensitic matrix of similar phase fractions formed by acicular units of bainitic ferrite with thin films of retained austenite between them, besides tempered martensite and fresh martensite laths. When the applied holding time is 422 s ('t2') (Figure 7.5.d), the martensitic-bainitic matrix evolves towards a matrix that is mainly formed by bainitic ferrite units. In both microstructures, tempered martensite is characterized by large elongated laths with carbides (Cb). Since the austenite regions untransformed during the isothermal holding are reduced from the isothermal treatment 't1' to 't2', laths of fresh martensite become smaller, and large fresh martensite areas are progressively converted into isolated martensite-austenite (MA) islands.

At 300°C (below M_s), prior athermal martensite represents a 0.50 volume fraction of the final microstructure. After the heat treatment 't1' (see Figure 7.5.e), in which the

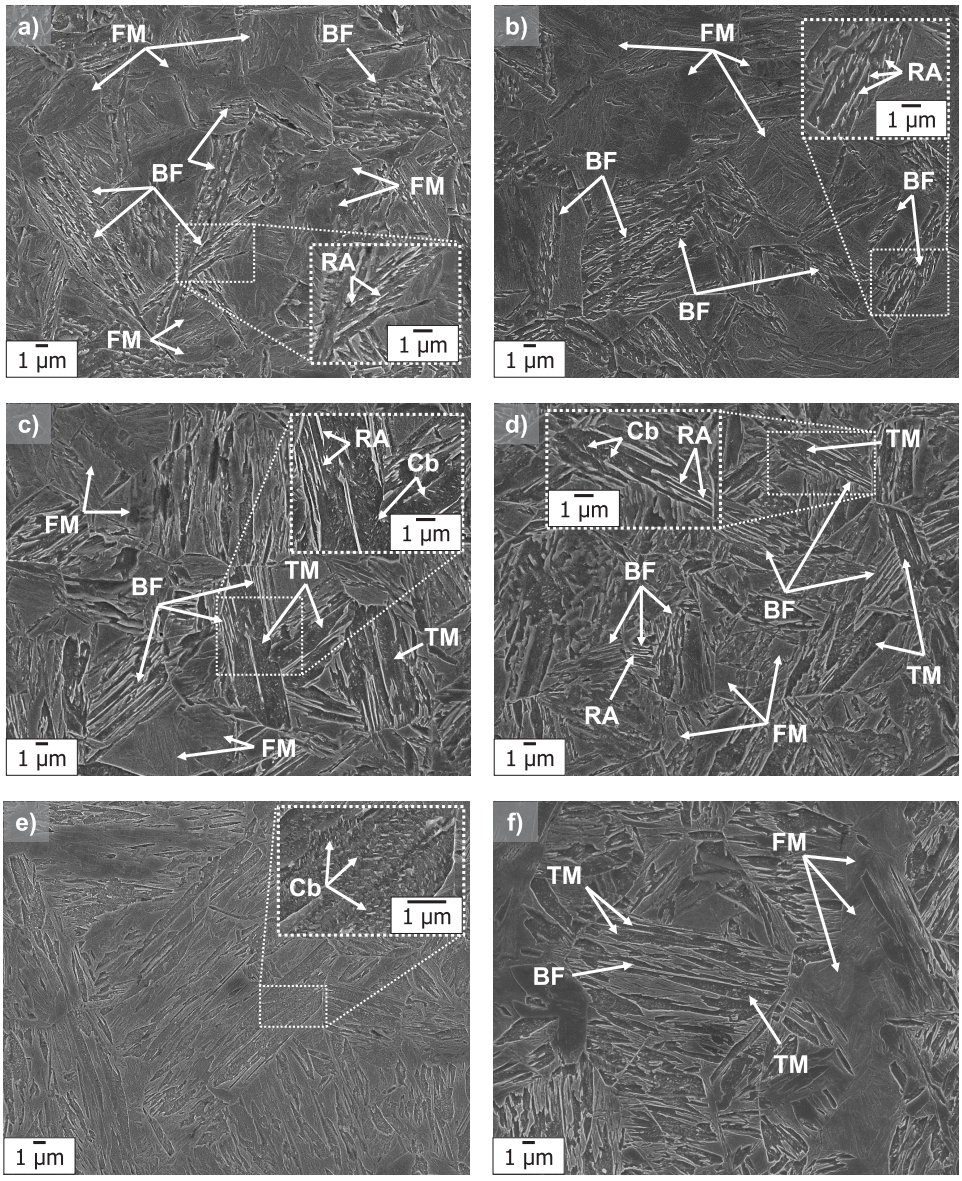

Figure 7.5. Evolution of microstructures obtained from different isothermal holding times at temperatures of a-b) 340°C (t1-t2), c-d) 320°C (t1-t2), and e-f) 300°C (t1-t2). The following terms refer to: 'TM: tempered martensite', 'BF: bainitic ferrite', 'FM: fresh martensite', 'RA: retained austenite', and 'Cb: carbides'. In this work, the term TM refers to PAM which is tempered during isothermal holding.

holding time is only 7 s, the microstructure is similar to the one obtained in a direct-quenched specimen (see Chapter 6). Carbides (Cb) are present within the martensite laths, as observed in the dashed-rectangular magnified area of Figure 7.5.e, which

indicates possible auto-tempering of martensite. Despite obtaining similar fractions of prior athermal martensite (PAM) and fresh martensite, approximately 0.50 and 0.44, respectively, the microstructural characteristics defining tempered martensite at higher temperatures cannot be distinguished in this microstructure. Moreover, it is not possible to ascertain the presence of bainitic ferrite due to its small volume fraction (less than 0.05). For the heat treatment 't2', in which the holding time is increased to 151 s, tempered martensite can be distinguished from fresh martensite (see Figure 7.5.f). Tempered martensite is present as elongated laths and laths with a sharp tip at one of its edges. Both types of martensitic laths contain carbides. Small bainitic ferrite units are identified in the surroundings of tempered martensite laths. Large areas of fresh martensite are also observed in this microstructure.

7.3.3. Mechanical Behaviour

Figures 7.6.a, c, e show the engineering stress-strain curves obtained from uniaxial tensile tests performed to the specimens heat treated for the selected isothermal temperatures and holding times. As observed in these engineering curves, all specimens exhibit a continuous yielding behaviour in spite of differences in the phase mixture obtained after the application of distinct isothermal treatments. This means that there is a smooth transition from elastic to plastic behaviour in all specimens, but the 0.2% yield stress is unambiguous. Extracted from these engineering curves, the evolution of the yield stress (YS) as well as the ultimate tensile strength (UTS) with holding time at the selected temperatures is presented in Figures 7.6.b, d, f. The yield stress as well as the ultimate tensile strength decrease with holding time independently of the applied isothermal temperature.

Figure 7.6 also shows mean values of uniform elongation (UEL) and strain hardening ('*YS/UTS*' ratio) of all heat-treated specimens at the selected temperatures. Uniform elongation increases with holding time for all isothermal holding temperatures. Once the maximum UEL is reached (at UTS), necking takes place within the gauge length until fracture. As observed in Figure 7.6, fracture strains of all heat-treated specimens are in the range of 17-23%. Note that the sub-size dimensions of double T-shaped specimens used in this work affect the elongation values obtained in tensile tests since the contribution from the necked region to the overall elongation is greater due to the reduced gauge length of the specimens [12]. Therefore, any comparison of these results with literature data must be performed with care.

Concerning the '*YS/UTS*' ratio, which represents the potential of a material to be hardened by plastic deformation, all heat treated tensile specimens present similar strain hardening potential. The mentioned ratio varies from 0.65 to 0.75, which are considered typical '*YS/UTS*' ratios in multiphase steels [4,13]. The specimens isothermally treated

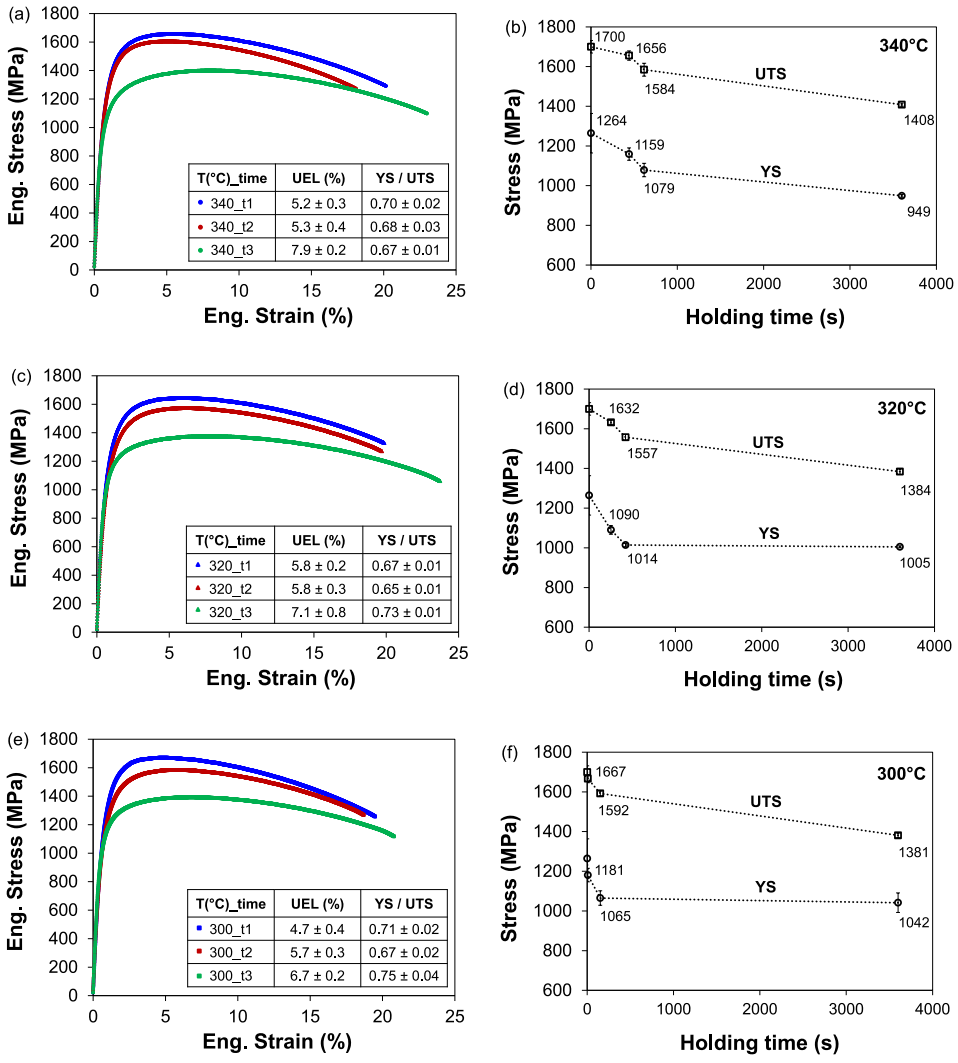

Figure 7.6. Engineering stress-strain curves and evolution of 0.2% offset yield stress (YS) and ultimate tensile strength (UTS) of specimens isothermally treated for holding times 't1', 't2', and 't3' at (a-b) 340°C, (c-d) 320°C, and (e-f) 300°C, respectively. Average values of uniform elongation (UEL) and strain hardening ('*YS/UTS*' ratio) of these specimens are also indicated for each thermal condition. The phase mixture of the direct quenched specimen is considered as the reference value at holding time '0 s'.

above M_s present a slight increase of their strain hardening potential with increasing holding time. On the contrary, specimens heat treated below M_s exhibit a slight decrease of their strain hardening potential with increasing holding time.

7.4. Discussion

7.4.1. Effect of Multiphase Microstructure on Strength

The evolution of the phase mixture with holding time leads to a decrease of the yield stress (YS) and ultimate tensile strength (UTS) in specimens thermally treated at temperatures above and below M_s (see Figure 7.4 and Figure 7.6). In specimens heat treated above M_s, the continuous decrease of YS and UTS with increasing holding times is directly related with a marked increase of the fraction of the softer bainitic ferrite at the cost of the decrease of the fraction of the harder fresh martensite (see Figures 7.4.a and 7.6.b). In specimens heat treated below M_s, a similar evolution of YS and UTS is observed up to holding times of 600 s (see Figures 7.6.d and 7.6.f). However, for longer holding times, the YS hardly decreases in spite of the formation of a higher fraction of bainitic ferrite and a lower fraction of fresh martensite. This dissimilar yielding behaviour after holding time 't2' should be attributed to the presence of prior athermal martensite (PAM) in the multiphase microstructure of specimens isothermally treated below M_s compared to that of specimens treated above M_s.

The observed evolution of the yield stress with holding time in specimens isothermally treated below M_s is partially in agreement with experimental observations reported by Yan et al. [5] and Zinsaz et al. [8]. Both authors studied the mechanical response exhibited by specimens isothermally treated for several holding times at temperatures below M_s in similarly compositional low-carbon steels as the one investigated in this study. In both investigations, there is a decrease of the YS exhibited by specimens treated below M_s up to short holding times (approximately 100 s). As the holding time is increased, the yielding response of these specimens radically changes and the YS increases continuously. Both authors suggest that the tempering of a high fraction of PAM dictates the yielding response of these specimens.

For a better comprehension of the yielding behaviour of PAM formed in isothermal treatments below M_s, the derivative of the true stress-strain curves, which represents the instantaneous work hardening rate (Θ), as a function of the true stress, known as the extended (since also the pre-yield range is included [14]) Kocks-Mecking (K-M) curves [15], is used in this analysis. Extended K-M curves have been demonstrated to be a reliable physically based method, alternative to the 0.2% offset criterion, to determine the yield stress of single-phase ferritic steels [14]. For such materials, two stages are commonly distinguished before uniform elongation is exceeded: 1) a gradual, although initially slow, decay of Θ corresponding with the anelastic reversible behaviour due to bowing of dislocations, and 2) a marked transition to the plastic regime when dislocations begin to massively multiply.

Figures 7.7.a-b show the instantaneous work hardening rate (Θ) of the specimens heat treated at temperatures of 340°C and 300°C, respectively. The extended K-M curves of a direct-quench specimen, and quenched and tempered (Q&T) specimens heat treated at both temperatures are also included for comparison. These latter treatments consisted of a one-hour holding stage (tempering) at either 340°C or 300°C after a rapid cooling from full austenitization. Both Q&T specimens exhibited a final microstructure which consisted of 0.97-0.98 of tempered martensite with 0.02-0.03 of retained austenite.

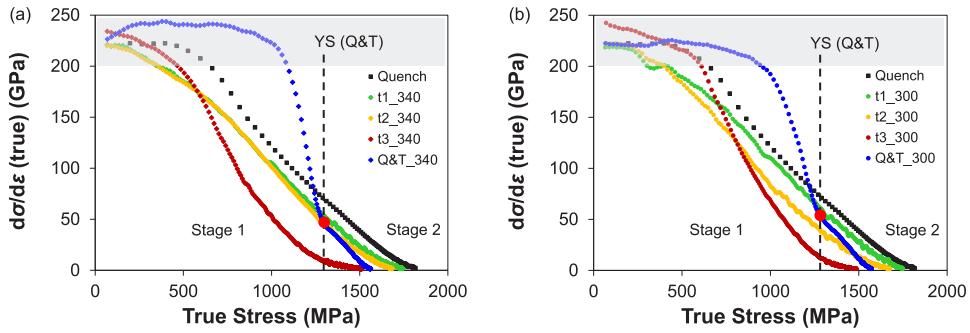

Figure 7.7. Instantaneous work hardening rate (Θ) as function of true stress of specimens thermally treated by a rapid cooling ('Quench'), isothermal holdings for several times ('t1', 't2', and 't3'), and quenching and tempering ('Q&T') at temperatures of (a) 340°C (above M_s) and (b) 300°C (below M_s).

In quenched specimens, the extended Kocks-Mecking curves exhibit an almost linear behaviour beyond stresses of 800 MPa, so no clear transition from elastic to plastic regime is visible. As the microstructure is only formed by quenched martensite, this yielding behaviour is related to the high density of dislocations within this phase together with a probably heterogeneous distribution of dislocation segment lengths. On the other hand, Q&T specimens exhibit extended Kocks-Mecking curves in which the pre-yield and plastic stages are well defined, showing a marked transition between both. The true stress at which an abrupt change of the instantaneous work hardening rate occurs (marked by a red circle in Figures 7.7.a-b) coincides with the yield stress of these specimens [14]. This yielding behaviour is related to all processes inherent to tempering, such as segregation/precipitation of carbon and reduction of dislocations density, which structurally modifies the initial matrix of as-quenched martensite [16].

Regarding isothermally treated specimens, the initial very slow decrease of Θ is barely observed, but a continuous decay of Θ is taking place. Values of Θ at very low stresses which exceed typical elastic modulus of around 210 GPa (the shaded range in Figures 7.7.a-b) arise from inaccuracies of the measurements. The lack of a clear transition from stage 1 to stage 2 denotes continuous yielding, which is typical of martensitic steels, but, for the current alloys, it is also a consequence of a multiphase microstructure. Differences

in the shape of the extended K-M curves of the different heat-treated specimens are related with the different mixture of product phases formed after the application of the thermal treatments.

In Figure 7.7.a, the specimen isothermally treated above M_s for 't1' exhibits an evolution of Θ similar to the direct-quenched specimen since fresh martensite is the dominant phase in the mixture (see Figure 7.4.a). The same yielding behaviour is observed in the specimen isothermally treated for 't2'. In this case, although the phase mixture evolves to a martensitic-bainitic matrix of similar volume fractions, the harder character of the fresh martensite prevails and, consequently, determines the overall yielding behaviour. However, in the specimen isothermally treated for one hour ('t3'), where the volume fraction of bainitic ferrite is 0.78, the instantaneous work hardening rate decreases faster during stage 1 of the extended K-M curve. This is an indication that bainitic ferrite yields at lower stress than fresh martensite, and its yielding behaviour prevails over the one of the fresh martensite.

In Figure 7.7.b, the specimen isothermally treated below M_s for 't1' also exhibits an evolution of Θ similar to the direct-quench specimen. This means that, after the formation of 0.48 volume fraction of PAM, a holding time of 7 s ('t1') is not sufficient to temper it, which indicates that PAM mechanically behaves as fresh martensite for these thermal conditions. In the specimen isothermally treated for 't2', a higher volume fraction of bainitic ferrite is formed (0.15), but the overall yielding behaviour is still dominated by martensitic phases, either the harder fresh martensite (0.29) or the softer PAM (0.50), which is tempered to a certain degree. When the holding time is increased up to one hour ('t3'), the isothermally treated specimen exhibits a decay of Θ before yielding more comparable to the one exhibited by the Q&T specimen (see Figure 7.7.b). The similarity of both curves is consequence of the presence of a higher fraction (0.48) of PAM tempered to a moderate degree, which becomes the dominant phase within the martensitic-bainitic mixture. However, two differences can be observed by comparing both extended K-M curves. The first is that the transition from the elastic to the plastic regime is not yet clearly marked as it is in the extended K-M curve of the Q&T specimen. The second difference is that the gradual decay of Θ occurs at lower stress. This is due to the presence of bainitic ferrite in the phase mixture, which indicates that bainitic ferrite yields at lower stress than tempered martensite.

According to this analysis, and taking into consideration the reported results in refs. [5] and [8], the tempering of PAM strongly affects its yielding behaviour, giving rise to a general decrease of the YS of specimens isothermally treated below M_s for short holding times (< 200 s). Tempering leads to the loss of carbon atoms in solid solution contained in the initial carbon-supersaturated PAM via diffusion into the surrounding

untransformed austenite during holding and segregation to the dislocation strain fields in the PAM [17,18]. These processes entail the softening of this product phase and, as a consequence, the decrease of the overall YS and UTS. The precipitation of carbon atoms in the form of carbides, a phenomenon that is also associated to tempering, will be minor during the isothermal holding since, in the present work, the formation of carbides within the PAM already takes place during the initial cooling before the isothermal holding. Figure 7.5.e shows the early precipitation of carbides in the specimen isothermally treated at 300°C (below M_s) for 7 s ('t1'), confirming the auto-tempering of PAM. On the other hand, the recovery process, which implies the reduction of the dislocation density, can contribute to the softening of the PAM with a moderate degree of tempering, but this effect may be minor in comparison with the ones previously described since the isothermal temperatures applied are lower than 400°C, the limit temperature above which the recovery of dislocations certainly becomes an important effect of the tempering [19].

As the applied holding time increases (> 200 s), it is presumable that processes leading to the softening of PAM are mostly finished, thus the yielding behaviour of PAM does not significantly vary with holding time, becoming similar to the tempered martensite of typical Q&T treatments. The insignificant variation of the yielding behaviour of PAM partially leads to the nearly constant YS exhibited by specimens treated below M_s after a certain holding time ('t2'). This fact is in agreement with the results reported by Cupertino et al. [20] and Liu et al. [21], concerning the yielding response of Q&T specimens of similarly compositional steels as the one investigated in this study. In both studies, results show that the yield stress of these Q&T specimens remains nearly constant after the application of a certain holding time at tempering temperatures below 350°C.

In addition to the minor effect of the tempering on the yielding response of the PAM at low temperatures and long holding times, the nearly constant YS in specimens heat treated below M_s after a certain holding time ('t2') is supported by the smaller variation of bainitic ferrite and fresh martensite fractions between holding times 't2' and 't3' in these specimens, compared to those treated above M_s. However, this fact does not explain by itself the nearly constant YS since, in principle, the formation of bainitic ferrite at the cost of fresh martensite should lead to the reduction, to some extent, of the YS and UTS of specimens isothermally treated below M_s. For these specimens, the strengthening effect due to the refinement of bainitic structures may partially counteract the expected decrease of YS [9].

The higher refinement of bainitic structures with the decreasing temperature has been experimentally reported in conventional low-carbon bainitic steels obtained above M_s

[22,23]. This refinement stems from the higher nucleation rate of bainitic ferrite due to the larger driving force for its formation at lower temperatures and from the larger resistance of the untransformed austenite to the motion of bainite-austenite interfaces [22]. However, the strengthening caused by the refinement of bainitic structures is further enhanced in specimens isothermally treated below M_s due to the formation of PAM before the bainite reaction. This fact leads to the initial formation of finer bainitic structures, compared to specimens isothermally treated above M_s, due to the fragmentation of the initial austenite grains [6] and the higher strengthening of the untransformed austenite as consequence of the dislocations introduced by the martensitic transformation. These dislocations will be inherited by the further formed bainitic ferrite [24], resulting into a higher overall strengthening in terms of YS of the specimens isothermally treated below M_s and, consequently, maintaining a nearly constant YS with holding time.

The extended K-M curves have been demonstrated to be a powerful method to analyse the mechanical response of these advanced multiphase steels since relevant differences in terms of yielding were observed between heat treated specimens containing PAM with different degrees of tempering. This new approach can thus give reliable information concerning the mechanical response of the bainitic phase formed below M_s. Figure 7.8 shows the extended K-M curves of the specimens isothermally treated for the holding time 't3' at the three selected temperatures. As observed, the specimens treated at 340°C (above M_s) and 320°C, (below M_s) with a similar high fraction of bainitic ferrite in their microstructure exhibit nearly the same yielding behaviour, i.e., a rapid decay of Θ at low stress. This mechanical response is similarly reproduced in the specimen treated at 300°C, below M_s, where a considerable fraction of bainitic ferrite is present.

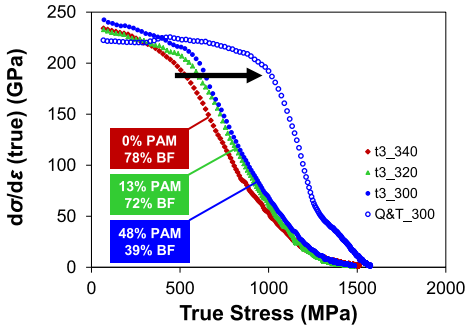

Figure 7.8. Extended K-M curves of specimens isothermally treated for the holding time 't3' at the selected temperatures above and below M_s. The corresponding K-M curve of the specimen quenched and tempered at 300°C for one hour has been included for comparison.

This unique observation via the K-M curves confirms, from the point of view of the mechanical behaviour, that the isothermal product formed below M_s has a bainitic character since the yielding behaviour of microstructures isothermally obtained below

M_s resembles well that of bainitic microstructures obtained above M_s. However, the formation of a certain fraction of PAM, tempered to a certain degree during the isothermal holding, modifies the yielding behaviour of the bainitic microstructures by delaying the rapid decay of Θ to higher stress, as indicated by a black arrow in Figure 7.8. This yielding behaviour may progressively evolve towards the one exhibited by Q&T specimens by increasing the volume fraction of PAM formed before the isothermal bainite reaction starts. Further investigations are needed to determine the volume fraction of PAM at which the yielding behaviour of the multiphase microstructure becomes similar to that of a fully tempered martensite.

7.4.2. Effect of Multiphase Microstructure on Strain Hardening

Uniform elongation increases with holding time in all heat treated specimens above and below M_s, as shown in Figures 7.6.a,c,e. This is due to the balanced evolution of product phases with holding time, in which the fraction of softer bainitic ferrite increases at the cost of the harder martensite formed during the final cooling after the isothermal holding. On the other hand, below M_s, the strain hardening potential slightly decreases with holding time, as opposed to what it is observed in isothermal treatments above M_s. This decrease may be consequence of three phenomena. The first two phenomena are presumably related to the pinning effect of dislocations derived from the precipitation of carbides within PAM and the grain refinement of bainitic structures occurring in specimens isothermally treated below M_s. The presence of carbides and finer structures can partially hinder the movement of dislocations until a higher level of tensile stress is reached [16]. The constrained movement of dislocations certainly contributes to a higher strengthening in terms of YS. However, further investigations are required for a better understanding of the hindering effect caused by both phenomena on the dislocation motion occurring within each phase contained in these multiphase specimens.

The third phenomenon derives from the softening of the phase mixture with holding time, leading to the decrease of UTS. This decrease is consequence of the formation of higher fractions of bainitic ferrite and lower fractions of fresh martensite, but also of the softening of PAM during tempering due to the partial loss of carbon contained in solid solution and the likely reduction of its dislocation density. For multiphase steels obtained by isothermal treatments below M_s, it can be assumed that the maximum carbon concentration in solid solution within PAM corresponds to that estimated from quenching and tempering (Q&T) treatments performed at the same isothermal temperature and holding time. Taking into consideration this assumption and following the experimental procedure described in Chapter 6, the carbon concentration in solid solution within PAM can be drastically reduced during one-hour tempering (as reported in Chapter 6), mainly due to carbon precipitation as carbides and carbon partitioning into other phases. The combined effect of the three described phenomena gives as result

the increase of the *'YS/UTS'* ratio, i.e., the decrease of the strain hardening potential in specimens isothermally treated below M_s.

Table 7.III. Volume fraction of retained austenite (f^{RA}) and its carbon concentration (X_C^{RA}) in wt. % in specimens isothermally treated at 340°C, 320°C, and 300°C for different holding times ('t1', 't2', 't3') before the application of tensile tests. The carbon concentration of retained austenite at room temperature was calculated according to the equation reported in ref. [25].

T (°C)	time	f^{RA}	X_C^{RA} (%)
340	t1 (441 s)	0.03 ± 0.01	0.79 ± 0.09
	t2 (615 s)	0.04 ± 0.02	0.85 ± 0.09
	t3 (3600 s)	0.10 ± 0.03	0.91 ± 0.06
320	t1 (253 s)	0.08 ± 0.01	0.79 ± 0.09
	t2 (422 s)	0.10 ± 0.03	0.85 ± 0.09
	t3 (3600 s)	0.09 ± 0.02	0.91 ± 0.03
300	t1 (7 s)	0.02 ± 0.01	0.79 ± 0.09
	t2 (151 s)	0.06 ± 0.01	0.79 ± 0.09
	t3 (3600 s)	0.09 ± 0.02	0.85 ± 0.06

The decrease of the strain hardening capacity can be partially counteracted by the mechanically-induced transformation of the retained austenite into martensite during the application of stress. This austenite-to-martensite transformation generally occurs within the uniform plastic deformation regime delaying the beginning of the necking, which implies an increase of the UTS. However, this counteracting effect on the UTS is challenging to be quantitatively analysed due to the complexity of the multiphase mixture created from these heat treatments. Investigations on the mechanical stability of the retained austenite in specimens isothermally treated for a holding time of 't3' at the same temperatures above and below M_s show a similar contribution of the retained austenite to the strain hardening capacity in all specimens, as is demonstrated in Chapter 6. This is attributed to the similar mechanical stability of the retained austenite as consequence of a similar carbon concentration (see Table 7.III), which leads to the mechanical transformation of approximately two thirds of the total fraction of retained austenite during the uniaxial tensile tests.

In the present work, the formation of similar retained austenite fractions with comparable carbon enrichment, especially for 't2' holding times (see Table 7.III), may lead to a similar effect of the mechanically-induced transformation of the retained austenite on the strain hardening in all heat treated specimens. However, the decreasing evolution of the strain hardening capacity from 't2' to 't3' holding times (below M_s) suggests that this transformation-induced effect cannot counteract by itself the opposing effects previously described that negatively affect the capacity of specimens isothermally treated below M_s to be hardened by deformation. Further research is needed to quantitatively determine

the contribution of the distinct morphologies (film-like or blocky) of retained austenite to the strain hardening of these multiphase steels.

7.4.3. Technological Implications

Figure 7.9.a shows the comparison of microstructure and properties of the specimens heat treated at two of the selected temperatures, 340°C (above M_s) and 320°C (below M_s), during similar holding times (441 s and 422 s, respectively). A higher fraction of bainitic ferrite is isothermally formed at 320°C compared to the volume fraction formed at 340°C during a similar holding time. This is mainly a consequence of the increasing number of preferential sites for bainite nucleation introduced as martensite-austenite interfaces due to the formation of PAM before the bainite reaction, as demonstrated in Chapter 2. The presence of these newly-created preferential sites triggers an accelerating effect in the kinetics of the bainitic ferrite formation at 320°C in comparison with the kinetics of the bainite reaction occurred at 340°C, where there is no presence of PAM. A higher formation of bainitic ferrite at 320°C subsequently leads to the formation of a lower fraction of fresh martensite during the final cooling after the isothermal holding. The resulting multiphase microstructure, where bainitic ferrite becomes the dominant phase, gives rise to a decrease of 100-150 MPa of the YS and UTS, as well as an increase of the uniform elongation and the strain hardening capacity, with respect to the multiphase microstructure formed above M_s.

In Figure 7.9.b, the comparison is made between two specimens with similar fractions of bainitic ferrite (approx. 0.46-0.49), heat treated at the same two temperatures above and below M_s, 340°C and 320°C, respectively. Due to the accelerated kinetics of bainite reaction derived from the formation of PAM, there is a strong reduction of the isothermal holding time applied at 320°C to obtain a similar bainitic ferrite fraction to that obtained at 340°C. Comparable YS and UTS are exhibited by both types of heat-treated specimens, although the difference in UTS is not negligible. According to these comparisons, the formation of martensite prior to the subsequent bainite reaction below M_s leads to a drastic reduction of the holding time needed to form similar fractions of bainitic ferrite as those formed above M_s, maintaining comparable mechanical properties between the specimens isothermally treated at both temperatures.

Finally, Figure 7.9.c shows the comparison of microstructure and properties of specimens exhibiting similar values of YS and UTS. The specimens isothermally treated at the lowest temperature (300°C) applying the shortest holding time (151 s) show intermediate values of YS and UTS compared to those exhibited by the other two specimens isothermally treated at higher temperatures and longer holding times. This implies a further step in the development of advanced multiphase steels with a bainitic-martensitic matrix. In this case, similar mechanical properties in terms of strength (YS

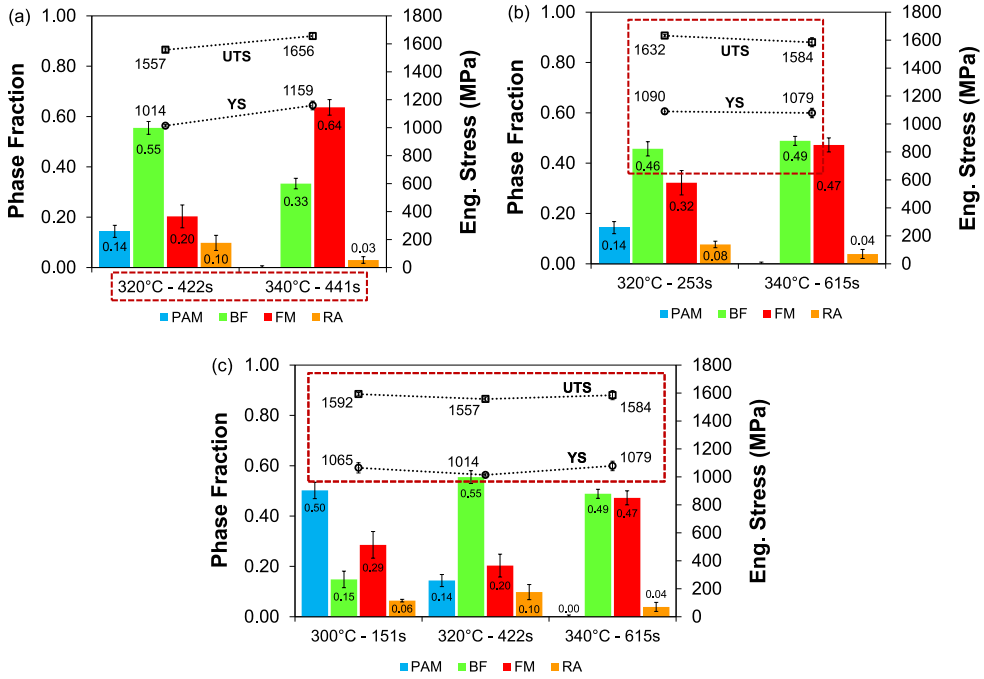

Figure 7.9. Comparison of the microstructure-properties relationships between specimens isothermally treated at distinct temperatures above and below M_s (a) for a similar holding time, (b) containing a similar bainite fraction, and (c) exhibiting similar yield stress and ultimate tensile strength.

and UTS), as well as of uniform elongation and strain hardening (see Figure 7.6), can be achieved with much shorter processing times by obtaining microstructures where bainitic ferrite is no longer the dominant phase, giving a greater relevance to the PAM with a certain degree of tempering.

The present study shows that the martensitic-bainitic steels developed by isothermal treatments above M_s can be replaced by those developed below M_s without compromising the mechanical performance under tensile deformation. To benchmark this new family of advanced high strength steels, the mechanical properties obtained in the present work through the application of isothermal treatments above and below the M_s temperature in a low-carbon high-silicon steel are compared with those obtained in similar thermal cycles and chemical compositions by other researchers [1,2-4,6]. Table 7.IV shows the original data extracted from the referenced works. Due to the use of different sub-size specimens, the values of total elongation were corrected by a simplified form of the Oliver formula [26], which is currently adopted by the existing standardised methodology [27]. This formula is expressed as

$$A_c = A_k \cdot \left(\frac{L_{0k}}{\sqrt{S_{0k}}} \right)^n \cdot \left(\frac{\sqrt{S_{0c}}}{L_{0c}} \right)^n \tag{7.1}$$

where A_c and A_k are the corrected and observed elongations, L_{0k} and S_{0k} are the gauge length and cross-section of the sub-size specimens, and L_{0c} and S_{0c} are the gauge length and cross-section obtained from the ASTM standards [28]. In this case, according to ASTM25, the standard specimen dimensions are: gauge length (L_{0c}) of 25 mm, width (w_{0c}) of 6.04 mm, and thickness (z_{0c}) of 3 mm, which implies S_{0c} = 18 mm^2. These dimensions were selected taking into consideration previous studies on the influence of the specimen dimensions on the tensile elongation of advanced high strength steels [29,30]. The exponent n is a geometrically dependent parameter that it is usually taken as 0.4 [26].

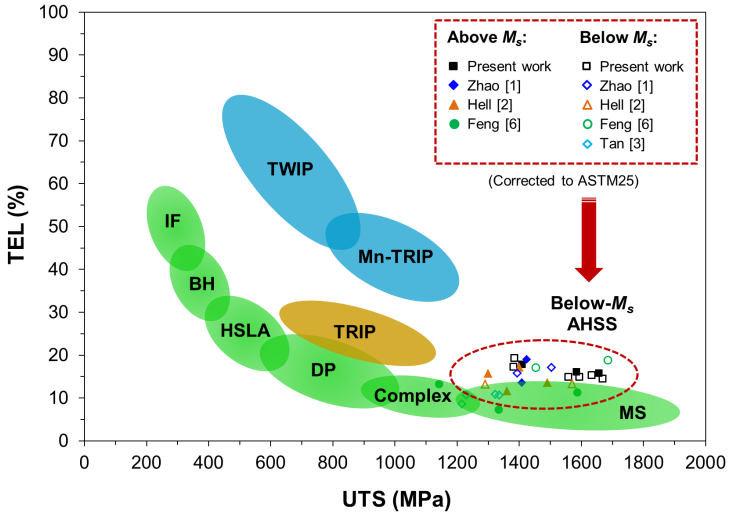

Figure 7.10. Diagram of steel properties in which the newly-designed advanced high strength steels (AHSS) through isothermal holdings below M_s are included [31]. Conventional bainitic steels isothermally obtained above M_s are displayed for comparison. Values of total elongation (TEL) were corrected according to the standardised methodology.

The corrected values of total elongation (TEL) of all specimens in relation to their ultimate tensile strength (UTS) are included in the steel properties diagram of Figure 7.10. As observed, the mechanical properties obtained in the present work are comparable to the ones obtained in similar studies performed with low-C steels. Therefore, new advanced high strength steels based on the presented approach can lead to a competitive advantage for steel industry, since faster processing and, thus, more sustainable routes can be implemented through isothermal holdings below M_s to manufacture steels with mechanical properties comparable to those obtained by conventional treatments above M_s.

Table 7.IV. Chemical composition, specimen dimensions, and original tensile data of several steels heat treated by isothermal treatments above and below M_s (L_{0k}, w_{0k}, and z_{0k} are the gauge length, width, and thickness, respectively (in mm) of the tensile specimens; UTS: ultimate tensile strength (MPa); TEL: total elongation (%)).

Reference	Alloy Composition (wt.%)	L_{0k}	w_{0k}	z_{0k}	Above or Below M_s	UTS (MPa)	TEL (%)
Present work	0.2C-3.5Mn-1.5Si-0.25Mo-0.04Al	10	4	2	Above	1408	21.9
						1584	19.7
						1656	19.4
					Below	1384	23.7
						1381	21.3
						1557	18.4
						1592	18.4
						1632	18.9
						1667	17.8
[1]	0.15C-1.9Mn-1.4Si-1.9Cr-0.4Ni-0.3Mo	25	10	3	Above	1408	15.0
						1424	21.0
					Below	1393	17.5
						1504	19.0
[2]	0.2C-2.5Mn-1.5Si-0.8Cr	15	9	1.4	Above	1360	13.2
						1400	19.6
					At M_s	1300	17.9
						1490	15.4
					Below	1290	15.1
						1570	15.2
[3]	0.2C-1.7Mn-1.7Si-0.2V	20	12.5	4	Below	1336	14.3
						1323	14.6
						1229	14.3
						1215	11.5
[6]	0.4C-0.82Mn-0.35Si-0.9Cr-0.1Mo	100	13	6	Above	1142	10.2
						1586	8.7
						1333	5.6
					Below	1452	13.2
						1684	14.5

7.5. Conclusions

The relationships between microstructure and properties of different multiphase microstructures obtained through the application of isothermal holdings at temperatures above and below M_s in a low-C high-Si steel are analysed at different holding times up to one hour. The microstructure-properties relationships are globally benchmarked within the family of advanced high strength steels (AHSS). The main conclusions obtained are the following:

1. The degree of tempering of prior athermal martensite with holding time has a primary effect on the overall mechanical response of specimens heat treated below M_s. Prior athermal martensite yields as quenched martensite after short holding times (< 200 s), whereas its yielding behaviour becomes comparable to that of tempered martensite as the holding time is increased.

2. Analysing the mechanical response by extended Kocks-Mecking plots confirms that the isothermal product formed below M_s has a bainitic character. The increased formation of bainitic ferrite within the phase mixture leads to a faster decrease of the instantaneous work hardening at low stresses, indicating that bainitic ferrite yields at lower stress than fresh martensite and tempered martensite.

3. The yield stress of multiphase microstructures formed below M_s remains practically unchanged with holding time after the first minutes compared to the progressive decrease of the yield stress with holding time observed in conventional bainitic steels. Also, an opposite evolution of the strain hardening capacity is observed between both types of multiphase steels. The mechanical response of multiphase microstructures formed below M_s is a direct consequence of the microstructural refinement, carbide precipitation, and matrix softening, which are phenomena derived from the formation and tempering of prior athermal martensite.

4. Combinations of product phases can be tailored varying processing temperatures and times in treatments below M_s to manufacture steels grades with similar properties to those obtained by conventional heat treatments performed above M_s, but with a considerable reduction in energy consumption. This energetic advantage stems from shorter processing times as a consequence of the accelerating effect of prior athermal martensite on the subsequent bainite reaction.

References

[1] L. Zhao, L. Qian, J. Meng, Q. Zhou, F. Zhang. Below-M_s austempering to obtain refined bainitic structure and enhanced mechanical properties in low-C high-Si/Al steels. Scripta Mater., 2016, vol. 112, pp. 96-100.

[2] J.C. Hell, M. Dehmas, S. Allain, J.M. Prado, A. Hazote, J.P. Chateau. Microstructure-properties relationships in carbide-free bainitic steels. ISIJ International, 2011, vol. 51, pp. 1724-1732.

[3] X. Tan, Y. Xu, X. Yang, D. Wu. Microstructure-properties relationship in a one-step quenched and partitioned steel. Mater. Sci. Eng. A, 2014, vol. 589, pp. 101-111.

[4] G. Mandal, S.K. Ghosh, S. Bera, S. Mukherjee. Effect of partial and full austenitisation on microstructure and mechanical properties of quenching and partitioning steel. Mater. Sci. Eng. A, 2016, vol. 676, pp. 56-64.

[5] S. Yan, X. Liu, W.J. Liu, T. Liang, B. Zhang, L. Liu, Y. Zhao. Comparative study on microstructure and mechanical properties of a C-Mn-Si steel treated by quenching and partitioning (Q&P) processes after a full and intercritical austenitization. Mater. Sci. Eng. A, 2017, vol. 684, pp. 261-269.

[6] J. Feng, T. Frankenbach, M. Wettlaufer. Strengthening 42CrMo4 steel by isothermal transformation below martensite start temperature. Mater. Sci. Eng. A, 2017, vol. 683, pp. 110-115.

[7] J. Tian, G. Xu, M. Zhou, H. Hu. Refined bainite microstructure and mechanical properties of a high-strength low-carbon bainitic steel treated by austempering below and above M_s. Steel Research Inter. 2018, pp. 1-10.

[8] A. Zinsaz-Borujerdi, A. Zarei-Hanzaki, H.R. Abedi, M. Karam-Abian, H. Ding, D. Han, N. Kheradmand. Room temperature mechanical properties and microstructure of a low alloyed TRIP-assisted steel subjected to one-step and two-step quenching and partitioning process. Mater. Sci. Eng. A, 2018, vol. 725, pp. 341-349.

[9] A. Navarro-Lopez, J. Hidalgo, J. Sietsma, M.J. Santofimia. Influence of the prior athermal martensite on the mechanical response of advanced bainitic steel. Mater. Sci. Eng. A, 2018, vol. 735, pp. 343-353.

[10] G. Krauss. Tempering of martensite in carbon steels. Book 'Phase transformations in steels, Volume 2: Diffusionless transformations, high strength steels, modelling and advanced analytical techniques'. Chapter 5, pp. 126-150, Woodhead Publishing Limited, 2012.

[11] C.F. Jatczak, J.A. Larson, S.W. Shin. Retained austenite and its measurements by X-ray diffraction. Society of Automotive Engineers, 1980, 453, Special Publication.

[12] G.E. Dieter. Mechanical Metallurgy, SI Metric Edition, McGraw-Hill, 1988.

[13] E.P. Bagliani, M.J. Santofimia, L. Zhao, J. Sietsma, E. Anelli. Microstructure, tensile and toughness properties after quenching and partitioning treatments of a medium-carbon steel. Mater. Sci. Eng. A, 2013, vol. 559, pp. 486-495.

[14] Z. Arechabaleta, P. van Liempt, J. Sietsma. Quantification of dislocation structures from anelastic deformation behaviour. Acta Mater., 2016, vol. 115, pp. 314-323.

[15] U.F. Kocks, H. Mecking. Physics and phenomenology of strain hardening: the FCC case. Prog. Mater. Sci., 2003, 48, pp. 171-273.

[16] G. Krauss. Steels: processing, structure, and performance. 2nd edition, ASM International, Materials Park, OH, USA, 2015, Chapters 17 & 18.

[17] M.K. Miller, P.A. Beaven, G.D.W. Smith. A study of the early stages of tempering of iron-carbon martensites by atom probe field ion microscopy. Metall. Trans. A, 1981, vol. 12, pp. 1197-1204.

[18] L. Chang, S.J. Barnard, G.D.W. Smith. The segregation of carbon atoms to dislocations in low-carbon martensites: studies by field ion microscopy and atom probe microanalysis. Symposium of fundamentals of aging and tempering in bainitic and martensitic steel products, Warrendale, PA, 1992, ISS, pp. 19-28.

[19] G.R. Speich, W.C. Leslie. Tempering of steel. Metall. Trans., 1972, vol. 3, pp. 1043-1054.

[20] L.R. Cupertino, E.A. Pachon, A. Arlazarov. Mechanical behaviour of tempered martensite: characterization and modeling. Mater. Sci. Eng. A, 2017, vol. 706, pp. 38-47.

[21] D. Liu, B. Bai, H. Fang, W. Zhang, J. Gu, K. Chang. Effect of tempering temperature and carbide free bainite on the mechanical characteristics of a high strength low alloy steel. Mater. Sci. Eng. A., 2004, vol. 371, pp. 40-44.

[22] S.B. Singh, H.K.D.H. Bhadeshia. Estimation of bainite plate-thickness in low-alloy steels. Mater. Sci. Eng. A, 1998, vol. 245, pp. 72-79.

[23] S.H. He, B.B. He, K.Y. Zhu, M.X. Huang. On the correlation among dislocation density, lath thickness and yield stress of bainite. Acta Mater., 2017, vol. 135, pp. 382-389.

[24] S.H. He, B.B. He, K.Y. Zhu, M.X. Huang. Evolution of dislocation density in bainitic steel: Modeling and experiments. Acta Mater., 2018, vol. 149, pp. 46-56.

[25] J.B. Seol, D. Raabe, P.P. Choi, Y.R. Im, C.G. Park. Atomic scale effects of alloying, partitioning, solute drag and austempering on the mechanical properties of high-carbon bainitic-austenitic TRIP steels. Acta Mater., 2012, vol. 60, pp. 6183-6199.

[26] D.A. Oliver. Proposed new criteria of ductility from a new law connecting the percentage elongation with size of test-piece. Proc. Inst. Mech. Eng., 1928, 2, 827–864.

[27] ISO 2566-1. Steel – Conversion of elongation values – Part 1: Carbon and low alloy steels. International Organization for Standarization (ISO), Geneve, Switzerland, 1984.

[28] ASTM E8/E8-09. Standard test methods for tension testing of metallic materials. ASTM International, Philadelphia, PA, 2009.

[29] G.M. Cola Jr., B. Hanhold, T. Lolla, B. Radhakrishnan, S. Babu. On the tensile elongation of advanced high-strength steels. AIST Trans., 2013, vol. 10 (3), pp. 1-6.

[30] D.N. Hanlon, S.M.C. van Bohemen, S. Celotto. Critical Assessment 10: Tensile elongation of strong automotive steels as function of testpiece geometry. Mat. Sci. & Techn., 2015, vol. 31, pp. 385-388.

[31] www.dierk-raabe.com/steels-brief-introduction/

8

CHAPTER 8

General Conclusions and Recommendations

8.1. General Conclusions

This Ph.D. thesis has led to the fundamental understanding of phase transformations and the interactions between the phases formed during isothermal treatments below the M_s temperature in a low-carbon high-silicon steel, as well as of the relationship of the formed multiphase microstructures with their final mechanical performance. The most relevant outcomes from this research work are highlighted as follows:

1. The formation of a certain fraction of athermal martensite is quantitatively proven to significantly accelerate the transformation kinetics at the onset of the isothermal decomposition of austenite below M_s, compared to isothermal transformations occurring without the presence of prior athermal martensite. This accelerating effect is attributed to the higher density of potential nucleation sites for the isothermal transformation at martensite-austenite interfaces. Consequently, there exists a dependency between the accelerated transformation rate at the onset of the isothermal reaction and the interfacial area of martensite-austenite interfaces.

2. The product phase formed from the decomposition of austenite in isothermal holdings below M_s is identified as bainitic ferrite. Microstructurally, bainitic ferrite appears in the form of thin acicular units and/or irregularly shaped laths, similar to the morphology exhibited by the bainitic structures formed after isothermal holdings above M_s. Mechanically, the bainitic character of this isothermally formed product phase is confirmed by extended Kocks-Mecking curves, which show that multiphase microstructures mainly formed by this isothermal product phase exhibit a similar yielding behaviour to the bainitic ones formed above M_s.

3. Significant differences in the microstructural development of martensitic-bainitic structures are observed between the surface and the bulk of specimens isothermally treated below M_s. These microstructural differences are shown to be caused by the reduced strain energy needed to accommodate the transformation strains originated by martensite formation at the free surface compared to the bulk. As a consequence, the onset of the martensitic transformation occurs at a higher M_s temperature at the free surface, which leads to the formation of different combinations of product phases at the surface and in the bulk. The martensitic-bainitic structures formed also differ in terms of grain size and growth direction due to effects derived from the free surface. These effects are experimentally observed to be the coalescence of martensitic and/or bainitic structures as well as their preferential growth nearly parallel to the surface.

4. Experimental observations by in-situ high energy X-ray diffraction measurements reveal the development of carbon-rich and carbon-poor austenite regions at the

early stage of the isothermal bainite formation above and below M_s. The formation of both austenite regions is attributed to the slower kinetics of carbon redistribution within untransformed austenite grains in comparison with the kinetics of bainite formation. The rate of carbon redistribution mainly depends on the combined effect of carbon diffusivity and the remaining austenite fraction at each temperature.

5. The formation of different fractions of prior athermal martensite as well as its degree of tempering with the isothermal holding time have a primary effect on the overall mechanical response of multiphase microstructures obtained below M_s. A grain boundary strengthening mechanism is triggered within these multiphase microstructures as a consequence of the fragmentation of the initial austenite grains by martensite-austenite interfaces formed before the isothermal bainite reaction. Tempering of the prior athermal martensite also triggers other strengthening mechanisms derived from the higher carbon concentration in solid solution of the prior athermal martensite, compared to bainitic ferrite, and the precipitation of carbides within martensite laths. These phenomena modify, to some extent, the overall mechanical response of multiphase microstructures formed below M_s.

6. Variations of tempering time in isothermal holdings below M_s lead to significant changes of the mechanical behaviour of the prior athermal martensite, besides the microstructural changes inherent to the isothermal progress of the bainite reaction. The yielding response of prior athermal martensite tempered for short times (several minutes) is similar to that of as-quenched martensite while, at long holding times (approximately one hour), prior athermal martensite typically yields as tempered martensite.

7. Small variations of temperature and holding time in the application of isothermal treatments below M_s enables to obtain bainitic-martensitic microstructures with comparable mechanical properties to those exhibited by conventional bainitic steels obtained above M_s. Furthermore, the multiphase microstructures are generally obtained in shorter holding times due to the accelerating effect caused by the formation of martensite on the isothermal bainite formation below M_s. The reduction of processing temperatures and times for the development of these multiphase steels without compromising their mechanical performance, compared to the conventional existing ones, entails a remarkable technological advance for the manufacturing of more sustainable advanced high strength steels, due to a lower energy consumption and the consequently reduced environmental footprint.

8.2. Recommendations for Future Work

These outcomes generate, however, new challenges for the scientific community regarding the understanding of new phenomena and/or mechanisms not only in similar steel compositions, but also in a wider range of carbon concentrations and alloying elements. Based on the described findings of this research work, the following recommendations are suggested for future work:

- The acceleration phenomenon caused by the formation of prior athermal martensite on the subsequent isothermal transformation kinetics has been mainly reported in alloyed steels with carbon concentrations lower than 0.4 wt.%. It is well known that the increase of carbon concentration implies a higher stability of the austenite, so the onset of its isothermal decomposition can be expected to occur at lower temperatures and longer times. Alloying additions of austenite stabilizers such as manganese, chromium, molybdenum, or nickel in these types of advanced high strength steels also contribute to the increasing stabilization of austenite. All these elements can potentially counteract the possible accelerating effect introduced by the prior athermal martensite. The reproducibility of this phenomenon in alloyed steels with high carbon concentrations, from 0.6 wt.% onwards, can therefore be questioned. The isothermal transformation kinetics is suggested to be studied in holdings below M_s in high-carbon low-alloy steels to determine the kinetic effect of prior athermal martensite.

- Based on the in-depth microstructural characterization of the product phases formed in isothermal treatments below M_s, the appearance of ledge-like protrusions in the wavy boundaries of prior athermal martensite, tempered to a certain degree, remains unclear. These protrusions present a similar orientation relationship as the core of martensite laths. In the present work, it is suggested that these protrusions are related to the formation of bainitic ferrite at martensite-austenite interfaces at the onset of the isothermal bainite reaction. If this is so, the accelerating effect introduced by the prior athermal martensite could be the triggering phenomenon for the formation of bainitic structures with an orientation relationship inherited from this martensite. To elucidate the veracity of this hypothesis, high-resolution transmission electron microscopy (HR-TEM) measurements are proposed to study the protrusions characterized at wavy boundaries of prior athermal martensite at the atomic scale.

- Based on the free surface effects observed on phase transformations occurring in isothermal treatments around the M_s temperature, microstructural differences can appear along the thickness of steel sheets that can be critical for the performance of these multiphase steels under fatigue. Since automotive structural components are

made of thin steel sheets internally formed by a multiphase microstructure, a detailed analysis of fatigue in steel sheets thermally treated around the M_s temperature is highly recommended. The interest of this analysis lies in determining the effect of the preferential growth of bainitic-martensitic structures at the free surface as well as the microstructure-properties gradient along the thickness formed in these steels on crack propagation due to fatigue.

- Understanding all strengthening mechanisms of the formed complex microstructures and the interactions between the phases formed in holdings below M_s is crucial for the optimization of the microstructure-properties relationship of these multiphase steels. In the present work, a clear insight is given regarding the contribution of grain boundaries and carbon in solid solution to the strengthening of multiphase microstructures obtained in these thermal treatments. However, the strengthening contribution of carbide precipitation within prior athermal martensite, tempered to some extent, is still unexplored. An accurate determination of the evolution of carbide precipitation in prior athermal martensite during holdings below M_s is thus recommended to be performed in order to characterize the type of carbide formed after the application of distinct holding times. Transmission electron microscopy (TEM) and atom probe tomography (APT) are the most appropriate high-resolution techniques to characterize the nature of the carbides formed as well as its morphology and carbon concentration, respectively.

- The use of empirical formulae introduces several uncertainties in the determination of the contribution of the strengthening mechanisms acting in multiphase microstructures isothermally formed below M_s. On the other hand, the need of using high resolution characterization techniques in combination with an extraordinary amount of working time significantly increases the development costs of these multiphase steels before industrial implementation. The development of a general physically-based model that accurately describes the yielding behaviour of these multiphase steels is suggested to provide a better fundamental understanding of the multiple interactions between the strained phases and to reduce the need of experimental measurements with the consequent decrease of industrial development costs of these advanced multiphase steels.

- Advanced high strength steels, such as Q&P and TRIP-aided bainitic steels, are generally used for structural automotive components. The mixture of martensitic-bainitic structures with retained austenite of these steels provides a good combination of strength and ductility, favouring the strain distribution in case of car crashing. The recent development of advanced multiphase steels through isothermal holdings below M_s means that there is still limited knowledge concerning the mechanical

properties derived from these multiphase microstructures. As these multiphase steels are a promising alternative for similar automotive components currently made of Q&P and TRIP-aided bainitic steels, it is recommended to complete the mechanical study of the present work by performing Charpy measurements of fracture toughness to determine the ductility of the multiphase mixture obtained after the application of distinct holding times. These measurements will provide fundamental knowledge with respect to variations of ductility stemming from microstructural changes and, specifically, from the different tempering degree of prior athermal martensite.

- Small variations of temperature and time around the M_s temperature imply significant microstructural differences which can lead to a drastic reduction of processing times for the development of advanced high strength steels. Thus, it is necessary to highlight the need of an effective temperature control system during steel manufacturing for an effective implementation of the newly-designed processing route of complex multiphase steels through isothermal holdings below M_s.

Acknowledgements

Firstly, I would like to express my sincerest gratitude to my promoters, Prof. dr. Maria Santofimia and Prof. dr. ir. Jilt Sietsma, for giving me the opportunity of developing professionally as a scientist, for their guidance and advice, and for their confidence in me and my work. I also want to thank my daily supervisor and co-promoter, Dr. Javier Hidalgo, for our numerous scientific discussions, our work collaborations, and the continuous support along all these years.

During my Ph.D., I visited other academic institutions to develop my research work and I always found wonderful scientists who helped me to achieve my goals. I thank Prof. dr. ir. Roumen Petrov, from University of Gent (Belgium), for his help on EBSD measurements, and Dr. Goro Miyamoto and Prof. dr. Tadashi Furuhara, from Tohoku University (Japan), for the warm hospitality, the continuous support, and their direct contribution to the work presented in this Ph.D. thesis. I also want to thank Prof. Jan van Turnhout for his help with the translation of the summary of my Ph.D. thesis in Dutch.

I would like to thank the technical staff of the department labs: Nico Geerlofs (dilatometry), Hans Hofman (furnaces and salt bath), Sander van Asperen (metallography), and Kees Kwakernaak (SEM) for their assistance and help during my experiments, and specially, Richard Huizenga who helped me enormously with his support and work on the performance and analysis of high-energy X-ray diffraction measurements.

These years of the Ph.D. process would not have been the same without all wonderful people with whom I have interacted on my daily basis not only in the department, but also outside it: Jun, Ashwath, Tungky, Qin, Ankit, Pina, Behnam, Casper, Lucia, Ann-Sophie, Jesús, Sudhindra, Wei, Viviam, Arthur, Konstantina, Tim, and Marilia. Thanks to everyone for the scientific discussions, the given advice, the good moments lived together and, of course, for having the door of your office open to help me whenever I needed it.

This great adventure of doing a Ph.D. in a foreign country started with happiness for the new life to begin, but also with some tears in my eyes for the family and friends to leave behind. Nobody could have told me that I would find a second family in The Netherlands. As in all families, there were two branches. On the one hand, I found a new Spanish family, with lovely people coming from all over Spain. They were and still are my support, this kind of people that they are always there for you in all the

unforgettable moments you live and, specially, in the worst ones. My whole-heartedly thanks to Paloma and Rubén, Diana and Juan, Patricia and Jose, Jesús, Javier, BijNa and Jesús, Zaloa, Javier and Elena, Carola and Javier, and Jose Julián. Although our lives will separate, all of you will be an important part of my life and my house will always be opened for you.

On the other hand, I can proudly say that I also found a Greek family. Since we met, I can count on them for everything I need no matter what and when. For this, my whole-heartedly thanks also goes to Constantinos, Marina and Konstantinos, Nikolas, Sotiria, Chrysoula, Evangelos, and Artemis. From all of them, I would like to give special thanks to Constantinos for his support since the first day of the Ph.D. process and all the unforgettable and, sometimes crazy, moments and experiences lived along these years. All of you make me feel that a part of me has always belonged to Greece.

I do not want to forget to thank my closest friends living in Albacete, my hometown, for keeping the contact despite the distance between us, being available to meet whenever I could visit Albacete, and supporting me during all these years. Our friendships have never changed no matter the distance and time without seeing or talking each other. This has demonstrated who my true friends are: Javier, David, Silvia, Eva, Raúl, Joaquín, and Francisco José.

Lastly, I want to express my greatest gratitude to my family and, especially, to my parents Alfonso and Valentina. To them, thank you so much for being always by my side when I have needed you and for supporting me in all the decisions that I have made throughout my life. I could not have reached so far in my professional career without your sacrifice and effort to give me the best possible education, that education you could not receive since you had to work from your childhood to get your family ahead. Both of you are my pride!

List of Publications

1. A. Navarro-López, J. Hidalgo, C.A. Fitriani, R.M. Huizenga, B. Kim, J. Sietsma, M.J. Santofimia. *In-situ investigation of carbon enrichment in austenite during isothermal holdings around the M_s temperature by high energy X-ray diffraction*. To be submitted for publication.

2. A. Navarro-López, J. Hidalgo, G. Miyamoto, T. Furuhara, J. Sietsma, M.J. Santofimia. *Free surface effects on low temperature phase transformations in a multiphase steel by laser confocal microscopy*. To be submitted for publication.

3. C. Ioannidou, A. Navarro-López, A. Rijkenberg, R.M. Dalgliesh, S. Kölling, C. Pappas, J. Sietsma, A.A. van Well, S.E. Offerman. *Evolution of the precipitate chemical composition during annealing of vanadium micro-alloyed steels by in-situ SANS*. Submitted for publication.

4. A. Navarro-López, C. Ioannidou, E. van der Wal, Z. Arechabaleta, R. van der Oever, M. Verleg, R.M. Dalgliesh, J. Sykora, F. Akeroyd, N. Geerlofs, J. Sietsma, C. Pappas, , A.A. van Well, S.E. Offerman. *Furnace for in-situ and simultaneous studies of nano-precipitates and phase transformations in steels by SANS and neutron diffraction*. Submitted to Review of Scientific Instruments.

5. X. Zhang, C. Ioannidou, G.H. ten Brink, A. Navarro-López, J. Wormann, J. Campaniello, R.M. Dalgliesh, A.A. van Well, S.E. Offerman, W. Kranendonk, B.J. Kooi. *Microstructure, precipitate, and property evolution in cold-rolled Ti-V high strength low alloy steel*. Mater. Design, 2020, vol. 192, 108720.

6. A.M. Ravi, A. Navarro-López, J. Sietsma, M.J. Santofimia. *Influence of martensite/austenite interfaces on bainite formation in low-alloy steels below M_s*. Acta Mater., 2020, vol. 188, pp. 1-12.

7. A. Navarro-López, J. Hidalgo, J. Sietsma, M.J. Santofimia. *Unravelling the mechanical behaviour of advanced multiphase steels isothermally obtained below M_s*. Mater. Design, 2020, vol. 188, 108484.

8. C. Ioannidou, Z. Arechabaleta, A. Navarro-López, A. Rijkenberg, R.M. Dalgliesh, S. Kölling, V. Bliznuk, C. Pappas, J. Sietsma, A.A. van Well, S.E. Offerman.

Interaction of precipitation with austenite-to-ferrite phase transformation in vanadium micro-alloyed steels. Acta Mater. 181 (2019) 10-24.

9. A. Navarro-López, J. Hidalgo, J. Sietsma, M.J. Santofimia. *Influence of the prior athermal martensite on the mechanical response of advanced bainitic steel*. Mater. Sci. Eng. A, 2018, vol. 735, pp. 343-353.

10. A. Navarro-López, J. Hidalgo, J. Sietsma, M.J. Santofimia. *Characterization of bainitic/martensitic structures formed in isothermal treatments below the M_s temperature*. Mater. Charact., 2017, vol. 128, pp. 248-256.

11. A. Navarro-López, J. Sietsma, M.J. Santofimia. *Effect of prior athermal martensite on the isothermal transformation kinetics below M_s in a low-C high-Si steel*. Metall. Mat. Trans. A, 2016, vol. 47A, pp. 1028-1039.

12. A. Navarro-López, J. Sietsma, M.J. Santofimia. *Effect of pre-existing martensite on the isothermal transformation kinetics below the M_s temperature in a low-C high-Si steel*. Proceedings of the International Conference on Solid-Solid Phase Transformations in Inorganic Materials (PTM 2015), pp. 559-560.

13. J.M. Torralba, A. Navarro-López, M. Campos. *From the TRIP effect and Quenching and Partitioning steels concepts to the development of new high-performance, lean powder metallurgy steels*. Mater. Science & Eng. A, 2013, vol. 573, pp. 253-256.

14. A. Martínez, V. Miguel, J. Coello, A. Navarro-López, A. Calatayud, M.C. Manjabacas. *Analysis of the influence of the multipass welding, welding pre-heat and welding post heat treatments on the behaviour of GMAW joints of HARDOX 400 microalloyed steel*. Journal of Metallurgy of CENIM, 2011, vol. 47, pp. 61-75.

List of Conferences

1. A. Navarro-López, J. Hidalgo, C.A. Fitriani, R.M. Huizenga, J. Sietsma, M.J. Santofimia. *In-situ evolution of carbon partitioning during phase transformation below M_s in advanced multiphase steels*. European Congress & Exhibition on Advanced Materials and Processes (EuroMat 2019), Stockholm, Sweden, September 1-5, 2019. (Oral presentation).

2. C. Ioannidou, A. Navarro-López, X. Zhang, A. Rijkenberg, R.M. Dalgliesh, S. Kölling, B. Kooi, A.A. van Well, S.E. Offerman. *Precipitation and phase transformation in V-microalloyed steels studied by in-situ simultaneous small-angle neutron scattering and neutron diffraction*. European Congress & Exhibition on Advanced Materials and Processes (EuroMat 2019), Stockholm, Sweden, September 1-5, 2019. (Oral presentation).

3. M.J. Santofimia, A.M. Ravi, A. Navarro-López, J. Sietsma. *Influencing the kinetics of bainite formation in low carbon steels*. International Conference on Processing & Manufacturing of Advanced Materials (THERMEC 2018), Paris, France, July 9-13, 2018. (Invited Oral presentation).

4. A. Navarro-López, J. Hidalgo, J. Sietsma, M.J. Santofimia. *Towards a more sustainable manufacturing of advanced multiphase steels through the acceleration of bainite formation*. European Congress & Exhibition on Advanced Materials and Processes (EuroMat 2017), Thessaloniki, Greece, September 17-22, 2017. (Oral presentation).

5. A. Navarro-López, J. Hidalgo, J. Sietsma, M.J. Santofimia. *The effect of martensite/bainite microstructures obtained above and below M_s on the mechanical properties in a low-C steel*. Materials Science and Engineering Congress (MSE), Darmstadt, Germany, September 27-29, 2016. (Oral presentation).

6. A. Navarro-López, J. Hidalgo, J. Sietsma, M.J. Santofimia. *Characterization of product phases formed from austenite during isothermal treatments around the M_s temperature in a low-C high-Si steel*. International Conference on Processing & Manufacturing of Advanced Materials (THERMEC 2016), Graz, Austria, May 29 – June 3, 2016. (Poster).

7. A. Navarro-López, J. Sietsma, M.J. Santofimia. *Effect of pre-existing martensite on the isothermal transformation kinetics below the M_s temperature in a low-C high-Si steel*. International Conference on Solid-Solid Phase Transformations in Inorganic Materials (PTM 2015), Displacive Transformations; Whistler, BC, Canada, June 27 – July 3, 2015. (Oral presentation).

8. A. Navarro-López, S.MC. van Bohemen, J. Sietsma, M.J. Santofimia. *Effect of pre-existing martensite on subsequent transformation kinetics in a low-C high-Si steel*. Materials Science and Engineering Congress (MSE), Darmstadt, Germany, September 23-25, 2014. (Oral-poster presentation).

9. A. Navarro-López, S.MC. van Bohemen, J. Sietsma, M.J. Santofimia. *Effect of pre-existing martensite on subsequent transformation kinetics in a low-C high-Si steel*. Materials Science and Engineering Congress (MSE), Darmstadt, Germany, September 23-25, 2014. (Poster).

About the Author

Alfonso NAVARRO LÓPEZ

Born on 3rd August 1985, in Albacete, Castilla-La Mancha, Spain

Professional Experience

09.2019 - Present Junior Researcher
Delft University of Technology, Delft, The Netherlands
Project: A new interface standard for integrated virtual material modelling in manufacturing industry (RVE-based material modelling).

02.2018 - 04.2019 Junior Researcher
Delft University of Technology, Delft, The Netherlands
Project: Resource efficient NANO-steels through in-situ and simultaneous studies of the precipitation and phase transformation kinetics.

02.2013 - 08.2017 Ph.D. Researcher
Delft University of Technology, Delft, The Netherlands
Project: Phase transformations and interactions between non-equilibrium phases in isothermal treatments below the M_s temperature.

10.2016 - 12.2016 Guest Researcher (internship within Ph.D. project)
Institute for Materials Research (IMR), Tohoku University, Sendai, Japan

10.2008 - 05.2009 Research Assistant (internship within Bachelor)
Institute for Regional Development (IDR), Albacete, Spain

Education

02.2013 - 08.2017	Ph.D. in Materials Science and Engineering Delft University of Technology (TUD), Delft, The Netherlands
09.2009 - 09.2012	Second stage (Master of Science) in Industrial Engineering University Carlos III (UC3M), Madrid, Spain
09.2004 - 07.2009	Bachelor in Mechanical Engineering with honours University of Castilla-La Mancha (UCLM), Albacete, Spain

Awards

2016	5 days of beam time at the European Synchrotron Radiation Facility (ESRF), placed in Grenoble, France
2009	Bachelor Extraordinary Award for the best academic record in Mechanical Engineering, University of Castilla-La Mancha, Albacete, Spain

Languages

Spanish	Native
English	Advanced Level C1. Full Professional Proficiency.
Dutch	Beginners Level A1/A2.

Extracurricular Activities

09.2014 - 09.2016	Board member of the Materials Student Association "Het Gezelschap TUBALKAIN" (Re-founder, secretary, and activity commissioner) Delft University of Technology (TUD), Delft, The Netherlands